UNIVERSITY OF CALIFORNIA,
IRVINE

Dynamics of Power Demand, Carbon-Footprint, and Process Performance of Primary and Secondary Separations in Water Resource Recovery Facilities

DISSERTATION

submitted in partial satisfaction of the requirements for the degree of

DOCTOR OF PHILOSOPHY

in Civil and Environmental Engineering

by

Mani Firouzian, P.E.

Dissertation Committee:
Professor Diego Rosso, Chair
Professor Sunny Jiang
Assistant Professor Adeyemi Adeleye

2021

DEDICATION

This dissertation is dedicated to my parents (Abdollah Firouzian and Fatemeh Mahboub) who have provided me invaluable educational opportunities and support through my life and to the memories of my grandparents (Mohamad Hosein Mahboub and Fakhri Haghshens) and my uncle (Mohamad Reza Mahboub) who believed in me through their entire lives.

I would thank my wife, my family, and friends for being patient with me over the course of the past 5 years that I had to work and study fulltime in order to make this PhD degree happen. Finally, I would like to thank my brother for encouraging me to complete this journey through these past 5 years.

TABLE OF CONTENTS

LIST OF FIGURES

LIST OF TABLES

LIST OF EQUATIONS

ACKNOWLEDGEMENTS

I would like to express the deepest appreciation to my committee chair and graduate adviser, Professor Diego Rosso, who believed in me and the fact that a PhD degree could be completed while working full-time as an engineer. Without his guidance and persistent help this dissertation would not be possible.

I would like to thank my PhD advancement and defense committee members, Professor Sunny Jiang, Professor Soroosh Sorooshian, and Assistant Professor Adeyemi Adeleye, whose guidance and suggestions though my graduate research proposal or defense stages added a great value to this dissertation.

Lastly, I would like to thank the utility personnel who supplied data and information for this research effort. Without their support, this research work would not be possible.

VITA

EDUCATION:

- **Doctor of Philosophy, Civil and Environmental Engineering**, University of California Irvine, Irvine **(Present)**
- **Master of Science in Engineering, Environmental Engineering**, University of California Irvine, Irvine **(2010)**
- **Bachelor of Science, Chemical Engineering,** California State Polytechnic University, Pomona **(2008)**

WORK EXPERIENCE:

- **Senior Air Quality Engineer at South Coast Air Quality Management District,** Diamond Bar/CA **(2015-Present)**
- **Teaching Assistant at University of California Irvine Mechanical and Aerospace Engineering Department,** Irvine/CA **(2019-2020)**
- **Environmental Engineer/Senior Consultant at Trinity Consultants,** Irvine/CA (**2010-2015)**
- **Environmental Engineer Intern at B. Braun Medical,** Irvine/CA **(2009-2010)**
- **Associate Process Engineer at Fluor Corporation,** Irvine/CA (**2008- 2009)**
- **Project Manager in Rio Tinto Minerals Distillation Column Design Project, California State Polytechnic University,** Pomona/CA **(2008-2009)**
- **Process Engineer Intern at Inland Empire Utilities Agencies,** Chino Hills/CA **(2008)**
- **Process Engineer Intern at Trussell Technologies Inc,** Pasadena/CA **(2007-2008)**

PUBLICATIONS:

- Caniani, D., Caivano, M., Pascale, R., Bianco, G., Mancini, I., Masi, S., Mazzone, G., Firouzian, M., Rosso, D. (2019, Jan 15). CO_2 and N_2O from water resource recovery facilities: Evaluation of emissions from biological treatment, settling, disinfection, and receiving water body. Science of the Total Environment, 648, 1130-1140. doi:10.1016/j.scitotenv.2018.08.150

ABSTRACT

Dynamics of Power Demand, Carbon-Footprint, and Process Performance of Primary and Secondary Separations in Water Resource Recovery Facilities

by

Mani Firouzian, P.E.

Doctor Of Philosophy in Civil and Environmental Engineering

University of California, Irvine, 2021

Professor Diego Rosso, Chair

Recent changes to the diurnal trend of power demand curves for the electrical grid and its new duck looking shape (Duck-Curve), as a result of increase in photovoltaic electricity generation, has also changed the power tariff structures and, in many cases, resulted in significant hike in the cost of power during the peak of demand (16:00-21:00). The significant effect of primary treatment on reducing the overall power demand in water resource recovery facilities, whose peak coincides with the Duck-Curve and power tariff peaks, placed this process at the center of attention for many recent studies focusing on power demand and cost. In contrast with the previous studies that only reviewed overall power demand optimization, this research effort focuses on the dynamics of power demand optimization for treatment facilities. Our approach elucidates the role of time-dependent power demand on the overall ability to perform treatment and the actual treatment cost and specific carbon emissions. This approach not only amplifies the cost-saving of this optimization due to higher electricity prices during the power demand peak periods, but also relieves the unexpected impacts associated with the Duck-Curve.

A series of dynamic models were developed here to study the effect of different primary treatment technologies on the electricity demand, operating cost, and carbon-footprint of a large water resource recovery facility in California. This comparison demonstrated primary filters or its

combination with the conventional clarifiers as the best option in terms of power, carbon-footprint and cost savings. Despite the different extents of secondary treatment required for these scenarios, activated sludge aeration electricity demand were the dominating electricity consumer. As such, the last three configurations of this facility's activated sludge processes were also compared using the dynamic models developed here to assure that the power, cost, and carbon-footprint reductions demonstrated by some of the primary treatment options here are maximized. This comparison demonstrated that the evolution of the activated sludge in this facility was performed with the goal of lowering its operating cost, electricity demand, and effluent load. However, the current configuration has additional room for energy optimization.

INTRODUCTION

Recent growth and wide use of photovoltaic (PV) electricity generation have been changing the diurnal trend of power demand curves for the electrical grid (i.e., power grid, the grid, and electricity grid), turning it into a duck-shaped curve (i.e. Duck-Curve phenomenon) [1, 2]. The evolution of Duck-Curve phenomenon (D-C) during the past 8 years has been illustrated in Figure 1 below for state of California in the U.S. where penetration of PV electricity has been growing significantly recently. Similar trends are expected to be observed in other states of the U.S. and European Union with adoption of regulations that require significant contribution of renewable (i.e. PV) sources to their total power generation [3, 4, 5, 6].

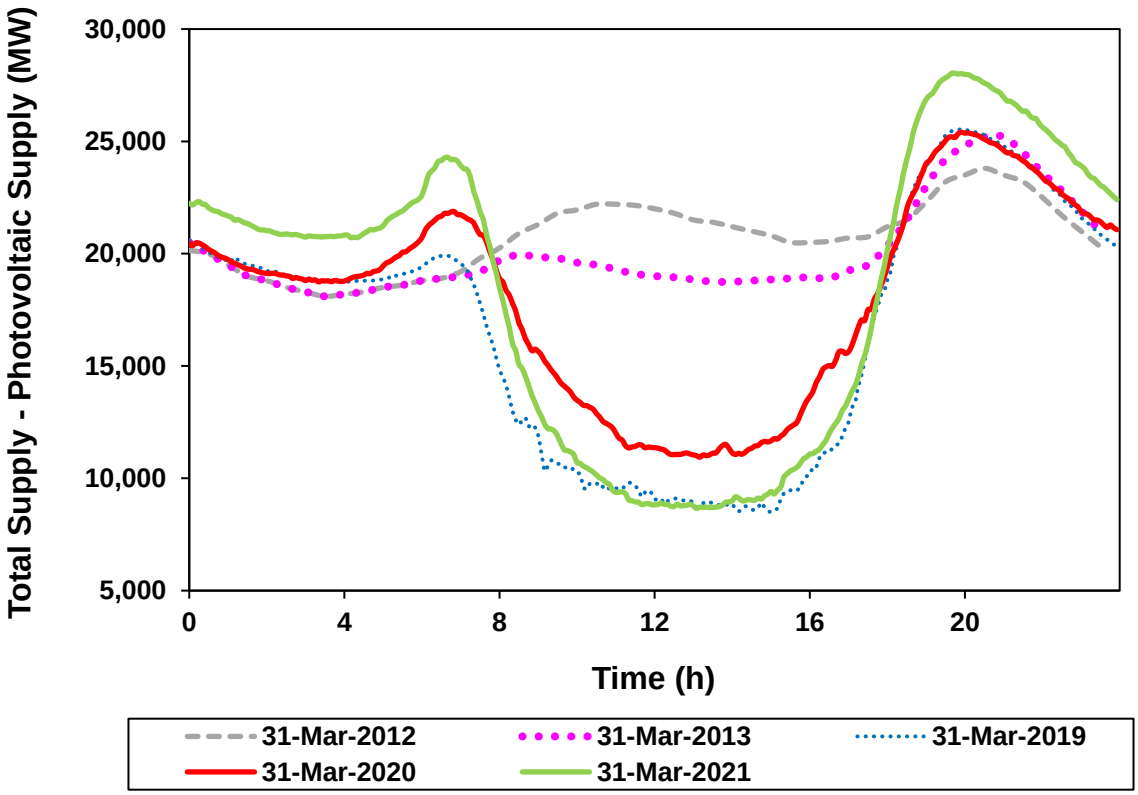

Figure 1. **California Independent System Operator (CAISO) actual and predicted net load (total supply - photovoltaic) curves for March 31, 2012, 2013, and 2019 to 2021. This figure has been generated using the data gathered by CAISO [7, 8].**

The change in the number and duration of diurnal power demand peak illustrated in Figure 1 above has changed the power tariff structure and cost of power and in many cases resulted in significant hike in the cost of power during the new peak of demand (16:00-21:00). The main reason for this cost increase is limited number of power generation sources that can respond to the short yet sharp ramp up period prior to peak of D-C and their higher cost of operation [2, 6]. Examples of few old and new power tariffs for Southern California Edison Company (SCE) have been compared in Figure 9 in the Methods Chapter (Chapter 2) demonstrating this change of electricity tariff structures.

In addition to higher cost, carbon intensity of the grids' electricity (i.e., greenhouse gas emissions produced to generate unit grid electricity in CO_2eq kWh^{-1}) during these peak periods are higher. This is because most of these power generation sources that are widely used during this ramp up periods currently rely on combustion of fossil fuels [2]. Diurnal trend of grid electricity carbon intensity for different months of 2019 demonstrating this phenomenon has been provided in Figure 8 in the Methods Chapter (Chapter 2), which was derived from data obtained from California Independent System Operators (CAISO).

One of the main solutions suggested by many studies for the grid instability and D-C's related shortcomings discussed above is load leveling using electricity storage systems. In other words, storing power during high renewable (i.e., PV) generation or low demand periods, and using it during low renewable production or high demand periods [9, 10, 1, 2, 7]. Recent popularity and advancements of Lithium-Ion (Li-Ion) batteries have encouraged many power providers to invest in load leveling using this type of power storage. However, a recent comprehensive review of current energy/electricity storage technologies by Argyroua, et al., 2018 suggests that Li-Ion battery by its own cannot be a feasible power storage option for load leveling due to its high cost, shorter durability (5-15 year) comparing to other storage options (e.g., decades if not centuries for Pumped Hydro Energy which forms 96% of global power storage), as well as risk of explosion

when over-charged or over-discharged [9]. Other shortcomings of this storage technology includes: limitation of source of critical metals used in its production (Li, Co, and graphite) to only few countries; limitation of its manufacturing technology to only four countries (i.e. China, Japan, United States, and South Korea); its rapidly growing demand in auto industry; and lack of the economically feasible recycling technology or environmental regulation requiring recycling it [11]. As such, more time is needed for Li-Ion batteries to improve and become cost-effective as recent studies suggest.

The other solution to the D-C effect on the power grid, which is more technologically and economically achievable, in absence of cost-effective large-scale batteries, is demand-side energy management strategies [12, 13]. One of these energy management strategies is load leveling or reduction at large sinks of the grid's electricity. This approach relies on reducing these large sinks' power demands during the gird's peak time or shifting it from demand peak periods (16:00 to 21:00 in Figure 1) to the off-peak periods which is the concept behind demand-side flexibility projects [14] in these large sinks. Water resource recovery facilities (WRRFs) are an attractive target for such demand-side flexibility projects [14]. This is because WRRFs require significant amount of electricity to operate due to the large amount of wastewater that they process daily and size of their equipment [15].

In addition to their large power demand, as shown in Figure 2 below and similar to power grid, WRRFs are subject to diurnal cycles and their peak of electricity demand typically coincide with peak of power grid [14]. Therefore, any reduction to their electricity demand during these load peak periods can directly reduce the power gird's peak when cost of power is significantly high. This approach not only alleviate the D-C, but also significantly reduces these facilities' electricity cost. As such, this coincidence of the peaks is another reason that makes WRRFs an attractive target for demand-side flexibility projects.

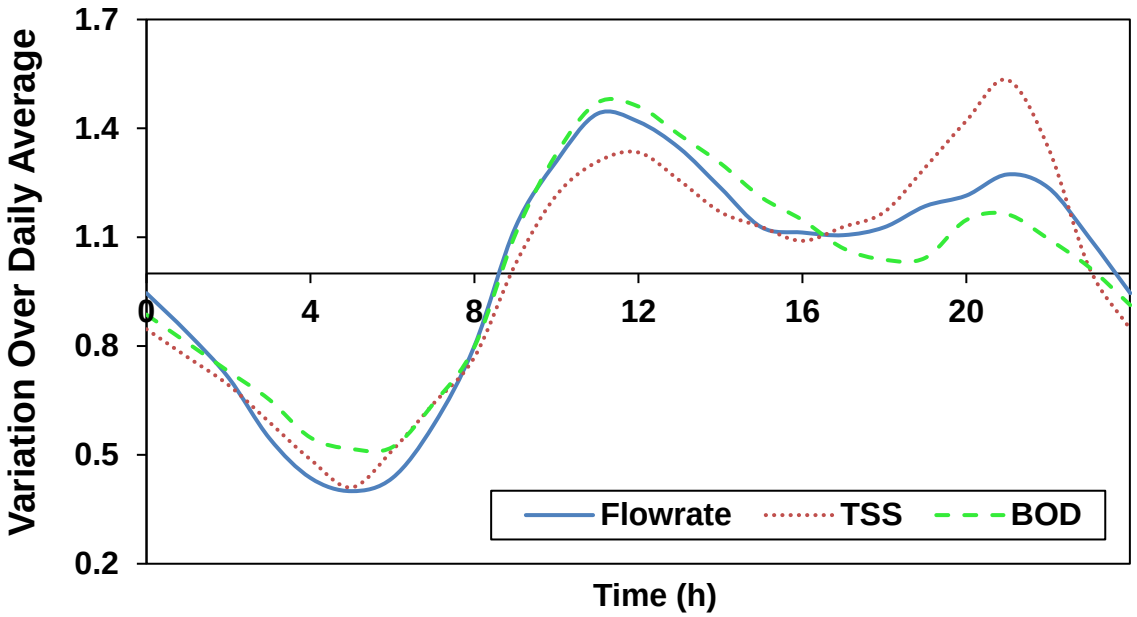

Figure 2. Typical diurnal variations observed in flow, biological oxygen demand (BOD), and total suspended solids (TSS) in domestic wastewater normalized to their average hourly values [16].

Since aeration in the biological treatment is the main contributor to the overall electricity demand at WRRFs by exceeding half of the total treatment process energy requirements [17, 18, 15, 19], reduction in aeration requirements should be the main objective of WRRF's demand-side flexibility projects.

WRRFs aeration requirements are function of the influent chemical oxygen demand (COD). In addition, wastewater contaminants (i.e., surface active agents) and soluble COD (sCOD) concentration are recognized as the main depressants of the oxygen transfer efficiency in aeration tanks. As such, reducing the COD load prior to aeration tank not only reduces the aeration requirement by reducing the influent load, but also by increasing the oxygen transfer efficiency of aeration [17, 18]. This is why the primary treatment (PT) is typically performed prior to biological treatment and aeration in all WRRFs with the exception of very small plants [20, 21] in addition to its effect on reducing the reactor volume in WRRFs' downstream processes.

The effect of PT on WRRFs' aeration and overall power demand whose peak coincides with the peak of D-C and power tariffs have made this process unit the center of attention for many recent studies focusing on WRRFs' power demand and cost optimizations including this research study. In contrast with the previous studies that only reviewed overall power demand optimization using steady state models, this study focuses on dynamics of this power demand optimization in order to develop different methods to concentrate this optimization on the peak of WRRF's power demand. This approach not only amplifies the cost-saving of this optimization due to higher electricity prices during the power demand peak periods, but also alleviates the D-C phenomena and its negative impacts. Therefore, it can be a great example of a demand-side flexibility project at WRRFs.

In this study the effect implementing three advances primary treatment (APT) technologies on electricity demand, operating cost and extent of treatment is assessed for a large WRRF in the state of California. This is accomplished by comparing the results of a fully dynamic model of this plant for each of these APT technologies and comparing it with a scenario where conventional primary treatment is utilized. The details about the model developed for this study and the challenges that had to be coped with to develop this model have been explained in Chapters 2 and 3 respectively. More details about different PT technologies compared in this study have been provided in the Background (Chapter 1) section. Upon comparing the scenarios representing each of the PT technologies, different combinations of two of these APT technologies with conventional PT are reviewed and compared with the other scenarios. This comparison allows the assessment of coupling these APT technologies as demand-side flexibility strategy and electricity load shifting in this large WRRF. This comparison is captured in Chapter 6.

As indicated earlier in this section, the activated sludge aeration is the largest contributor to the facility overall electricity demand; therefore, it needs to be the center of all demand-side flexibility project. Therefore, using the dynamic model developed in this study and the facility

historical data, this study also evaluates the effect of evolution of the secondary treatment activated sludge configurations in this facility and how it has impacted the facility electricity demand, carbon-footprint, and operating cost. This evaluation or comparison consists of binary comparisons of the last three activated sludge configurations at this facility. The latest or current configuration consists of simultaneous use of two different activated sludge configurations which provides the opportunity of defining another new demand-side flexibility project that results in power savings by maximizing the use of the more electricity-efficient of these two configurations. These assessments are discussed in Chapters 4 & 5.

CHAPTER 1: BACKGROUND

Primary treatment (PT) consists of separation and removal of suspended solids and floatables (e.g., fats, grease, oils, plastics, etc.) from wastewater using physical-chemical techniques. GRAVITY Quiescent sedimentation or clarification also referred to as sedimentation tank, clarifier, and settler is the most common form of primary treatment (conventional clarifiers). In recent years, advanced primary treatment (APT) technologies have been emerged which provide higher extent of primary treatment at lower footprint, operational, and maintenance requirements compared to conventional primary clarifiers [20, 22]. In addition to lowering aeration and its power requirements, APTs' higher extent of primary treatment will allow higher capture of primary sludge which is more carbon-rich and highly degradable resulting in higher production of biogas in water resource recovery facilities (WRRFs) that are equipped with anaerobic digesters. Many of these WRRFs use the produced biogas to produce electricity in addition to the thermal energy required to operate their digesters. As such, APTs' higher extent of primary treatment not only reduces the power consumption of the facility by reducing aeration requirement, but also can further reduce WRRFs dependence on grid power by increasing the in-house power generation when digesters and in-house power generation are available. This is another factor that makes PT optimization a more desirable option for grid load leveling/reduction.

Chemically enhanced primary treatment (CEPT), primary filtration (PF) and rotating belt filtration (RBF) or micro-screening which are explained in more details below are three APT technologies that are focused on in this study. It needs to be noted that PF and RBF are also referred to as barrier separations or barrier separation methods through this dissertation which is a general name based on the same separation principles that they utilize.

- **Chemically enhanced primary treatment (CEPT)** is primary sedimentation that is equipped with pre-chemical coagulation and flocculation. Addition of chemicals typically accompanied

with mixing prior to sedimentation of the raw wastewater promotes clumping and agglomeration of fine solids into more settle-able flocs resulting in higher total suspended solids (TSS), chemical oxygen demand (COD), biochemical oxygen demand (BOD), phosphorus, and heavy metals removal in the primary sedimentation. Iron and aluminum salts are typically added as coagulants while anionic polymers are added in the flocculation step to promote floc formation from agglomerated and clumped particles formed in coagulation step [20].

- **Primary filtration (PF)** achieves high primary TSS and organic removal by filtration using a media with a relatively small pore size [e.g., 5 to 10 micrometer (μm) for example in cloth depth filtration] [23, 24]
- **Rotating belt filtration (RBF) or micro-screening** removes solids by a continuous-loop fine mesh belt screen [20].

The extent of removal for primary clarifiers (conventional and chemically enhanced/CEPT) and these two emerging barrier separation technologies have been compared in Table 1 below:

Table 1.Primary treatment technologies performance ranges.

Primary Treatment Process	TSS Removal (%)	COD or BOD_5 Removal (%)	Phosphorus Removal (%)	Reference
Conventional primary clarifier*	25–70	25–40	5–10	[20] [16] [25] [26]
Chemically enhanced primary treatment (CEPT)	60-90	40-70	70-90	[16] [27]
Primary filtration*	60–80	40–60	N/A	[23]
Rotating belt filtration/ Micro-screening*	30–60	25–40	N/A	[28]

* Without chemical enhancement.

In PFs and RBFs, rotational speed during WRRF's hydraulic load peak can be increased to maintain their high solid removals while increase of hydraulic load reduces retention time; therefore, removal efficiency of conventional clarifiers [29]. The main difference between PF and

RBF is their medium pore size, which will influence the treatment performance. Larger pore size in RBFs comparing to PFs results in lowering their treatment removal as illustrated in Table 1; however, it is improved as retained material (especially cellulose) builds up on the screen during filtration, which is referred to as filter cake [30, 31]. The dependence of removal efficiency of conventional clarifiers on hydraulic load can be alleviated by chemically enhancing the extent of the removal in CEPT. As such, the extent of removal in these three APTs in contrast with conventional clarifiers is independent of their hydraulic load. This is one of the key elements that this study will take advantage of in order to optimize the PT and WRRF's power demand.

Many recent studies (inter alia, [32, 23, 24, 22, 33, 21, 29]), reviewed the benefit of additional primary treatment and compared APTs with conventional clarifiers. Gori, et al., 2011 and 2013 demonstrated the significant effect of additional COD removal prior to biological treatment on WRRFs' energy and carbon-footprint reductions [21, 33]. Pasini, et al., 2020 showed limited advantage on operational costs when using primary screening technologies [29]. Caliskaner, et al., 2016, 2017, and 2018 analyzed and demonstrated the benefit of primary filtration in some recent installations in the U.S. [23, 24, 22].

These studies demonstrate the overall cost, carbon-footprint, and energy savings of one of these APTs over their period of studies or on average basis in comparison with conventional clarifiers; however, fail to show their dynamic effects and benefits especially on reducing WRRFs' electricity consumption whose cost and carbon intensity (footprint) are dynamic during the day. In addition, due to use of averaged influent characteristics in steady-estate models, these studies fail to account for the effect of diurnal trends of influent on the removal efficiency; aeration demand and efficiency; energy consumption; and biogas generation of WRRFs' they reviewed especially the ones with conventional clarifiers (their baselines). This is another fact that suggests the need for a dynamic comparison here.

The dynamic analysis in this research effort also reveals the possibility of utilizing barrier separation technologies (PF and RBF) in a WRRF that is originally equipped with only conventional primary clarifiers during the time periods that these technologies outperform conventional clarifiers in order to maximize the removal performance and minimize energy demand and carbon-footprint of the facility (i.e. decoupling the primary treatment performance from hydraulic load). The dependence of conventional primary clarifiers on the hydraulic load is only disadvantageous during the high hydraulic load when clarifier's removal will be minimized; however, as Table 1 suggests the extent of the removal of conventional clarifier can exceeds some of its alternatives'. Thereby, combining two treatment methods can maximize the overall extent of primary separation and its benefits for this facility by increasing the minimum extent of conventional clarifier to the constant and higher removal of barrier separation's during the peak of hydraulic load. Identifying the possibility of this combination approach is another gap that previous studies have failed to address and all they have focused on are comparing a baseline scenario of only conventional primary clarifier with a scenario that fully employs a standalone APT.

The last gap that the review of previously published literature reveals is the lack of critical review or comparison of RBFs and PFs. Despite their different extend of removal which is explained to be due to their different mediums' pour size, and the effect of filter cake formation on improving the removal performance of RBF, no additional performance comparison of these barrier separation technologies has been found in the literature. The table below summarizes the existing literature reviewed as part of this study and highlights the necessity for a more comprehensive analysis of the research gaps explained above:

Table 2. Research gap analysis summary.

SUBJECT MATTER	AVAILABILITY	REFERENCE
Role of Extent of Primary Treatment (Carbon Diversion) on WRRF's Energy Demand, Recovery and Carbon-footprint	Yes	[20] [33] [21] [17] [18] [29]
Primary Treatment Technologies	Yes	[20] [23] [24] [22] [16]
Primary Filtration (PF)	Yes	[20] [32] [23] [24] [22] [30] [31]
Rotating Belt Filters (RBFs) or Micro-screens	Yes	[20] [30] [29] [31]
Significant Effect of Aeration on WRRF's Electricity Demand	Yes	[17] [18] [15] [34] [19]
Dynamic Modeling of Aeration O_2 Transfer	Yes	[17] [18]
Critical Review and Comparison of Primary Filtration and Rotary Belt Filtration or Micro-screening	No	Research gap.
Decoupling the Primary Treatment Removal from Flow	No	Research gap.
Power Load Leveling/Reduction by Combining Use of Conventional Settling and Barrier Separation to Lower WRRFs' Overall Operational Cost and Carbon-footprint	No	Research gap.

Except for the gap for critical review and comparison of PF and RBF other gaps listed in the table above will be addressed in the research study summarized in this dissertation.

CHAPTER 2: METHODS

Current Plant Description

This research study was performed on a large WRRF located in state of California whose current peak of influent flow is 5.30×10^5 m^3 d^{-1} (140 million gallons per day, or MGD). This facility is currently the main facility of a two-plant network that treats on average a combined flow of 7.57×10^5 m^3 d^{-1} (200 MGD). More than half of this network's effluent is utilized for reuse purposes, specifically groundwater recharge and sea-water barrier intrusion, and the remainder is discharged to the Pacific Ocean. At the time of this project, further infrastructural expansion for water reclamation and reuse was already planned for this two-plan network.

Prior to pumping into the ground injection wells for reuse, the effluent of the WRRF studied here goes through microfiltration, reverse-osmosis, and ultraviolet disinfection at a neighboring facility to meet the reuse specifications. As such, this plant's primary treatment goal is the removal of TSS and BOD to prepare the effluent for its downstream microfiltration. Although nitrogen (i.e., ammonia, nitrate, and nitrite) removal is not a concern for this facility, it is performed here to improve secondary solids separation and as an energy-savings measure [35] .

The plant employs chemically enhanced primary treatment (CEPT) using ferric chloride and anionic polymers for its primary treatment stage. On average, about 20% of the primary effluent is sent to the plant's two trickling filters equipped with one clarifier (settling unit) each. The remaining 80% of the primary effluent is distributed between Activated Sludge Unit #1 (AS1) and Activated Sludge Unit #2 (AS2) at a 40/60 ratio, respectively, on average. AS1 configuration is a step-feed Ludzack-Ettinger (L-E) while AS2 is a Modified Ludzack-Ettinger (MLE), each has its own secondary clarifiers network. Figure 3 illustrates the overall process configuration of the current plant.

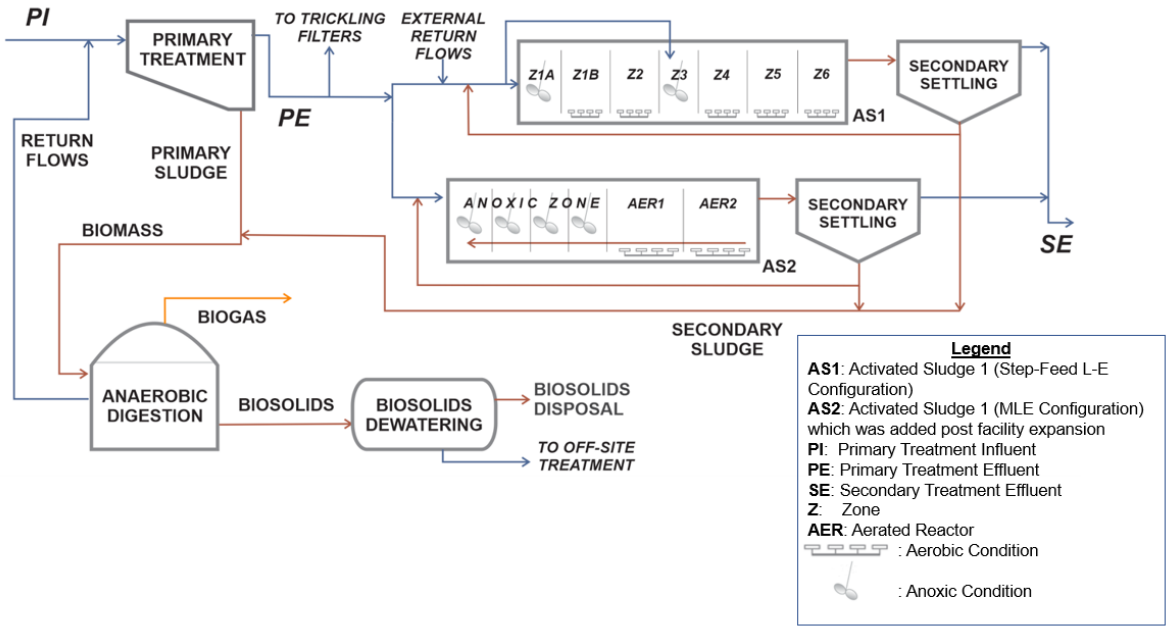

Figure 3. Current plant configuration after the expansion.

In the L-E configuration, the influent, which is the mixture of primary treatment effluent and return sludge from secondary settling, is fed to an anoxic zone and then to an aerobic zone. The nitrate in the return sludge from the secondary settling is consumed as substrate by denitrifying microorganisms in the anoxic zone and is converted to nitrogen gas that is released to the ambient air. The MLE configuration is an improved version of L-E process, achieved by adding internal recirculation to the biomass (i.e., by circulating from the end of the aerated zone back to the anoxic zone). It provides higher extent of nitrification and denitrification, by increasing the amount of nitrate delivered to the anoxic zone and converted to nitrogen gas, which otherwise would be limited to the nitrate in the return sludge [16].

The AS1 in this facility uses the L-E configuration in a step-feed layout where two L-E units are placed in series. About 40 percent of this activated sludge unit's influent is delivered to the anoxic zone of the upstream L-E unit and the remainder 60 percent is mixed with the effluent of the upstream L-E unit in the downstream L-E's anoxic zone. This configuration improves the

nitrogen removal of an individual L-E process as it sends more nitrate to the anoxic zone of the downstream L-E unit. Depending on the internal recycle stream flow in the MLE and the flow distribution in the step-feed L-E configurations, they can achieve total effluent nitrogen less than 10 mg l^{-1}. The step-feed L-E provides higher treatment capacity per tank volume comparing to the MLE. However, the MLE process is expected to provide improved nitrogen removal without adding to the aeration electricity demand as the recirculating stream has already undergone BOD oxidation. The internal recirculation pumps in MLE process have high flow, but very low head, hence its energy requirements are minor when compared to the aeration blowers. The MLE is also less complex to operate comparing to the step-feed [16].

The thickened sludge from primary and secondary treatment units of this plant is digested anaerobically in the plant digesters. The produced biogas in this process is consumed by the facility's cogeneration unit to generate electricity and steam for the plant's operations. This WRRF also imports natural gas and electricity to meet the remainder of its energy requirements. Natural gas supplements biogas for electricity generation, especially during the summer months when grid electricity costs are higher.

A small portion of AS1 effluent is used in the treatment operations for this facility and its adjacent advanced treatment plant. Specifically, it is used for this facility's cogeneration system cooling and the microfiltration backwash process in the adjacent reuse facility. These applications add contaminants to the water; as such, the effluents of these processes need to be returned to AS1 for treatment. The presence of nitrate in AS1 effluent which is retuned to this activated sludge unit through these return streams promotes the nitrogen removal of AS1 (as explained above in the definition of the MLE process in this section). As such, the presence of these return streams in the facility AS1 slightly deviates the operation of AS1 from an only L-E to a de facto Hybrid L-E/MLE.

The current plant's activated sludge configuration, parallel use of step-feed L-E (AS1) and MLE (AS2) configuration, described in this section is result of an expansion project that added AS2 to the plant existing step-feed L-E. Prior to this expansion project the activated sludge section of this plant went through another major configuration changes and that was conversion of the AS1 from carbon-oxidizing or plug-flow to nitrogen removing step-feed configuration. The dynamic models to portray these two old configurations can be simply developed by making slight changes to the current plant's. As such, the effect of these activated sludge configuration changes on the plant extent of treatment, electricity demand, and operating cost are also studied as the secondary goal of this study. The results of these comparison also illustrates whether these configuration changes can be qualified as demand-side flexibility project for the facilities that are still using these old configurations. These old configurations are further explained in the next section of this chapter.

Current Plant Preceding Activated Sludge Configurations

I. Old Plant with Step-Feed Activated Sludge

This activated sludge configuration was employed at this facility before the current plant's. The old step-feed plant scenario can be simply described as the current plant without the AS2 or MLE activated sludge configuration in Figure 3. In other words, the expansion project resulting in the current plant plant's configuration, added AS2 (i.e., MLE configuration) to the plant's existing activated sludge unit (i.e., AS1) that utilized step-feed L-E configuration. As such, prior to the plant expansion, the entire primary effluent minus the constant portion that was sent to the trickling filters would be treated in the AS1 or step-feed L-E process. Without the AS2, the pre-expansion facility had a lower treatment capacity with the peak of influent flow of about 3.79×10^5 m^3 d^{-1} (100 MGD). The two-plant network would however treat the same average combined flow of 7.57×10^5 m^3 d^{-1} (200 MGD).

II. Old Plant with Plug-Flow Activated Sludge

Old carbon-oxidizing or plug-flow plant utilized the same activated sludge basins as the old step-feed. However, in this configuration the entire influent of the activated sludge goes through all the basins as opposed to being split up between the first and the third basins as demonstrated in Figure 3. All the activated sludge basins in this configuration are aerated as such no denitrification is performed in this configuration. In addition, lower sludge retention time of the activated sludge unit in this configuration does not allow oxidation of the ammonia to nitrite (nitrification). This is why this configuration is called carbon-oxidizing. The operating capacity of this configuration is close to the capacity of old step-feed configuration that superseded this configuration. Figure 4 compares these two old, activated sludge configurations.

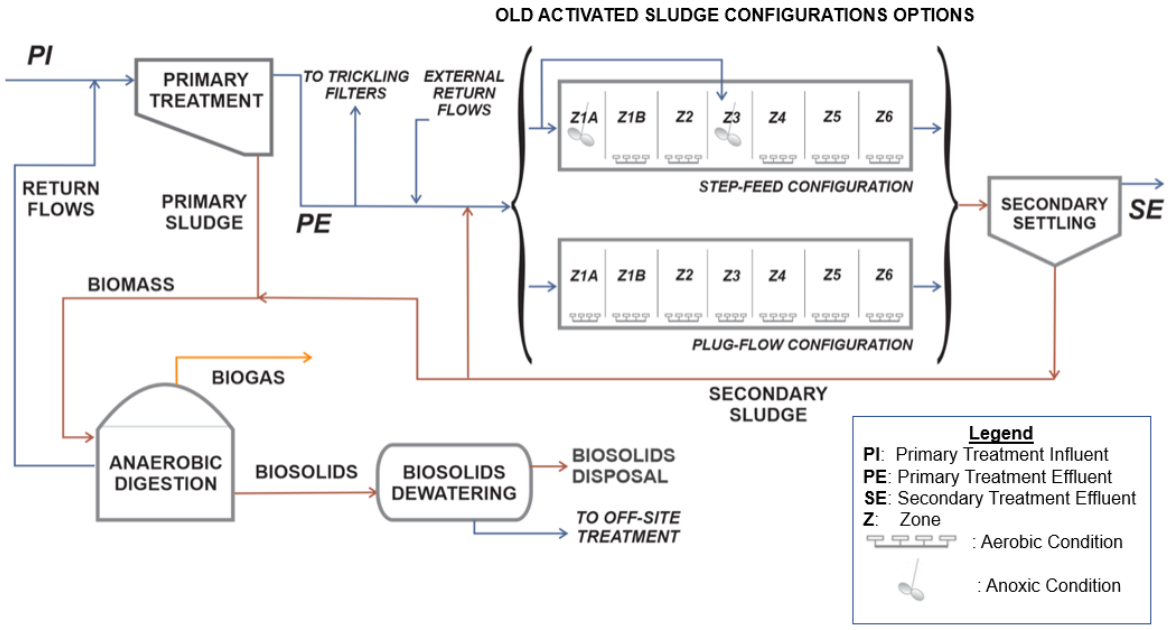

Figure 4. Plant activated sludge old configurations.

The process equipment details such as total equipment count, count of units in service for each of the configurations explained above, dimensions and other required process information for this modelling effort have been listed in Appendix B.

Modelling Tool and Protocol

To perform this dynamic modelling effort, BioWin 6.1 (EnviroSim; Hamilton, ON) was utilized using the Good Modelling Practice Protocol [36]. The monthly average process data from the facility was utilized for calibration and validation. Specifically, October through December 2018 monthly data were used for calibration, and January through September 2019 data was used for validation. Dynamic hourly influent flow and constituents' hourly trends were derived from these monthly averages as descried in more details in the next few sections of this chapter. Default values in the simulation software [37] were also utilized in developing the models in this study unless otherwise described.

In addition to modelling the treatment processes, electricity demand was also quantified for main equipment units (e.g., pumps and blowers) in this effort. The additional electricity demand for the unit operations not available in the process simulation software (e.g., minor process pumping, odor control, process control equipment, etc.) was quantified by subtracting the power demand of the calibrated model from the total power demand from the field data. This additional electricity demand was entered into the simulation as a ratio of this difference to the plant total influent flow. The supplemental natural gas consumed for power generation was also accounted for. The plant blowers, plus the cogeneration power and thermal energy efficiencies were also calibrated using field data.

The trickling filters were excluded from the dynamic model to increase computational efficiency and speed of simulations because they received a constant aliquot of primary effluent, with the dynamic portion of the flow going to the activated sludge units. However, the trickling filters' electricity demand was entered into the model to estimate their contribution to the plant's total power demand. This was achieved by entering the electricity demand rating of these process units per their unit influent flow into the simulation. The effluent of the trickling filters is mixed with the effluent of AS1 and AS2 effluents and the mixed effluent is delivered to the neighboring facility

for further treatment. The effluent characteristics of the trickling filters were assumed to be the same as for the activated sludge units for this research study.

Each of this facility's treatment processes consist of multiple identical units (e.g., AS basins, clarifiers). The total count and count the in-service equipment ere summarized in Appendix B. Simulating all these active, identical, repetitive equipment slows down the simulations. It is common practice to simplify the modelling, by treating the plant as the single smallest functional unit that could be scaled back to the plant total using a constant multiplication. Therefore, the entire plant was divided into 6 identical trains and only one of these was simulated using one sixth of the plant influent flow to optimize the simulation's run time. As indicated before, this approach is common for efficient modelling of processes with redundancies such as WRRFs. The numbers of trains selected for this modeling effort is the smallest set of identical process units that this facility could be reduced to. The results of the single-line simulations were subsequently scaled up to the total by multiplying the results times 6 (i.e., the total number of trains).

Influent and Temperature Profiles

To perform the dynamic simulation, hourly influent profiles including at least flow, COD, and total Kjeldahl nitrogen (TKN) concentration are required. The data collection system at this plant only records monthly averages. However, the plant hourly influent flow data for one month immediately preceding the study period here which was recorded for a different project at the facility could be also provided. This hourly flow data was utilized to calculate an average daily flow and then average instantaneous (hourly) to average daily flowrate ratio (or hourly flow-factors) for each hour of the day. The average and standard deviation of these flow-factors calculated for each hour of the day, for all days of the month when data was available is illustrated in the Figure 5.

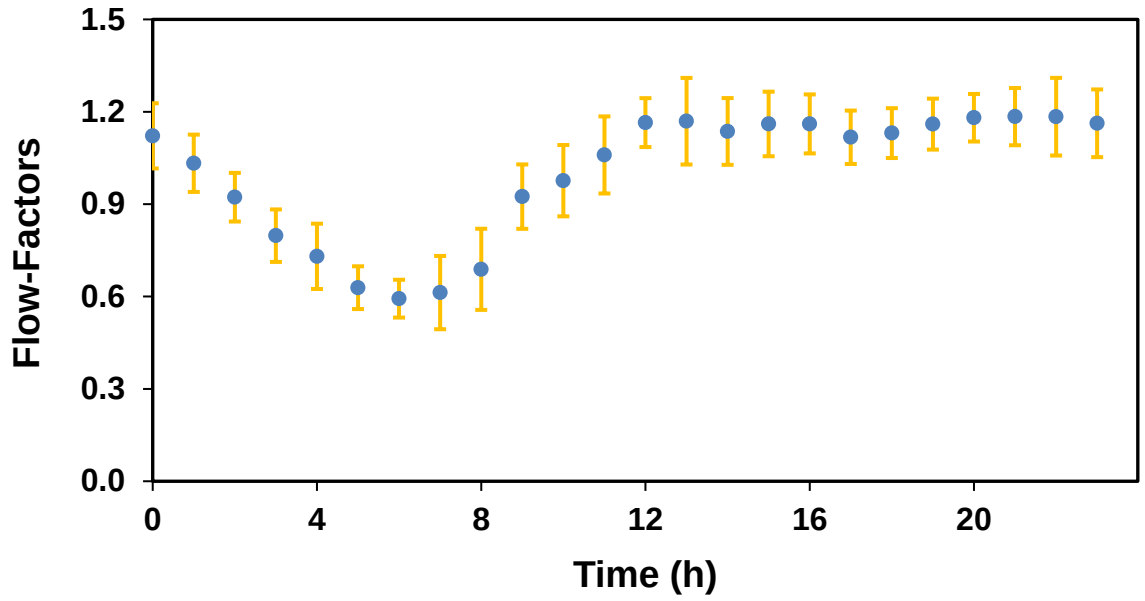

Figure 5. Statistical analysis of hourly flow-factors demonstrating the average (blue dots) and standard deviation (orange error bar) values for each hour of the day, for all days of the month when data was available (September 2018).

These average instantaneous ratios were then applied to each average monthly influent entity to develop hourly profiles for each hour of the day in that month upon consulting and confirming with the plant personnel and in the absence of hourly concentration data.

Figure 6 demonstrates the hourly influent flow and concentration profiles derived for the twelve months study period in this study. These hourly profiles were also used to perform the final calibration of the model after calibrating it with monthly averages. In the absence of field COD data sets, the facility typical Carbonaceous BOD (CBOD) to COD ratio (0.38) provided by the plant engineers was used to prepare COD data from CBOD field measurements.

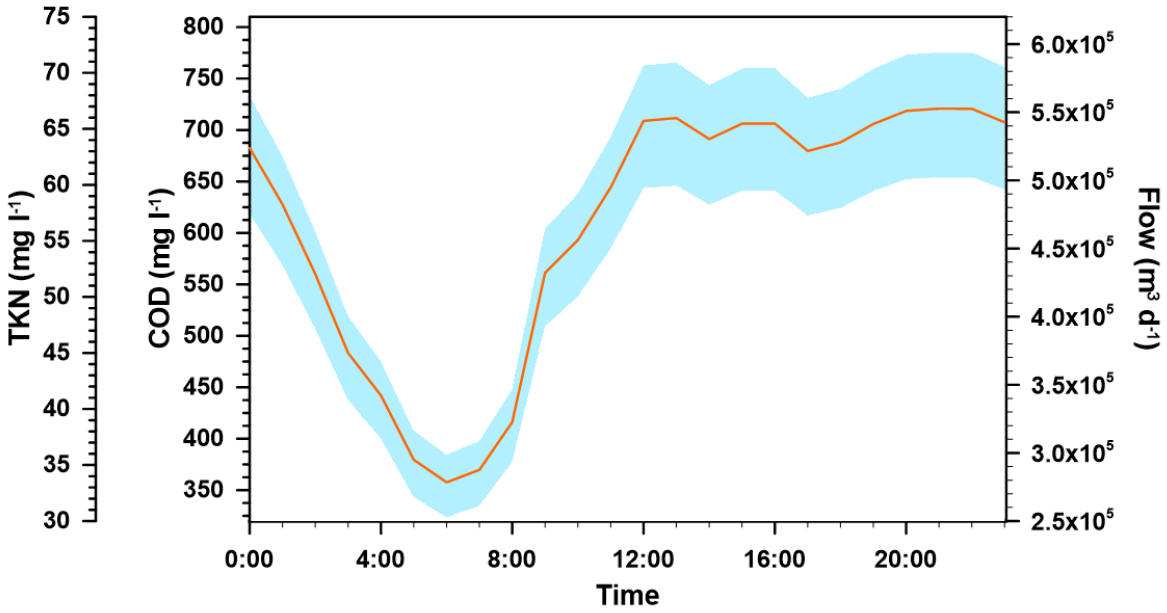

Figure 6. Current plant influent dynamic trends for October 2018 through September 2019 derived from monthly averages multiplied by an hourly flow-factor based on the ratio of instantaneous to average monthly flows. All three Y-axis apply to the data points plotted. Shaded in blue is the range of the entities shown on each Y-axis during this 12-month period and the red line represents their hourly averages over one year.

The current plant influent dynamic trends in Figure 6 were used to model the current plant configuration. However, to model the old plant scenarios (i.e., old plant with step-feed AS and old plant with plug-flow AS) the dynamic flow trend in Figure 6 was adjusted to account for the lower treatment capacity and influent flow of these old plant scenarios (74.97% and 73.85% of the current plant's respectively). These old plant scenarios' average influent flow rates were back-calculated from the average activated sludge process' total influent flow and hydraulic retention time (HRT) data collected during field-testing campaigns at the old plant with the goal of measuring its AS's oxygen transfer efficiency in process conditions for each of these old activated sludge configurations. In this back-calculation, the trickling filters' average influent flow at the old plant was assumed to be the same as the current plant's.

Temperature effects on process physical-chemical and biokinetics constants are well documented and temperature-based calibrations have been extensively used in the past [36]. As

such, temperature dynamics were also incorporated here in addition to the dynamic influent concentrations, by using average daily ambient temperature data for October 2018 through September 2019 from the weather station closest to this facility [38]. The wastewater temperature in this collection area spans between maximum and minimum temperatures of 30°C and 20°C, occurring in September and March, respectively. Therefore, the wastewater temperature was varied over the yearly cycle using a sinusoid with a 12-month period, average of 25^{o}C, amplitude determined by the temperature variation, and peak on the nineth month of the year.

Oxygen Transfer Efficiency and Alpha Factor

A field-testing campaign was carried out to measure in situ the oxygen transfer efficiency in process conditions (OTE, %). The OTE is the ratio of mass of oxygen transferred to the water over the mass of oxygen fed to the water through the compressed air line. In practical terms, the OTE represents the efficiency of the aeration process. We measured OTE using the off-gas method following the American Society of Civil Engineers (ASCE) testing protocol [39]. The field water temperature and dissolved oxygen measurements were used to correct OTE to standard conditions in wastewater (alpha × SOTE, %). Utilizing oxygen transfer efficiency data in clean water, from the air diffusers manufacturer, a posteriori alpha factor was calculated which is the ratio of the oxygen transfer rate in process water to that in clean water. The alpha factor is used for calculating aeration electricity demand and represents the effects of wastewater pollutants on oxygen transfer efficiency [40].

To model the activated sludge basins dynamically, a dynamic alpha trend for each aerated basin was required. Although the simulation software used here did not provide for a dynamic alpha, it allowed the user to enter a time-dependent alpha diurnal schedule for each aerated reactor. The result of off-gas testing on AS1 was used for modelling AS1 for all the current and old plant scenarios. Since no alpha data was available for AS2 in the current plant, the alpha

values of AS2 were estimated matching the calculated DO with field data during the calibration period. The field alpha values used for the simulation of AS1 and AS2 are presented in Table 3.

Table 3. Field alpha factors used to simulate the aeration dynamics in all the activated sludge reactors configurations in this study. The alpha factor is not defined for anoxic zones.

Current Plant (Activated Sludge 1)							
Zone:	**Zone 1A**	**Zone 1B**	**Zone 2**	**Zone 3**	**Zone 4**	**Zone 5**	**Zone 6**
Max	Anoxic	0.66	0.79	Anoxic	0.91	0.94	0.75
Min	Anoxic	0.37	0.66	Anoxic	0.55	0.62	0.65
Average	**N/D**	**0.48**	**0.74**	**N/D**	**0.69**	**0.83**	**0.71**
Old Plant with Step-Feed							
Zone:	**Zone 1A**	**Zone 1B**	**Zone 2**	**Zone 3**	**Zone 4**	**Zone 5**	**Zone 6**
Max	Anoxic	0.66	0.79	Anoxic	0.91	0.94	0.75
Min	Anoxic	0.37	0.66	Anoxic	0.55	0.62	0.65
Average	**N/D**	**0.48**	**0.74**	**Anoxic**	**0.69**	**0.83**	**0.71**
Old Plant with Plug-Flow							
Zone:	**Zone 1A**	**Zone 1B**	**Zone 2**	**Zone 3**	**Zone 4**	**Zone 5**	**Zone 6**
Max	0.3	0.30	0.30	0.26	0.28	0.29	0.27
Min	0.23	0.23	0.28	0.24	0.25	0.25	0.26
Average	**0.26**	**0.26**	**0.29**	**0.25**	**0.26**	**0.28**	**0.27**

Current Plant (Activated Sludge 2)			
Zone:	**Anoxic Zone**	**Aerobic Zone 1**	**Aerobic Zone 2**
Max	Anoxic	0.59	0.82
Min	Anoxic	0.33	0.50
Average	**N/D**	**0.43**	**0.62**

Similar to the plant influent data, dynamic alpha trends needed to be derived from this field data. This was achieved by using the dynamic alpha equation from Jiang, Garrido-Baserba et al. (2017) for each aeration basin, where alpha is a function of the applied COD [17]. Equation 1 demonstrates this dynamic alpha equation:

$$\mathbf{Ln}\,(\boldsymbol{\alpha}) = -\mathbf{1.82} \times \mathbf{10^{-3}} \times \mathbf{sCOD} - \mathbf{0.213} \qquad (\mathbf{Equation\ 1})$$

Where **α** or **alpha** is unit-less ratio of the oxygen transfer rate in process water to that in clean water (αSOTE/SOTE), and **sCOD** is concentration soluble chemical oxygen demand in the plant influent in (mg l^{-1}).

The dynamic alpha trends generated using Jiang and Garrido-Baserba equation then was applied to the average field data in Table 3 using Equation 2, developed for this study, to create a dynamic alpha trend from this field data

$$\alpha_{\text{Dyn for Hour i}}|_{\text{Areation Tank j}} =$$

$$\left[\alpha_{\text{Field-Ave}} + \frac{\alpha_{\text{J-G for Hour i}} - \alpha_{\text{J-G Houly Ave}}}{\frac{\alpha_{\text{J-G Houly Max}} - \alpha_{\text{J-G Houly Min}}}{2}} \times \frac{\alpha_{\text{Field Max}} - \alpha_{\text{Field Min}}}{2}\right]|_{\text{Areation Tank j}} \qquad \textbf{(Equation 2)}$$

Where **i** is hour of the year (0 to 8759), **j** is the aeration tanks number/identifier, $\alpha_{\text{Dyn for Hour i}}|_{\text{Aeration Tank J}}$ is dynamic α for hour i in tank j, $\alpha_{\text{Field-Ave}}$ is the average **α** from field data for the aeration tank j, $\alpha_{\text{J-G for Hour i}}$ is calculated α from sCOD calculated in the simulation for tank j in hour i using J-G equation, $\alpha_{\text{J-G Hourly Ave}}$ is average of all $\alpha_{\text{J-G for Hour i}}|_{\text{i=0 to 8759}}$ for tank j, $\alpha_{\text{J-G Hourly Max}}$ is maximum of all $\alpha_{\text{J-G for Hour i}}|_{\text{i=0 to 8759}}$ for tank j, $\alpha_{\text{J-G Hourly Min}}$ is minimum of all $\alpha_{\text{J-G for Hour i}}|_{\text{i=0 to 8759}}$ for tank j, and $\alpha_{\text{Field Max}}$ and $\alpha_{\text{Field Min}}$ are maximum and minimum α values from the field data respectively for tank j.

The dynamic alpha values from Equation 2 above are derived from direct field data that was already impacted by diffusers' fouling. Thus, all of the references to alpha in this study already accounted for fouling and no fouling factor needed to be applied in all the calculations that these alpha values were used for. Since sCOD and alpha are dependent, a series of trial-and-error iterations need to be performed using the result of the simulation to determine the values of corresponding sCOD and alpha in the dynamic alpha calculations explained above. These iterations are illustrated in the flowchart portrayed in Figure 7.

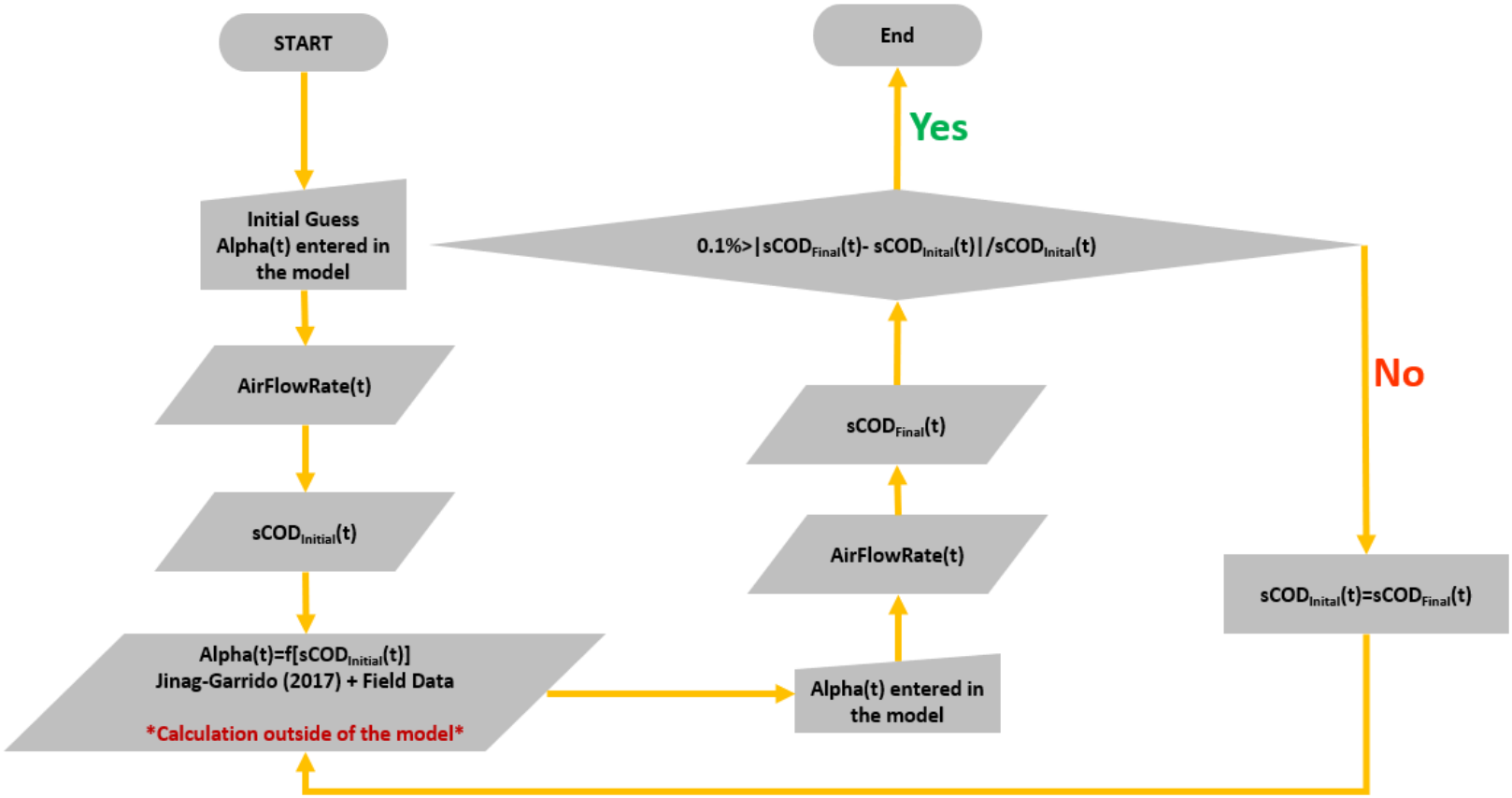

Figure 7. Dynamic alpha factor calculation flowchart.

Energy Calculation Parameters

The natural gas caloric value used for fuel demand calculations in the simulation software was set to be the same as the default high heat value in the greenhouse gas (GHG) combustion emission calculation protocol by the U.S. EPA, which is also used for GHG emission calculations in this study [41]. The simulation software default biogas calorific values were used for calculating the energy generation (electrical and thermal) from the combustion of biogas. The electricity and thermal energy generation quantification was performed in the simulation software using the cogeneration efficiency and energy usage specification provided by the facility or calculated using the facility energy usage data. The facility electricity demand was also calculated in the simulation software using the process units' electricity demand ratings and blower efficiency entered into the software. These ratings and efficiency entries either were derived from the field data as part of the current plant model calibration or obtained from literature research. The blower or aeration power demand was calculated in the simulation software based on the software calculated airflow demand. In addition to blower efficiency, air diffusers specifications and dynamic ambient air temperature profiles entered by the user in the simulation software were utilized for aeration electricity demand calculations. All the parameters entered into the simulation software for energy calculations are listed in Appendix B.

Greenhouse Gas Emissions Calculation Parameters

To estimate the greenhouse gas (GHG) emissions associated with the electricity imported from the grid, the dynamic hourly average carbon intensity for the grid's electricity was calculated from the data obtained from the California Independent System Operators (CAISO) [8] for each month of the year. These calculations were described in more details in the next section of this chapter. In addition to electricity importation (indirect GHG emissions), the direct GHG emissions associated with combustion of biogas and natural gas; CO_2, N_2O, and CH_4 emissions associated with activated sludge biological treatment; CO_2 emission associated with sludge digestion; and

CH_4 from biogas fugitive leaks were calculated and accounted for in assessing each scenarios' carbon-footprint. No other source of GHG emissions was accounted for in this study.

Emission factors obtained from the U.S. EPA GHG combustion emission calculation protocol [41] were used to calculate the biogas and natural gas combustion emissions. This calculation was performed outside of the simulation software and in a Microsoft Excel spreadsheet using the biogas and natural usages calculated by the simulation software. GHG emissions associated with the activated sludge and anaerobic digestion proceses were calculated in the simulation software using its default parameters. Fugitive methane emission associated with biogas leak was assumed to be 1% of the total methane generation in the digesters. The total GHG emission was then calculated and reported in CO_2eq units by multiplying each GHG mass flow times their respective global warming potential obtained from U.S. EPA GHG emission calculation protocol [42].

Due to the renewable nature of biogas fuel and natural occurrence of oxidation performed in the activated sludge and digester units in the nature (i.e., biogenic nature), the GHG emissions from these sources are not considered as concerning GHG emissions that need to be capped and reduced by many carbon-footprint reduction regulation. California air Resources Board Cap and Trade regulation is an example of such regulations or protocols [43]. As such, anthropogenic GHG emissions is defined in this chapter as total GHG excluding biogenic (i.e., non-anthropogenic) emissions to only present the portion of these emissions that is the concern of these environmental regulations. CO_2 portion of biogas combustion emissions is an example of this biogenic category per California air Resources Board Cap and Trade regulation [43]. Since the influent to the WRRF may contain traces of fossil fuel-based organics, not all the biological process emissions can be assumed to be biogenic, and a portion of these emissions should be accounted toward the anthropogenic GHG here. According to the data gathered by Tseng, et al., (2016), 87.18% of the biological process emissions in the activated sludge unit and all the CO_2

emission in the digesters on average can be assumed to be biogenic at this facility [44]. In other words, 12.82% of the activated sludge process emissions needs to be accounted for toward the anthropogenic emissions. As such, the anthropogenic emissions are quantified by subtracting these three biogenic categories from total GHG emission when this category of GHG emissions is of an interested in the assessments performed in this dissertation.

Grid Electricity CO_2 Intensity

To obtain dynamic hourly average CO_2 intensity for unit of grid's electricity, total electricity supply and total grid's CO_2 emission data were obtained from the California Independent System Operator's (CAISO's) website [8] for each month of the year. With California's different regulations targeting zero-carbon electricity by 2045 [45], the grid's CO_2 emissions in this state were expected to have a different trend every year and to descend toward zero by 2045. Therefore, the most recent grid power supply and emission data needed to be extracted for the most accurate representation of the grid's carbon intensity calculations. However, with the start of the COVID-19 pandemic and the stay-at-home order in the beginning of 2020, the grid electricity demand and emission data for 2020 and 2021 could not be a trustworthy representation of the grid's normal dynamics. This could be explained by the increase in residential power usage and decrease in industrial power usage across the state during this pandemic and the stay-at-home order. As such, for the purpose of this study, 2019 grid power supply and emission data were extracted from the CAISO website as the most recent yet representative available data and used to develop average hourly grid power CO_2 intensity values needed for this dynamic modelling effort.

When accessed in 2020 and 2021, the CAISO website had individual daily data sets of 5-minute intervals for each power supply type (e.g., renewables, natural gas, large hydro, imports, batteries, nuclear, etc) and total grid's CO_2 which could only be extracted separately and for a single day at a time. As such, extracting this data would require tremendous amount of time if all of the 2019 data needed to be extracted and used to develop the grid dynamic CO_2 intensity

profile. This data then needed to be carefully reviewed and adjusted for outlier days when the grid power trends had been impacted by extreme weather conditions and other causes which would amplify this significant effort. Examples of such other causes are gusty winds and fires leading to intentional or unintentional grid service interruptions which are common in California especially in recent years as the state has been dealing with extreme drought and fire conditions. As such, a subset of more representative data for one third of the days in each month was selected in this study to simplify the detection and elimination of outlier days and to reduce the extent of effort required for CAISO data extraction.

Ambient temperature was used here to determine extreme weather conditions and eliminate the biased and outlier historical grid data associated with them. An example of such an extreme condition is a hot day in the middle of the cold season resulting in abnormally high grid power demand due to increase in the use of commercial and residential air conditioning units. This biased data elimination was performed by selecting one third of the days in each month that had the closest daily average temperature to the monthly average. These selected days were subsequently verified against the CAISO website grid data not to include days with any abnormal power interruptions. If they did, that day would be replaced by the next day with the closest daily average temperature to the monthly average outside of the domain of days selected in the first step. Ambient average daily temperatures from the closest weather station to the WRRF studied here in 2019 were extracted for this purpose [38]. The approach explained above translated into selecting days with average temperatures within ±1.5 to ±3% of each month's average monthly temperature in 2019.

The average grid CO_2 intensity for each hour of every month was calculated then using the data extracted from CAISO website for the selected one third of the days in each month. First, the average total grid CO_2 emission value is divided by the average total electricity supply for the corresponding 5-minute interval CAISO data for these selected days of each month.

Subsequently, these calculated average intensities of the 5-minute intervals within each hour are averaged to form the average intensity of that hour for a typical day of each month.

The calculated average hourly CO_2 intensity trends for each month of 2019 that were used for the dynamic modelling in this study were illustrated in Figure 8. This figure clearly presents the Duck-Curve phenomenon explained in the Introduction section of this article and the impact of the increase in solar power generation in CAISO grid's carbon intensity (i.e., significantly dropping it during the daylight: 9:00 through 16:00). It also demonstrates the coincidence of maximum grid's CO_2 emission intensity with this plant's peak of influent flow and constituent concentrations presented in Figure 6.

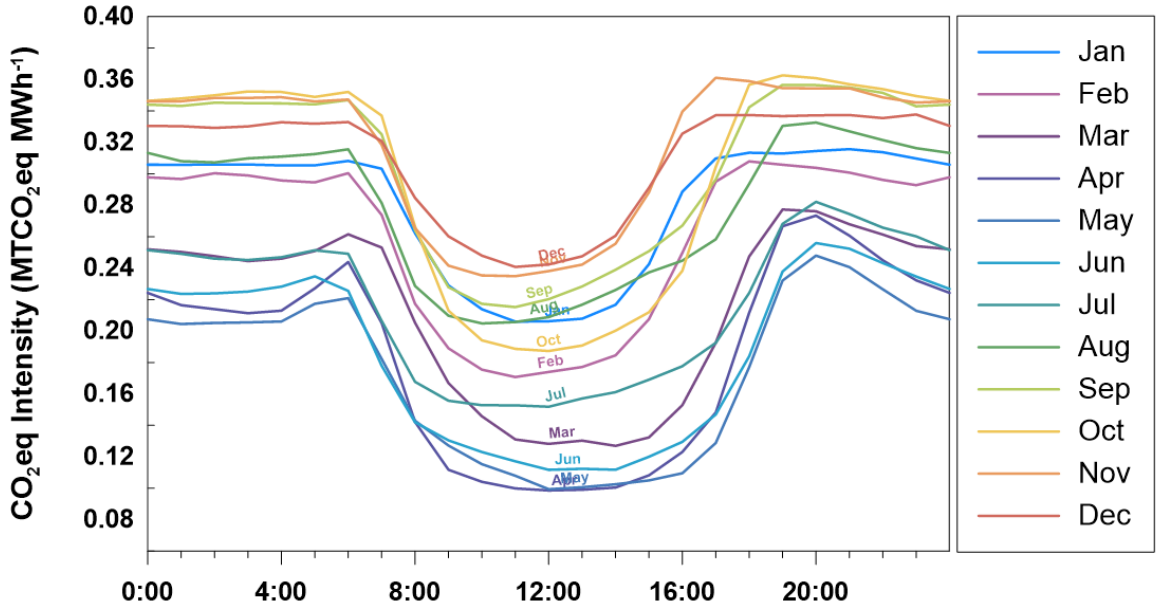

Figure 8. CAISO grid average hourly CO_2eq intensity diagram for each month of 2019.

The calculated CO_2eq intensity values illustrated in Figure 8 above have been also included in Table 4 as a useful resource for similar dynamic modelling effort for WRRFs in the CAISO jurisdiction, which covers great portion of state of California.

Table 4. Calculated CAISO grid hourly average CO_2eq intensity values for each month and entire 2019.

Average CO_2 Intensity for Total Electricity Demand ($MTCO_2eq\ MWh^{-1}$) for Each Month of 2019													
Hour	**January**	**February**	**March**	**April**	**May**	**June**	**July**	**August**	**September**	**October**	**November**	**December**	**Annual Average**
0	0.3058	0.2978	0.2520	0.2242	0.2075	0.2267	0.2514	0.3133	0.3440	0.3464	0.3461	0.3305	0.2872
1	0.3057	0.2967	0.2503	0.2165	0.2045	0.2236	0.2491	0.3080	0.3432	0.3479	0.3461	0.3303	0.2852
2	0.3060	0.3004	0.2476	0.2139	0.2051	0.2240	0.2460	0.3073	0.3453	0.3500	0.3483	0.3292	0.2852
3	0.3059	0.2989	0.2445	0.2113	0.2055	0.2251	0.2452	0.3098	0.3449	0.3524	0.3483	0.3301	0.2852
4	0.3053	0.2958	0.2460	0.2129	0.2061	0.2282	0.2470	0.3110	0.3448	0.3521	0.3487	0.3328	0.2859
5	0.3054	0.2945	0.2509	0.2271	0.2173	0.2348	0.2514	0.3126	0.3442	0.3489	0.3460	0.3319	0.2887
6	0.3082	0.3004	0.2616	0.2439	0.2209	0.2255	0.2492	0.3156	0.3469	0.3521	0.3473	0.3329	0.2920
7	0.3032	0.2739	0.2531	0.2051	0.1823	0.1779	0.2065	0.2815	0.3251	0.3370	0.3185	0.3209	0.2654
8	0.2622	0.2173	0.2053	0.1422	0.1429	0.1420	0.1677	0.2286	0.2641	0.2664	0.2654	0.2847	0.2157
9	0.2290	0.1890	0.1669	0.1118	0.1272	0.1305	0.1557	0.2098	0.2279	0.2130	0.2416	0.2602	0.1885
10	0.2139	0.1754	0.1458	0.1041	0.1153	0.1231	0.1528	0.2048	0.2173	0.1941	0.2354	0.2480	0.1775
11	0.2060	0.1707	0.1311	0.0999	0.1080	0.1172	0.1528	0.2057	0.2152	0.1887	0.2349	0.2408	0.1726
12	0.2062	0.1740	0.1282	0.0986	0.0994	0.1117	0.1519	0.2088	0.2203	0.1873	0.2381	0.2423	0.1722
13	0.2078	0.1771	0.1303	0.0991	0.1007	0.1124	0.1571	0.2168	0.2284	0.1908	0.2422	0.2475	0.1758
14	0.2167	0.1845	0.1270	0.1004	0.1025	0.1118	0.1611	0.2261	0.2390	0.2002	0.2555	0.2606	0.1821
15	0.2425	0.2075	0.1323	0.1082	0.1050	0.1200	0.1691	0.2373	0.2508	0.2119	0.2882	0.2911	0.1970
16	0.2886	0.2497	0.1529	0.1231	0.1096	0.1295	0.1776	0.2448	0.2671	0.2383	0.3396	0.3255	0.2205
17	0.3098	0.2950	0.1926	0.1482	0.1288	0.1469	0.1925	0.2583	0.2964	0.3044	0.3611	0.3373	0.2476
18	0.3134	0.3079	0.2474	0.2116	0.1770	0.1839	0.2242	0.2936	0.3423	0.3567	0.3589	0.3374	0.2795
19	0.3129	0.3058	0.2773	0.2667	0.2321	0.2378	0.2682	0.3305	0.3566	0.3626	0.3545	0.3367	0.3035
20	0.3145	0.3038	0.2762	0.2734	0.2480	0.2560	0.2822	0.3326	0.3564	0.3609	0.3544	0.3372	0.3080
21	0.3157	0.3008	0.2679	0.2607	0.2407	0.2524	0.2744	0.3270	0.3549	0.3569	0.3544	0.3374	0.3036
22	0.3137	0.2961	0.2614	0.2450	0.2266	0.2432	0.2657	0.3215	0.3515	0.3539	0.3486	0.3354	0.2969
23	0.3097	0.2928	0.2540	0.2322	0.2129	0.2346	0.2602	0.3163	0.3429	0.3494	0.3453	0.3377	0.2907
Average	**0.2795**	**0.2586**	**0.2126**	**0.1825**	**0.1719**	**0.1841**	**0.2150**	**0.2759**	**0.3029**	**0.2968**	**0.3153**	**0.3083**	**0.2503**

Operating Cost

The overall operating cost of the plant in this study was calculated by summing up the costs of chemicals used to enhance the primary treatment (for scenarios with CEPT only), chemical additives used for primary and secondary sludge thickening and dewatering, sludge disposal, natural gas, and electricity imports.

The costs of chemicals used for the treatment processes that are accounted for in this study's operating cost assessments were calculated using the simulation software defaults [37] except for the anionic polymers used for chemically enhanced primary treatment (CEPT) whose cost (32.13 USD per 1000 m^3 of primary treatment influent) was obtained from the chemical provider (NSF Polydyne Inc.; Riceboro, GA). As mentioned before, only the cost of ferric chloride and anionic polymers used for primary treatment enhancement as well as chemical additives used in sludge dewatering and thickening processes were accounted for in this study. To calculate the sludge disposal cost the simulation software's default cost option for dry sludge disposal (cost per unit mass of TSS) was used [37]. Natural gas imports cost was also estimated using this software's default price factor [37].

The cost of power imported from the grid was calculated using Southern California Edison's (SCE's) Time-of-Use tariffs provided in the cost schedules TOU-8-S and TOU-8-RTP-S [46]. These price schedules are for facilities with electricity demand higher than 500 kW and in-house electricity generation capabilities which was determined to be the most representative tariffs for this WRRF comparing to other available price schedules on SCE's website at the time of this study. Metering, energy usage (delivery and generation), as well as fixed and time-dependent demand charges from these tariff schedules were used to calculate the cost of imported electricity for all the simulation scenarios studied here. Other charges such as voltage discount and power factors adjustment were not used as they were not applicable to this facility

or the necessary data for calculating them (i.e., kVAR) could not be produced in this modelling effort.

TOU-8-RTP-S provides real time hourly pricing for the energy usage charges while TOU-8-S offers constant pricing for each time-of-use periods (e.g., on-peak, off-peak, mid-peak, etc). These fee schedules also provide different pricing based on the voltage range at which the electricity is delivered (i.e., below 2kV, from 2kV to 50 kV, and above 50 kV). Average of the pricing for 2kV to 50 kV and above 50 kV for each charge category was used as a hybrid cost to simplify the power calculation yet addressing the typical and different voltages utilized at a typical large water resource recovery facility (WRRF). In addition, the meter charge for only one meter was accounted for in the cost calculation for this study.

Figure 9 compares the total energy usage charges (i.e. sum of delivery and generation) for hybrid of 2kV to 50 kV and above 50 kV voltage categories for each of the tariffs listed in these two fee schedules for summer (i.e., June through September) and winter (non-summer) months. The usage charges presented in this figure are for weekdays and selected to be used for this modelling effort as it dominates more than 70% of the study period.

Comparison of these energy usage cost trends with the plant dynamic influent profiles in Figure 6 clearly substantiates the coincidence of the peak of the plant influent diurnal trends and peak of these electricity tariffs. In addition, comparison of the legacy (old) tariffs with the new ones (illustrated in Figure 9) also demonstrates how the new diurnal cost and peak periods are different. It also demonstrates an increase in the electricity cost and shifting or compressing of the peak period to 16:00 to 21:00 as a result of duck-curve phenomenon as explained in the Introduction section of this article.

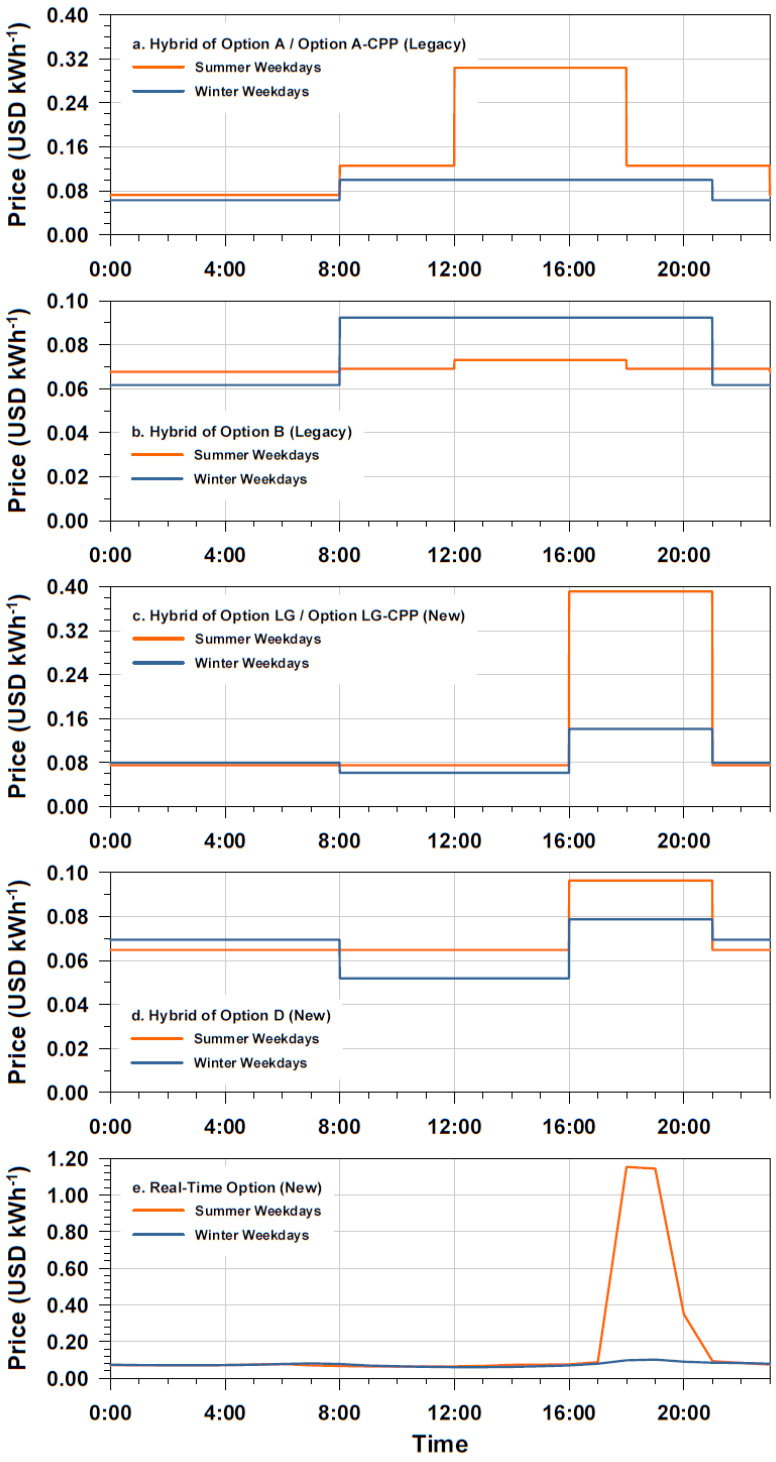

Figure 9. Southern California Edison's tariff structures. (a) to (d): new and old (legacy) time-of-use schedule for total energy use charges (sum of delivery and generation charges) for facilities with internal generation capacity and with the demand larger than 500kW (TOU-8-S) for weekdays derived from the average of fees scheduled for 2-50kV and >50kV grids [Effective as of March 1, 2019]. (e): current real-time schedule for total energy use charges (sum of delivery and generation charges) for facilities with internal generation capacity and with the demand larger than 500kW (TOU-8-RTP-S) for weekdays derived from the average of fees scheduled for 2-50 kV and >50kV grids [Effective as of March 1, 2019] [46].

The hybrid metering and demand charges were also calculated by averaging of the charges for 2kV to 50 kV and above 50 kV categories are provided in Appendix C [46]. Also, the standby demand value of this facility which is required for demand charge calculations was assumed to be 5.2 MW. This is the typical average in-house generation capacity at the plant being studied here and was selected per consultation with plant engineers.

Normalization of Results

In order to compare different simulation scenarios fairly in this research study, their electricity demand, GHG emissions, and operating cost, need to be normalized to different parameters representing the extent of treatment. Possible normalization methods that could be and were used for this purpose are summarized here.

I. Normalization per Unit Influent Flow

The facility influent flow treated was used to normalize the simulations results for comparing the effluent quality and the net and total electricity demands where net electricity demand is calculated by subtracting the facility in-house electricity generation from the total electricity demand. The normalized net and total electricity demand values per unit influent flow are referred to as net and total electrical energy intensities in this research study.

II. Normalization per Unit Activated Sludge Theoretical Oxygen Requirement

Theoretical oxygen requirements, defined as the amount of oxygen required for removal of carbonaceous material and oxidation of ammonia and nitrite to nitrate, were used to normalize the electricity demand in comparing the activated sludge units in this research study. This normalized electricity demand is referred to as activated sludge energy intensity in this dissertation.

III. Normalization per Unit Quality Index Removal

The cumulative extent of removal of all pollutants from wastewater for each scenario has been accounted for by normalizing the net and total electricity demand, GHG emissions, and operating cost of each scenario to the plant's quality index [47, 48] removal. Quality index removal (QIR) is defined as the difference between the weighted sum of TSS, TKN, COD, Nitrate, and BOD in the facility influent and effluent and calculated by subtracting effluent quality index (EQI) influent quality index (IQI) where:

Effluent quality index (EQI), defined as weighted sum of the pollutants in the effluent [47, 48], is calculated in Equation 3 as following:

$$\mathbf{EQI} = \mathbf{1}/(\Delta\mathbf{t}\,.\,\mathbf{1000}) \int_{\mathbf{t_1}}^{\mathbf{t_2}} [\boldsymbol{\beta}_{\mathbf{TSS}}.\,\mathbf{TSS_e}(\mathbf{t}) + \boldsymbol{\beta}_{\mathbf{COD}}.\,\mathbf{COD_e}(\mathbf{t}) + \boldsymbol{\beta}_{\mathbf{TKN}}.\,\mathbf{TKN_e}(\mathbf{t}) + \boldsymbol{\beta}_{\mathbf{NO_3^-}}.\,\mathbf{NO_{3e}^-}(\mathbf{t}) + \boldsymbol{\beta}_{\mathbf{BOD_5}}.\,\mathbf{BOD_{5e}}(\mathbf{t})]\mathbf{Q_e}(\mathbf{t})\mathbf{dt} \qquad (\mathbf{Equation\ 3})$$

Where **Δt** is the total evaluation period; **Q_e(t)** is instantaneous effluent flow rate during the evaluation period; **TSS_e(t)**, **COD_e(t)**, **TKN_e(t)**, $\mathbf{NO_{3e}^-}(\mathbf{t})$, **$BOD_{5e}$(t)** are these wastewater constituents' instantaneous concentrations in the effluent; **β** represents weighted factors for different wastewater constituent which are β_{TSS}= 2, β_{COD}=1, β_{TKN}=30, $\beta_{NO_{3e}^-}$=10, β_{BOD5}=2 [47, 48]. **1000** is the SI unit conversion factor which can be replaced by other factors depending on the desired unit for EQI and units in which concentrations and flow data is collected.

Using the same logic as EQI's, influent quality index (IQI) can be defined in Equation 4 as following:

$$\mathbf{IQI} = \mathbf{1}/(\Delta\mathbf{t}\,.\,\mathbf{1000}) \int_{\mathbf{t_1}}^{\mathbf{t_2}} [\boldsymbol{\beta}_{\mathbf{TSS}}.\,\mathbf{TSS_i}(\mathbf{t}) + \boldsymbol{\beta}_{\mathbf{COD}}.\,\mathbf{COD_i}(\mathbf{t}) + \boldsymbol{\beta}_{\mathbf{TKN}}.\,\mathbf{TKN_i}(\mathbf{t}) + \boldsymbol{\beta}_{\mathbf{NO_3^-}}.\,\mathbf{NO_{3i}^-}(\mathbf{t}) + \boldsymbol{\beta}_{\mathbf{BOD_5}}.\,\mathbf{BOD_{5i}}(\mathbf{t})]\mathbf{Q_i}(\mathbf{t})\mathbf{dt} \qquad (\mathbf{Equation\ 4})$$

Where **Δt** is the total evaluation period; **Q_i(t)** is instantaneous influent flow rate during the evaluation period; **TSS_i(t)**, **COD_i(t)**, **TKN_i(t)**, $\mathbf{NO_{3i}^-}(\mathbf{t})$, **$BOD_{5i}$(t)** are these wastewater constituents' instantaneous concentrations in the influent; **β** represents weighted factors for different wastewater constituent which are β_{TSS}= 2, β_{COD}=1, β_{TKN}=30, $\beta_{NO_{3e}^-}$=10, β_{BOD5}=2 [47, 48]. **1000** is the SI unit conversion factor which can be replaced by other factors depending on the desired unit for IQI and units in which concentrations and flow data is collected.

IV. Normalization per Unit Oxidized Load

Another approach used to compare the net electricity demand of different scenarios in this research effort is to normalize the net electricity demand to oxidized load or load removed. It is defined as biodegradable COD (bCOD) load and nitrogen removed by oxidation. The bCOD represent the portion of the COD that can be biochemically oxidized. In calculating the oxidized load, the oxygen associated with oxidation of bCOD by denitrifying bacteria in the denitrification process (i.e., denitrification credit) needs to be subtracted if no supplemental carbon (e.g., methanol) is added to support the denitrification. The plant studied here does not add any supplemental carbon; therefore, this adjustment needs to be implemented to distinguish the actual oxidized load from the theoretical oxygen requirements used in the normalization method presented earlier in this section.

CHAPTER 3: CHALLENGES IN FULL-SCALE MODELING OF WATER RESOURCE RECOVERY FACILITIES

Most of the challenges that had to be encountered to develop the full-scale dynamic model in this study were related to the data collection phase and quality of the data. The data collection for this dynamic modelling effort took more than two years. This chapter provides a list of the major examples of these challenges. This list of was also presented in 2021 WateReuse California Annual Conference in Los Angeles, California in September 2021.

1. **Missing and Inconsistent Data**: not all the data needed for performing the simulations in this study was available. Therefore, different methods such as averaging, mass balance, or typical values from literature had to be used to fill in the blanks. There were also cases that the values for the same parameter were available from multiple sources but were contradicting. Different remedies such as mass balance or follow-up communication with the plant engineers were employed to determine the most accurate of these values. The other factor that was observed in this modelling effort was that intermediate process streams such as recycle streams had less priority for sampling and process data collection comparing to the plant influent and effluent streams. Therefore, these streams' data was more difficult to be obtained from the plant.
2. **Plant's Staff Busy Schedule**: only the facility officials had access to the field data needed for this modelling effort. As such, all the data request and data validation questions had to be addressed by the facility staff, who were usually busy with the plant's daily operation and other priorities. For this study, there were many instances that multiple requests, follow-ups, and reminders were needed to be sent to obtain a piece of information. The waiting period to receive this data not only slowed down the modelling process, but also resulted in repeating many steps of the simulation where literature data or educated assumptions were used as place holders in the dynamic model. Replacing these placeholders in many cases required

extensive amount of time as it would require recalibration of the model and repeating the simulation runs for all the scenarios in this study which would take weeks.

3. **Difficulty of Finding Appropriate NH_3/TKN**: NH_3-N/TKN-N was needed for converting the influent field ammonia concentrations to TKN-N to create the influent profile of the simulations. Upon influent profiles input to the simulation software, this ratio was also used by the software to convert TKN-N back to ammonia. Since no ratio could be provided by this plant nor from other local projects, literature research was conducted to find a typical value for this ratio preferably in warm climates same as California. Different values ranging from 50 through 80% were observed in this research; however, except a few, most of them seemed not to be precise, from testing, or backed up by a clear source. The most defensible data obtained from this literature research was from Zorpas, et al., (2010) study on the operation and physicochemical characteristics of influent, effluent, and tertiary treatment of a water resource recovery facility (WRRF) in eastern Cyprus under warm climates [49]. In their study, Zorpas, et al., compiled average concentrations of influent constituents for 7 years (2003 through 2009) for the WRRF they studied in Cyprus and compared this data with other WRRFs in Turkey, which is not considered a warm climate. The influent concentrations of this Cyprus plant especially its COD's, which was the main influent parameter used for simulating the California WRRF studied in this dissertation, were the same as this California facility. Therefore, the NH_3-N/TKN-N ratio derived from Zorpas et al. could be a great representative for this facility. The ratio calculated for the Cyprus plant in Zorpas et al. research varied from 58% to 80% with average and median of 69% and 67% respectively. The average ratios calculated from the concentrations provided for other plants in Istanbul in Zorpas, et al., paper varied from 45% to 67%.

This literature review concluded that the NH_3-N/TKN-N could be highly site specific and even could have significant variation for the same plant; therefore, it should be obtained from field measurements for future modeling efforts. In the absence of the field data to derive

this ratio for the California plant studied in this dissertation, the default ratio of 66% from the simulation software which was also close to the average and median values in Zorpas et al. article was used.

4. **Process Data Frequency**: the frequency of process data records available by the plant were at the most average monthly values. As indicated before to perform a dynamic modelling that captures the influent's and power grid's diurnal trends, higher frequency data preferably hourly data was needed. This was why hourly data trends were generated synthetically for this study as explained in the Methods section of this dissertation.
5. **Biased Concentration Data**: the concentration data especially solid concentrations can be biased due to infrequent sampling. Even when sampling is performed more frequently in case of composite sampling, and more accurately by auto-samplers, samples may be collected inconsistently or from an improper location. In many instances samples are collected when plant operators find an opportunity to do so; therefore, sampling may be performed at different time of the day each time. Thus, the results may not be true representatives of the plant's operations. In this study, many inconsistent solid concentration values were observed and substituted by yearly averages or average of preceding and subsequent monthly values.
6. **Outdate Data Collection System**: in this study it was observed that the data collection database of the facility was not updated in response to changing the plant's sludge dewatering and thickening technology to centrifuges. This resulted in some data gaps in the operation data reports populated by the plant toward the end of 2019.
7. **Missing Energy Data and Its Breakdowns**: WRRFs' focus is usually treatment of water and not energy usage. The energy data that is usually compiled in their operation reports are limited to total in-house thermal and electrical energy production as well as fuel and electricity imports and exports that are mainly meant for verifying the plant utility bills and accounting purposes. As such, it is difficult to determine the energy usage (especially electricity) breakdown for each process unit at these facilities as the data is not metered; metered but

not recorded; or metered and recorded but in aggregation with other process units. Same difficulties were observed and highlighted in other modelling efforts for example in an energy footprint modelling of 5 large WRRFs in the U.S. and Europe by Rosso, et al., 2012 [50]. The plant studied here was not an exception. Therefore, literature research or field aggregated power usage data for combination of process units had to be used for energy calculations and model calibration here.

8. **Meter Accuracy**: metering accuracy is another factor that impacts the accuracy of the collected field data especially when the meter is not calibrated and maintained as recommended by the manufacturer. The other concern here is the spread or amplification of this degree of error to other model input parameters that are calculated from the metered parameter. Flowmeters are the main example of metering devices extensively used at WRRFs and are discussed in more details here.

   The range of accuracy of more common flowmeters in wastewater industry as well as newer flowmeter technologies used in the water industry are listed in Table 5.

Table 5. Common flowmeter types and accuracy ranges.

Closed Conduit Flow Measurement Devices	Accuracy (%Error)	Data Source
More Common for Wastewater		
Venturi Meter	±1% to 2% of flow reading	[51]
Orifice Meter	±0.5% of flow reading	
Electromagnetic Meter	±1% of full scale	
Example of Newer Technology		
Vortex–shedding Meters	±0.7% over 30:1 range of flow	[52]
Ultrasonic Meter /Clamp–on Transit–time Type	±2% of flow reading	
Ultrasonic Meter /Doppler Type	±5% of full scale	

As shown in this table, these meters not only have different range of accuracy, but also have different scales to demonstrate their accuracy (i.e. “% of flow reading”, “% of full scales”, and “% over range of flow”). The simplified interpretations of these accuracy scales are provided in the following examples:

- % Error of ±1 to 2% of flow reading in case of Venturi meters means that any readings from this meter can be within the ±1 to 2% of the true flow value.
- % Error of ±1% of full-scale in case of Electromagnetic meters means that the true flowrate can be within of ±1% of the meter’s maximum reading scale; therefore, the percent error increases if the measured flow falls below this maximum. In other words, the accuracy of the flowmeter varies by the flowrate and is lower when smaller flows are measured.
- % Error of ±0.7% over 30:1 range of flow in Vortex–shedding meters means that the % error provided applies to flow ranges from maximum possible reading going down to 1/30 of this maximum.

The margins of error provided in the Table 5 are for the ideal case when these meters are installed, calibrated, and maintained as instructed by the manufacturer which is highly unlikely at the field applications seen in WRRFs. Thus, the range of error is expected to be greater than Table 5 values.

The effect of flowmeters’ error on calculating the process parameters becomes more visible when readings from different types of meters with different range of accuracy installed across the same plant are used to perform mass or flow balance around major process units or the entire plant. An article by J. Davis, demonstrates this issue in few mathematical examples and explains why flow data history in many wastewater treatment plants erroneously demonstrate significant amount of wastewater generation or evaporation within these plants’ boundary [53]. This explains the negative or unrealistic flows and concentrations

calculated in some of the mass-balance calculations performed in this research study performed to obtain the missing monthly process data required for the simulation.

The operating condition of meter can also further lower its performance and expand its margin of error. An example of this, is the negative effect of sludge settling in the inner line of certain type of flowmeters in WRRFs installations [53]. The other factor that impacts the accuracy of the collected flow data beyond the flowmeter accuracy is the fact that a flow meter accuracy does not fully represent the accuracy of the entire flow system. The accuracy of other components of such a system needs to be also accounted for to determine the accuracy of the collected readings. In his article, Davis demonstrates how accounting for the entire flow systems in an example will raise the margin of the error of collected flow data by more than 60% of the flowmeter's alone [53]. The flow system in his example consisted of a magnetic flowmeter sending an analogue signal to an operator's workstation via a programmable logic controller (PLC).

Validating the flow data and compensating for all its measuring system components' inaccuracy is very challenging and require significant amount of process details. This substantiates the great value of installing and operating of identical flow meters per manufacturer standards and within their maximum accuracy operating margins across the same plant to simplify the validation and correction of the collected data.

Although analysis provided above has been focused on wastewater flow measurement, its conclusions can be expanded to the meters used for natural and biogas flow measurements. In fact, some of the flow meters listed in Table 5 are also used for gas service. However, gas meters' degree of accuracy especially for biogas service whose corrosive constituents damage the meter components over time is expected to be higher. Gas streams' compressibility increases the effect of flow obstruction and fitting components on the

flow measurement accuracy. Gas meters also have higher flow system network error due to their additional components such as temperature and pressure gages which may not be present in liquid service.

It is worthy to mention that the extent of accuracy of biogas flow meters becomes more crucial in case of calculating biogas transmission fugitive emissions using mass or flow balance. Reviewing the margin of errors in Table 5 for few types of the meters that can be used for gas service (0.5% to 2%) not accounting for the additional error contribution of the other flow system's components, also demonstrates the difficulty of calculating biogas leak via flow or mass balance. These meters accuracy range also exhibits the great margin of error for the typical biogas fugitive emission factor of 2% of total biogas production used in previous carbon-footprint assessment efforts by other researchers for WRRFs [33, 21]. The significance of the extent of biogas fugitive emissions on the plant's overall carbon-footprint has been further discussed in other chapters of this dissertation.

9. **Unverifiable Parameters:** Calculated parameters provided by the plant whose calculations and independent measured variable were not provided could not be verified; therefore, had to be assumed to be accurate. Examples of these calculated parameters in this study are activated sludge mean cell retention time (MCRT) and airflow to BOD ratios.
10. **Incorrect or Unclear Parameters' Measurement Units**: during the course of data verification and validation, there were instances that the process data provided by the plant were incorrectly or unclearly labelled. For example, AS2 MLE recycled stream flow for one out of 6 basins were labelled such that it suggested the value was for all 6 basins. Another example was for the natural gas and biogas flowrates where it was not clear whether the values are presented in standard conditions or not. In this case, the natural gas data which seemed to be obtained from utility bills or at least compared with them assumed to be adjusted

to standard condition. However, biogas data assumed to be at operating condition and was adjusted to standard condition assuming standard condition of 1atm and 20°C.

11. **Inability of Modelling All the Processes**: Due to lack of process information not all the process units could be modelled in this simulation effort. Trickling filter was the main example of such a process in this modelling effort.
12. **Site Specific Wastewater Fractions**: For this modelling effort, influent COD concentration was entered ino the simulation software to calculate other influent constituents (ex. TSS, VSS, cBOD etc) except for TKN, ammonia and nitrate. For these calculations, the software relied on a series of default fractions including: Unbiodegradable Soluble/ Total COD; Readily Biodegradable/Total COD; Ordinary Heterothrophic COD Fraction; and Unbiodegradable Particulate/Total COD. Through the course of the current plant model calibration here, it was discovered that not all of these default wastewater fractions were representative of the plant being modeled here. Specifically, these default fractions resulted in underestimation of the influent's TSS and VSS and overestimation of its cBOD concentrations in the model which would also impact other streams of the model. This discrepancy also resulted in overestimation of the biogas production in the simulated plant's digesters. As such, these fractions were calculated using the plant influent data pursuing the methodology summarized by Gori, et al., 2011 [21] for each month of the year and averaged for the 12 months study period for this facility. Since the simulation software only allowed a single entry as opposed to data trends for these factions, the average of the calculated fractions for the calibration period was used to calibrate the model. Utilization of these average calculated fractions resolved the TSS, VSS, and cBOD discrepancy in the modelled streams; however, caused a significant underestimation of the plant's biogas production in the model comparing to the field data in the calibration period.

After few trial-and-error calibration runs using different ranges of COD fractions and analyzing their effect on the influent constituents and biogas production errors, only the default

fraction of the Unbiodegradable Particulate/Total COD was replaced. This faction was changed to the average of the software default and calculated average value for the calibration period which came out to be double of the software's default. This change allowed resulted in minimizing the discrepancies or error in the output of simulation comparing to the field data.

A brief literature review on the sources of typical default influent factions, shed light on the reason for why this simulation software's default fractions might not be a good fit for this California WRRF. Most of the gathered data for the COD fractions in the activated sludge modeling protocols are based on samplings at European WRRFs. An example these sampling events is fractions gathered by Roeleveld and Van Loosdrecht based on the 5 years of study for 100 WRRFs in Nederland's [54]. Roeleveld and Van Loosdrecht study has been referenced in many activated sludge modeling efforts and protocols (e.g., Dutch Foundation of Applied Water Research or STOWA's protocols). This may explain the need for increasing the default Unbiodegradable Particulate/Total COD ratio in the simulation of our California plant here which treats wastewater containing kitchen garbage disposer wastes.

Disposal of this kitchen waste consisting of more cellulosic material, that are not biodegradable in a typical wastewater treatment plant, increases the unbiodegradable fraction of COD in California wastewater comparing to Europe where garbage disposers are uncommon. As such, utilizing the COD fractions based on studies in Europe overestimates the biodegradable portion of wastewater COD in modelling this California plant. This is what we observed in this study and the possible reason for the need for increasing Unbiodegradable Particulate/Total COD default factor in the simulation software for this sudy.

This finding substantiates the need for providing more location-specific COD fractions in activated sludge modeling protocols or simulation software such as BioWin that are used by many users across the globe. These location specific default fractions allow more accurate modelling results and eliminate the need for COD fractions calibration where sufficient detailed field data for calibration may not be available. The importance of such location

specific factions is also increasing due to recent adoption of regulations promoting the diversion of food wastes to WRRFs as opposed to landfills for digestion and biogas production. Enforcing this process change may impact the COD fractions of influent streams sent to digesters or other process units of WRRFs at regions where such regulations are being implemented. California Senate Bill 1383 (SB1383) is an example of such regulations [55, 56].

13. **Modelling a Component Instead of a System of the Plants**: as indicated before the plant being modelled in this study is the primary plant of a two WRRFs network. This network supplies water to an advanced treatment facility that employs microfiltration, reverse-osmosis, and Ultraviolet disinfection before delivering the water to underground injection wells. To perform an accurate energy and carbon-footprint assessment, the entire network of these two WRRFs and the advanced treatment facility needs to be modelled simultaneously. This is because any changes to the primary WRRF will also impact the operation and energy demand of the facilities in parallel or downstream of this plant. Few examples of such impacts were explained in the other chapters of this dissertation.

    However, modelling the network of these three plants was difficult if not impossible for this study as:

    - Not all the process units in these three plants were available in the simulation software used here. Therefore, these processes could not be modelled in this software.
    - Even if all the process equipment existed in the software, dynamic modelling of all these processes in the same simulation would require extensive amount of simulation run time. This could be easily explained when only one dynamic scenario for one sixth of the primary plant of this network required 3 hours after implementing all the possible optimizations with the help of the software developing company (EnvioSim).

- The simulation software used here also did not allow simulation of these three plants independently in separate simulation files and linking the results. As such, this cumulative simulation effort could not be broken down to different phases to reduce the simulation run time by distributing the work among different project teams.
- Data required for simulating this network of plants had to be obtained from different jurisdictions and utility boundaries. This would make it very challenging to align the data and perform a mass balance that is coherent to find missing data. In addition, the time and effort needed to compile and validate this amount of data would be expected to be very extensive when it took 2 to 3 years to obtain and validate the data just for the primary WRRF of this network.

In sum, the data collection and validation were the most challenging phase of this research effort and required years of expert investigator work. One of the main challenging factors in data collection was the low frequency of data collection and recording (mostly monthly). Additionally, the patchwork of data acquisition and storage systems, typical of large facilities that underwent a succession of upgrades and expansions, increased the challenge in accessing data. Higher frequency of data sampling and recording that at least represents the on- and off- diurnal influent peaks is recommended to be performed by WRRFs for future studies and modelling effort. This not only results in more accurate dynamic modelling results, but also simplifies data validation and missing data substitution efforts.

The influent fractions required by the modelling software utilized in this research needed to also be verified in the field or at least be derived from collected field data. Comparison of these field fractions with the simulation software's defaults and changing these defaults, when extensively different than field's values, can reduce or eliminate errors. In this modelling effort, not all influent fractions could be derived from field data collected by the plant (e.g., COD fractions,

NH_3/TKN). As such, additional sampling to derive these rations and fractions before starting the modelling effort in the future is greatly recommend. The accuracy of the flow data used for modelling and validating the simulation of different process units is also crucial. As such, calibrating and operating the flowmeter systems according to manufacturers' guidelines by the facility as well as using the data from such metering systems, when available, are also strongly recommended here. A lack of dynamic power demand data broken down to major process units, which is necessary for developing a complete dynamic facility power demand model, was another challenge that had to be confronted here. Equipment models can assist in this task; however, collecting and recording field power demand data is recommended to for best results.

CHAPTER 4: PLANT EXPANSION TO CURRENT CONFIGURATION

As explained int the Introduction section, water resource recovery facilities' (WRRFs') significant power consumption, their electricity demand peaks' coincidence of with the grid's, and the effect of the increase in variable-generating renewable sources on the grid's diurnal dynamics and cost (hence, WRRFs electricity cost) had made these facilities an attractive target for demand-side flexibility projects [14]. These projects rely on modifying the WRRF's operation to lower their electricity imports from the grid during the gird's peak of demand resulting in lowering their electricity import cost and carbon-footprint.

In order to demonstrate the effectiveness of a demand-side flexibility project at a WRRF, experimental and simulation efforts [14] that correctly capture the diurnal cycles or dynamic trends of its influent and electricity grid are required. This is achieved by feeding the dynamic grid's electricity fee schedules and carbon intensity as well as dynamic influent characteristics profiles into the developed dynamic simulations or models for the selected WRRF. Using this dynamic model, the impact of such a project on other aspects of treatment such as effluent quality and overall operating cost of the plant needs to be also simultaneously assessed with the electricity savings to assure the practicality and feasibility of the proposed demand-side flexibility project.

This chapter summarizes the preliminary feasibility assessment of a demand-side flexibility project that relies on changing the distribution ratio of primary effluent between the two different activated sludge (AS) configurations (i.e. MLE and step-feed L-E) in the current process configuration of the large California WRRF studied in this dissertation which has been described in more details in the Methods chapter. The simultaneous and parallel operation of these two different AS configurations allows electricity savings by maximizing the use of the more electricity efficient configuration. As such, the first step of this assessment is to compare these configurations and determine which of them is more electricity efficient. This comparison is

performed indirectly by comparing the current plant's process configuration demonstrated in Figure 3 (current plant scenario) with the facility's older configuration that only utilized one of these two configurations (i.e., step-feed L-E) illustrated in Figure 4 (old step-feed scenario).

The current plant configuration here is in fact the outcome of expanding the old step-feed plant by adding the MLE activated sludge configuration to its existing step-feed L-E configuration. Although this expansion increased the facility's treatment capacity, the results of the dynamic models developed to compare these pre- and post- expansion scenarios can be fairly compared by normalizing them to the extent of treatment using the methods introduced in the Chapter 2 (Methods). This indirect comparison was selected over a direct comparison of the two configurations in the current plant as the available field data from the facility and the simulation software's blower electricity calculations tool would not allow separate energy calibration for each of these two configurations in the same facility simulation. As such, the current plant or post-expansion scenario including both configurations were developed and calibrated first. The old step-feed model was then developed by eliminating the MLE configuration from the current plant's calibrated model and adjusting its influent flow. Details about these scenarios' model preparation have been provided in Methods chapter.

In this indirect comparison we assessed the effect of the addition of the second configuration on the power demand, overall operating cost, carbon-footprint, and effluent quality of this facility. This comparison portrays the more electricity efficient option of these two configurations and its facility wide overall operating cost, carbon-footprint, effluent quality. This is the first step to determine whether the two parallel activated sludge configuration at this plant could be used to define demand-side flexibility projects. Depending on this first step findings, then future detailed studies can be coordinated and performed on technicality and the extent of changing the primary effluent distribution between these two activated sludge configurations as a demand-side flexibility project.

Effluent Quality

Simulations for both post and pre-expansion scenarios (or current and old step-feed plants) were completed using dynamic influent and process profiles and after running the alpha factor iterations as discussed in the Methods chapter. The effluent concentrations of TSS, CBOD, ammonia and nitrate for these two scenarios have been compared in Figures 10 through 13.

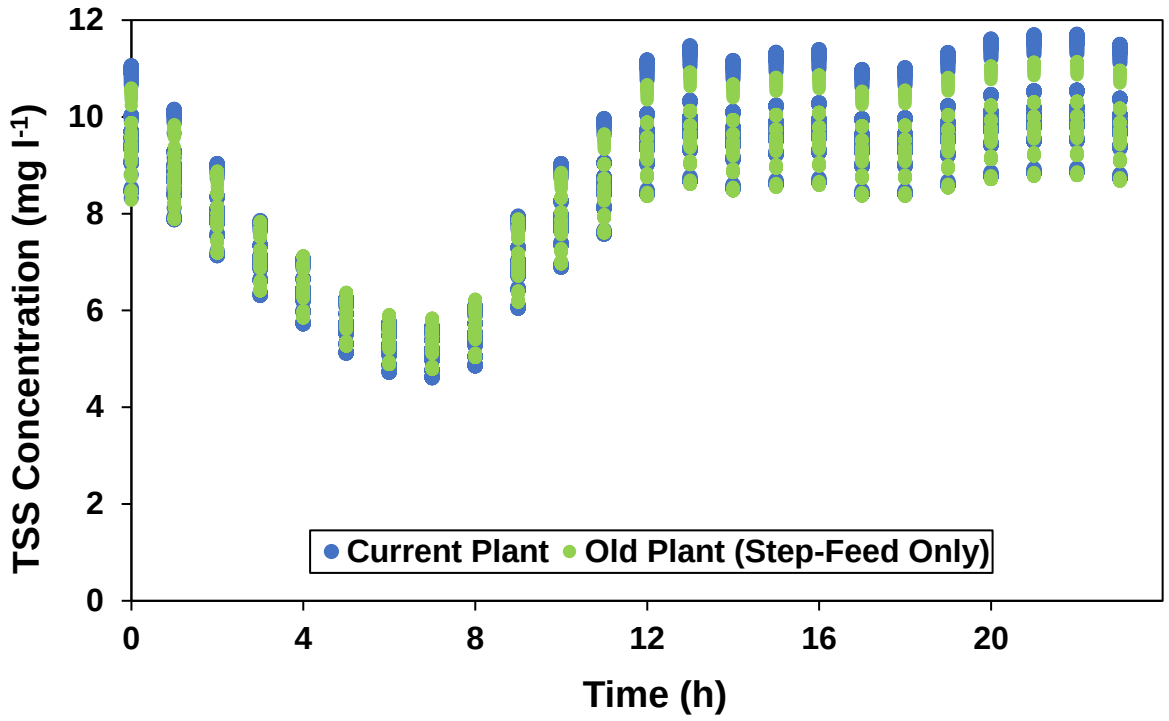

Figure 10. Plant's effluent TSS concentration comparison for current and old step-feed scenarios.

As illustrated in Figure 10 TSS concentrations during the peak of WRRF's influent (12:00 to 23:00) is slightly lower in the old step-feed plant for some of the months of the year and is comparable for the remainder of the day. Comparing the CBOD concentrations of these two scenarios in Figure 11 demonstrates about 1 mg l^{-1} less of this pollutant in effluent of the current plant comparing to the old step-feed plant for the entire day during the study period.

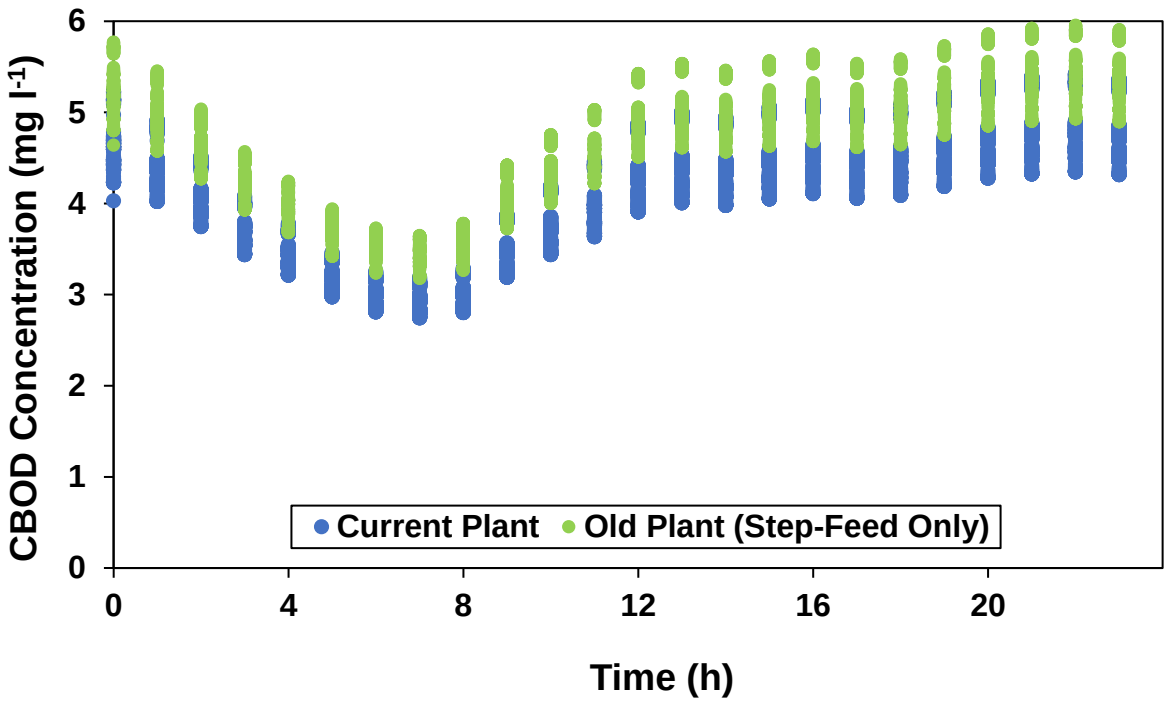

Figure 11. Plant's effluent CBOD concentration comparison for current and old step-feed scenarios.

Higher CBOD and TSS in the effluent sent to the downstream advanced treatment facility would result in the need for higher extent of removal in its microfiltration and reverse-osmosis units at the cost of higher electricity demand. As such, combining these two pollutants discrepancies suggests that old step-feed plant's effluent quality would slightly require more electricity at the downstream facility. This higher electricity demand would also translate into higher greenhouse gas emissions and costs associated with the electricity imports at this neighboring advanced treatment facility which were assumed to be outside the scope of this study.

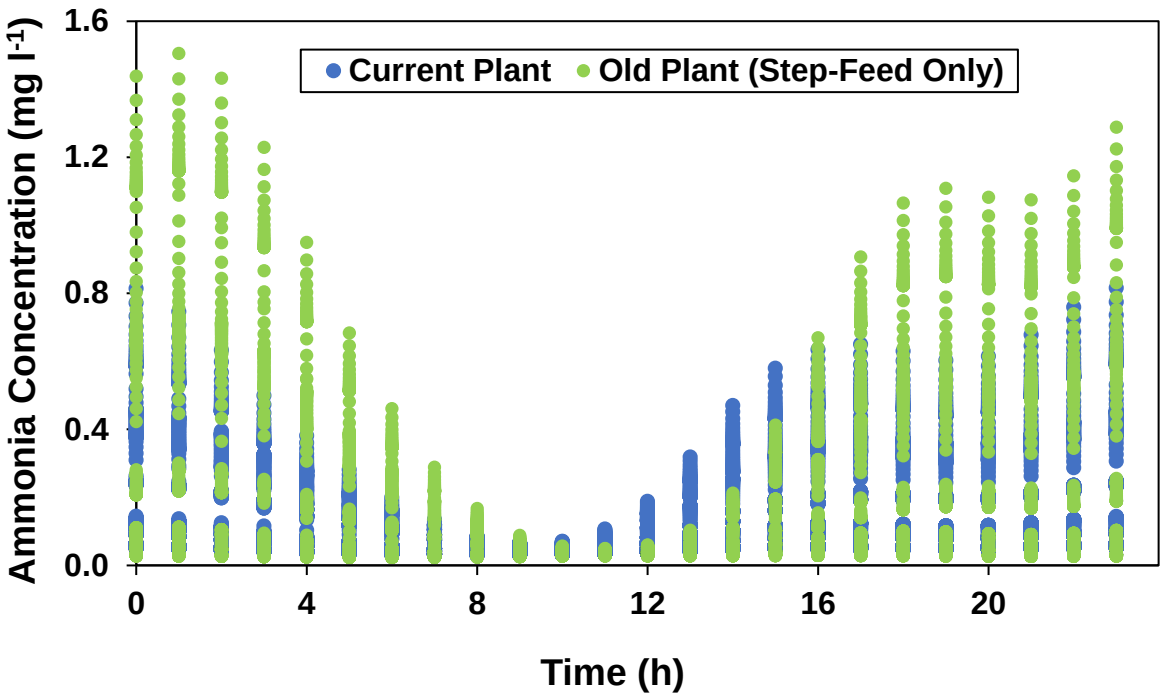

Figure 12. Plant's effluent N-NH3 concentration comparison for current and old step-feed scenarios.

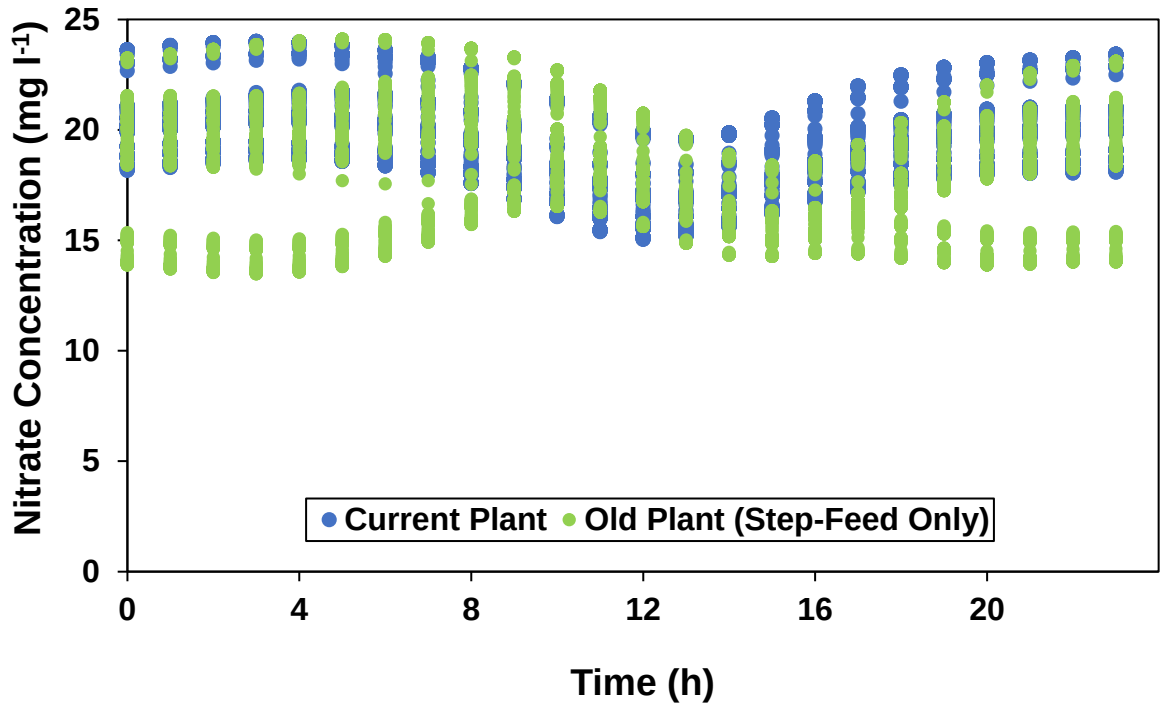

Figure 13. Plant's effluent N-NO_3^- concentration comparison for current and old step-feed scenarios.

Comparing the ammonia concentrations in Figure 12 suggests a slightly less ammonia removal in the old step-feed plant. A closer look at the concentration of nitrate in the effluent of two scenarios in Figure 13 substantiates that both scenarios' effluent contained almost the same amount of nitrate except during the peak of the plant load when old step-feed plant's is slightly lower. Traces of nitrite were also observed in the effluent of both scenarios which was negligible in the current plant (0.0 to 0.3 mg l^{-1} on average annually) and more considerable in the old step-feed plant scenario (0.0 to 3.0 mg l^{-1} on average annually). The presence of nitrite which was considerably observed in March through April 2019 was assumed to be due to biomass limitation in these months. It can be also explained side effect of overestimation of dynamic flow and therefore influent load due to rain events in these months. Since the effluent sampling data from the plant did not provide any information about nitrite and nitrate concentrations, the model's results for nitrate and nitrite could not be verified against the field data and play a role in the calibration stage. In summary, comparing the overall simulation nitrogen trends in the effluent (ammonia, nitrite, and nitrate) with the plant's influent ammonia's (66% of influent TKN-N in Figure 6) illustrated that the extent of nitrification and denitrification is slightly lower in the old plant scenario.

To simplify the comparison of effluent quality for these scenarios, a cumulative comparison was conducted using the effluent quality index (EQI) which has been explained in the Methods Chapter [47, 48]. It needs to be noted that EQI is a weighted measure of pollution, hence higher EQI is opposite to effluent quality. Since the post-expansion (current plant) scenario treats higher influent flow comparing to pre-expansion (old step-feed plant), the EQI values were normalized to the plant total influent flow for this comparison in Figure 14.

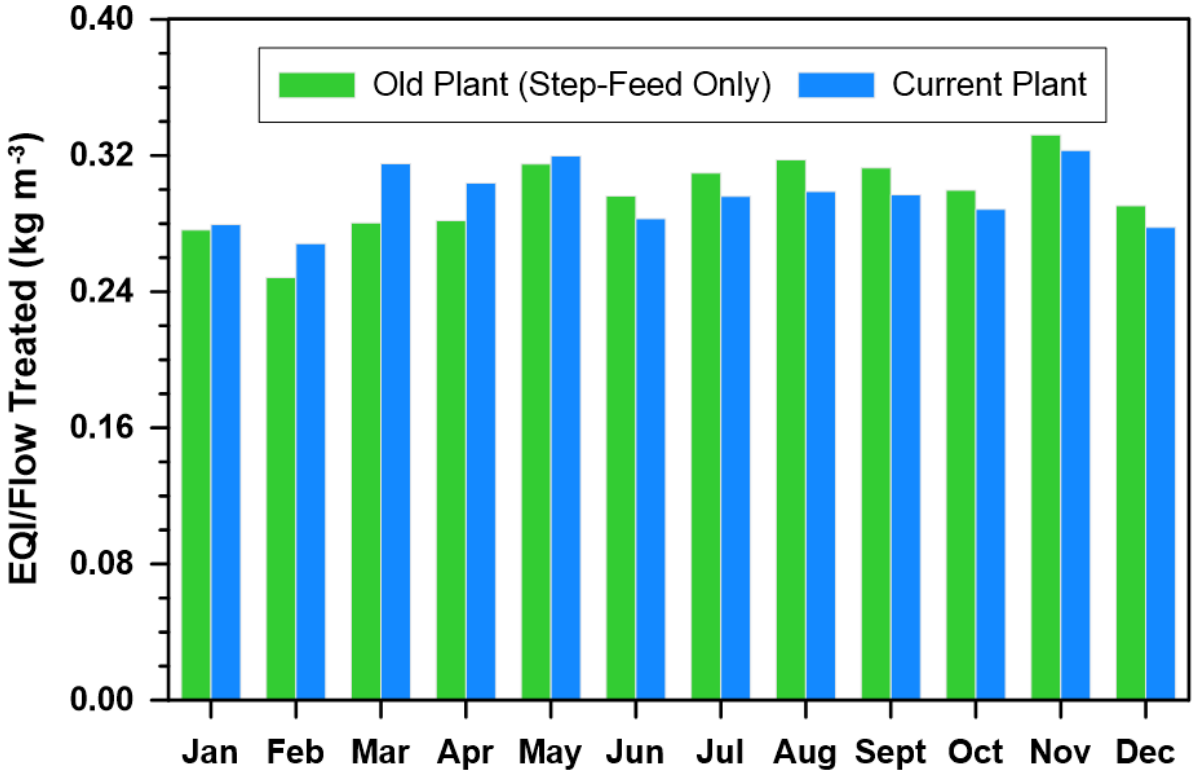

Figure 14. Monthly effluent quality index (EQI), normalized per unit flow treated, for current and old step-feed plants scenarios. Note that lower values in the vertical axis imply better quality of effluent water.

Comparing the monthly EQI for these two scenarios in Figure 14 demonstrates that the current plant's index is lower by 3 to 6% from June through December; slightly higher in January and May (1.2 to 1.5 % respectively), and higher by 6 to 12% in February through April when compared to the old step-feed plant's. The facility received significant amount of rain in February through March resulted in significantly higher influent flow which may contributed to the significant discrepancy between the overall EQI trend observed for these months comparing to the other months. As such and overall, the expanded plant delivers same or better quality of treatment comparing to pre-expansion.

Electricity Demand Dynamic Trends and Annual Breakdown

Dynamic net and total electrical energy intensities (i.e., electricity demand divided by influent flow) for both scenarios were demonstrated in Figure 15. This figure shows that the overall improved effluent quality after the expansion (current plant) corresponds to an increase of up to 0.07 kWh m^{-3} in total electrical energy intensity when compared to the old step-feed plant. Similar range of increase (0.02 to 0.10 kWh m^{-3}) is observed in the net electrical energy intensity which accounts for the plant's internal electricity generation.

The total electrical energy intensity is minimum or close to it at the peak of plant influent load (between 12:00 and 23:00) while the net intensity is maximum. This is despite the fact that the hourly trends for both the net and total electricity demands follow the same trend as influent flow's and net power demand energy intensity's and all peak between 12:00 and 23:00. Thus, the reciprocal trend of total and net electrical energy intensity in Figure 15 is explained to be due to a different magnitude of the net and total power demand values compared to influent flows where these demand values are normalized to the same influent flows to calculate the net and total energy intensity values here.

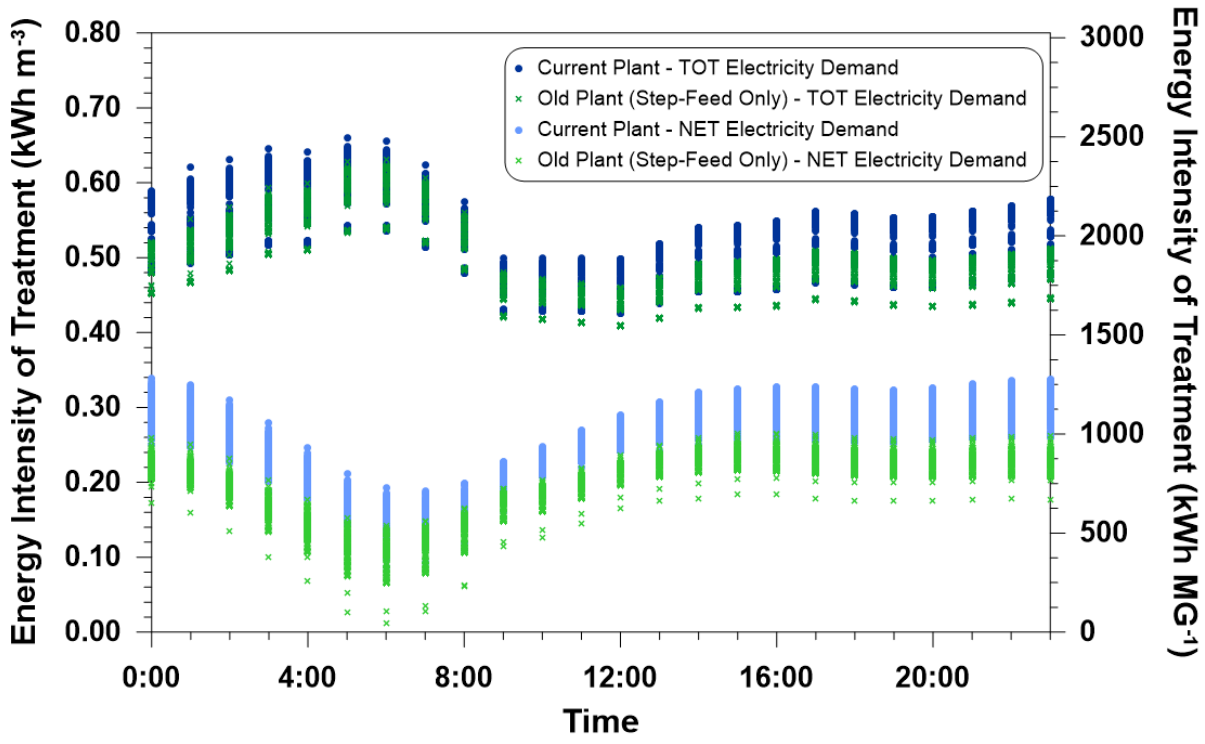

Figure 15. Dynamic net and total treatment electrical energy intensities (demand normalized to plant influent flow) for current and old step-feed plants' scenarios. Both Y-axes apply to the data points plotted.

Comparing the dynamic net power intensity trends in Figure 15 with the grid's electricity CO_2 intensity and tariffs diurnal trends in Figures 8 and 9, respectively, elucidates the coincidence of the peak of these three parameters for both scenarios at this WRRF similar to the references mentioned in the Introduction chapter. This coincidence results in the amplification of the peak of the grid's electricity import cost and greenhouse gas (GHG) emissions during the peak of these scenarios' net power demand, a phenomenon identified earlier in Emami et al., (2018) [57]. This is why the operating cost and GHG emissions need to be assessed along with the energy impact analysis in studies such as this.

Figure 16 illustrates the overall annual total power demand breakdown for the main treatment process units for each of these two scenarios.

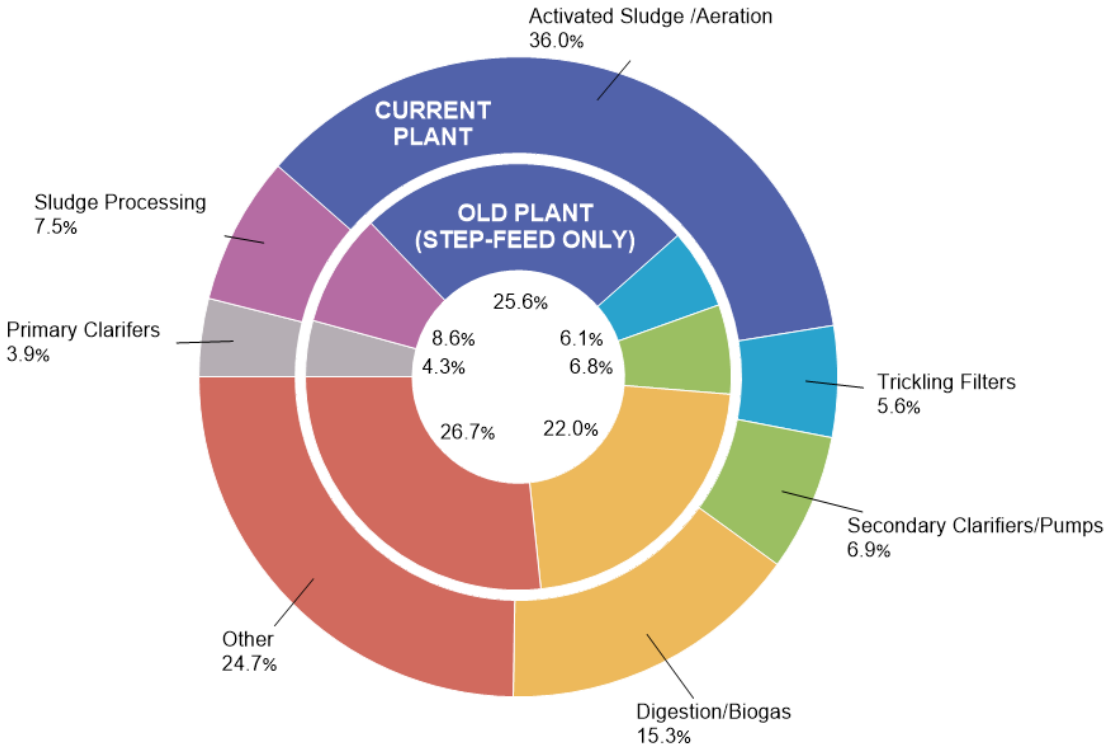

Figure 16. **Total electricity demand breakdown by treatment process unit for current and old step-feed plants' scenarios. The total average daily electricity demand of current and old plant step-feed's normalized to their influent flows are 0.53 kWh m^{-3} and 0.49 kWh m^{-3}, respectively.**

The main difference in electricity demand breakdown for these two scenarios is in the activated sludge aeration power demand, with a larger proportion for the current plant (i.e., 36.0% vs. 25.6%). This was anticipated in the Introduction chapter of this dissertation, where aeration was suggested to be target of electricity demand saving projects.

This difference can be attributed to the different depth for the two processes, with the new expansion in the current plant (MLE configuration) being deeper (>7m, compared to the previous ~4.5m) and the consequent effect of this on the weighted sum of the two processes in the current configuration. Deeper tanks require more pressure from the blowers to support air discharge [16], and have also the associated limitation of lower floor area per unit tank volume. Hence, the diffusers installed in the MLE configuration must be operated at higher air flux, which is inevitably

linked to lower oxygen transfer efficiency [40, 34]. Since the total electricity demand of this scenario is higher than the old step-feed plant's, this higher percentage represents a relevant increase in aeration electricity demand after the facility expansion. In other words, the addition of the new configuration has increased the plant's overall activated sludge electricity demand; thus, did not have expanded its options for demand-side flexibility projects by providing a process change that saves electricity.

The only other category that shows an increase in the electricity demand after addition of the second configuration is secondary treatment pumping and clarifiers. This small increase is mainly result of the additional pumping power associated with the AS2 MLE recycle stream in the current plant. This is a small contribution since in this facility the MLE pump of AS2 consumes less than 5% of the AS2 aeration energy. All other categories of the process energy demand breakdown show a small reduction after expansion.

The electrical energy intensity and demand breakdown comparison discussed here does not account for the better extent of treatment and effluent quality post expansion. Therefore, the effect of expansion on monthly electricity demand is reviewed further in the next section of this chapter using other normalization method explained in the Methods chapter that account for the extent of treatment.

Monthly Electricity Demand

The monthly power demands of these two scenarios are compared using the following three normalization methods that account for extent of treatment. These normalization methods have been discussed in more details in the Methods Chapter.

I. Activated Sludge Energy Intensity

Since the main difference between the two scenarios' electricity demand is driven by the secondary treatment process energy (dominated by aeration), the comparison in aeration power demand is highlighted here using activated sludge energy intensity in Figure 17.

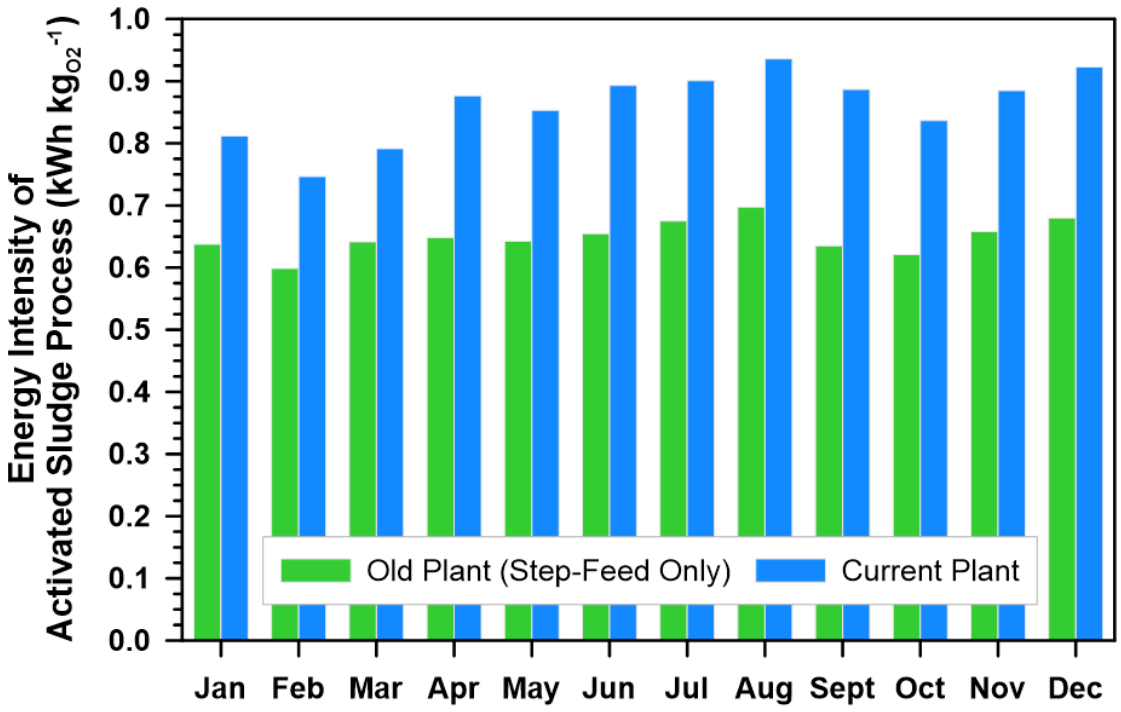

Figure 17. Comparison of the activated sludge electrical energy intensity, defined as the electrical demand per unit of theoretical oxygen requirements, for current and old step-feed plants' scenarios.

As Figure 17 elucidates, the activated sludge energy intensity of the current plant is consistently higher than the old plant's by approximately 33%, on average. As such, after accounting for the higher extent of removal in the current plant's activated sludge, it appears that in this scenario the activated sludge process is less energy-efficient. This conclusion is driven by the energy-intensity of the AS2 MLE activated sludge units added after expansion, which includes the MLE internal recirculation beside aeration and sludge return. This demonstrates the higher electricity efficiency of the step-feed L-E configuration comparing to MLE.

Since no alpha factors for the AS2 were available, the assumptions made for this basin's alpha were selected conservatively, which could have resulted in a conservative estimation of the electrical demand for AS2. Only a direct measurement of the alpha factors could verify these assumptions. Despite this seemingly higher energy intensity, the current plant offers the benefits of increased nitrogen removal, which contributes to the oxygen requirements in the normalization used in Figure 17. This suggests that alternate methods of normalization which are fair to the increased quality of the effluent water are needed here. Additionally and more importantly, the plant reaches a now improved solids separation in secondary effluent, a characteristic of plants with longer sludge retention time [58, 59]. This benefit is welcomed by the downstream reuse operations, whose efficiency is marred by suspended solids [60]. In addition, processes operating at longer sludge retention time are associated with improved removal of trace organics [61], which further enhances the quality of effluent water.

II. Electricity Demand to Quality Index Removal Ratio

Normalized net and total electricity demands to each scenario's quality index [47, 48] removal (QIR) for each month of the year are compared in Figure 18.

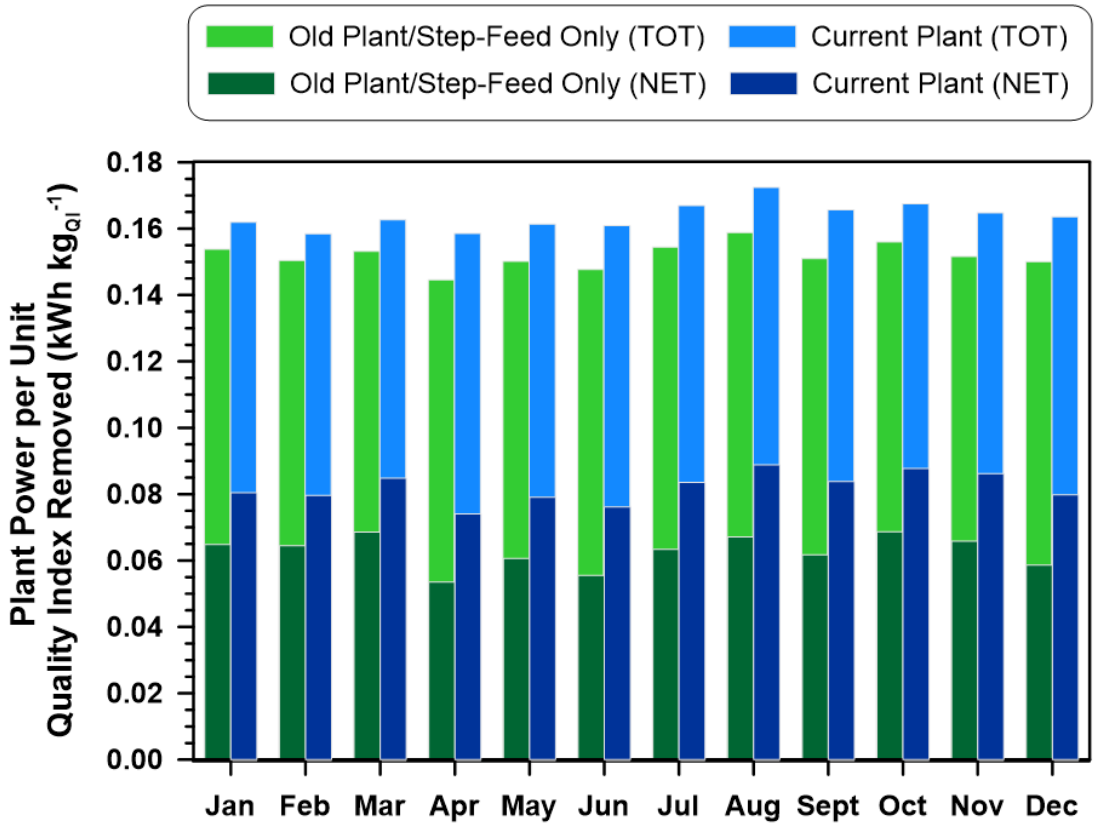

Figure 18. Plant total and net power demand normalized per unit quality index removal for current and old step-feed plants' scenarios.

Figure 18 demonstrates that both total and net power demand to QIR ratios are lower for the old plant by 5-9% and 19-28% of the current plant's, respectively. In other words, even after accounting for the plantwide higher cumulative extent of removal in the current plant scenario, it still requires more electrical energy for treatment. The extent of this power demand discrepancy doubles when net power demand is compared as shown in Figure 18.

III. Electricity Demand to Oxidized Load Ratio

Figure 19 compares the normalized net power demand to oxidized load for both scenarios without supplemental carbon addition.

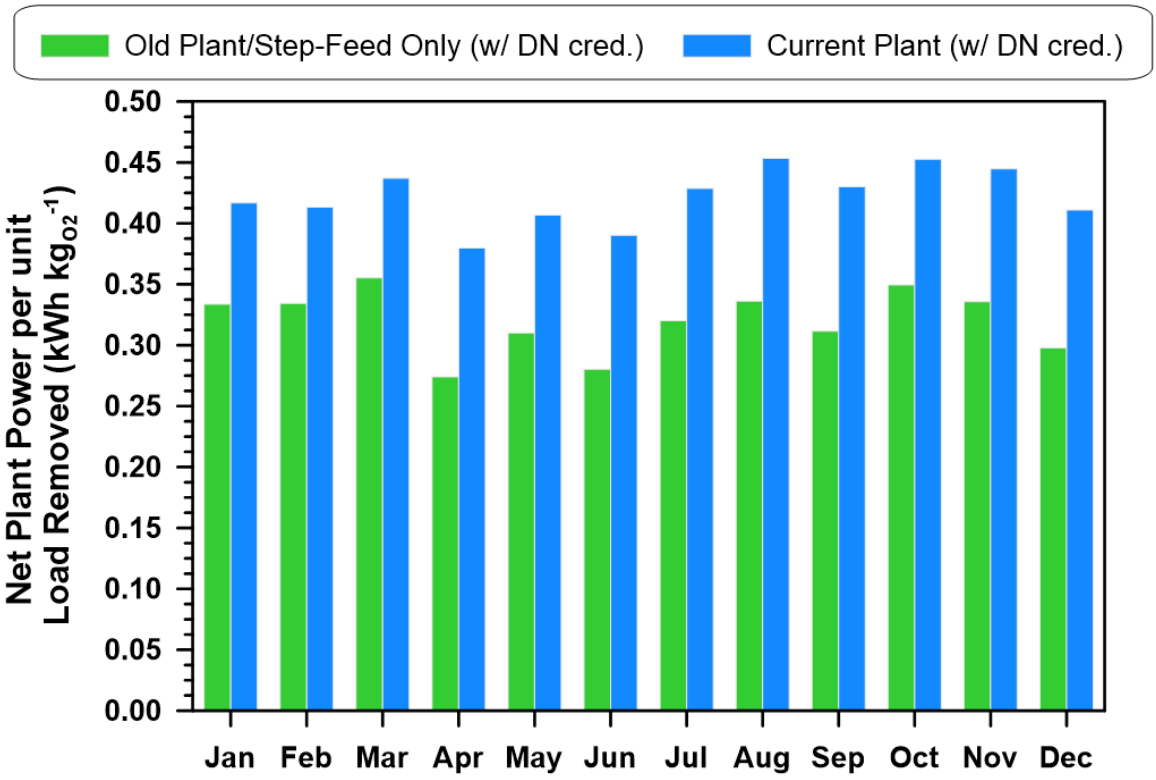

Figure 19. Net power demand normalized per unit of total oxidized load for current and old step-feed plants' scenarios with denitrification credit (i.e., without supplemental carbon).

Similar to the other electricity demand normalizations options, normalizing the net power demand per unit of oxidized load without supplemental carbon also confirms that the old plant scenario is the more energy-efficient option by 19-28%.

In summary all the normalization methods used to compare these scenarios electricity demand concludes the current plant to be less electricity efficient. This translates into demonstrating the MLE configuration as the less electricity efficient comparing to the step-feed L-E in this facility. We attribute this difference to the depth of the MLE process, which places the operating point and efficiency of the aeration diffusers at a disadvantage compared to the L-E process. In addition, the current MLE recycle stream flow is another suspect for this lower efficiency which is recommended to be further evaluated in future studies. More details on this

suspicion have been provided in the Recommendations and Future Research section of this paper.

Greenhouse Gas Emissions

The average daily GHG emissions breakdown by each emission source category as defined in the Methods chapter are compared in Figure 20. The major sources of GHG emissions are the total biological process emissions (i.e., activated sludge and digester processes) which consist of CO_2, CH_4, and N_2O emissions generated by activated sludge and CO_2 emission generated by the anaerobic digesters. The combined combustion emissions of biogas and natural gas consist of CO_2, CH_4, and N_2O emissions constitute the second major source of emissions followed by power import CO_2 and biogas fugitive leak (CH_4) emissions.

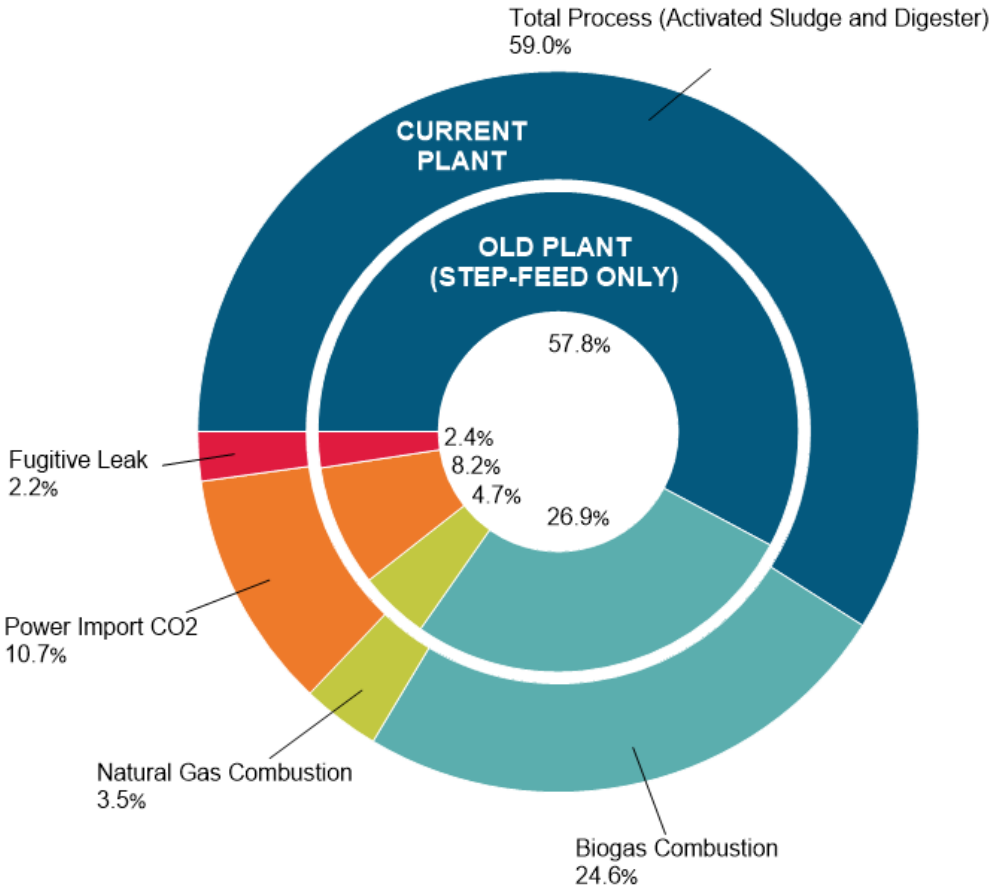

Figure 20. Greenhouse gas emissions breakdown by source type for current and old step-feed plants' scenarios. The total average daily emissions per unit influent flow treated for current and old plants are close (0.623 kgCO_2eq m^{-3} and 0.619 kgCO_2eq m^{-3}, respectively).

The biogas fugitive leak emissions calculated here is heavily dependent of the calculation's assumptions used as there are no direct measurements of the fugitive digester gas, and biogas flow metering is not sufficiently accurate to quantify these emissions. Therefore, its emission quantification has not been captured in GHG quantification protocols [62]. As explained in more details in the Chapter 3, the margin of accuracy of the flow meters also makes the estimation of biogas fugitive emissions using mass or flow balance from field data very difficult if not impossible. The fugitive emission assumption of 1.0% of the total biogas production employed in this study can easily fall within the range of accuracy of the typical flowmeters capable of reading gas flows at a wastewater treatment plant, ranging from 0.5 to 2.0% [51]. Previously, the

assumption of 2% was used in several studies (inter alia, [33, 21]) since it was within the typical margin of error for most large-scale biogas flow meters (i.e., >5%) and corresponded to the assumption by [63]. This range of assumptions has been highlighted as a knowledge gap as early as 2008 [64] and has yet to be addressed fully. A sensitivity analysis was performed to demonstrate the effect of increasing fugitive emissions from 1% to 15% on the plant's overall GHG breakdown for these two scenarios in Figure 21.

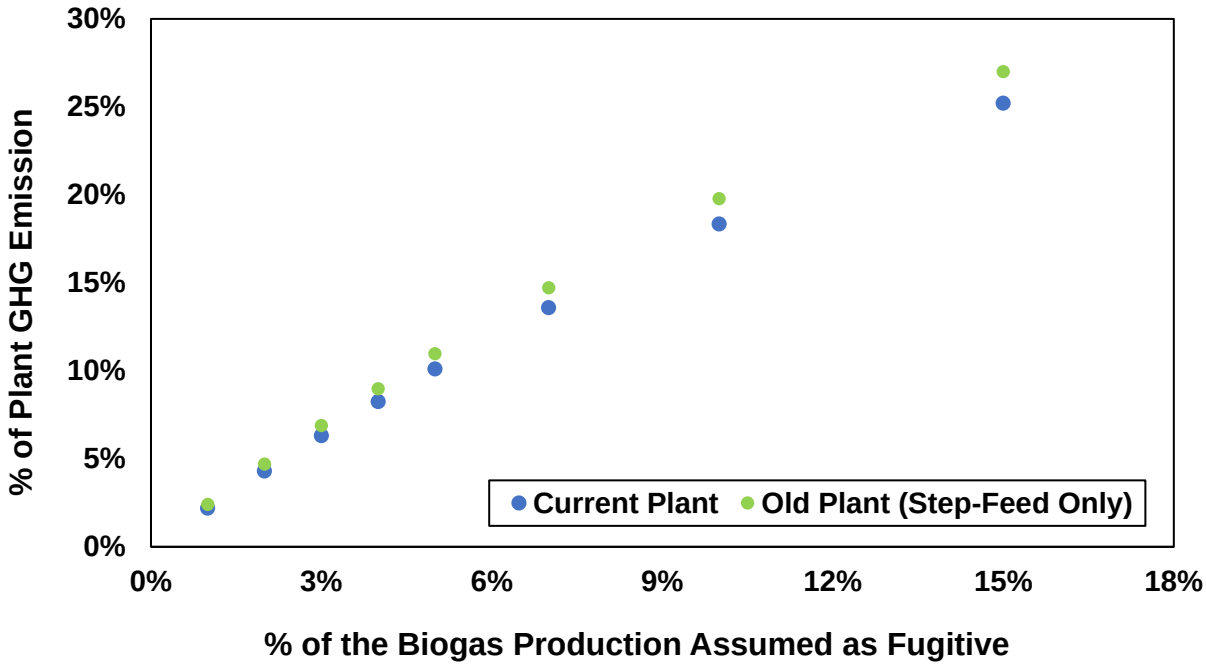

Figure 21. Biogas leak contribution to the total plant greenhouse gas emissions sensitivity analysis.

Incrementally including the fugitive emission in the total GHG calculations results in almost doubling its overall emissions contribution in this sensitivity analysis (2% to 25% in this study). This is due to methane's global warming potential of 25 [42] .

Comparison of monthly GHG emissions normalized to QIR for these scenarios was also presented in Figure 22. This comparison illustrates an insignificant difference of ± 2% between

these scenarios. It also elucidates a subtle seasonality with the current plant having slightly lower emissions in the hotter months (May through September).

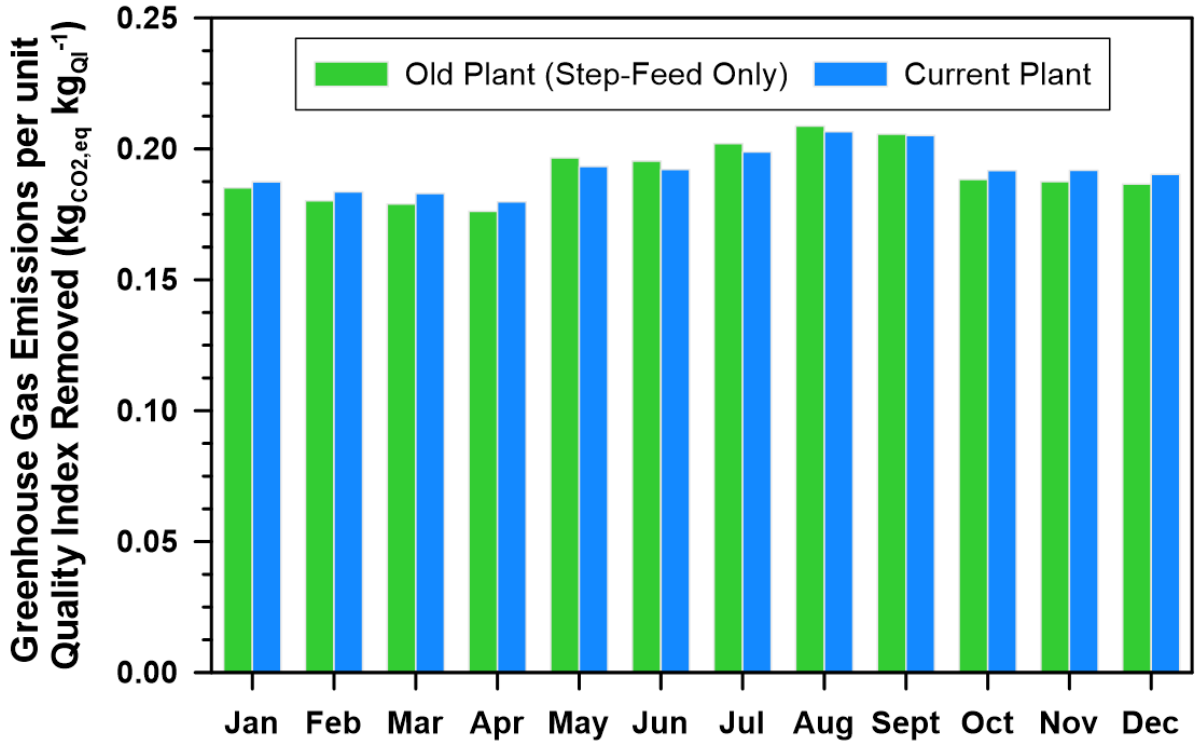

Figure 22. Greenhouse gas emissions to quality index removal ratio comparison for current and old step-feed plants' scenarios.

In summary, the plant expansion seems not to have a considerable impact on the facility carbon-footprint normalized to the extent of treatment. In other words, addition of the less electricity efficient activated sludge configuration to this plant as part of the expansion is not impacting its GHG emissions per unit overall removal quantified by QIR. This conclusion however may change with changing the assumption used to estimate the biogas fugitive emissions per sensitivity analysis performed in this section.

Operating Cost

For the two scenarios discussed in this chapter the operating cost based on the 5 different power tariff structures presented in Figure. 9 were compared. In addition to the grid's electricity import cost, costs of following activities have been calculated and captured here: chemicals used for enhancing primary treatment; sludge dewatering and thickening chemical additives; biosolid disposal; and natural gas imports. More details about the methodologies used for each of these activities' cost estimation are provided in the Methods chapter.

These costs are normalized per unit QIR similar to other comparisons performed in this chapter to also account for the extent of the treatment in each scenario. Since each treatment scenario would have 5 tariff sub-scenarios, the ratio of the normalized total operating cost of the current plant scenario to the old step-feed plant scenario's are estimated and used here to simplify the comparison. These ratios for each month of the year in the study period are presented in the Figure 23 below.

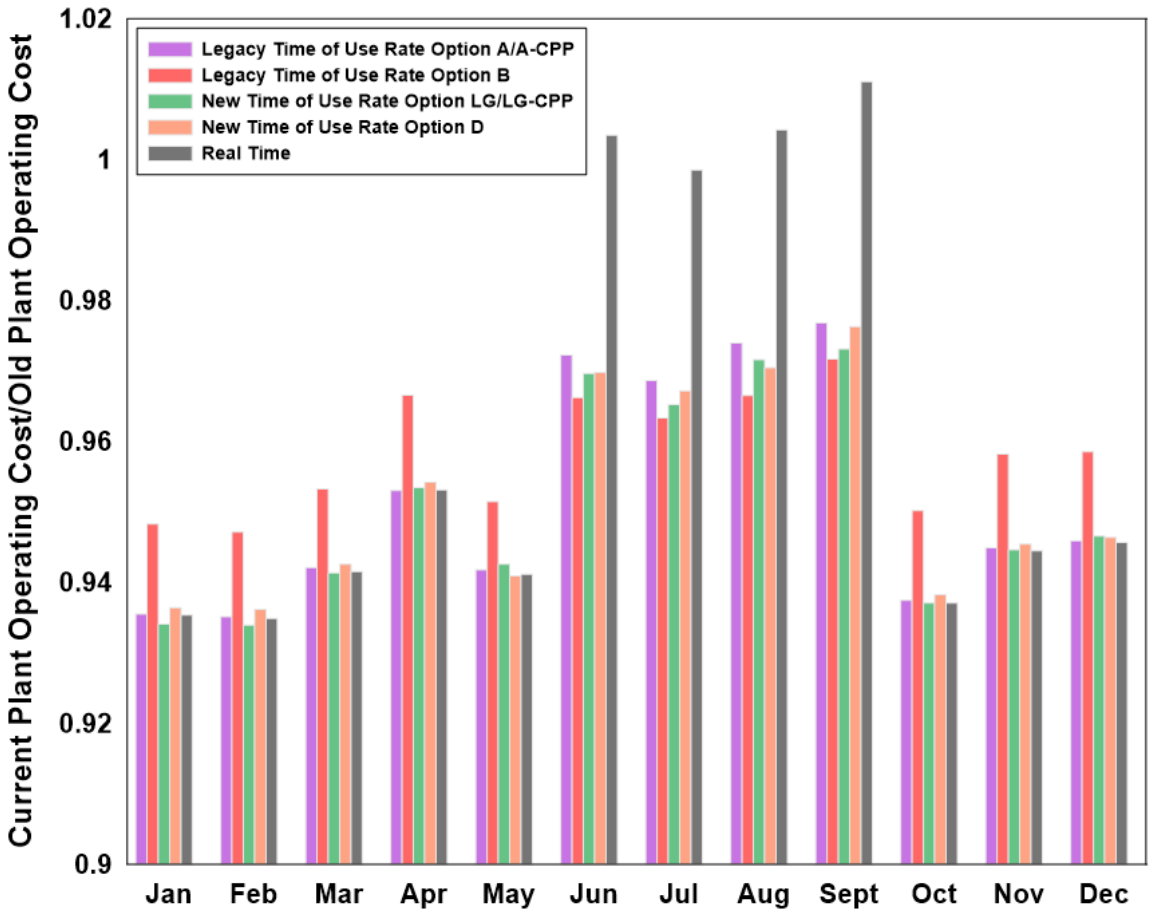

Figure 23. Operating cost per unit quality index removal for current and old step-feed plants' scenarios, applying the five power tariffs in Figure 9. The results are presented as dimensionless ratios, with the past configuration (old step-feed plant) in the denominator. Annual operating cost to unit quality index removal ratio calculated using the average of these 5 tariffs annual electricity cost for current and old step-feed plant are 41.98 USD per metric ton and 43.90 USD per metric ton respectively.

Figure 23 demonstrates that the normalized operating cost calculated using all the five electricity tariffs for this plant have been reduced post expansion for every month except for Real Time tariff in summer months when the cost is almost the same or about 1% higher. It also shows that overall operating costs estimated using tariff options B (a legacy tariff) and Real Time (a new tariff) are significant different than the other four tariffs' in winter and summer months respectively. This elucidates the significant effect of different tariff structures on the economic outcome of this expansion project and why changes in the electricity tariff structure in response to the increase of

renewable electricity sources, captured in new tariff (e.g., Real Time), can significantly impact WRRFs operating cost.

The significantly higher operating cost of the Real Time option in the summer months comparing to the other tariffs can be explained by it significantly higher summer energy usage charges during peak demand periods, comparing to all other tariffs. The higher cost of Option B in the winter months can be substantiated by having the highest excess capacity reserve charge component of the facility electricity demand charge among these 5 electricity tariffs. This reserve charge applies to the portion of the facility total electricity demand that exceeds a standby demand value that is agreed upon between the facility and the electricity provider and is usually based on the facility historical electricity generation data. This standby demand is assumed to be the same as the facility typical average electricity generation nameplate capacity for this study (5.2 MW). More details about the demand charges for each of these tariffs are provided in the Methods chapter. This higher facility demand charge for Option B should have affected all the months of the year and not only winter's. However, this tariff's lower total energy usage charges in the summer compared to the winter, which is unique to this tariff option, alleviates its high demand charge in the summer months resulting in comparable overall operating cost with the other tariffs except for Real Time's.

Figure 23 also clearly demonstrates the effect of electricity seasonality on the overall cost comparison here and how higher cost of electricity in summer months can significantly increase the operating cost of the WRRF. In other words, all the tariff options show significantly higher operating cost difference for these two scenarios in the summer months, which can be explained by the higher electricity cost (i.e., total energy usage or demand charges) especially during the peak of electricity demand, as reported in the Methods chapter. This observation is also another proof for the role of applying the dynamic power tariff profiles in the accuracy of WRRFs' modelling

efforts such as this one, and how using an average value for the entire year instead will ignore the effect of this significant seasonal tariff increase.

The overall lower operating cost of the current plant, illustrated by ratios of less than 1, in Figure 23 for almost all the tariff options, demonstrates that the non-electricity portion of operating cost components accounted for in this study compensates this scenario's slightly higher electricity cost. Comparing the other annual operating cost components values normalized to the QIR for current and old-step-feed plants suggests that these compensating components are chemical and natural usage costs with the chemical usage being the dominating one. Since the primary treatment has not been impacted by the expansion project, the chemical usage for enhancing its performance and its sludge thickening and dewatering normalized to total QIR is expected to be the same for both scenarios. Therefore, the chemical usage cost saving observed here can be narrowed down to the secondary treatment's waste sludge dewatering and thickening. The lower normalized secondary sludge waste stream flow that goes through dewatering and thickening in the current plant scenario comparing to the old step-feed plant scenario clearly substantiates the chemical usage cost saving of this option which is calculated from this stream flowrate using a constant cost to flow ratio. This lower secondary sludge waste generation can be explained by better solids separation in secondary treatment of the current plant due to its activated sludge longer sludge retention time in the MLE reactors [58, 59].

In addition to less chemical demand, the lower secondary sludge waste production in the current scenario reduces its thermal energy demand at the facility digesters and increases the digesters' capacity (i.e., their retention time). This results in reducing this scenario's natural gas import by lowering its overall thermal energy demand and increasing its biogas production, which is largely driven by primary sludge conversion to methane [33]. This phenomenon can be clearly demonstrated by the lower normalized natural gas usage cost to QIR in the current scenario comparing to the old step-feed's.

In short, the expansion of the plant had other benefits than just increasing the facility treatment capacity which included improvement of the overall effluent quality of the facility as well as reducing its natural gas and chemical demands resulting in overall reduction of the treatment cost and ultimately of its environmental footprint. The observed overall operating cost reduction here demonstrates that the combined chemical and natural gas demands cost savings of the expansion overcomes its electricity cost increase. In other words, it substantiates the less electricity efficient combination of the AS configurations post-expansion is more cost effective. Thus, lowering the plant's electricity demand by increasing the use of more electricity efficient activated sludge configuration (AS1 or step-deed configuration), will increase its overall operating cost and effluent pollution which makes such an electricity saving undesirable and infeasible from economic and environmental standpoints.

This inverse effect of reducing this facility's electricity demand, by increasing the use of its more electricity efficient activated sludge configuration of the two, on its overall operating cost also demonstrates the infeasibly of the proposed demand-side flexibility project in beginning of this chapter. This conclusion and inverse effect; however, can be reversed by increasing the electricity efficiency of the MLE configuration to exceed the step-feed's. In this case, the electricity cost savings associated with maximizing the use of the more efficient configuration (MLE) is added to this configuration's chemical and natural gas demand cost savings. Thus, such power saving project in this plant also becomes economically feasible. This electricity savings is also expected to lower the plant overall carbon-footprint by lowering the contribution of the indirect GHG emissions associated to the imported electricity from the grid. This reduction in the plant carbon-footprint along with the higher extent of the treatment in the MLE configuration (as demonstrated earlier) further reduces the overall environmental footprint of the expanded plant.

The positive economic and environmental impact of improving the electricity efficiency of the MLE section of the current plant's and its role on making the proposed demand-side flexibility

project in this chapter feasibility, motivated a brief side-research. This side-research focused on introducing different strategies that can increase the electricity efficiency of this AS configurations for future research. The findings of this brief research effort are summarized in the Recommendations and Future Research section of this chapter.

Recommendations and Future Research

Comparing the effluent nitrogen (ammonia, nitrite, and nitrate) trends with the plant's influent ammonia (~66% of influent TKN-N; Appendix F) for the two activated sludge scenarios compared in the Effluent Quality section of this chapter, concludes slightly higher nitrification and denitrification in the current plant scenario. This is despite the fact that much higher denitrification and lower effluent nitrate and ammonia concentrations are expected from the current plant after addition of the MLE configuration as part of the plant expansion. This lower denitrification performance is likely due to high MLE recycle-stream flow and is a potential explanation for higher aeration electricity demand post-expansion. Thus, further studies to investigate this issue are recommended for the large WRRF studied here in addition to collecting field alpha data for MLE configuration as remarked in electricity demand analysis summarized in this chapter.

The MLE recycle stream at the current plant is set at about 200% of the AS2 influent. High flow recycle streams in the AS2 bioreactors in series deviates the performance of these reactors from plug-flow to continuous stirred tank reactor (CSTR) configuration, which is characterized by lower conversion rates. Thus, the extent of denitrification may have been lowered by excessive MLE internal recycling here which is a great hypothesis for future energy efficiency studies at this plant. The effect of lowering this recycle stream flow on the normalized electricity demand would be twofold: reduction of pumping energy and increased plug-flow characteristics (hence, higher pollutant removal in the same reactor volume). As such, future studies are needed and recommended to optimize the MLE recycle stream at this plant. Once and if optimized, the same

assessment performed in this chapter shall be repeated to determine the feasibility and technicality of the demand-side flexibility project proposed in the beginning of this chapter.

Limitations and Considerations

The results of this study shall not be blindly extended to other plants as each plant has its own characteristics, treatment targets, and distinct geometry and equipment. In the facility studied here, the concentration of nitrogen in the effluent is almost immaterial and effluent solids concentration is the main treatment concern. Thus, optimizing the nitrogen in effluent is a minor priority in contrast with other plants where water reclamation results in distribution (e.g., for irrigation). In order to extrapolate the results of activated sludge basins in this study to other plants with similar volumes, the geometry must also be accounted for as the distribution of the flow depends on the length of the basin not its volume. Therefore, in such a comparison, a large difference in the reactors' length causes the geometry to suffer; therefore, different results should be expected. The reduced length deviates this reactor from plug-flow configuration and makes it more like a CSTR at the cost of lowering the extent of reaction and removal as explained earlier in this chapter. Additionally, for a given volume, reactors with reduced surface area must be deeper, which reduces the number of diffusers that can be installed on the tank floor and forces their operating point at higher flux (i.e., less efficient). Therefore, analyzing the geometry in a case-specific basis and optimizing the flow rate for returns to make sure the denitrification meets the target of that specific utility is more important than us trying to infer that our findings in this chapter are true for every plant with the same process volumes. Similarly, site-specific dynamic electricity tariffs, power grid GHG intensities, and alpha factors need to be considered before extending the results of this study to other plants.

Summary

This chapter underlined how the diurnal cycles and peaks of the grid electricity tariffs and carbon intensity coincide with a large WRRF's peak of influent load and power demand in California. Illustrating the coincidence of these parameters and the amplifying effect of these coincidence in the facility electricity import cost and carbon-footprint, it also demonstrated the importance of dynamic modelling of these facilities to correctly assess their electricity demand cost and carbon-footprint.

The coupled bioprocess and power dynamic analysis summarized in this chapter was performed to study the effect of an expansion project on power demand, carbon-footprint, and the operating cost of this facility. Having two independent parallel activated sludge process configurations after this expansion which are fed the same influent was the reason for selecting this plant. This parallel set up allows reducing the current facility's overall electricity demand by increasing the more electricity efficient configuration's share of the influent treatment. The coincidence of this plant's peak of electricity demand with the power grid's peak of cost and carbon intensity here suggested additional benefit for this potential power-saving option during the grid's peak of demand, which could be a target for demand-side flexibility incentives.

Both net and total electricity demand of this WRRF for pre- and post-expansion scenarios, accounting for these scenarios' extent of treatment using different normalization methods, were compared in this chapters. This comparison demonstrated that the addition of the second activated sludge configuration (MLE) as part of the expansion lowered the activated sludge and plant's overall electricity efficiency. However, it reduced the plant's operating cost (despite the increase in its electricity demand and cost) and slightly improved its effluent quality without significantly impacting its overall carbon-footprint. In other words, the increase in energy intensity due to this expansion project was ultimately compensated by a decrease in overall operating cost which was explained to be due to reduction in chemicals and natural gas usages. This inverse

correlation between electricity demand and overall operating cost of the expanded plant substantiated the infeasibility of the demand-side flexibility project (proposed in this this chapter) that would target electricity savings by maximizing the use of the more energy efficient activated sludge configuration in this plant.

By lowering the plant's overall activated sludge energy efficiency after the expansion, despite the expectation for improving it, the added activated sludge configuration (MLE) demonstrated to be in a need for optimization and further process geometry analysis. The MLE recycle stream flow adjustment was an area that this study recommended for such process optimization efforts in the future studies. Such an optimization is expected to also improve the effluent quality in addition to the cost and carbon-footprint reductions associated to electricity savings resulting from this optimization. In addition, such an optimization project can reverse the conclusion of this chapter on the infeasibility of the demand-side flexibility project that maximize the use of the more energy-efficient activated sludge configuration in the current facility. To achieve this goal the optimized MLE configuration shall exceeds the energy efficiency of step-feed L-E's.

Lastly, this chapter prohibits extending the results of this study to other WRRFs without considering these plants' characteristics, treatment goals, and distinct geometry differences as well as their site-specific dynamic grid electricity tariffs, GHG intensities, and alpha factors.

CHAPTER 5: BENEFIT OF NITROGEN REMOVAL FROM DYNAMIC ENERGY AND OPERATING COST STANDPOINT

As explained in the previous chapters, improving the secondary solids separation and energy-savings in the activated sludge were explained to be the theoretical justifications for performing nitrogen removal at this WRRF [35]. The coincidence of this plant's influent load and electricity demand diurnal cycles with the grid's electricity tariffs as well as significant contribution of activated sludge (where nitrogen removal is preformed) to the plant's overall electricity demand, as demonstrated in Chapter 4, suggests the translation of nitrogen removal energy-savings to a significant operating cost saving. However, improving the extent of water treatment has been always the focus of WRRFs not the operating cost savings [65]. As such, energy-saving and its associated cost-saving may have not been the focus of feasibility analysis performed to justify the implementation nitrogen removal at the activated sludge section of this facility when it was implemented. Comparing the plant's energy demand and operating cost before and after this change will reveal the advantages and disadvantages of nitrogen removal at this facility from the cost- and energy-savings standpoint.

Prior to implementing the nitrogen removing step-feed-only (or old plant step-feed) activated sludge (AS) configuration (discussed in detail in Chapter 4), the activated sludge at this plant employed standalone carbon-oxidation or plug-flow configuration which did not perform any nitrogen oxidation and removal. More details about these two AS configurations that are immediately preceding the plant's current configuration are provided in the Methods chapter. Simplicity of building the dynamic simulation model of the old plant plug-flow from the old step-feed configuration model developed for Chapter 4 analysis, and curiosity about the effect of new electricity tariffs on this configuration change's cost-savings were the motivating factors to compare these two scenarios in this chapter. Similar to Chapter 4, extent of treatment, electricity demand, carbon-footprint and operating cost of these two superseded activated sludge

configurations are compared using dynamic models incorporating the diurnal trends of this facility's influent load, as well as the electricity grid's cost and carbon intensity dynamics. This comparison will allow us to determine the pros and cons of addition of nitrogen removal which was implemented by changing this facility's AS configuration from standalone plug-flow (or carbon-oxidizing-only) to step-feed.

There has been a myth in the water treatment industry suggesting that addition of nitrogen removal in warm climates results in increasing the facility electricity demand and cost due to additional aeration requirement. The result of this study can also verify the validity of this myth at a large WRRF in the warm California climate. This analysis can also verify the findings by Rosso and Stenstrom, al., (2005) on the effect of nitrogen removal on increasing the efficiency of aeration and reducing the combined operating cost in this WRRF [34].

The process overview for the activated sludge (AS) configurations reviewed in this chapter (i.e., standalone old plant plug-flow and standalone old plant step-feed) have been compared in Figure 4 in the Methods chapter. The assumptions made, calculations performed, and data collected for developing these scenarios dynamic models are also explained in the Method chapter. As such this chapter only focuses on the results of these scenarios comparison. To simply the nomenclature used for these two scenarios, the reference to the "old plant" and "standalone" have been omitted from the scenario names and their names are shortened to plug-flow and step-feed in the text sections of this chapter.

Simulations for both step-feed and plug-flow scenarios were completed using dynamic influent and process profiles and by completing the dynamic alpha factor iterations as discussed in the Methods chapter. The results of these simulation are compared by their categories in following sections:

Effluent Quality

The effluent concentrations of TSS, CBOD, ammonia and nitrate for these two scenarios have been compared in Figures 24 through 27.

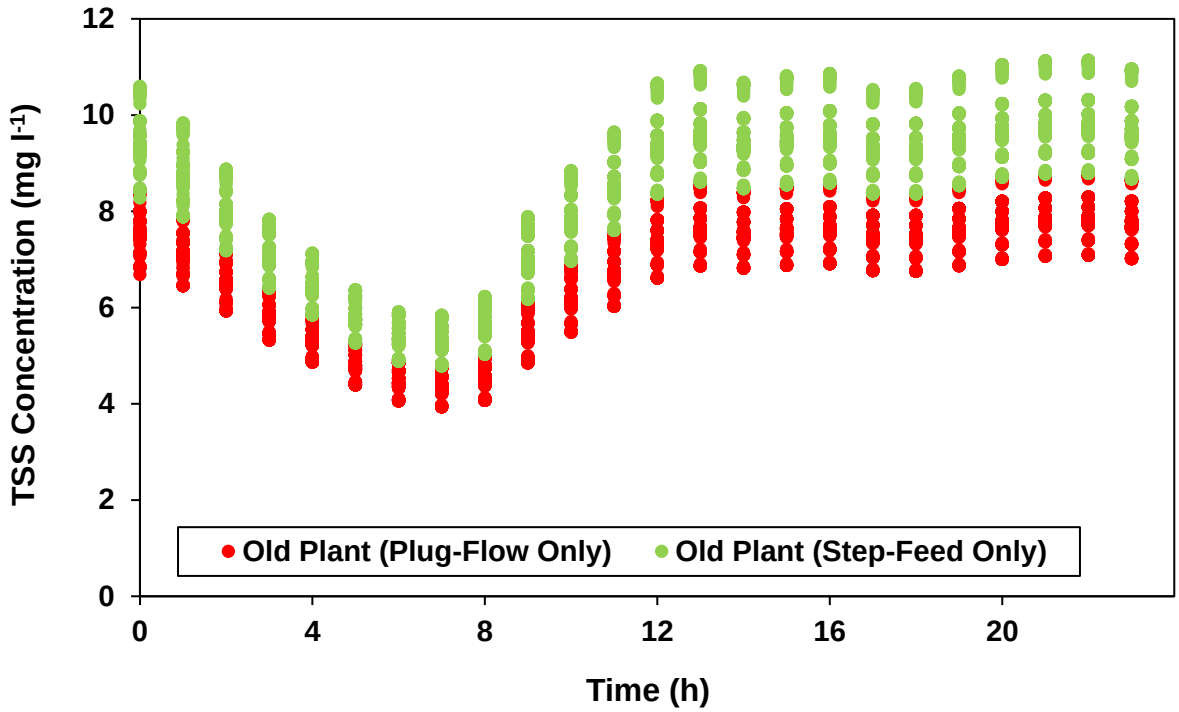

Figure 24. Facility's effluent TSS concentration comparison for plug-flow and step-feed scenarios.

Figure 24 demonstrates that effluent TSS concentration is higher in the step-feed scenario comparing to the plug-flow by 0.5 to 1.5 mg l^{-1}. The higher TSS can be explained by the step-feed configuration's higher mean cell residence time (MCRT) required for the growth and performance of microorganisms that perform the nitrogen removal (i.e., Autotrophs). The historical field sampling record used for this modeling effort provides average MCRT of 4.6 and 1.1 days for the step-feed and plug-flow configurations at this plant, respectively. This higher MCRT is achieved by increasing the flow of activated sludge recycled back to the beginning of the AS basin by reducing the waste activated sludge (WAS) stream which is sent to digesters. This higher recycling of AS in the step-feed scenario increases the concentration of solids in the activated

sludge reactors (a.k.e., mixed liquor suspended solids or MLSS); therefore, increases the load of the solids that enter the secondary clarifiers translating into higher effluent TSS concentration.

The CBOD effluent comparison in the Figure 25 shows the opposite trend of TSS's and demonstrates higher CBOD concentration in the effluent of plug-flow scenario. This can be also explained with higher MCRT of step-feed which increase the number of carbon consuming microorganism in the system (i.e., heterotrophs and autotrophs) resulting in higher extent of CBOD removal in the step-feed.

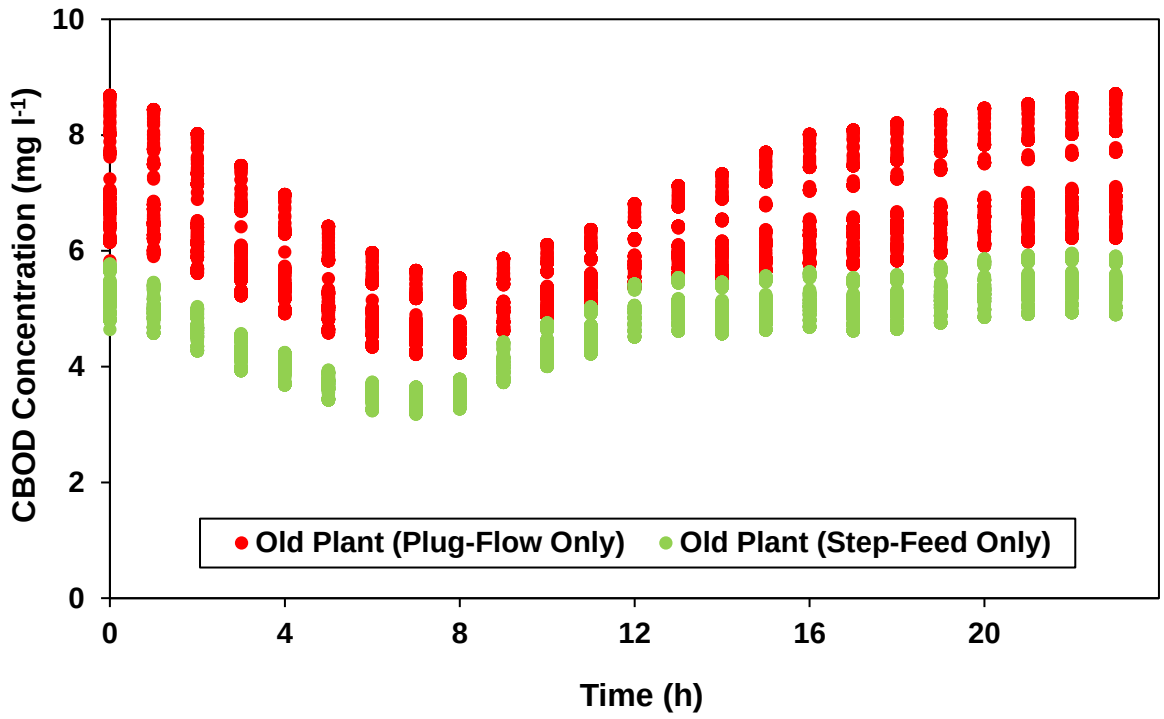

Figure 25. Facility's effluent CBOD concentration comparison for plug-flow and step-feed scenarios.

As explained before no nitrification and denitrification (i.e., nitrogen oxidation and removal) can be performed in the small MCRT of the plug-flow configuration, which explains the significantly higher concentration of ammonia in the effluent of this configuration comparing to negligible traces in the step-feed's in Figure 26. Same explanation can be provided for zero concentration of nitrate demonstrated in the Figure 27 for the plug-flow configuration.

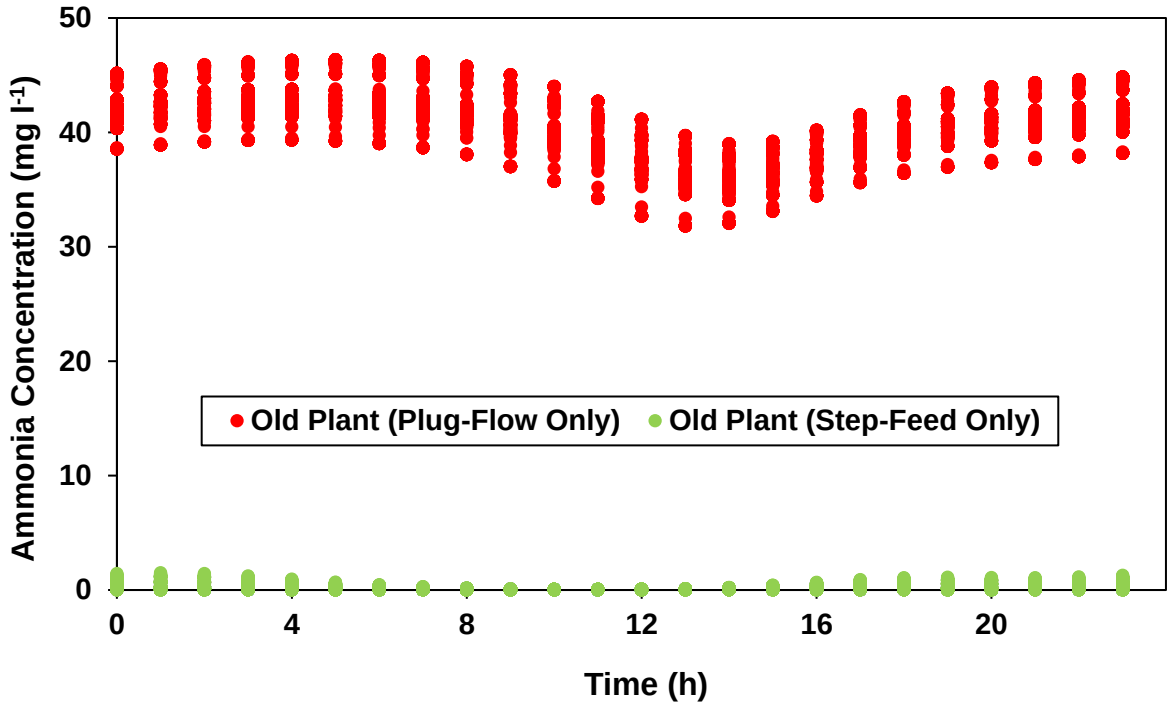

Figure 26. Facility's effluent N-NH_3 concentration comparison for plug-flow and step-feed scenarios.

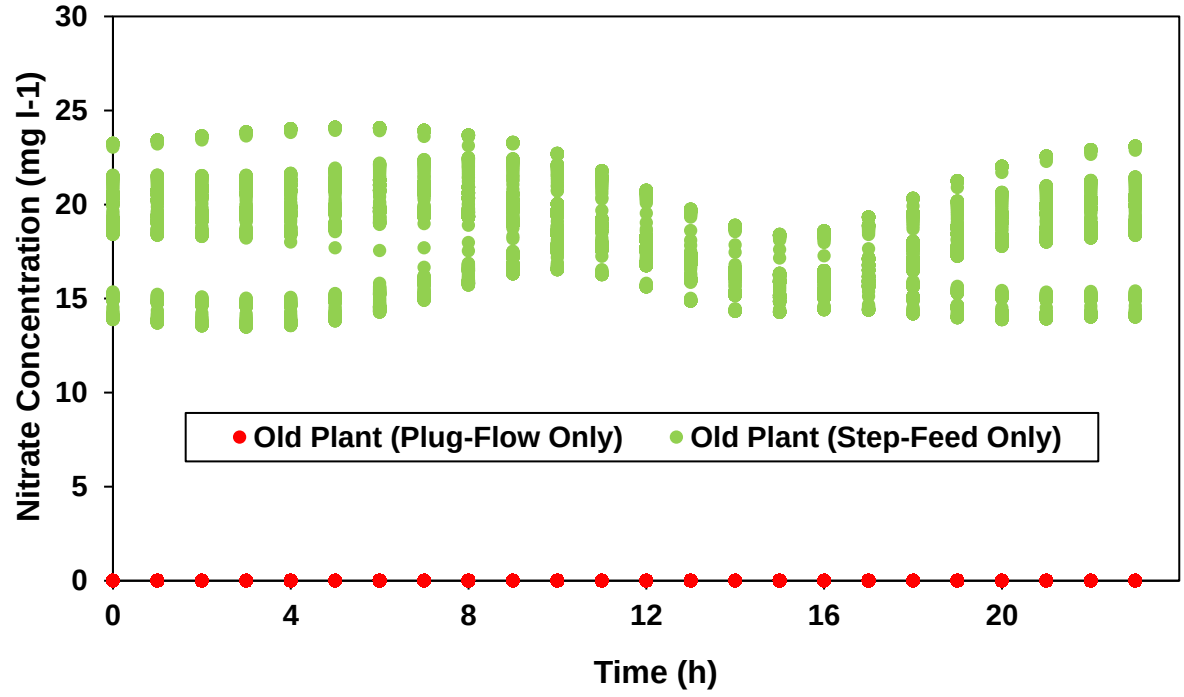

Figure 27. Facility's effluent N-NO_3^- concentration comparison for plug-flow and step-feed scenarios.

To simplify the comparison of the effluent quality for these scenarios, a cumulative comparison was conducted using effluent quality index (EQI) [47, 48] which explained in more details in the Methods chapter. EQI is defined as weighted measure of pollution; therefore, higher EQI is antithetical to effluent quality. Since the influent flow values used for modeling these two scenarios were slightly different (as explained in Methods chapter), the calculated EQI for these scenarios' comparisons were normalized to the plant influent flow to account for this slight difference and to have a fair comparison of these scenarios.

Comparing the monthly normalized EQI for the two scenarios here in Figure 28 demonstrates that plug-flow's normalized EQI is more than quadrupole of step-feed's, corresponding to worst effluent quality. In other words, the plant decision on converting the plant to step-feed from plug-flow is in line with the focus of every WRRFs which is improving the extent of treatment [65].

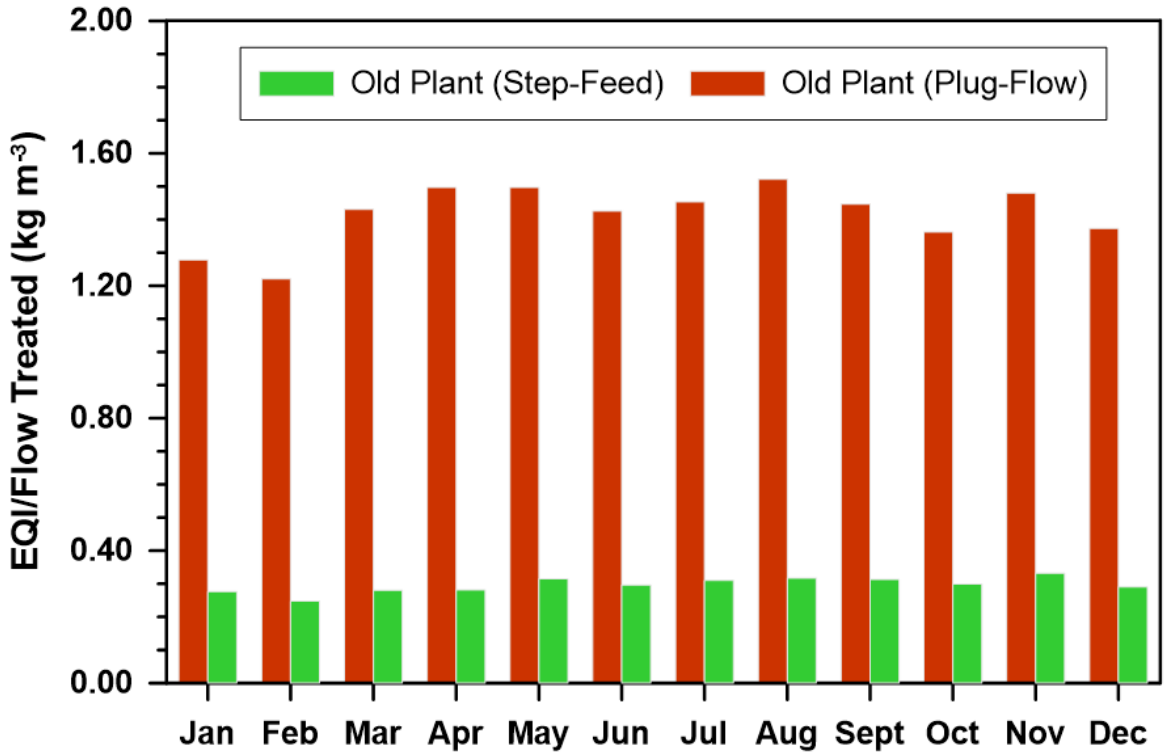

Figure 28. Monthly effluent quality index (EQI), normalized per unit flow treated, for plug-flow and step-feed scenarios. Note that lower values in the vertical axis imply better quality of effluent water.

The definition of the EQI assigns a low weight to the TSS in the effluent, given their reduced impact to the receiving water body when compared to more reactive nitrogenous species such as ammonia and nitrate. This explains the significantly lower extent of EQI in the step-feed scenario that removes larger amount of nitrogen comparing to plug-flow despite plug-flow's higher TSS removal. The removal of TSS is of much importance for the facility here as the effluent is fed to a water reuse facility where solids selectively affect the energy demand for filtration in that facility. Increasing the step-feed's TSS removal seems to be one of the reasons for expanding the plant to its current configuration by adding additional activated sludge and secondary settling capacity which has been discussed in Chapter 4.

Electricity Demand

Figure 29 illustrates the overall annual total electricity demand breakdown for the main treatment processes of each scenario.

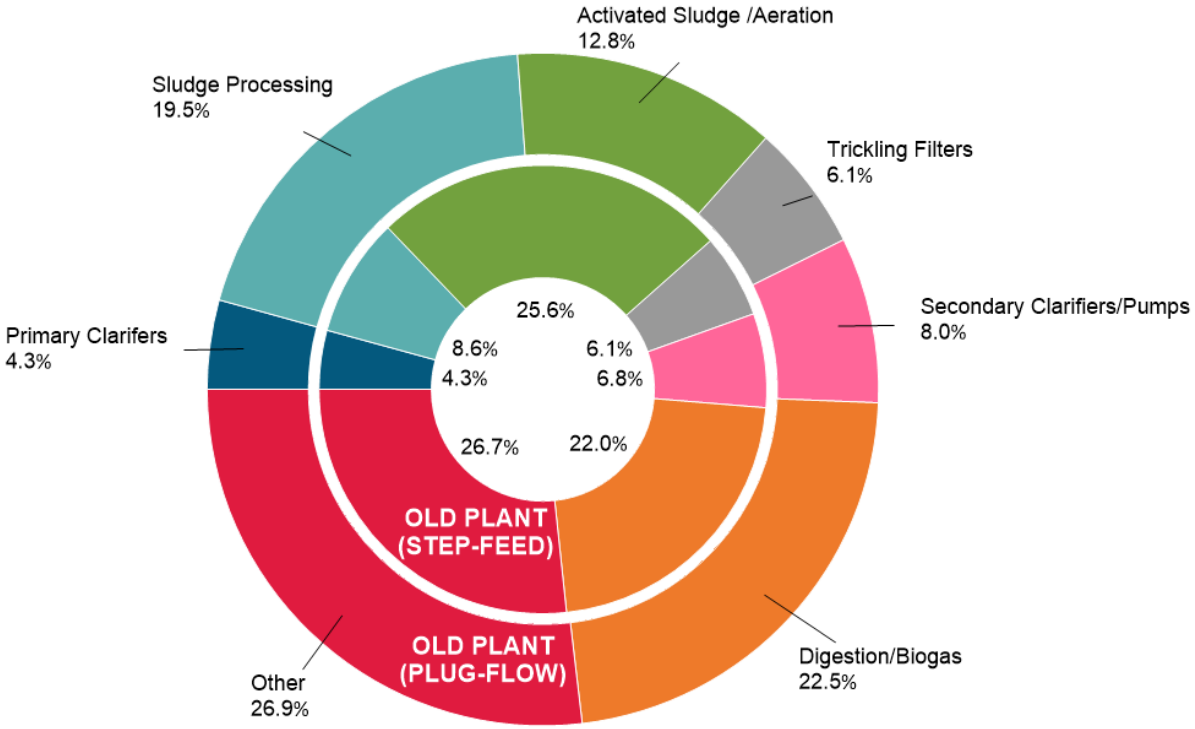

Figure 29. Total electricity demand breakdown by treatment process for plug-flow and step-feed scenarios. The total average daily electricity demand of old plant step-feed and plug-flow scenarios normalized to their influent flows are 4.93×10^{-1} kWh m^{-3} and 4.89×10^{-1} kWh m^{-3}, respectively.

Almost the same total average daily electricity demand normalized to plant influent flow (< 0.7% increase) and power demand breakdowns for most of the processes in these two scenarios are portrayed in Figure 29. As such, it can be concluded that addition of the nitrogen removal by switching from plug-flow to step-feed configuration does not change the power demand of most of this facility's process units. The only process units that demonstrate a change in electricity demand are sludge processing (i.e., sludge thickening and biosolids dewatering and loading) and activated sludge. However, a closer look at Figure 29 elucidates that sum of these two electricity demand categories are almost the same for both scenarios. In other words, addition of nitrogen

removal in the step-feed scenario only diverts some of the electricity demand from sludge processing of the plug-flow scenario to the activated sludge aeration in the step-feed. This invalidates the myth suggesting larger power demands in WRRFs that remove nitrogen in comparison with carbon-oxidizing treatment facilities.

To fairly compare these two scenarios' electricity efficiency, their extent of treatment needs to be simultaneously accounted for. As such, the monthly power demands of these two scenarios are compared using three normalization methods presented in the Methods chapter.

I. Electrical Energy Intensity

Dynamic net and total electrical energy intensity for both scenarios (as defined in the Methods chapter) have been compared in Figure 30. In this figure, we can see that the improved cumulative effluent quality after switching the activated sludge configuration to step-feed corresponds to change in total energy intensity ranging from -0.07 to 0.05 kWh m^{-3}. Closer comparison of total energy intensities in this study concludes that step-feed has larger total energy intensity than plug-flow during 58% of the study period and plug-flows is larger in the remaining 42%. This configuration change also results in changing in net energy intensity ranging from -0.04 to 0.07 kWh m^{-3}. For 74% of the study period step-feed's net energy intensity is higher than plug-flow. In short, changing the AS configuration to step-feed can be concluded to mostly lower the facility's net power demand efficiency when the facility influent flow is used as the normalizing parameter.

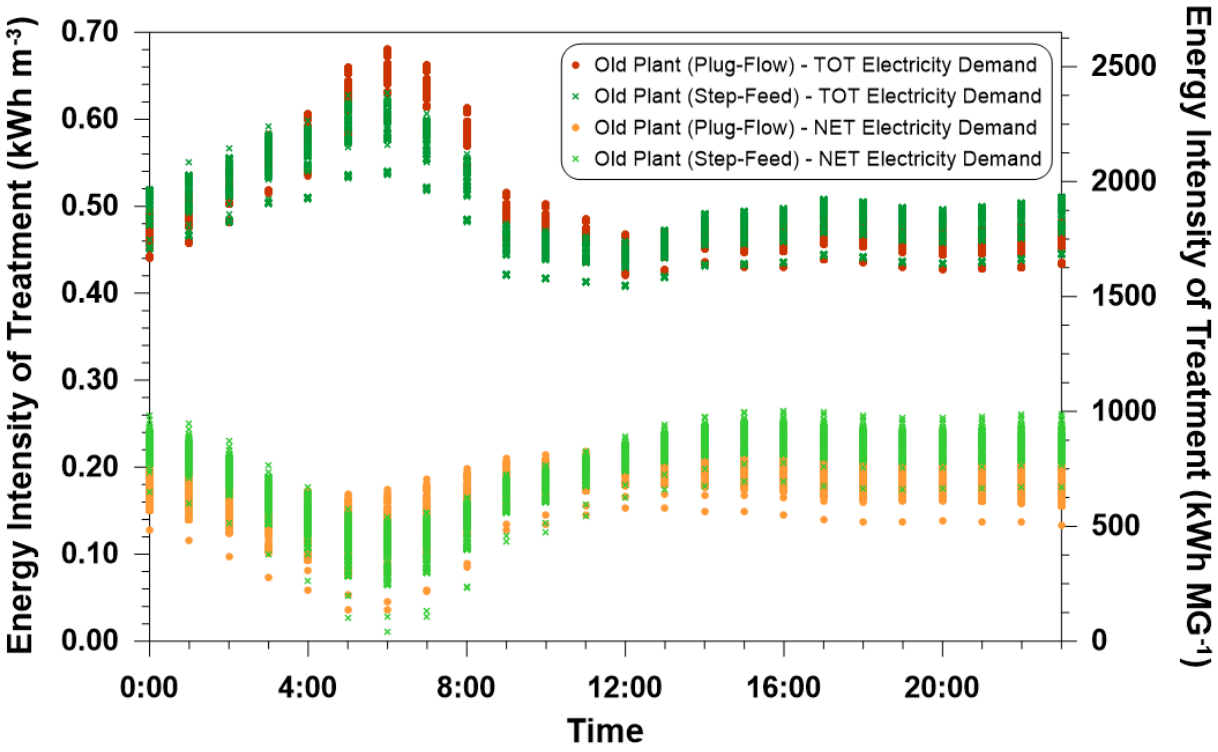

Figure 30. Dynamic net and total treatment electrical energy intensities (demand normalized to plant influent flow) for plug-flow and step-feed scenarios. Both Y-axes apply to the data points plotted.

The total electrical energy intensity is minimum or close to it at the peak of plant influent load (between 12:00 and 23:00) while the net intensity is maximum. This is despite the fact that the hourly trends for both the net and total electricity demands follow the same trend as influent flow and net power demand energy intensity's and all peak between 12:00 and 23:00. Thus, the reciprocal trend of total and net electrical energy intensity in Figure 30 is due to a different magnitude of the net and total power demand values compared to influent flows where these demand values are normalized to the same influent flows to calculate the net and total energy intensity values here.

Comparing the dynamic net power intensity trends in Figure 30 with the grid's electricity CO_2 emission intensity and tariffs diurnal trends in Figure 8 and Figure 9, respectively, elucidates the coincidence of the peak of these three parameters for both scenarios at this WRRF similar to the references mentioned in the Introduction. As indicated in the previous chapter, this

coincidence results in the amplification of the peak of the grid's electricity import cost and GHG emissions during the peak of these scenarios' net power demand, a phenomenon identified earlier in Emami et al., (2018) [57]. This is why the operating cost and GHG emissions need to be assessed along with the energy impact analysis in studies such as this. Since plant influent flow does not fully capture the extent of the removal for its different influent constituents, other normalization methods were used for the electricity demand comparison of these scenarios in the next few sections of this chapter.

II. Activated Sludge Energy Intensity

Since aeration power demand is the main concern of all the myths evolved around disadvantages of nitrogen removal, the comparison of aeration electricity demand is highlighted using activated sludge energy intensity (defined in the Methods chapter) in Figure 31.

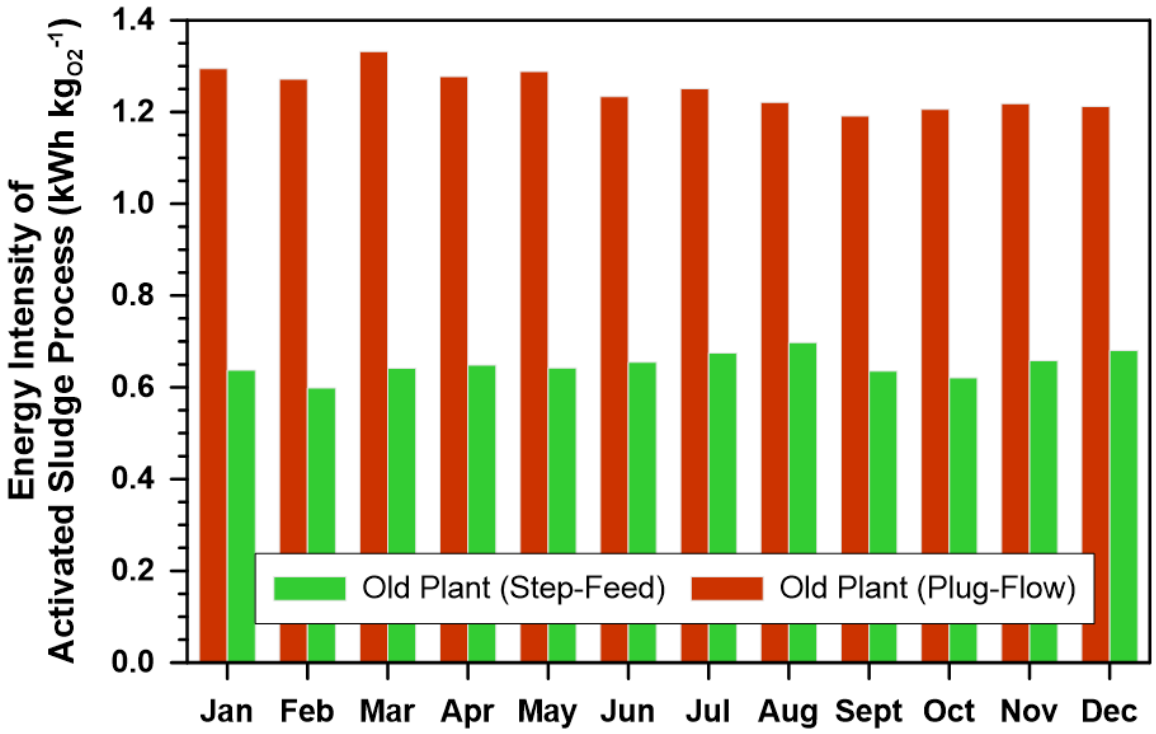

Figure 31. Comparison of the activated sludge electrical energy intensity (defined as the electrical demand per unit of theoretical oxygen requirements) for plug-flow and step-feed scenarios.

.

As Figure 31 illustrates, activated sludge energy intensity of the plug-flow configuration is close to double of step-feed's. In other words, the energy efficiency of the activated sludge process in the step-feed scenario is about twice of plug-flow's. This higher aeration efficiency can be explained by larger alpha factors of the step-feed scenario as illustrated in Table 3 in the Methods chapter. Denitrification process in the step-feed configuration selectively removes surfactant hence increases oxygen transfer efficiency (represented by alpha) with consequent decrease in the aeration power demand [34].

III. Electricity Demand to Quality Index Removal Ratio

To account for the facility's overall extent of removal beyond activated sludge unit's and accounting for all the pollutants, net and total electricity demand of each scenario for each month of the one year study period is normalized to quality index removal (QIR) [47, 48] and compared in Figure 32. Details about QIR definition and calculations methodology has been provided in the Methods chapter.

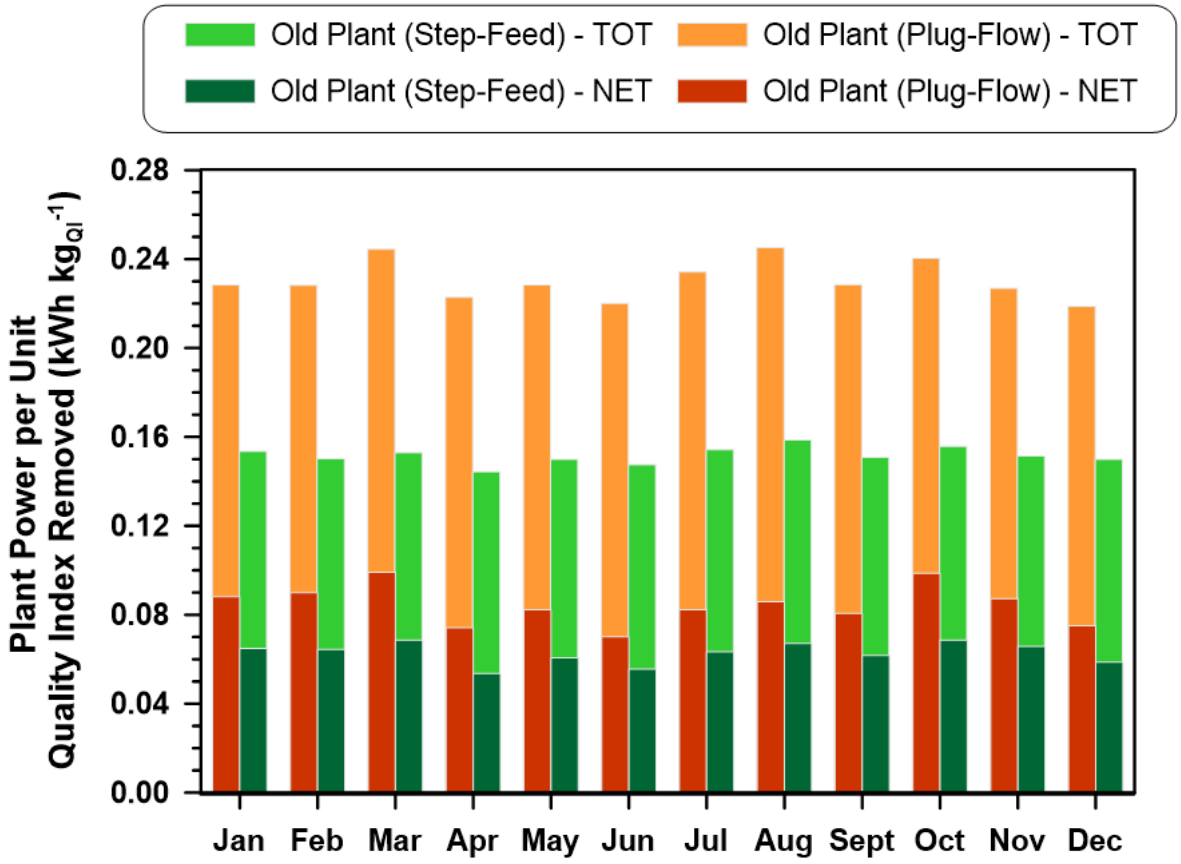

Figure 32. Plant total and net power demand normalized per unit quality index removal for plug-flow and step-feed scenarios.

Figure 32 illustrates that both total and net electricity demand to QIR ratios are lower for the step-feed scenario by 31-37% and 21-31% of plug-flow's, respectively. In other words, after accounting for the facility-wide higher cumulative extent of removal in the step-feed scenario, this scenario is still presented to be more energy-efficient. The lower extent of normalized net electricity demand difference between these two scenarios comparing to total electricity demand's is due to roughly 6% higher biogas productions in the plug-flow scenario. This higher biogas production which translates into higher inhouse electricity generation will compensate a portion of the difference observed in the normalized total electricity demand.

More biodegradable or digestible organics contents of plug-flow secondary sludge, due to its low MCRT, and its higher waste activated sludge stream (WAS) comparing to step-feeds results in this higher biogas production. This extra biodegradable content is consumed by the carbon oxidizing and denitrifying bacteria in the step-feed configuration at the cost of more aeration. The effect of this more biodegradable sludge in promoting the biogas production in the plug-flow scenario is so significant that despite this scenario's digester detention time of half of step-feed's, due to its higher WAS, it still produces more biogas than step-feed. This finding suggests addition of digestion volume as a strategy to further compensate the electricity deficiency of plug-flow or non-nitrogen removing AS configurations when in-house electricity generation from biogas is available and switching to nitrogen removing AS configuration is not possible.

Greenhouse Gas Emissions

The average daily greenhouse gas (GHG) emissions breakdown by each emission source category as defined in the Methods chapter are compared in Figure 33. According to this figure, one of the two major sources of GHG emissions for the two scenarios discussed here is the activated sludge and digester process emission, which consists of the CO_2, CH_4, and N_2O emissions generated by the activated sludge processes and CO_2 emission generated by the digesters. The combustion emission (biogas and natural gas) consists of CO_2, CH_4, and N_2O emissions is the other major source of emissions followed by power import CO_2 and fugitive leak CH_4 emissions.

As demonstrated in the Figure 33, the significance order of the two major contributing sources to the plant total carbon-footprint are different for the scenarios compared in this chapter. In case of the step-feed configuration the combined emissions generated by activated sludge and digester processes is the most significant contributor while this source category is the second

major contributor for the plug-flow scenario. For the plug-flow, GHG emissions from combustion of biogas and natural combined is the largest contributor while it is the second for in the step-feed.

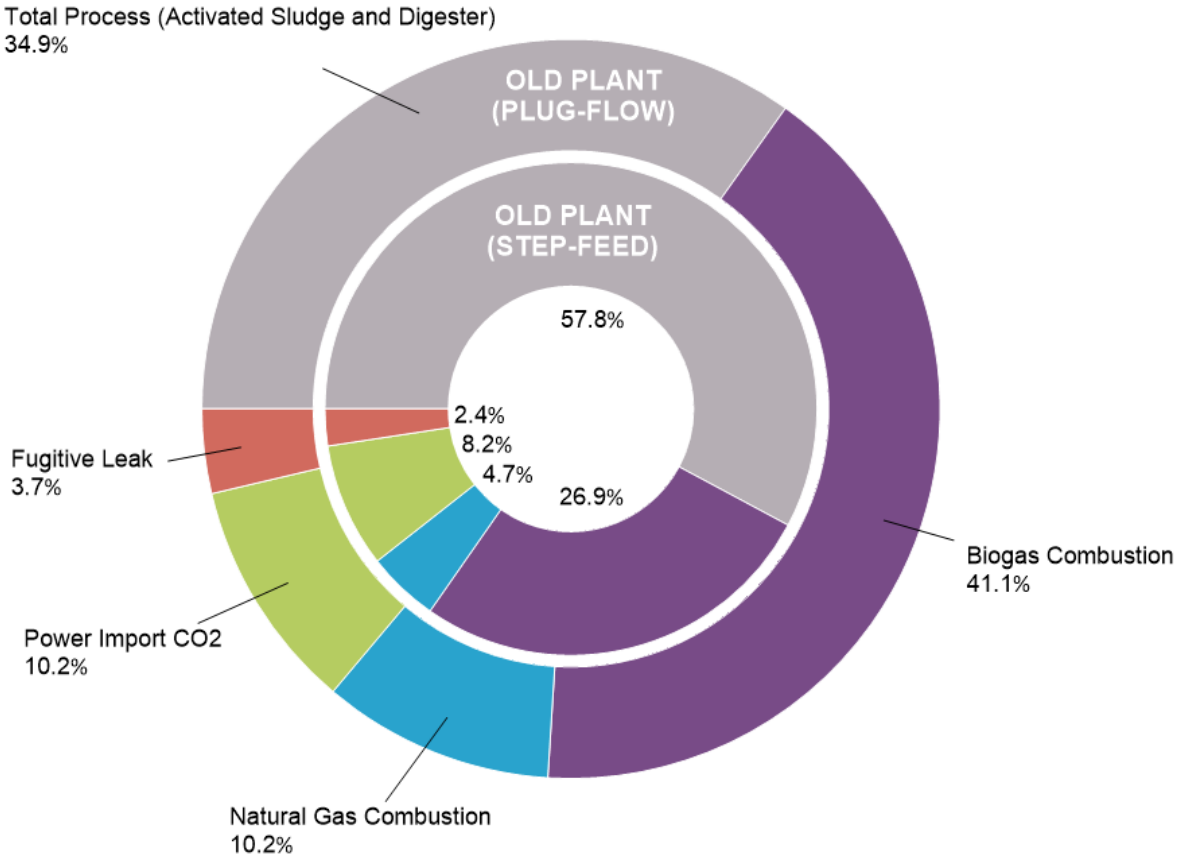

Figure 33. Greenhouse gas emissions breakdown by source type for plug-flow and step-feed scenarios. The total average daily emissions normalized per unit influent flow treated for old plant step-feed and plug-flow scenarios are 0.62 kgCO_2eq m^{-3} and 0.43 kgCO_2eq m^{-3}, respectively.

As illustrated in Figure 33, the conversion to step-feed from the plug-flow configuration has raised the facility's overall average annual GHG emission per unit flow treated by almost 43%. The main reason for this large discrepancy is the higher extent of influent constituent oxidation in the step-feed activated sludge scenarios which has higher sludge retention time than plug-flow. This results in generating more than triple of plug-flow's CO_2 emissions in activated sludge of step-feed scenario and more than doubling the overall process emissions after compensating the slightly higher CO_2 generation in digesters of plug-flow scenario.

Changing the activated sludge configuration to step-feed from plug-flow also increases the grid's electricity import emissions by 17%. This is explained by lower power generation in step-feed scenario because of its 6% lower biogas production. This modification; however, reduces the total combustion (biogas and natural gas) and fugitive emissions by 11% and 6% respectively due to lowering the facility's biogas production. Reduction of the WAS in the step-feed scenario also reduces the thermal energy demand for heating up the digesters' influent. This thermal energy savings translates into allocation of its associated fuel savings to inhouse power generation in the step-feed scenario and alleviating its higher electricity import emissions. Accounting for only anthropogenic GHG emissions, which is defined as total GHG emissions excluding 87.18% of activated sludge process emissions [44], total CO_2 produced in digesters, and CO_2 portion of biogas combustion, addition of nitrogen removal in the step-feed scenario results in on average 17% increase of the facility's GHG emissions.

As indicated under the electricity demand comparison section of these chapter to fairly compare these scenarios, the simulation results need to be normalized to parameters that truly and cumulatively demonstrate the extent of treatment here. Comparing the available alternatives in the electricity demand comparison section of this chapter suggest QIR to be the best option for this purpose. The normalized monthly GHG to unit of QIR ratios which account for these scenarios' cumulative pollutant removal from wastewater are compared in Figure 34.

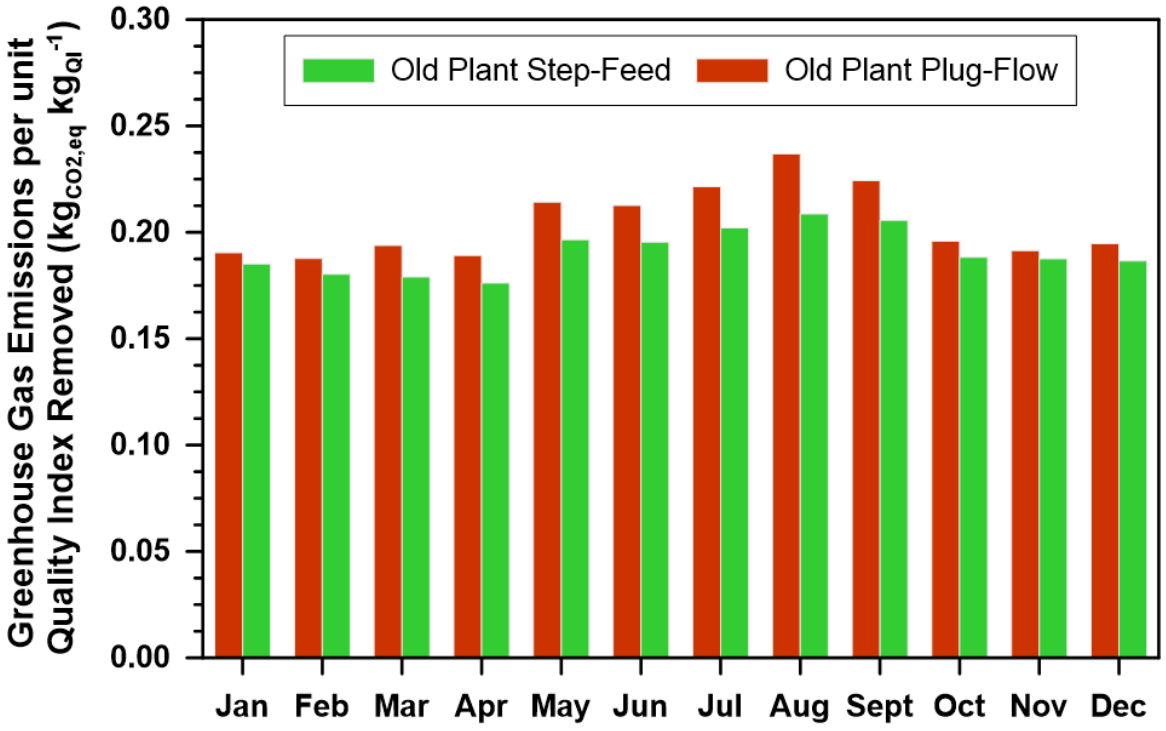

Figure 34. Greenhouse gas emissions to quality index removal ratio comparison for plug-flow and step-feed scenarios.

Figure 34 demonstrates that after accounting for the cumulative extent of removal in these scenarios, total GHG emissions are lower for step-feed scenario by 2-12%. This can be explained by the significantly higher extent of removal quantified by QIR in the step-feed scenario. Figure 34 also demonstrates slight seasonal trend in normalized GHG emissions with larger and lower ratios for both scenarios occurring during hot (May through September) and cold months (October through April) of the year, respectively. The higher normalized emissions in the hotter months can be explained to be due to the effect of temperature in promoting the biological process activities and consequently higher process GHG emissions production. The other explanations are the increase of inhouse power generation using natural gas in summer months in response to higher grid electricity tariffs and positive correlation between blowers' energy demand required to deliver unit airflow to AS units and ambient air temperature translating into higher electricity demand and its associated GHGs in the hotter months of the year.

Operating Cost

For the two scenarios discussed in this chapter the operating cost based on the 5 different power tariff structures presented in Figure. 9 were calculated. In addition to the grid's electricity import cost, costs of following activities have been calculated and captured here: chemicals used for enhancing primary treatment; sludge dewatering and thickening chemical additives; biosolid disposal; and natural gas imports. More details about the methodologies used for each of these activities' cost estimation are provided in the Methods chapter.

These costs are normalized per unit QIR to also account for the extent of the treatment in each scenario. Since each treatment scenario would have 5 tariff sub-scenarios, the ratio of the normalized total operating cost of the plug-flow scenario to step-feed's are estimated to simplify the comparison. These dimensionless ratios for each month of the year in the study period are presented in the Figure 35.

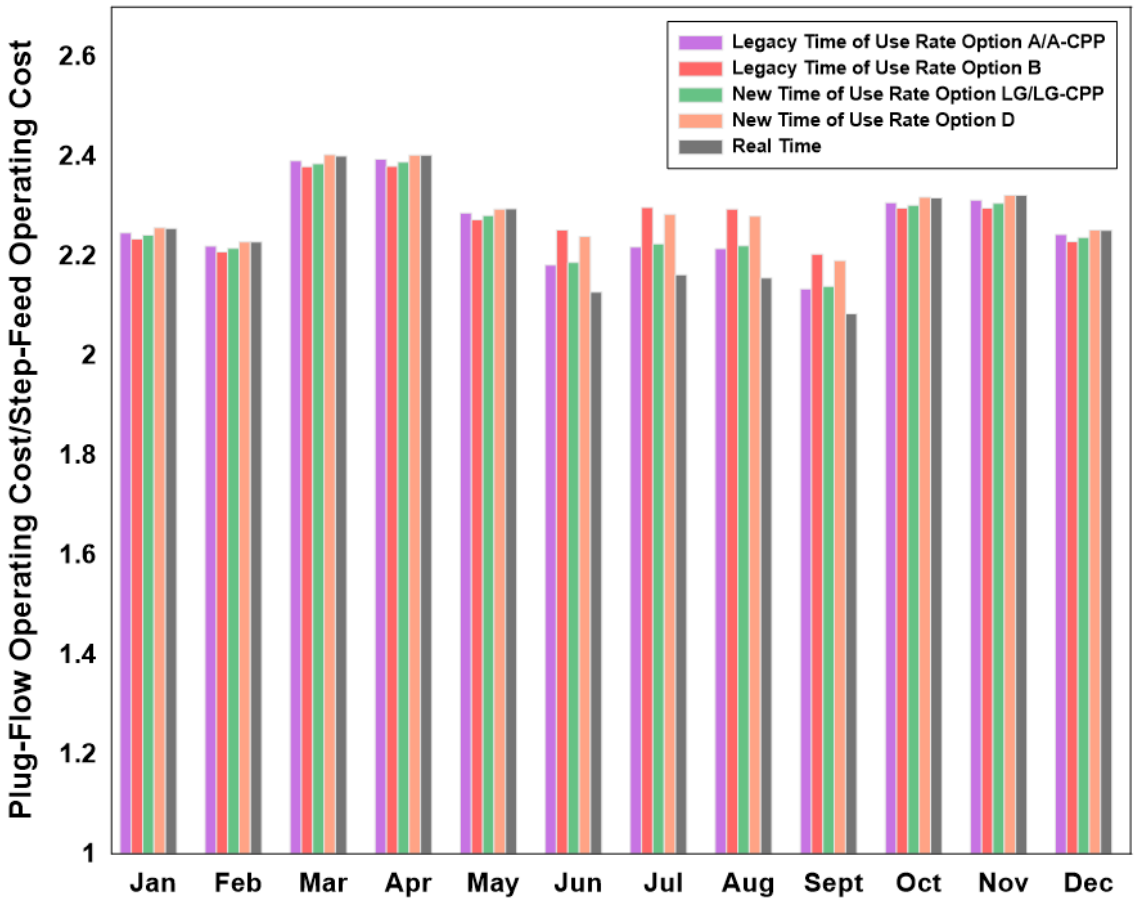

Figure 35. Operating cost per unit quality index removal for plug-flow and step-feed scenarios, applying the five power tariffs in Figure 9. The results are presented as dimensionless ratios, with the step-feed configuration in the denominator. Annual operating cost to unit quality index removal ratio calculated using the average of these 5 tariffs annual electricity cost for plug-flow and old step-feed plant are 99.36 USD per metric ton and 43.90 USD per metric ton respectively.

Figure 35 demonstrates that the normalized operating cost of the plug-flow is more than double of the step-feed's disregarding the tariff structure used. Therefore, modification to step-feed has provided a great amount of operating cost savings in addition to providing better overall effluent quality. This figure also shows that the cost ratios derived using different tariffs for each of the winter months (October through May) are comparable. In other words, the effect of tariff structures on the outcome of this operating cost comparison, is only considerable during the grid's summer months (June through September). This is due to more significant differences between

these tariffs' energy usage and demand charges in the summer months. More details about these tariffs and their components can be found in the Methods chapter.

Higher electricity imports, due to lower biogas production and slightly higher electricity demand, results in higher imported electricity cost of step-feed scenario. However, the additional operating cost associated with higher WAS production in the activated sludge of plug-flow scenario will significantly overcompensate the step-feed's higher electricity import cost. Higher cost of grid's electricity in the summer months (June through September) amplifies the step-feed's slightly higher electricity import cost resulting in further compensation of plug-flow's higher overall operating cost. This explains the slight decrease in the cost ratios demonstrated in the Figure 35 in the summer months.

Plug-flow's higher WAS results in higher usage and cost of chemical additives used in the sludge thickening and dewatering processes; higher thermal energy demand in digesters at the cost of higher natural gas imports; and larger disposal costs comparing to step-feed scenario. The most significant of all these three is the higher chemical additives cost in the plug-flow scenario. Since the primary treatment was assumed and configured to be the same for both scenarios, the chemical usage for enhancing its performance and its sludge thickening and dewatering normalized to total QIR is expected to be the same for both scenarios. Therefore, the significant chemical usage cost difference observed here can be narrowed down to the secondary treatment's waste sludge dewatering and thickening.

The WAS flow in the plug-flow scenario is on average more than five times of steps-feed's. This significant difference results in the same order of magnitude higher chemical additive cost (five-fold) in the secondary sludge thickening process of plug-flow scenario where the additive usage and its cost are directly calculated from the WAS flow using constant factor. Upon removal of the larger water content of plug-flow's WAS comparing to step-feed's in the sludge thickening process, the difference between the two scenarios sludge flows is reduced to slightly greater than

two-fold. Therefore, the digesters' influent thermal demand and their effluent dewatering chemical demand and their costs will be impacted with this smaller difference. This difference is further reduced to less than two-folds in case of sludge-disposal cost as a result of removing digested sludge's (i.e. biosolids) water in the sludge dewatering unit prior to disposal. This explains why the thickening and dewatering chemical additive cost is the most contributing factor to plug-flow to step-feed operating cost ratio in Figure 35.

Summary

The dynamic simulation of this large WRRF prior and post addition of nitrogen removal (i.e., plug-flow and step-feed activated sludge configurations, respectively) demonstrated that addition of nitrogen removal slightly increased the overall electricity demand of this facility. The more significant change observed in the power demand comparison of these two configurations was shifting of more than half of the power demand used for sludge thickening, biosolid dewatering and loading processes of the plug-flow scenario to the activated sludge aeration of the step-feed scenario upon switching to this configuration. Significant improvement in the cumulative effluent quality of this facility, measured in unit of quality index and normalized to the facility influent flow, was also observed after converting the facility's plug-flow activated sludge configuration to the nitrogen removing or step-feed at the cost of the shifting half of the activated sludge processing electricity demand to its aeration.

To fairly and closely compare the total and net electricity demands of these two scenarios, these values were normalized to different parameters representing the extent of the treatment. The comparison of these normalized values illustrated higher aeration energy efficiency in the activated sludge unit of step-feed scenario and presented this scenario as the more electricity-efficient one. The higher aeration energy efficiency observed in the step-feed was explained and demonstrated to be due to selective removal of surfactants by the denitrification process that increases oxygen transfer efficiency (represented by alpha).

Comparing the overall greenhouse gas emissions of the facility prior and post addition of nitrogen removal normalized to cumulative extent of removal quantified by quality index removal concluded a decrease in the emissions post nitrogen removal addition (step-feed). A comparative analysis of the facility total operating cost using different electricity tariff structures in this study also presented significant cost saving post addition of nitrogen removal. This was identified to be mostly due to reduction of the sludge and biosolids processing and handling costs.

Higher biogas production was observed in the plug-flow scenario. This was explained to be due to diversion of larger amount of waste activated sludge containing more biodegradable materials to digesters in this scenario, that otherwise would be oxidized in aeration process of step-feed configuration at the cost of additional electricity demand. This higher biogas production in the plug-flow scenario resulted in higher inhouse power generation and consequently reduced this scenario's power imports and its cost. This cost saving, however, could only alleviate a small portion of this scenario' higher cost of sludge and biosolids processing and disposal including the thermal energy and chemical additives cost. It is important to note here that the benefit of this additional biogas production prior to nitrogen removal addition is not applicable to the plug-flow configurations at facilities that do not have digesters (ex., facilities that utilizes sludge incinerations). As such, these facilities' energy-efficiency improvement and cost savings as a result of addition of nitrogen removal to their existing carbon-oxidizing activated sludge units will be more significant.

CHAPTER 6: BENEFITS OF ADVANCED PRIMARY TREATMENT TECHNOLOGIES OVER CONVENTIONAL PRIMARY SETTLING (CLARIFIERS) FROM A DYNAMIC MODEL POINT OF VIEW

Primary treatment (PT) consists of separation and removal of suspended solids and floatables (ex. fats, grease, oils, plastics, etc.) from wastewater using physical-chemical techniques which is performed to reduce the reactors volume requirement and aeration demand of biological treatment. As also demonstrated in the previous two chapters and for the three different activated sludge (AS) configurations at the large water resource recovery facilities (WRRF) studied in this research effort, aeration in the biological treatment is one of the main contributors, if not the main contributor, to WRRFs' total electricity demand [18, 66, 19]. This is why reducing the aeration demand and improving its efficiency by increasing the extent of the primary treatment has demonstrated considerable electricity demand savings in the previous studies of advanced primary treatments (APT) summarized in the Background chapter of this dissertation (inter alia, [32, 23, 24, 22, 33, 21, 29]).

In addition to lowering the aeration demand and its power requirements, APTs' higher extent of solid removal allows higher capture of primary sludge which is more carbon-rich and highly degradable [29]. This results in higher production of biogas in WRRFs that are equipped with anaerobic digesters. Many of these WRRFs use the produced biogas to produce electricity in addition to the thermal energy required to operate digesters similar to the one being studied here. As such, APTs' higher extent of treatment can further reduce WRRFs dependency on grid electricity by increasing the inhouse electricity generation when digesters and inhouse electricity generation are available.

The effect of implementation of three of these APT technologies at a large WRRF that is originally equipped with conversional settling (clarifier) is studied in this chapter. This chapter focuses on the impact of this process change on electricity demand, carbon-footprint, operating

cost of this facility. Chemically enhanced primary treatment (CEPT), primary filtration (PF), and rotating-belt filtration (RBF) or micro-screening are the three APT technologies that are selected for this analysis. Detailed explanation of these three technologies and their extents of removal are provided in the Background section of this dissertation.

The previous studies summarized in the Background section of this dissertation demonstrate overall cost, carbon-footprint, and energy reduction for few of these APTs on average basis in comparison with conventional clarifiers. Thus, they do not account for WRRFs operation dynamics especially their electricity imports whose cost and carbon intensity (footprint) are dynamic during the day. In addition, due to the use of averaged influent characteristics in steady-estate models, these studies do not account for the effect of diurnal trends of influent on the removal efficiency and consequently aeration demand and its efficiency; energy consumption; and biogas generation of the WRRFs' they reviewed especially the ones with conventional clarifiers (their baselines). Therefore, there is still a gap for comparing these APT technologies with conventional clarifiers in a complete dynamic modelling effort that accounts for both WRRF's and the electricity grid's dynamics. Filling this gap is the goal of the modeling effort that is being discussed in this chapter.

In addition to providing more accurate results, the dynamic analysis in this chapter also reveals the possibility of coupling barrier separation technologies (i.e., PF and RBF) with existing conventional primary clarifiers as a demand-side flexibility project (defined in the Introduction section of section of this dissertation) to reduce the plant electricity demand and overall operating cost during the peak of electricity grid demand. This is achieved by utilizing barrier separation technologies (BSTs) during the periods that these technologies outperform conventional clarifiers to maximize the removal performance and minimize energy demand and carbon-footprint of the facility (i.e. decoupling of conventional clarifiers' performance from their hydraulic load). It needs to be noted here that the dependency of primary clarifiers on the hydraulic load may be only

disadvantageous during the high hydraulic load periods when clarifier's removal will be minimized. However, as Table 1 in the Background section of this dissertation and Figure 40 in this chapter demonstrate the extent of the removal of conventional clarifiers can exceed some of its advanced alternatives outside of a WRFF's high hydraulic load periods. The coincidence of the WRRF hydraulic load peak with the peak of the electricity gird's demand, as demonstrated in Chapters 4 and 5, is the key element demonstrating the potential benefits of coupling BSTs with conventional clarifier as a great candidate for demand-side flexibility projects.

In addition to improving the performance, by increasing their rotational speed and consequently lowering their retention time, BSTs allow faster treatment in the primary stage which can be used as a process and electricity load shifting mechanism. This can be achieved by switching to a BST at the beginning of the electricity grid demand ramp-up period prior to its peak to take advantage of lower power cost at the aeration (the largest power consumer at the plant) and subsequently switching back to conventional clarifiers (the slower option) at the peak or toward the end of it to delay the power demand at the downstream processes. Note that instantaneous and complete alternation between these PT technologies can upset the primary treatment especially conventional clarifiers; therefore, gradual transition or hybrid (load distribution) approach need to be considered for the field applications.

In this chapter, the dynamic simulation developed for the current configuration of the large California WRRF studied in this research effort, which was explained in Chapter 4, is used as a starting point to develop the simulations for the different APT scenarios as well as conventional clarifier's. The results of these simulations then are compared to demonstrate the effect of these different standalone PT technology scenarios on electricity demand, operating cost, and carbon-footprint of this facility. Using the result of this comparison effort additional scenarios are defined and studied where BSTs are combined with the conventional clarifiers. These additional scenarios

explore alternative approaches that may interest facilities that are not interested or not able to completely switch to a BST from their primary clarifiers.

Since the cost of electricity and primary treatment enhancing chemicals (only for CEPT) play a key role on feasibility of each of the APT scenarios studied here, an analysis is also performed in this chapter to determine the instantaneous and cumulative electricity and primary treatment enhancing chemicals costs domains for which each standalone APT scenario is generating cost-savings over conventional clarifiers. This analysis and the methods being introduced here can be a great tool for the facility being studied here and any other WRRF to select the power tariff structures and primary enhancing agents that will maximize their operating cost savings when different options are available.

Simulation Scenarios

Following scenarios are simulated here using the current plant configuration described in the Methods chapter:

1. **Baseline:** standalone primary clarifiers without chemical enhancement (conventional clarifiers).
2. **Chemically Enhanced Primary Treatment (CEPT):** Same as baseline scenario; however, the primary treatment is chemically enhanced using Ferric Chloride ($FeCl_3$) and anionic polymers. This scenario represents the current plant whose simulation model is used as a starting point for other scenarios and whose simulation results are analyzed in Chapter 4.
3. **Standalone-RBF:** RBFs replace conventional clarifiers in the baseline scenario for the entire study period. Since the solid removal of this technology can be modified by the operator by changing its pump rate and electric powertrain speed, three different sub-scenarios are studied here for this technology that represent a) minimum, b)

average, and c) maximum percent TSS removals listed in Table 1 of the Background section of this dissertation (i.e., 30%, 45%, and 60% respectively).

4. **Standalone-PF:** PFs replace conventional clarifiers in the baseline scenario for the entire study period. Since the solid removal of this technology can be modified by the operator by changing its pump rate and electric powertrain speed, three different sub-scenarios were studied for this technology that represent a) minimum, b) average, and c) maximum percent TSS removals listed in Table 1 of the Background section of this dissertation (i.e., 60%, 70%, and 80% respectively).
5. **RBF-Conventional Clarifier Alternation:** same as baseline; however, the plant is capable of bypassing the primary clarifiers and utilizing RBF instead for a fixed period of time during the day. This scenario is one of the electricity load-shifting scenarios that was explained in the beginning of this chapter. To study the impact of this load shifting strategy, it has been studied through five different sub-scenarios where RBF replaces conventional clarifiers for a period of 5 continuous hours during:
    a. maximum solar power contribution to the grid or bottom of the Duck-Curve (i.e., 10:00-15:00, determined from the grid carbon intensity curves for this facility provided in the Methods chapter);
    b. minimum removal performance of the primary clarifier (12:00 to 17:00) as illustrated in Figure 40;
    c. peak of power grid demand or Duck-Curve ramp-up period (16:00 to 21:00);
    d. right after the peak of power grid demand (21:00 to 2:00); and
    e. right after the peak of the plant influent flow (i.e., 00:00 to 5:00, pursuant to the plant influent flow trend provided for this facility presented in Figure 6 of the Methods chapter).

    The average percent TSS removal of the RBF (45%) from Table 1 of the Background section of this dissertation was used for all these 5 sub-scenarios.

6. **Primary Filter (PF)-Conventional Clarifier Alternation:** same as baseline; however, the plant is capable of bypassing the primary clarifiers and utilizing PF instead for a fixed period of time during the day. This scenario is divided to the same 5 sub-scenarios listed in Scenario 5. The average percent TSS removal of the PF (70%) from Table 1 of the Background section of this dissertation was used for each of these sub-scenarios.
7. **RBF-Conventional Clarifier Hybrid:** same as baseline; however, both RBF and clarifier are operated in parallel simultaneously for a portion of the day when the plant's influent flow exceeds a certain threshold and only clarifiers are operated for the remainder of the day. This scenario is divided to three sub-scenarios where the threshold to operate the RBF is a) 70, b) 90, and c) 120 MGD (265, 341, and 454 × 10^3 m^3 d^{-1} respectively). For this scenario any flow up to the flow threshold is treated by the primary conventional clarifiers and the remainder is sent to the RBF whose percent TSS removal is the average value of the range (45%) provided in Table 1 of the Background section of this dissertation.
8. **PF-Conventional Clarifier Hybrid:** same as baseline; however, both PF and clarifier are operated in parallel simultaneously for a portion of the day when the plant's influent flow exceeds a certain threshold and only clarifiers are operated for the remainder of the day. This scenario consists of the same 3 sub-scenarios described under Scenario 7. The average percent TSS removal (70%) derived from the ranges provided for PF in Table 1 of the Background section of this dissertation is used for each of these sub-scenarios.

The schematics for these 8 scenarios have been illustrated in the Figure 36 through 39 below:

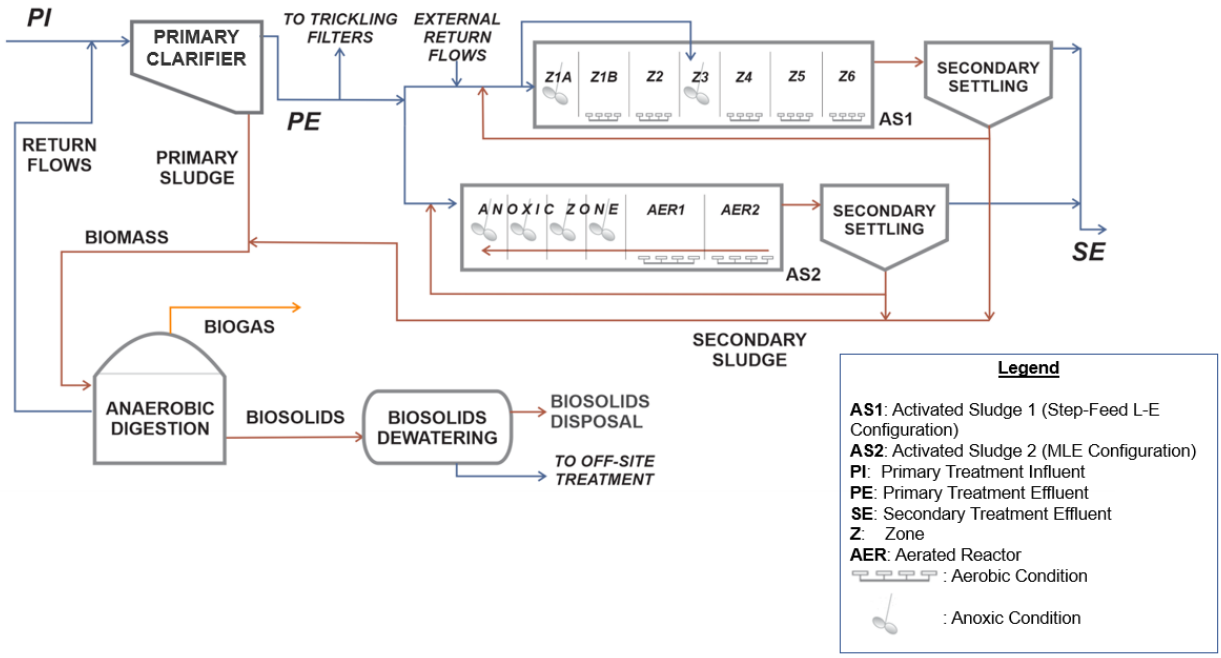

Figure 36. Process schematic for conventional primary clarifier (baseline) scenario (Scenario 1).

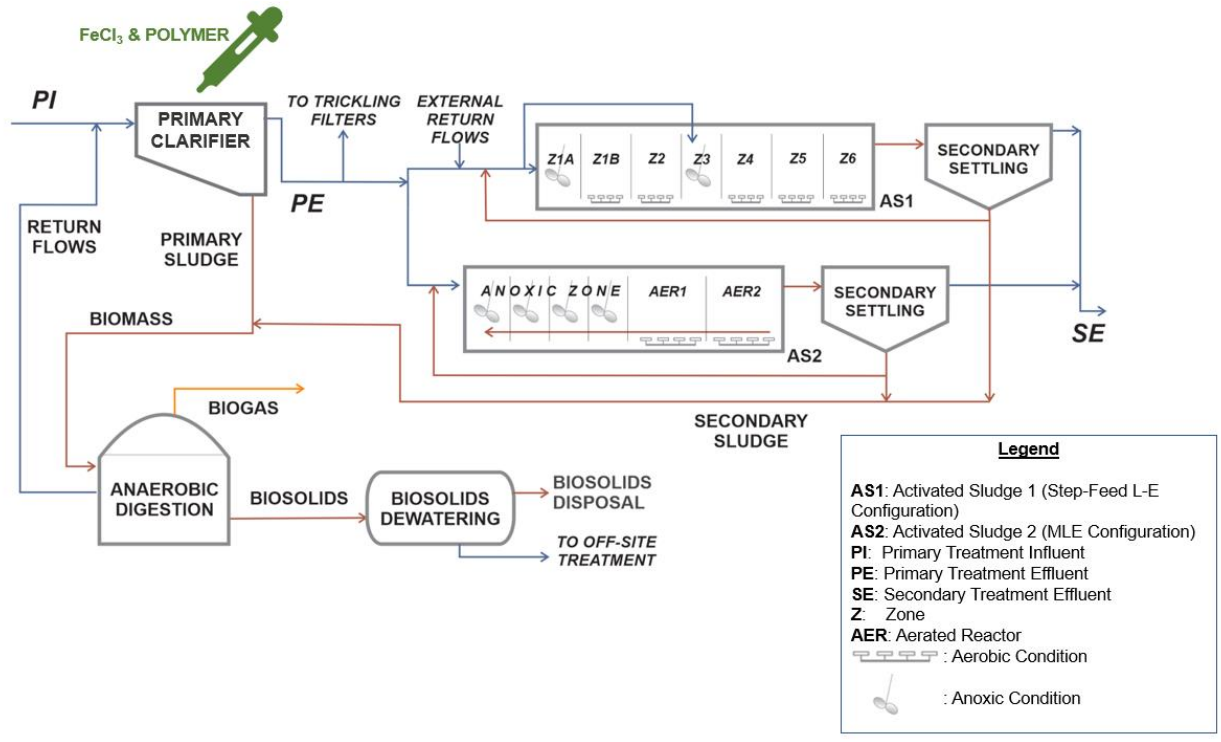

Figure 37. Process schematic for chemically enhanced primary treatment (CEPT) scenario (Scenario 2).

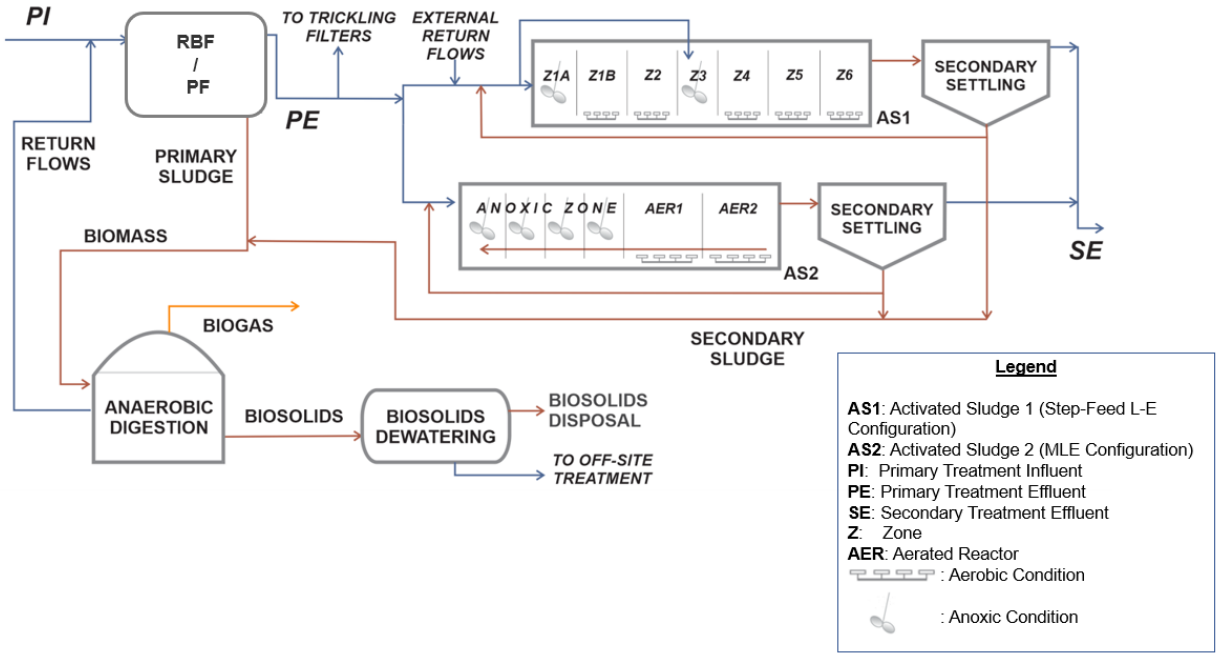

Figure 38. Process schematic for standalone-RBF or standalone-PF scenarios (Scenario 3 and 4).

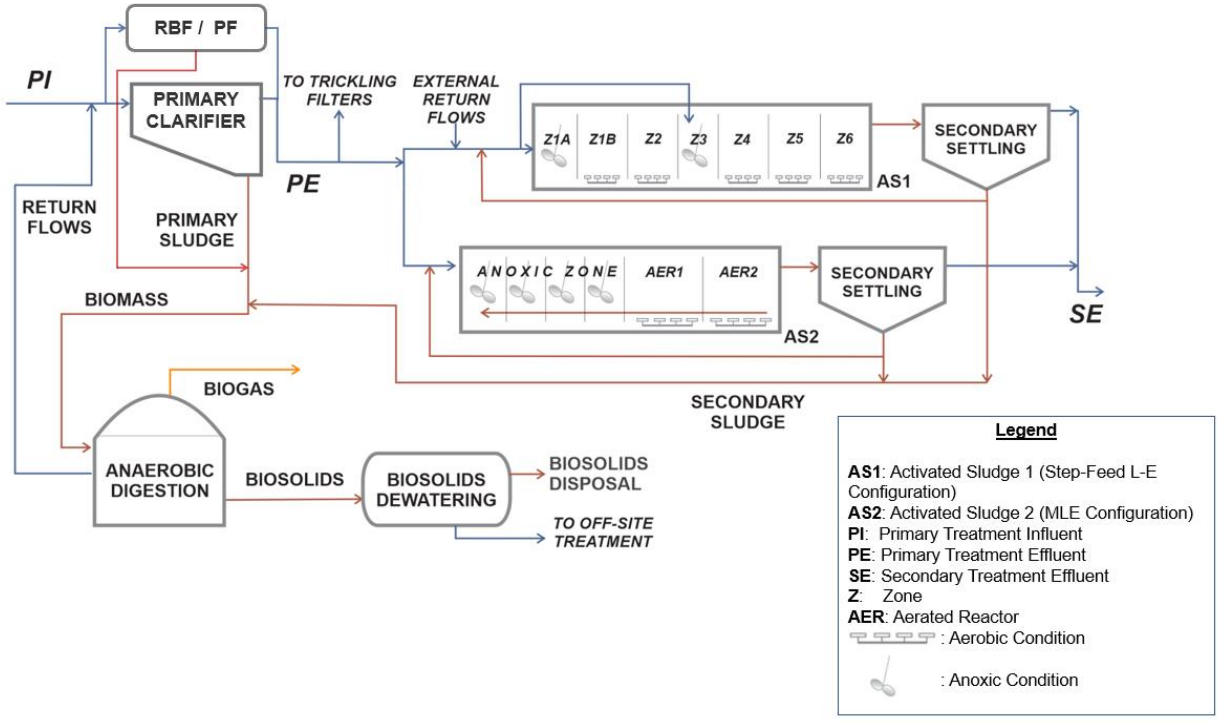

Figure 39. Process schematic for scenarios coupling PF or RBF with conventional clarifier (Hybrid and Alternation or Scenarios 5 to 8).

Conventional Clarifier Dynamic Solid Removal

As mentioned before, the solid removal of conventional clarifiers is inversely correlated to their hydraulic load. As such, they underperform at the peak of the plant influent flow. As demonstrated in Figure 6 in the Methods section, the WRRF in this study reaches its hydraulic load peak at 12:00 and remain at its peak until 00:00 and declines to its minimum hydraulic load at 6:00. Figure 40 illustrates the average diurnal trend of TSS removal of the conventional primary clarifiers in Scenario 1. This trend has been derived from the results of this scenario's simulation for the 12 months study period here (October 2018 to September 19) and clearly demonstrates this reverse correlation of extent of solid removal with the facility dynamic hydraulic load. TSS removal domain of the APT technologies focused on in this study are also compared with conventional clarifier scenario's in this figure. It needs to be noted that % removal of standalone BST (RBF and PF) can be set at a constant removal within the provided ranges; however, CEPT's still remain dynamic similar to conventional clarifier but within a range in the green zone demonstrated in Figure 40.

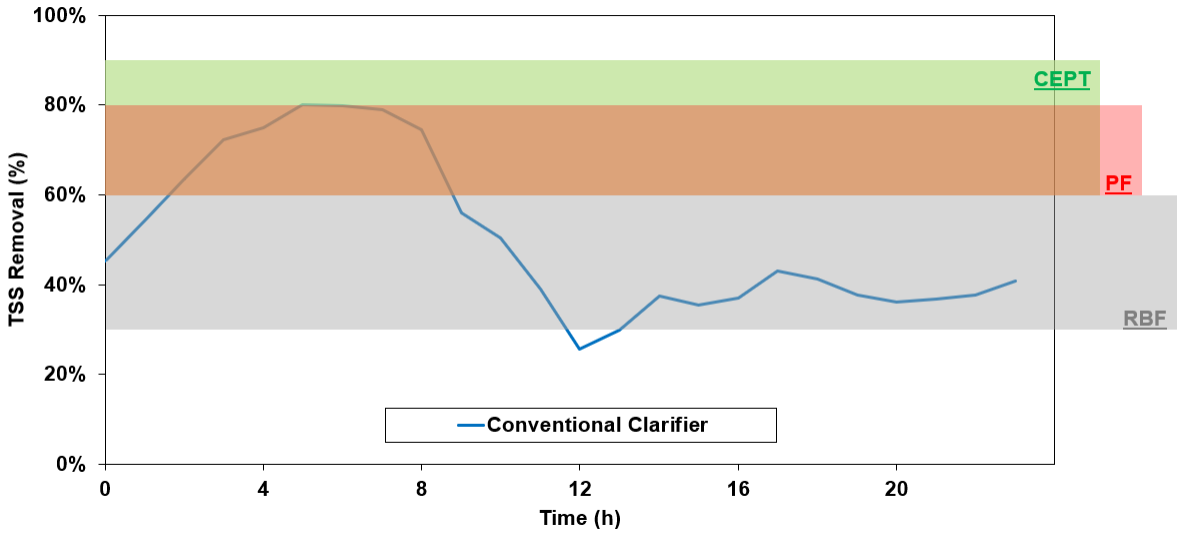

Figure 40. Comparison of conventional clarifier scenario's (Scenario 1) dynamic TSS removal (blue line) with the three advanced primary treatments technologies' (chemically enhanced primary treatment, primary filtration, and rotating-belt filtration) TSS removal domains. The dynamic trend (blue line) represents the average of all the TSS removal diurnal trends produced in Scenario 1's simulation for the 12 months study period here (i.e., October 2018 to September 2019).

By comparing this dynamic trend with the TSS removal domain of the APT studied here, this figure elucidates the additional extent of removal and its time frame that each of these APTs could offer to this facility's conventional primary clarifier scenario. As such, this figure must be the first step of the similar analysis for other facilities as, with a small amount effort, it illustrates how much of additional removal could be achieved with each alternative advanced treatment technology over conventional clarifier and whether BST load-shifting scenarios could be applied and are practical for that facility's electricity tariff structures. It also demonstrates the time periods that coupling a BST with the conventional clarifiers could boost up the primary treatment removal efficiency. The time frames selected for the proposed BST alternation scenarios in this study are selected following this logic and target the periods that clarifier efficiency is below its maximum.

Extent of Removal

In order for the facilities modeled in the scenarios presented in this chapter to be comparable they need to deliver the same extent of treatment or water pollutants removal. In other words, the effluent quality and environmental impact of all these scenarios should be close. As such, the simulation of all the scenarios in this chapter have been set up to deliver the same overall facility-wide extent of removal as of the current WRRF scenario described in the Chapter 4 which is the CEPT scenario or Scenario 2 in this chapter. The other advantage of this approach is that the result of the comparison performed in this chapter can be directly applied to this facility and determine whether it can achieve any energy or cost-saving by switching to other primary treatment technologies. Quality Index Removal (QIR) which represents the difference between the weighted sum of TSS, TKN, COD, Nitrate, and BOD in the facility influent and effluent as described in the Methods chapter [47, 48] is used in this chapter to monitor the overall extent of removal and effluent's environmental impact of each of these scenarios.

Due to different extent of solid removals in each of the primary treatment scenarios being studied here, the extent of the removal in the secondary treatment needs to be adjusted in order

to deliver the same overall facility-wide extern of treatment for all the scenarios here. As such the operating parameters of the secondary treatment (activated sludge) for each scenario needs to be adjusted accordingly. Waste activated sludge (WAS) stream flow rate which is one of the main operating factors to control the extent of activated sludge units' removal is utilized here as a control parameter to achieve the desired overall plantwide extent of removal. The extent of the removal in the activated sludge units of these scenarios are also monitored using mixed liquor suspended solids (MLSS) and mean cell residence time (MCRT) in each scenario's simulation as surrogates for the extent of removal. In other words, the MLSS and MCRT of the activated sludge units of all these scenarios are kept close to current plants' by adjusting their WAS flows.

Figure 41 compares the total QIR of all these scenarios' simulations for the entire 12 months study period (October 2018 to September 2019) after performing the necessary adjustments to their WAS flow as well as the necessary dynamic alpha iterations as explained in Methods chapter. In contrast with the comparisons performed in Chapters 4 and 5, the plant influent flow and load used for all these simulations are the same; thus, the total QIR values calculated from the results of these simulations do not need to be normalized to the plant influent flow for this comparison. To simplify the comparison of these calculated total QIR values and to demonstrate how close they are to CEPT's, these values are presented as dimensionless ratios, with the CEPT scenario's (current plant) in the denominator, in Figure 41.

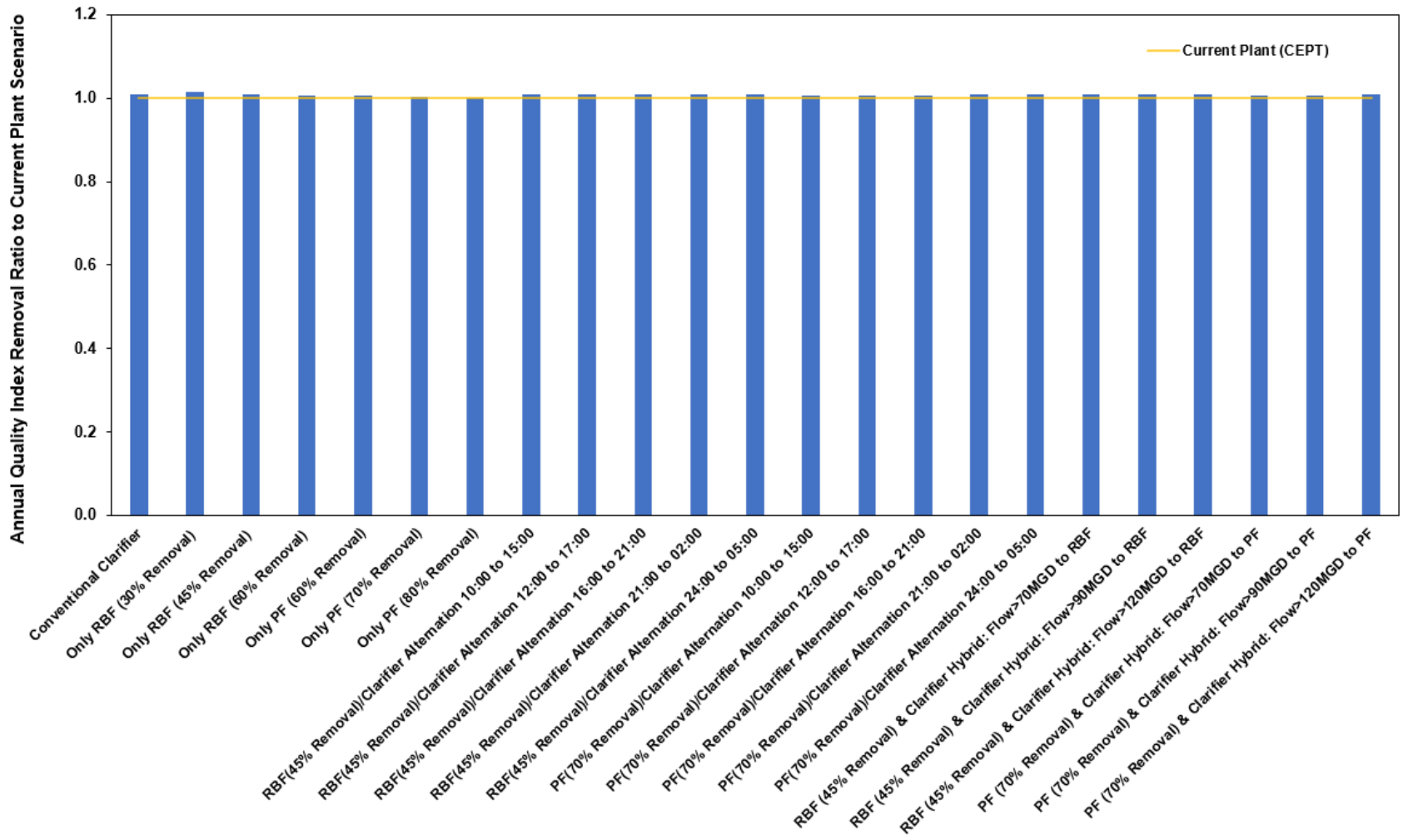

Figure 41. Sum of 12 consecutive months' total quality index removal for all the primary treatment scenarios. The results are presented as dimensionless ratios, with the chemically enhanced primary treatment (CEPT) scenario or the current plant in the denominator. These 12 months total index removal ratios are calculated using the 12 months total quality index removal of the current plant (CEPT scenario) which is 530.6 t y^{-1}.

As this figure illustrates, the dimensionless ratios for all these scenarios are close to 1 (within 0 to 1.5% of CEPT scenario's) which elucidates the close extent of removals of all these scenarios to CEPT's. In addition, to the quantitative comparison demonstrated in Figure 41, the diurnal effluent constituents' trends for these scenarios' final simulations for the entire 12-month study period were also visually compared and verified to be the comparable to current plants' (CEPT scenario's).

Electricity Demand

Similar to the other chapters to fairly compare the electricity demand and generation calculated by the simulation software for different scenarios, these values are normalized to the cumulative extent of removal represented by plant's QIR [47, 48] in this chapter.

To compare the standalone primary treatment technology scenarios (i.e., conventional clarifier, CEPT, RBF-only and PF-only) which are presented in Scenarios 1 through 4, their total and net power demand, total power generation, and total aeration power demand for the entire 12 months study period (October 2018 to September 2019 or annual) normalized to QIR [47, 48] have been compiled in Figure 42.

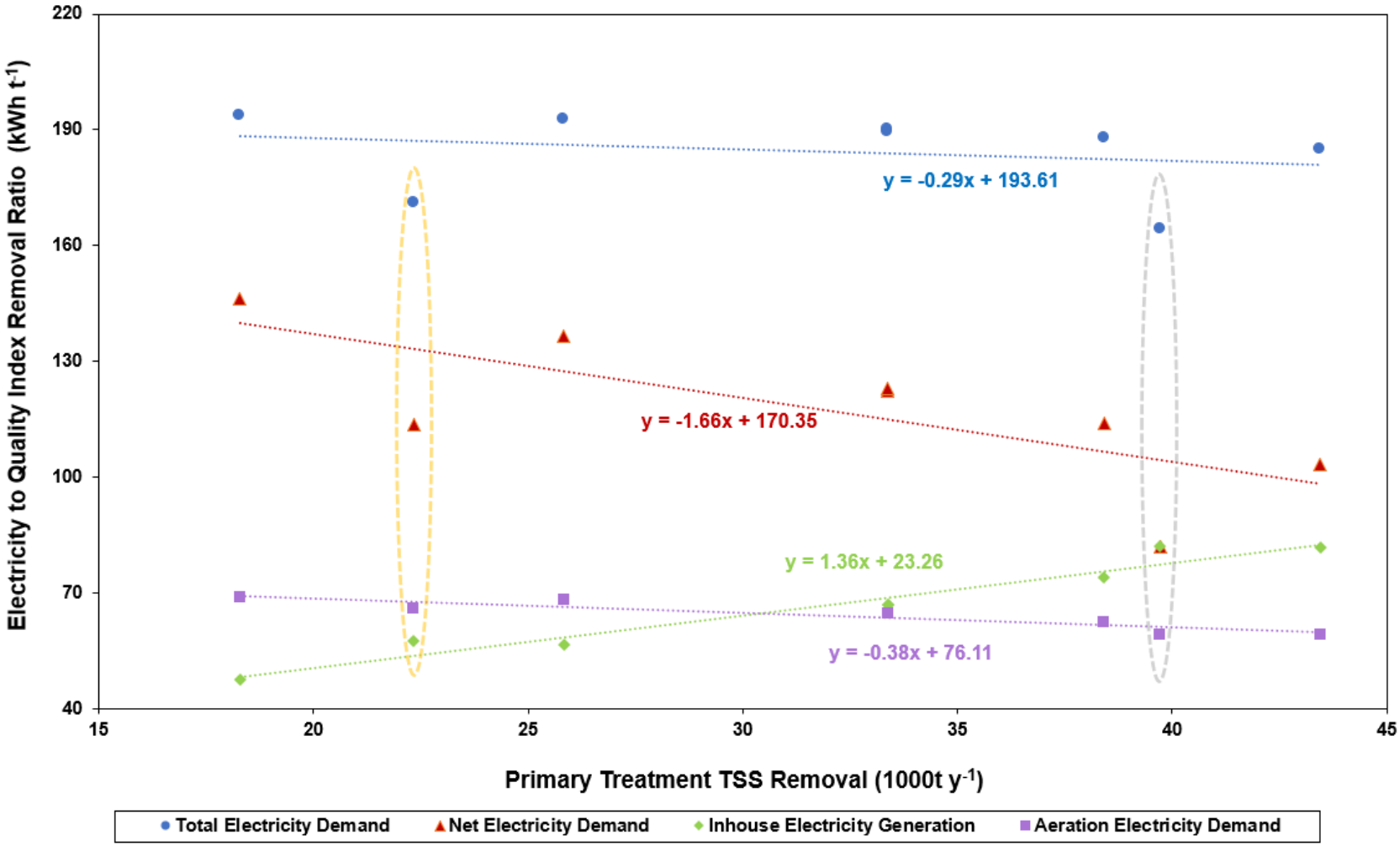

Figure 42. Comparison of sum of 12 consecutive months' electricity generations and demands normalized to total quality index removal for Scenarios 1 through 4: standalone conventional primary clarifier, chemically enhanced primary treatment, rotary belt filters (RBF) and primary filters (PF) scenarios respectively. Standalone conventional and chemically enhanced primary treatment scenarios' values are highlighted using the orange and gray dashed circles respectively. The remainder of data points represent standalone RBF and PF scenarios in the order of their extent of TSS removal from the left to right. The dotted trendlines and their matching color equations demonstrate the ascending and descending trend of each electricity data category.

Figure 42 demonstrates that increase in the extent of the primary treatment, represented by 1000 metric ton of TSS removal in X-axis, results in a reduction in the plant total electricity demand. The extent of the electricity demand reduction is more significant in the net electricity demand category, also known as electricity imports, due to combination of increase in the facility inhouse electricity generation and reduction in total demand. The increase in the facility electricity generation is due to increase in the facility biogas production by sending more primary sludge, which is more biodegradable and carbon-rich comparing to the secondary sludge, to the facility digesters. The aeration electricity demand also portrays a reduction with the increase in the extent of primary treatment removal. This can be explained to be due to reduction of the load going to the activated sludge, and better oxygen transfer efficiency in these units as hypothesized in the beginning of this chapter. The dynamic alpha trends developed and utilized for these scenarios' simulations, following the procedures in Methods chapter, also prove this hypothesis and the scenarios with higher extent of removal have higher alpha values. Similar figure to Figure 42 presenting the data for all the scenarios in this chapter is provided in the Appendix E. This figure also demonstrates the same findings as Figure 42.

To demonstrate the extent of electricity-savings of the three standalone APT technologies that are focused on in this chapter and their combinations with convention primary clarifier over the conventional clarifier scenario, the sum of their total and net power demand as well as their inhouse power generation for the entire study period are compared in Figure 43. The electricity demand and generation values for each scenario are normalized to each scenario's total QIR [47, 48] for the entire study period here and are presented as dimensionless ratios, with the conventional clarifier scenario's in the denominator, to simplify the comparison of scenarios in Figure 43.

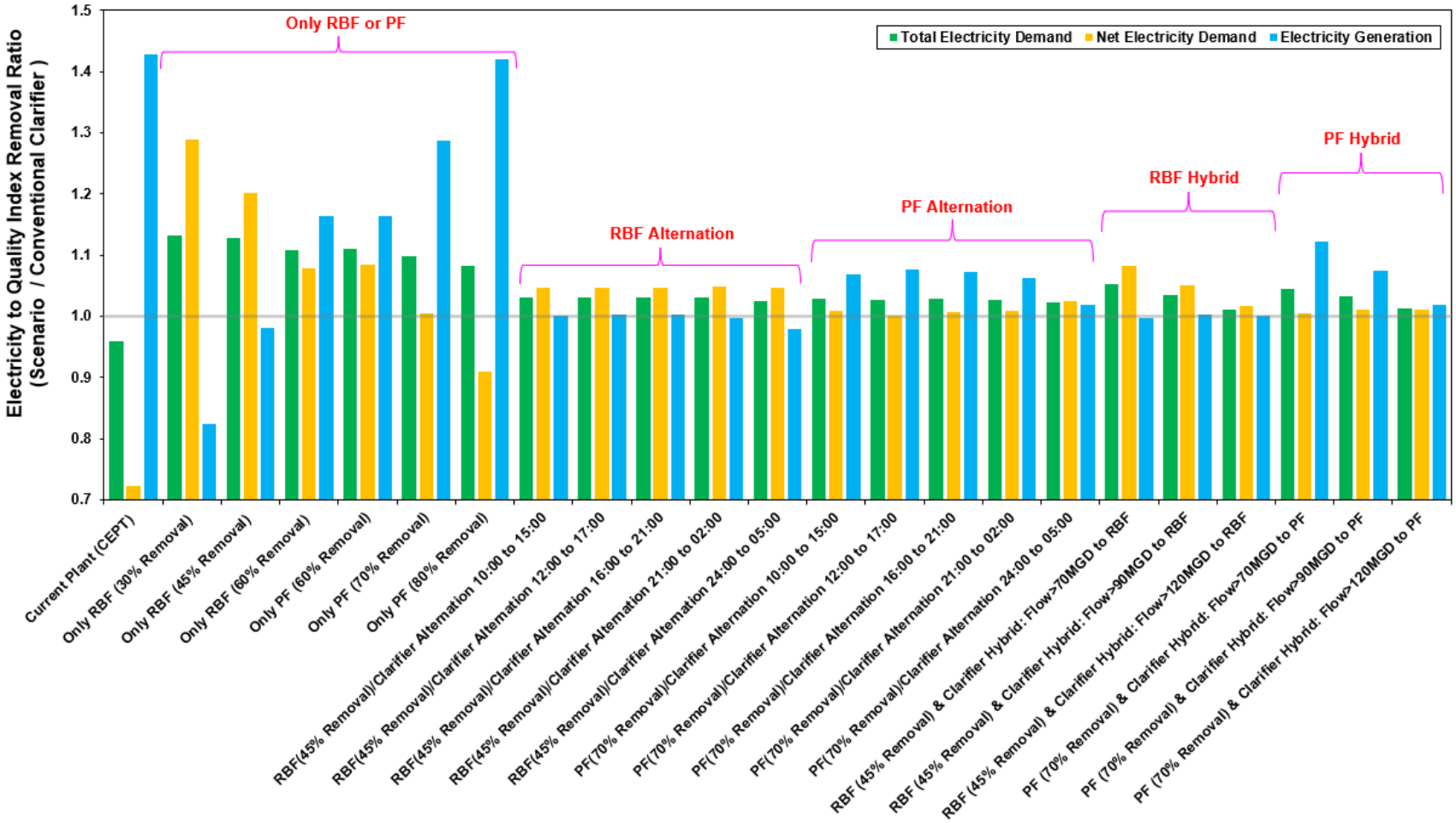

Figure 43. Sum of 12 consecutive months' total and net electricity demand and inhouse electricity generation values normalized to total quality index removal for all the scenarios with standalone advanced primary treatment and their combinations with conventional clarifier (Scenarios 2 to 8). These results are presented as dimensionless ratios, with the conventional clarifier scenario in the denominator. The light gray horizontal line represents the conventional clarifier scenario's ratio of 1 for all the three electricity categories presented here.

Figure 43 portrays that only CEPT and PF with precent solid removal of 80% result in a lower net electricity demand than conventional clarifier which can be explained with their extremely higher inhouse electricity generation comparing to the conventional clarifier scenario's. In other words, these are the only scenarios that provide net electricity demand savings over conventional clarifier scenario from overall demand standpoint. CEPT is the only scenario that has less total electricity demand than conventional clarifier scenario. This can be explained by the additional electricity required to operate BSTs on top of the influent pumping which is the main consumer of electricity in conventional clarifier and CEPT scenario. The electricity ratings used to simulate each of the PT technologies in this chapter are compared in Appendix B. Similar to Figure 42, Figure 43 also demonstrates the effect of the increase in extent of primary treatment on increasing and decreasing the electricity demand and generation respectively especially for the scenarios with a standalone primary treatment technology.

As emphasized through different chapters of this dissertation, in addition to the extent electricity demand, the dynamics of it is important for analyzing feasibility of different treatment configuration at WRRFs as the grid electricity tariffs and carbon intensities are also dynamic. The effect of electricity demand dynamics along with other cost and carbon-footprint benefits of APT technologies and their combinations over conventional clarifiers are discussed in more details in the operating cost and carbon-footprint sections of this chapter.

Greenhouse Gas Emissions

Similar to Figure 42, the sum of greenhouse gas (GHG) emissions from all the sources captured in this study for the entire 12 months study period, as explained in Methods chapter, after being normalize to QIR are compared in Figure 44 for all the standalone primary treatment technology scenarios in this chapter (Scenarios 1 through 4).

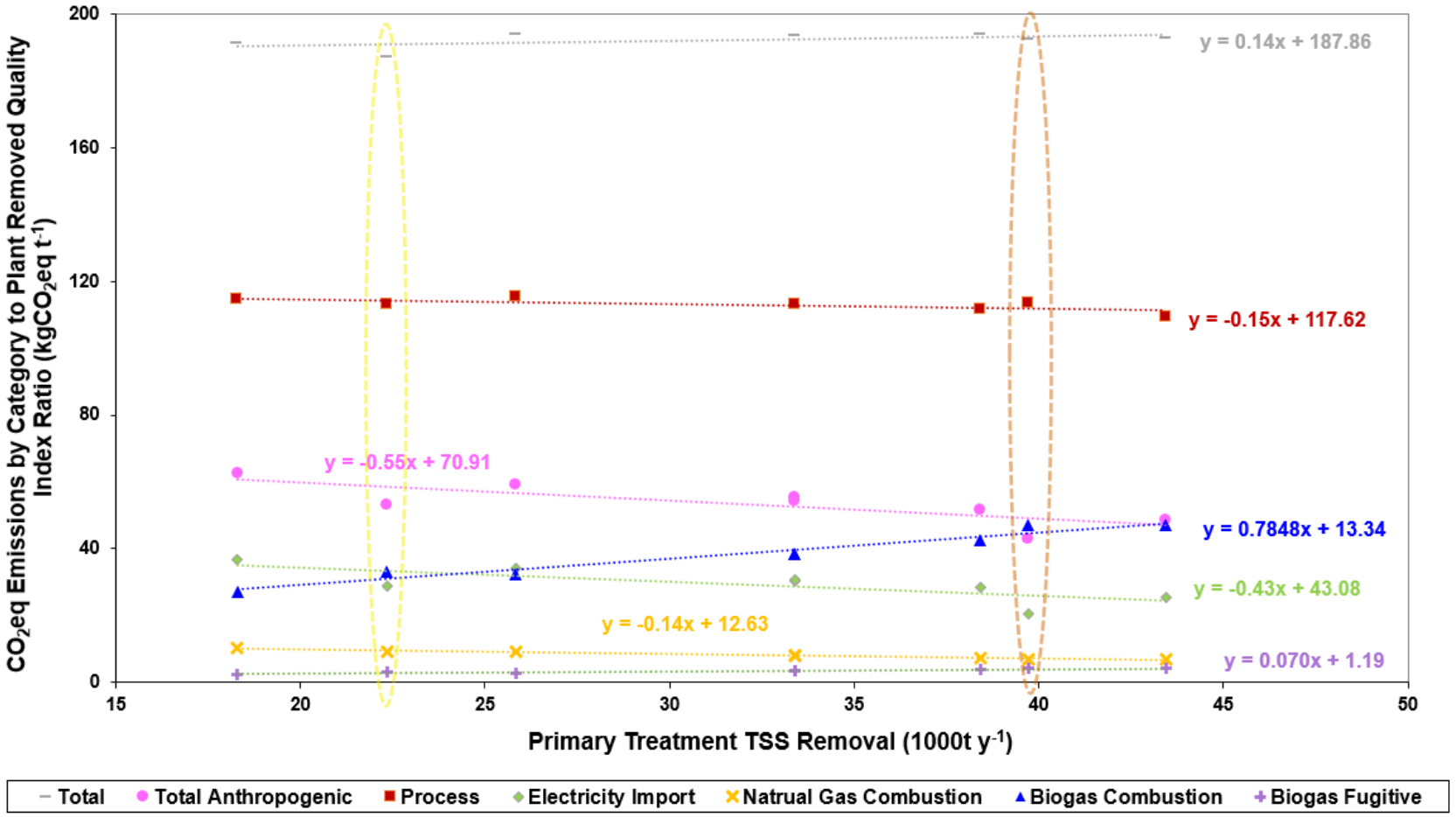

Figure 44. Comparison of sum of 12 consecutive months' greenhouse gas (GHG) emissions normalized to total quality index removal by GHG emission source category for Scenarios 1 through 4: standalone conventional primary clarifier, chemically enhanced primary treatment, rotary belt filters (RBF) and primary filters (PF) scenarios respectively. Standalone conventional and chemically enhanced primary treatment's values are highlighted using the yellow and brown dashed circles respectively. The remainder of data points represent standalone RBF and PF scenarios in the order of their extent of TSS removal from the left to right. The dotted trendlines and their matching color equations demonstrate the ascending and descending trend of each GHG emission data category. Anthropogenic total GHG emission is defined as total GHG excluding 87.18% of activated sludge process emissions [44], total CO_2 produced in digesters, and CO_2 portion of biogas combustion.

Among all the sources of GHG emissions accounted for here only biogas combustion and fugitive leak emissions show an increase with the increase in the extent of primary removal which is due to increase in the facility's biogas production. Process emissions which are associated to GHG (CO_2, CH_4, and N_2O) generated from the oxidation of the influent load in the activated sludge reactors and CO_2 production in digesters decline with the increase in the primary treatment extent of removal. This is due to the fact that higher extent of the primary removal diverts the biodegradable organics removal from oxidation in the activated sludge units to anaerobic digestion where these organics are converted to usable biogas as opposed to GHG emissions. The increase in biogas production as a result of higher extent of primary treatment reduces the facility's demand for natural gas and electricity imports which reduces the natural gas combustion and electricity import emissions although it increases the biogas combustion emissions. Despite the descending trend of most of GHG categories, the sum of all the GHG emissions presents a slightly ascending trend with increase in the extent of primary treatment.

Due to the renewable nature of biogas fuel and natural occurrence of oxidation performed in the activated sludge and digester units in the nature (i.e., biogenic nature), the GHG emissions from these sources are not considered as concerning GHG emissions that need to be capped and reduced by many carbon-footprint reduction regulation. California air Resources Board Cap and Trade regulation is an example of such regulations or protocols [43]. As such, anthropogenic GHG emissions is defined in this chapter as total GHG excluding biogenic (i.e., non-anthropogenic) emissions to present the portion of these emissions that is the concern of these environmental regulations. CO_2 portion of biogas combustion emissions is an example of this biogenic category per California air Resources Board Cap and Trade regulation [43]. Since the influent to the WRRF may contain traces of fossil fuel-based organics, not all the biological process emissions can be assumed to be biogenic, and a portion of these emissions should be accounted toward the anthropogenic GHG here. According to the data gathered by Tseng, et al.,

(2016), 87.18% of the biological process emissions in the activated sludge unit and all the CO_2 emission in the digesters on average can be assumed to be biogenic at this facility [44]. As such, 12.82% of the activated sludge process emissions needs to be accounted for toward the anthropogenic emissions. The anthropogenic emissions values, which are derived from subtracting these three biogenic categories from total GHG emission, have been also demonstrated in Figure 44. This figure illustrates a more extensive drop in the total anthropogenic emission with an increase in the extent of primary treatment comparing to each individual emission source and sum of all these emissions sources in total GHG values. This portrays the overall benefit of increase in the extent of the primary treatment by reducing the facility environmental impact from the global warming standpoint pursuant to the current regulations and protocols.

Figure 45 compares the total and anthropogenic GHG emissions of all the scenarios in this chapter for the entire study period (12 consecutive months). The emission values for each scenario here are normalized to each scenario's total QIR [47, 48] and are presented as dimensionless ratios, with the conventional clarifier scenario's in the denominator, to simplify the comparison of scenarios in this figure.

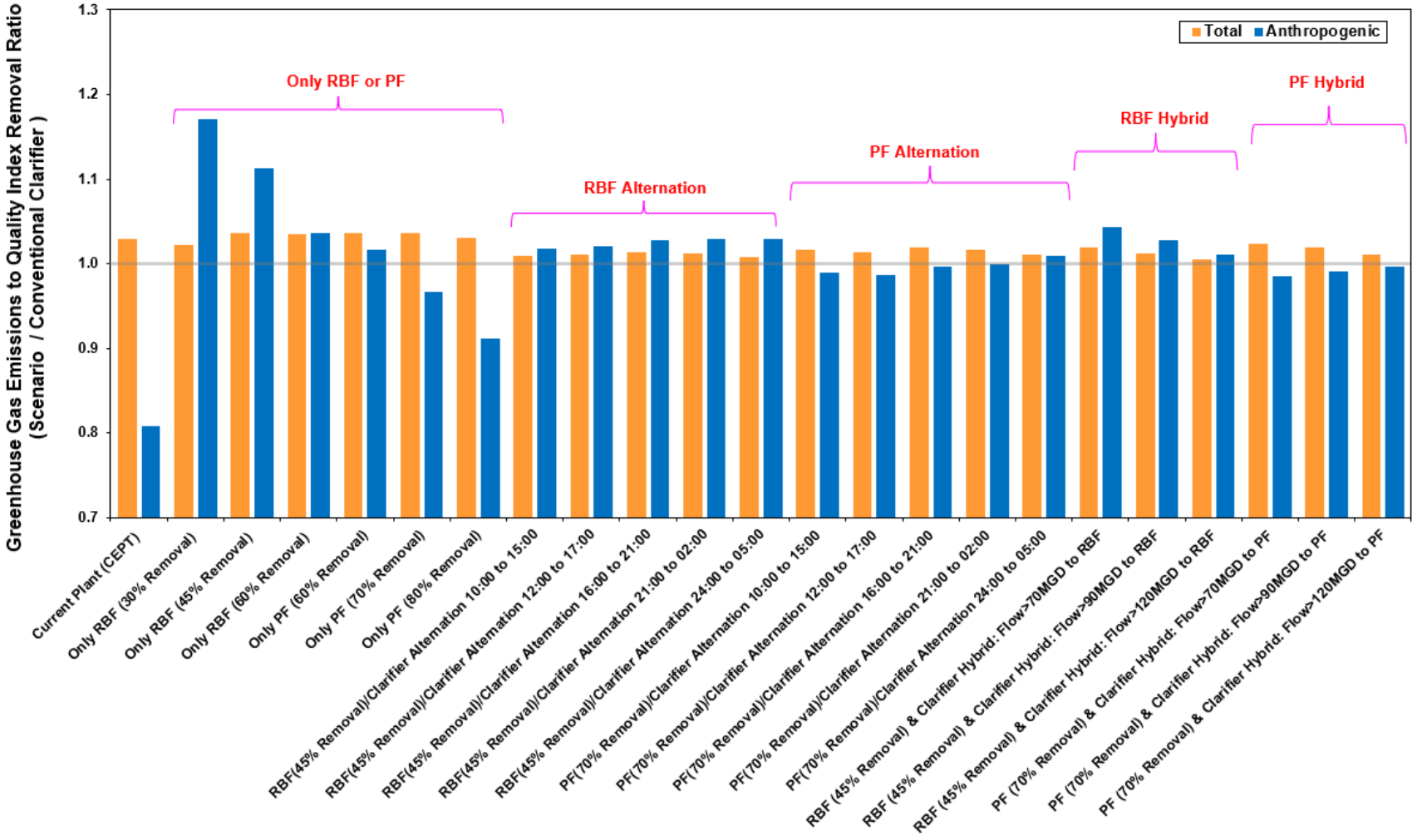

Figure 45. Sum of 12 consecutive months' total and anthropogenic greenhouse gas emissions normalized to total quality index removal for all the scenarios with standalone advanced primary treatment and their combinations with conventional clarifier (Scenarios 2 to 8). The results are presented as dimensionless ratios, with the conventional clarifier scenario in the denominator. The light gray horizontal line represents the conventional clarifier scenario's ratio of 1 for all the emission categories presented in this figure.

Figure 45 demonstrates that the total GHG emissions of all the scenarios are higher than the conventional clarifiers'. However, most of scenarios with higher extent of primary treatment than conventional clarifiers including CEPT, PF with % solid removal above 70%, all of the PF hybrid, and most of PF alternation scenarios have lower anthropogenic GHG emissions than standalone conventional clarifiers.

To better understand the impact of standalone APT technologies and their combination with the conventional clarifiers on the facility GHG emissions, each scenario's total GHG emissions for the entire study period by each emissions source category assessed in this study have been compared with the conventional primary clarifiers' in Figure 46. The emission values for each scenario are normalized to each scenario's total QIR [47, 48] and are presented as dimensionless ratios, with the conventional clarifier scenario's in the denominator, to simplify the comparison.

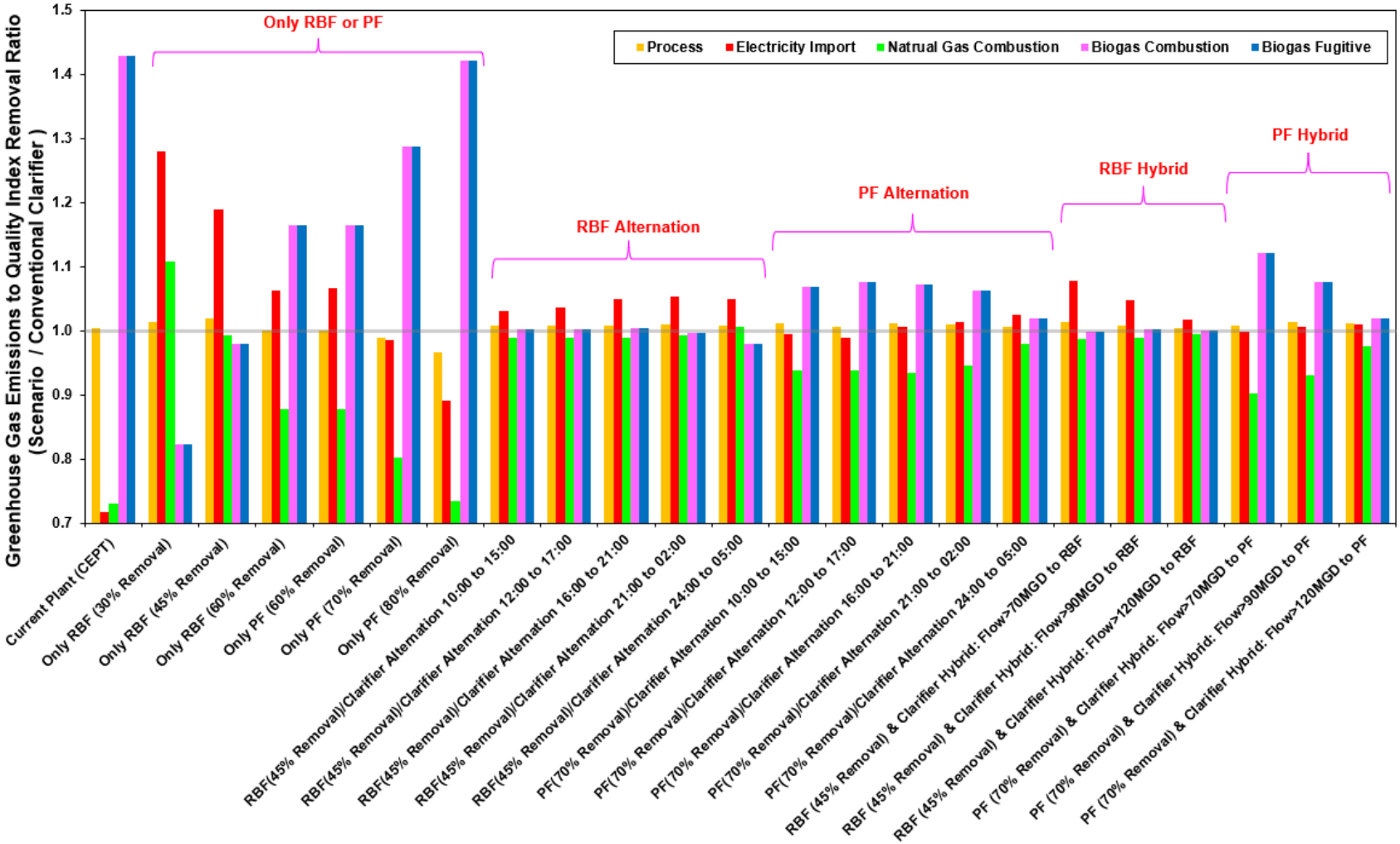

Figure 46. Sum of 12 consecutive months' greenhouse gas (GHG) emissions by source category normalized to total quality index removal for all the scenarios with standalone advanced primary treatment technologies and their combinations with conventional clarifier (Scenarios 2 to 8). The results are presented as dimensionless ratios, with the conventional clarifier scenario in the denominator. The light gray horizontal line represents the conventional clarifier scenario's ratio of 1 for all the GHG emission categories presented here.

As demonstrated in Figure 46, biogas combustion and fugitive emissions are directly correlated with the extent of primary solid removal as increasing the extent of the primary treatment increases the flow of more carbon-rich primary sludge to the digestors resulting in an increase in biogas production. This figure illustrates that all the scenarios including PF, CEPT and standalone RBF with % TSS removal of 60% in their primary treatment units produce more biogas than conventional clarifier scenario which results in their higher fugitive and biogas combustion emissions than conventional clarifiers. Natural gas combustion emission has a reverse correlation with biogas production. This can be explained by the role of natural gas as a secondary fuel in the absence of sufficient amount of biogas at this facility. As such, increase in the biogas production of the facility due to the increase in its extent of primary treatment leads to reduction in the facility natural demand and its combustion emissions.

Figure 46 also demonstrates comparable process emissions to of conventional clarifier scenario's for all of the scenarios except for standalone PF scenarios with percent TSS removal of equal to and higher than 70% whose process emissions are slightly lower. Figure 46 also illustrates the reverse correlation of the extent of removal and biogas production with electricity imports. This is due to the fact that increase in the biogas production at this WRRF in response to higher extent of primary solids removal increases the facility inhouse electricity generation which reduces the facility dependency on the grid's electricity and electricity imports. In addition to the extent of total power demand change, the timing of this change also impact the facility electricity import emissions in this dynamic assessment. This is due to the fact that carbon intensity of the grid is dynamic and varies through the day which can amplify or condense the extent of this emission source category.

Examples of this phenomenon can be observed by comparing the total net electricity dimensionless trends in Figure 43 with electricity import GHG emissions' in Figure 46. To simplify this comparison these dimensionless ratios are presented side-by-side in Figure 47 below:

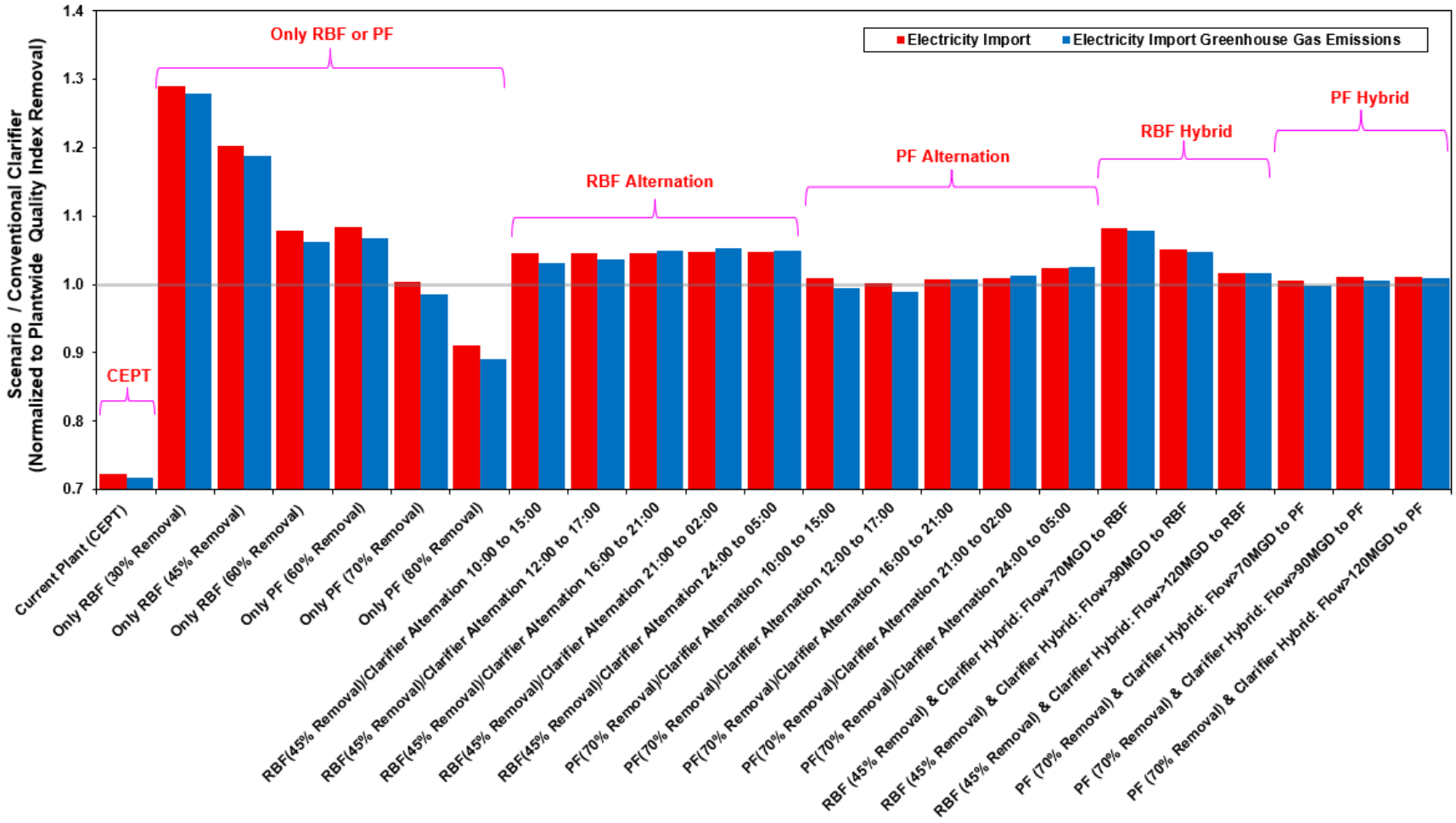

Figure 47. Sum of 12 consecutive months' electricity import and its greenhouse gas emissions normalized to total quality index removal for all the scenarios with standalone advanced primary treatment technologies and their combinations with conventional clarifier (Scenarios 2 to 8). The results are presented as dimensionless ratios, with the conventional clarifier scenario in the denominator. The light gray horizontal line represents the conventional clarifier scenario's ratio of 1 for all the electricity and emission categories presented here.

In Figure 47 the electricity imports, which is the same as net electricity demand, are reported to be close to conventional clarifier scenario's for standalone PF with 70% solid removal as well as PF and conventional clarifiers alternation between 10:00 to 15:00 and 12:00 to 17:00 scenarios. However, comparing the imported electricity GHG emissions for these scenarios in this figure demonstrates emissions lower than conventional clarifier scenario's for these scenarios. In other words, despite these scenarios' close total imported electricity during the study period here which is slightly greater than conventional clarifier's, their electricity import emissions which are calculated form these similar electricity imports come out to be lower than conventional clarifier scenario's at different magnitudes. This observation clearly demonstrates the effect of dynamic grid carbon intensity and how using averages average carbon intensities as opposed to their dynamic profiles may result in inaccurate conclusions. The opposite of this diminishing role of dynamic carbon intensity is observed in comparing the electricity imports and its GHG emissions of RBF-conventional clarifier alternation scenarios between 16:00 to 21:00, 21:00 to 2:00 and 00:00 to 5:00. For these scenarios, the electricity import emissions ratios to conventional clarifier scenario's seem to be slightly amplified after applying the gird dynamic emission intensities in calculating the electricity import GHG emissions.

To better illustrate the importance of calculating the electricity import GHG emissions as well as its cost dynamically, which is discussed in the next section, the average diurnal trend of each scenario's net electricity demand is developed by averaging the result of it's simulation for each hour of the day for the entire 12 months of this study period. These diurnal trends are compared in Figures 48 through 52. Similar to other electricity data comparison in this chapter, the net electricity trends developed in these figures are normalized to QIR [47, 48] and are presented as dimensionless ratios, with the conventional clarifier scenario's in the denominator, to simplify the comparison.

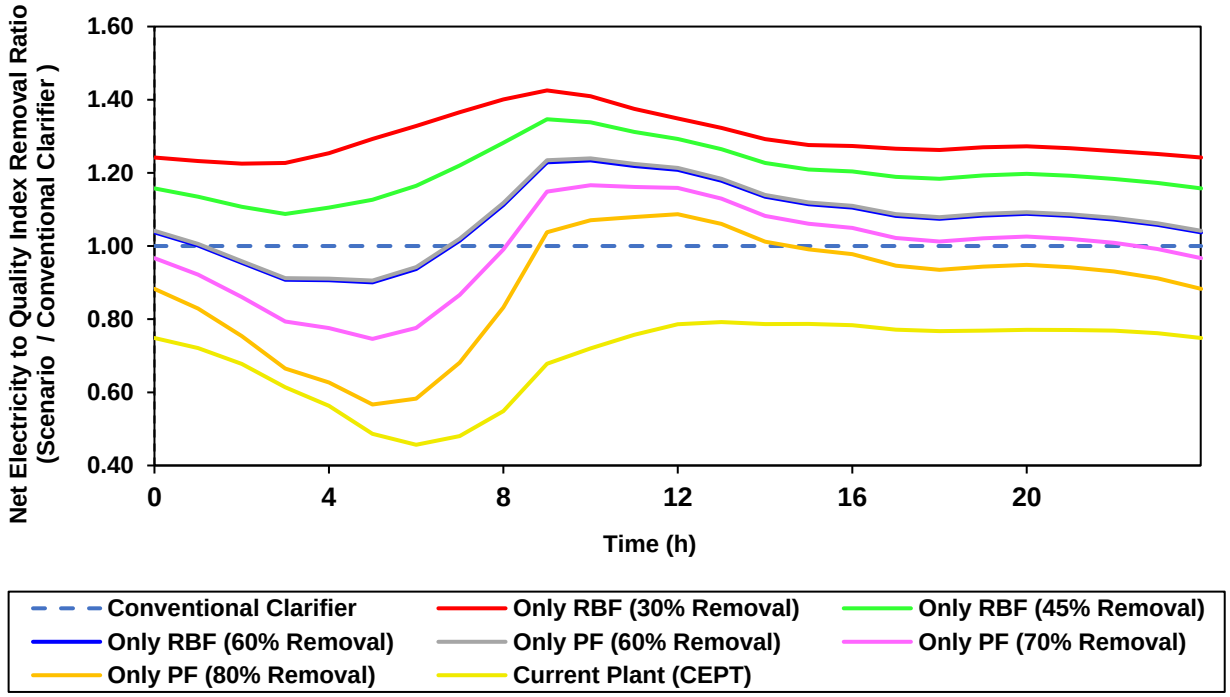

Figure 48. Comparison of standalone primary treatment technologies' average net electricity demand diurnal trends normalized to quality index removal presented as dimensionless ratios, with the conventional clarifier scenario's in the denominator.

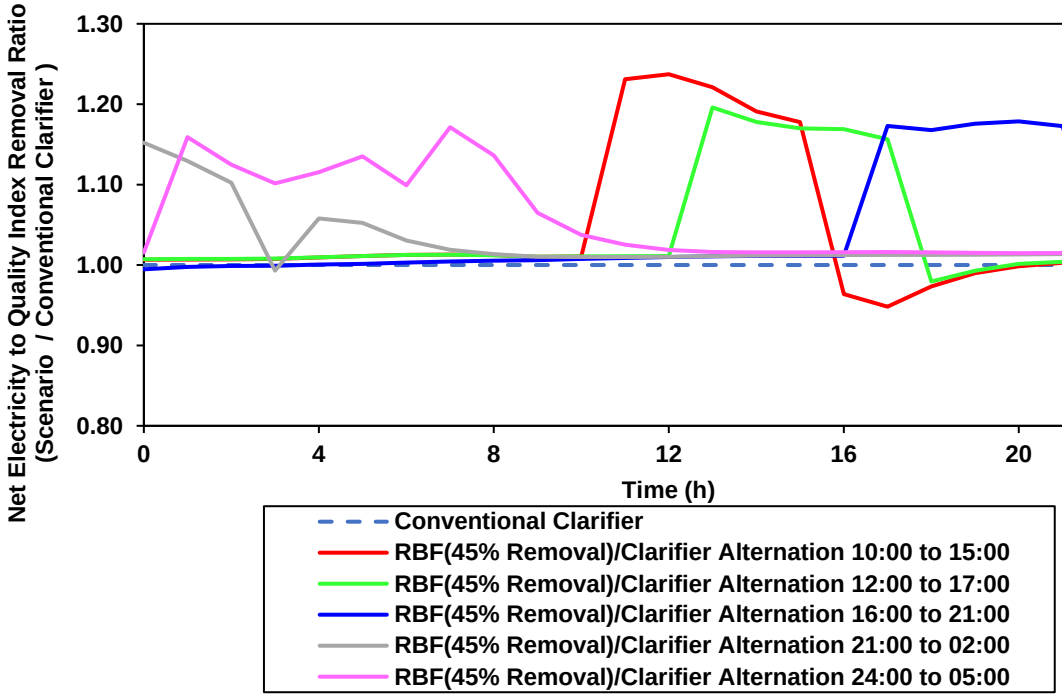

Figure 49. Comparison of rotating-belt filtration and conventional clarifier alternation scenarios' average net electricity demand diurnal trends normalized to quality index removal presented as dimensionless ratios, with the conventional clarifier scenario's in the denominator.

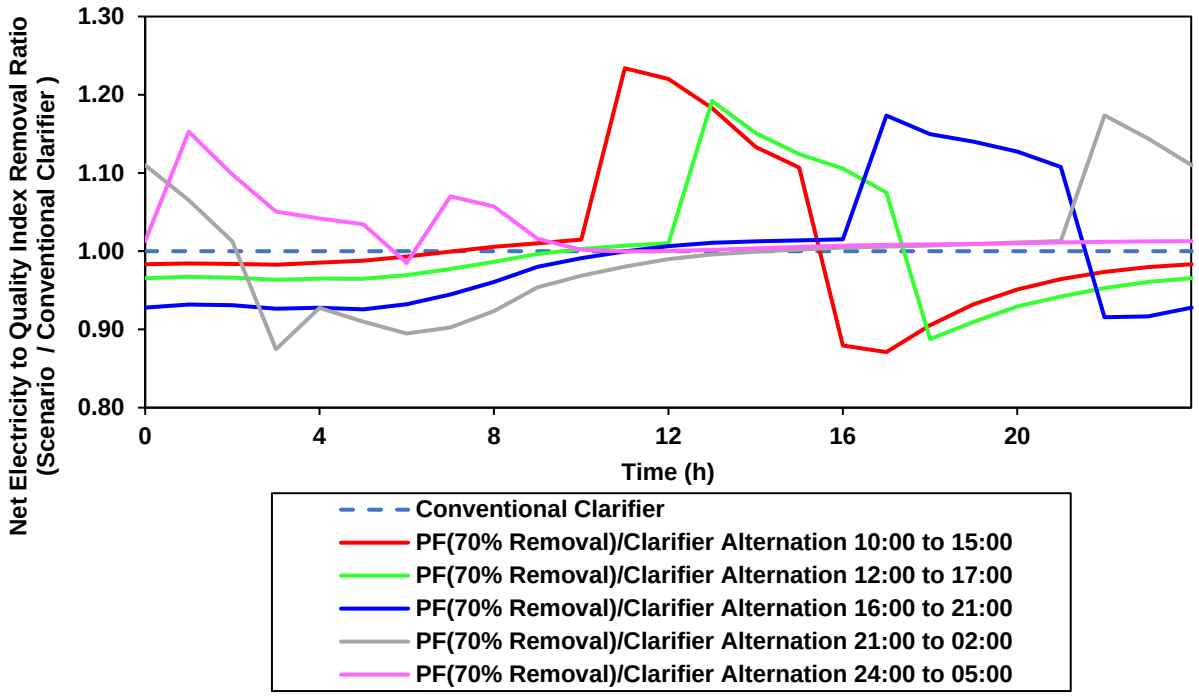

Figure 50. Comparison of primary filtration and conventional clarifier alternation scenarios' average net electricity demand diurnal trends normalized to quality index removal presented as dimensionless ratios, with the conventional clarifier scenario's in the denominator.

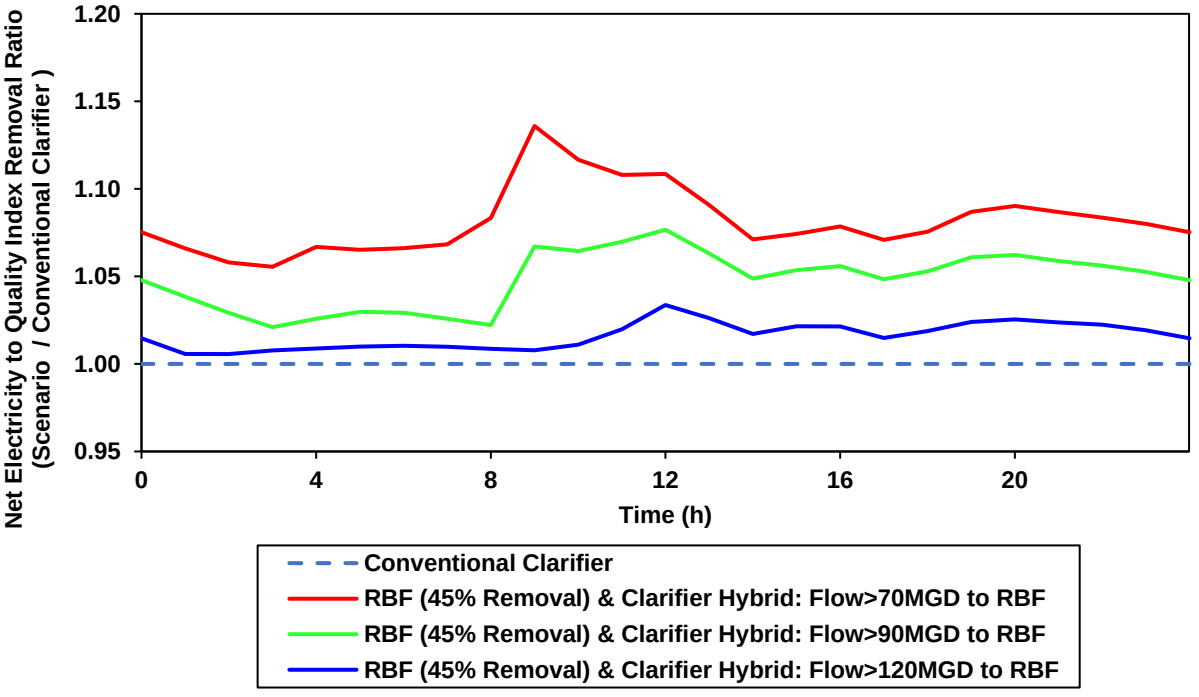

Figure 51. Comparison of rotating-belt filtration and conventional clarifier hybrid scenarios' average net electricity demand diurnal trends normalized to quality index removal presented as dimensionless ratios, with the conventional clarifier scenario's in the denominator.

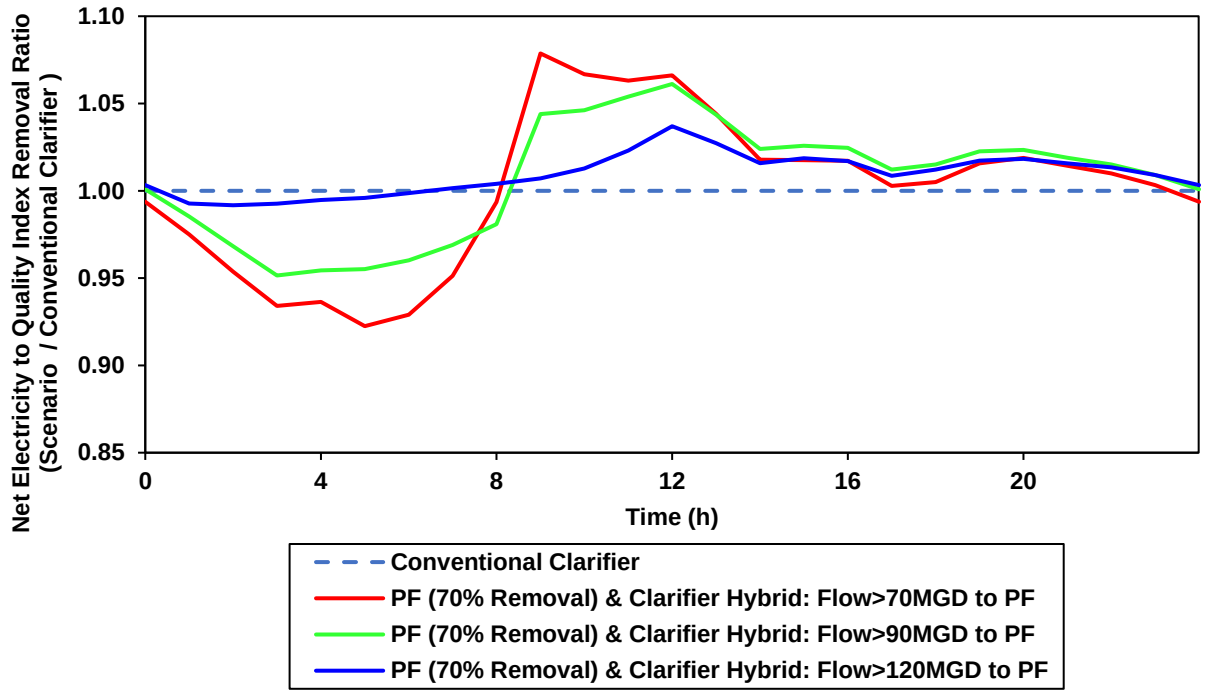

Figure 52. Comparison of primary filtration and conventional clarifier hybrid scenarios' average net electricity demand diurnal trends normalized to quality index removal presented as dimensionless ratios, with the conventional clarifier scenario's in the denominator.

Figures 48 to 52 demonstrates the dynamic blueprint of the net electricity demand for all the scenarios discussed in this chapter which can explain the amplifying and condensing effect of these dynamic profiles when they are coupled with dynamic grid tariffs and carbon intensity. For example, comparing the dynamic trends for RBF-conventional clarifier and PF-conventional clarifier alternation scenarios ins Figures 49 to 50 and California Independent System Operators' (CAISO's) grid carbon intensity dynamic trends in Figure 8 explains the discrepancy observed between the overall electricity imports and electricity impots GHG emissions in Figure 47 that was explained earlier.

In Figures 48 to 52, the area under each scenario's curve divided by conventional clarifiers' represents the dimensionless ratio of each scenario total average net electricity demand normalized to total QIR that is presented in Figures 43 and 47. In case of PF-conventional clarifiers alternation between 10:00 to 15:00 and 12:00 to 17:00 scenarios the area under the

curve for both of these scenarios in Figure 50 are comparable and close to conventional clarifier's represented by the dashed line. This is consistent with what Figures 43 and 47 demonstrate. However, comparing these scenarios' dynamic trends with CAISO's gird carbon intensities in Figure 8, demonstrates that peak and minimum of these scenarios' electricity imports coincide with the minimum and peak of the gird's carbon intensities respectively. Such coincidence results in the sum product of these trends to be smaller than of conventional clarifier's (condensing effect). This explains why these scenarios have lower electricity import GHG emissions than conventional clarifier scenario. The discrepancy in electricity imports and electricity imports' GHG emissions of RBF-conventional clarifier alternation scenarios between 16:00 to 21:00, 21:00 to 2:00 and 00:00 to 5:00 mentioned above can be explained similarly by comparing Figures 8 and49.

Figures 53 to 57 demonstrates the average diurnal trend of each scenario's electricity import GHG emissions which developed by averaging the product of each scenario's dynamic net electricity demand trends from its simulation and dynamic grid carbon intensities in Figure 8 for each hour of the day for the entire study period. Similar to other electricity comparison in this chapter, the net electricity trends used to develop this figure are normalized to QIR [47, 48] and final emission trends are presented as dimensionless ratios, with the conventional clarifier scenario's in the denominator, to simplify the comparison.

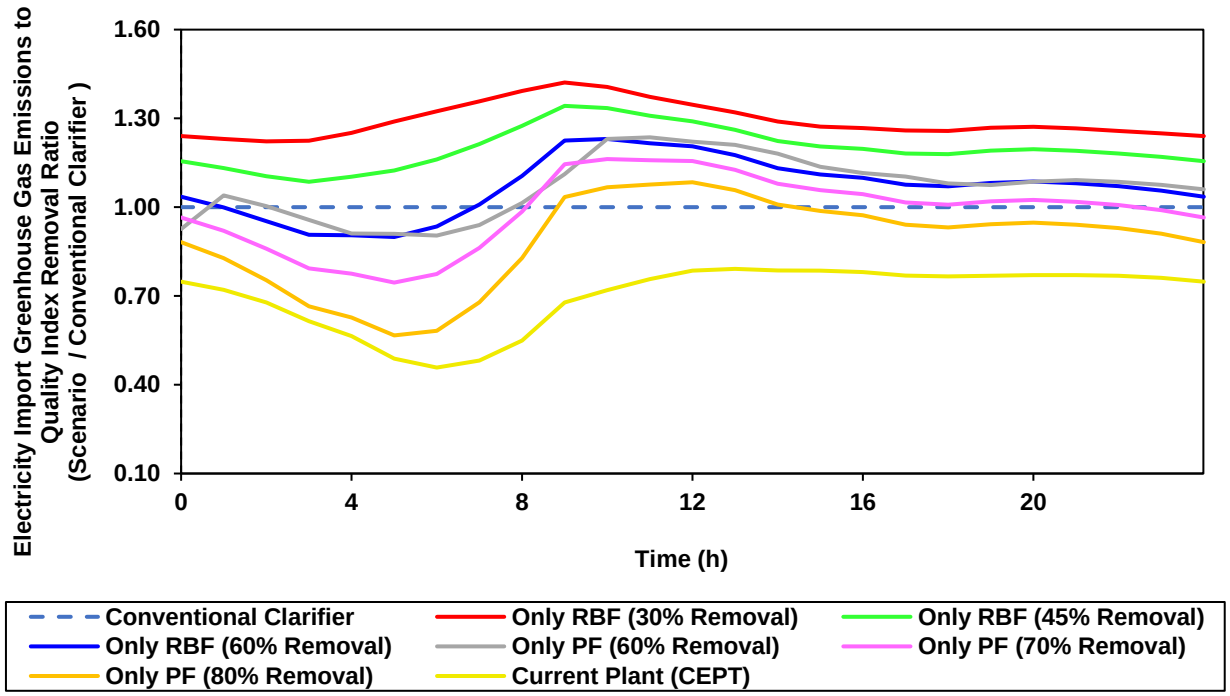

Figure 53. Comparison of standalone primary treatment technologies' average electricity import greenhouse gas emissions diurnal trends normalized to quality index removal presented as dimensionless ratios, with the conventional clarifier scenario's in the denominator.

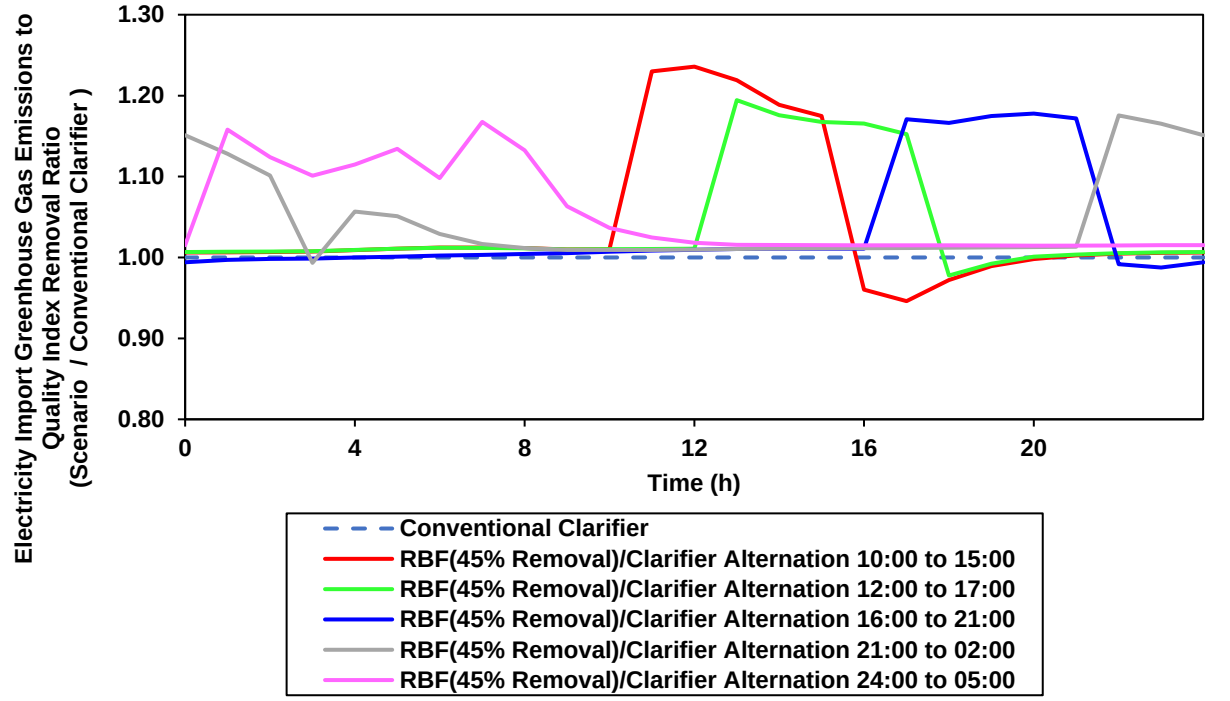

Figure 54. Comparison of rotating-belt filtration and conventional clarifier alternation scenarios' average electricity import greenhouse gas emissions diurnal trends normalized to quality index removal presented as dimensionless ratios, with the conventional clarifier scenario's in the denominator.

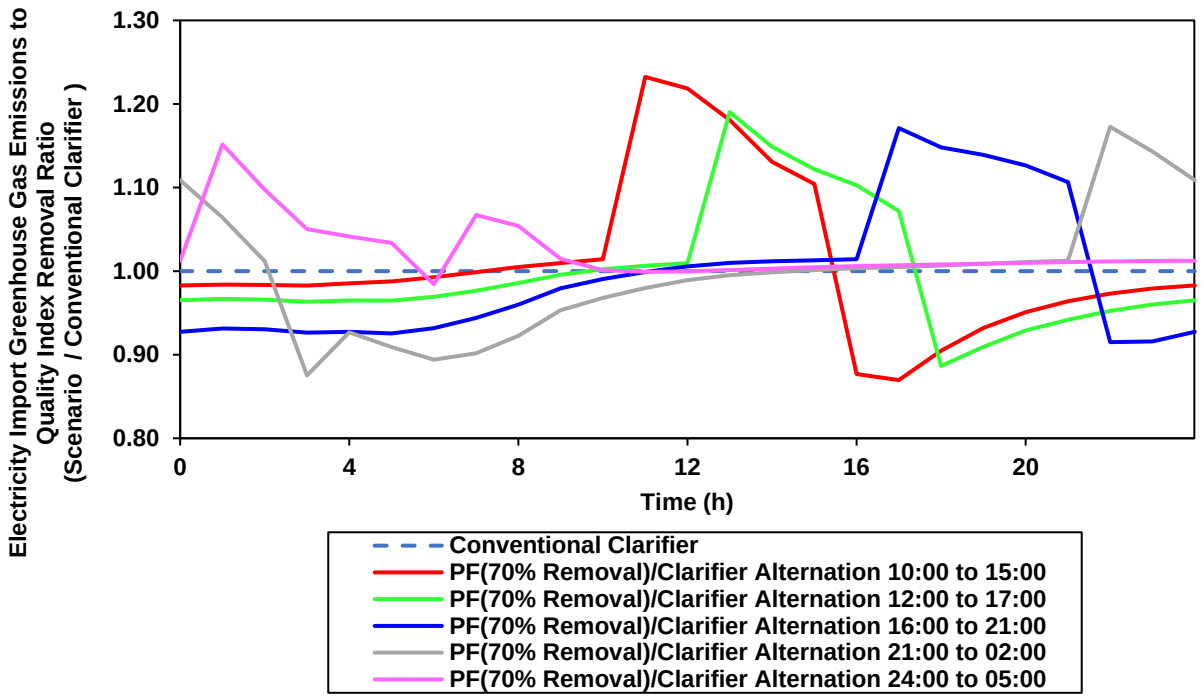

Figure 55. Comparison of primary filtration and conventional clarifier alternation scenarios' average electricity import greenhouse gas emissions diurnal trends normalized to quality index removal presented as dimensionless ratios, with the conventional clarifier scenario's in the denominator.

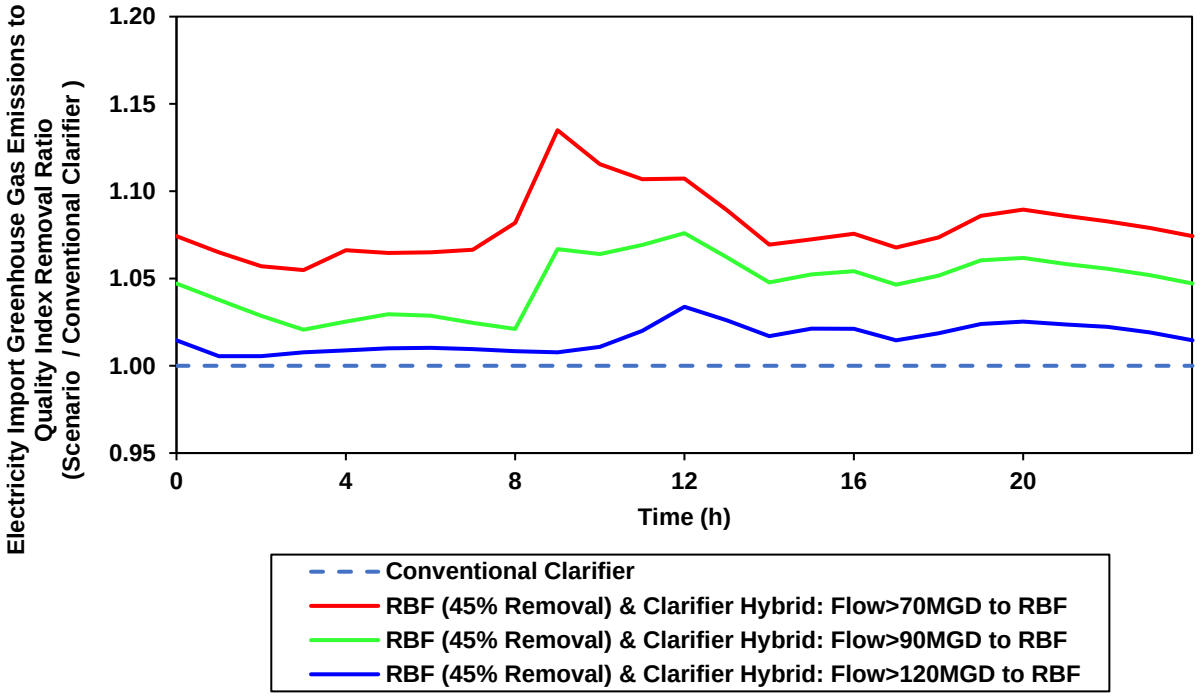

Figure 56. Comparison of rotating-belt filtration and conventional clarifier hybrid scenarios' average electricity import greenhouse gas emissions diurnal trends normalized to quality index removal presented as dimensionless ratios, with the conventional clarifier scenario's in the denominator.

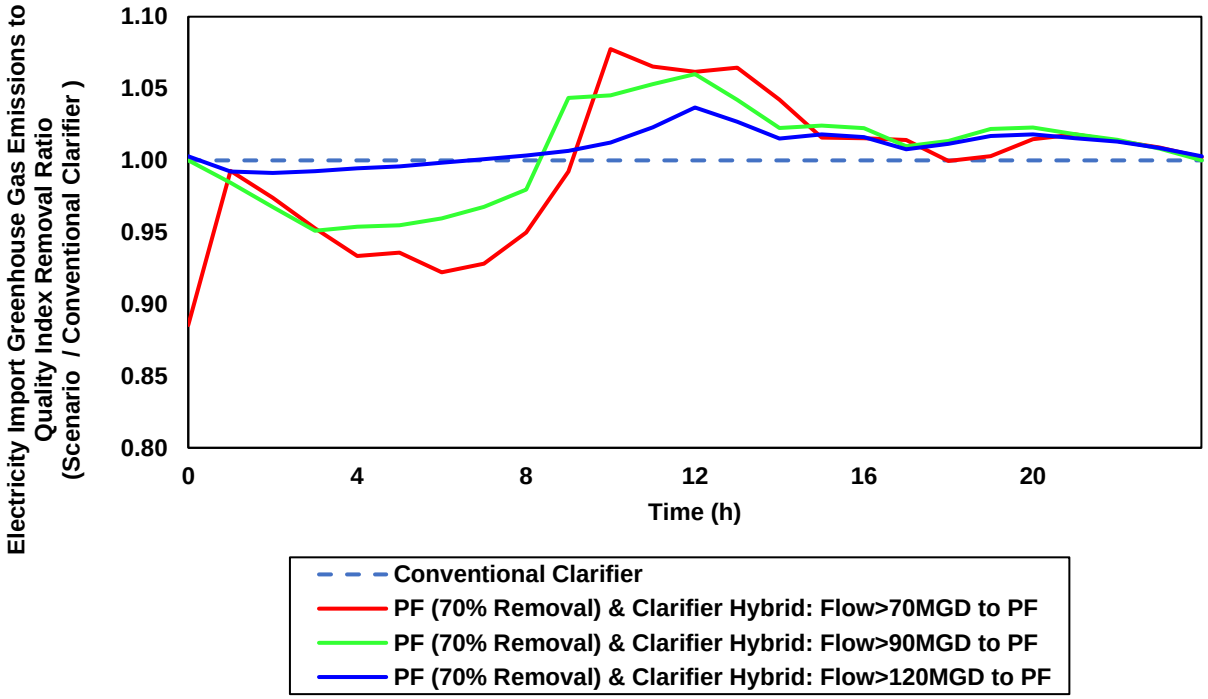

Figure 57. Comparison of primary filtration and conventional clarifier hybrid scenarios' average electricity import greenhouse gas emissions diurnal trends normalized to quality index removal presented as dimensionless ratios, with the conventional clarifier scenario's in the denominator.

These figures demonstrate the average diurnal trend of each scenario's electricity imports GHG emissions which can be used for detail comparison of the scenarios presented in this chapter. Similar to Figures 48 to 52 and 53 to 57, the diurnal average trends of facility-wide total and anthropogenic GHG emissions for all the scenarios have been developed and provided in the Appendix E of this dissertation as an additional reference for further analysis of the trends demonstrated in Figure 45.

Operating Cost

To assess the impact of different dynamic electricity tariffs on the total facility electricity import cost for each scenario, Figure 58 compares the total electricity import cost of all the scenarios presented in this chapter for the entire study period (12 consecutive months) and for each of the 5 tariffs presented in the Methods chapter. These cost values are normalized to each

scenario's total QIR [47, 48] and are presented as dimensionless ratios, with the conventional clarifier scenario's in the denominator, to simplify the comparison of these scenarios.

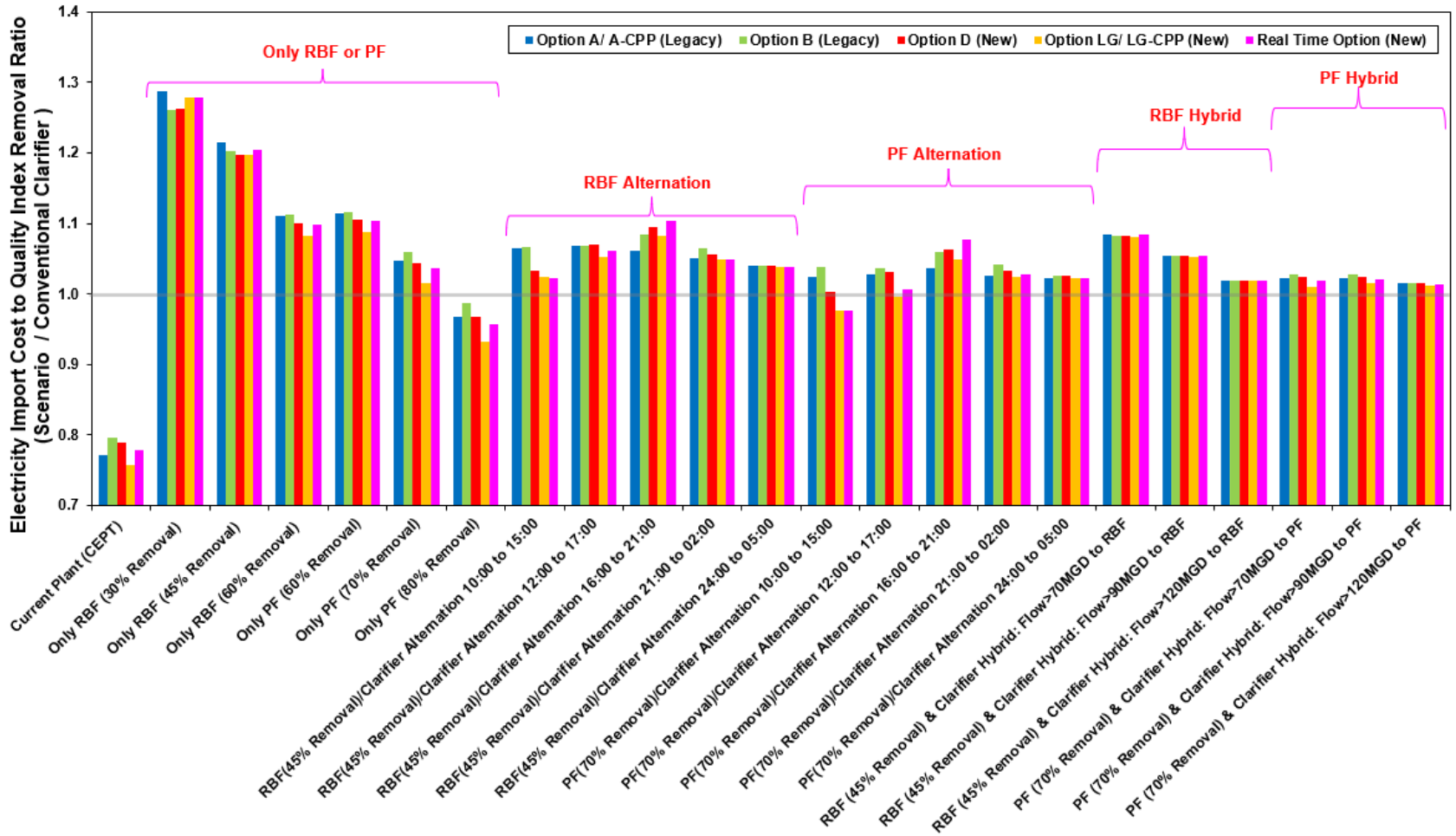

Figure 58. Sum of 12 consecutive months' electricity imports cost for each electricity tariff structure normalized to total quality index removal for all the scenarios with standalone advanced primary treatment technologies and their combinations with conventional clarifier (Scenarios 2 to 8). The results are presented as dimensionless ratios, with the conventional clarifier scenario in the denominator. The light gray horizontal line represents the conventional clarifier scenario's ratio of 1 for all the electricity tariffs.

Figure 58 demonstrates that in addition to the CEPT and standalone PF with 80% TSS removal scenarios, which are the only scenarios with lower net electricity demand (electricity imports) than conventional clarifier scenario according to Figure 43, PF-Conventional Clarifier alternation scenario between 10:00 to 15:00 also presents lower electricity demand cost than conventional clarifier for few of the tariff structures. Similar to greenhouse gas emissions analysis section of this chapter, this discrepancy demonstrates the importance of calculating the electricity import costs dynamically using dynamic tariff structures. This observation also elucidates that load shifting in this alternation scenario results in electricity cost savings for these tariffs although this scenario requires higher power imports than conventional clarifier's. As such, it can be concluded that it is not only the extent of the primary treatment that determines the cost-savings and feasibility of these technologies and electricity tariff structures play a key role too.

Similar to the electricity import GHG emission analysis in the previous section, closer comparison of the total electricity import cost ratios in Figure 58 with total electricity import (net demand) ratios in Figure 43 may identify more examples of scenarios with a discrepancy between their total electricity imports and cost ratios to conventional clarifier scenario's. As such, average diurnal trends for electricity import cost using each of the 5 tariff structures in the Methods chapter are included as a reference in Appendix E in case further investigation of such discrepancies are needed in the future.

Figure 58 also demonstrates that the increase in the extent of primary treatment in the standalone primary treatment technology options reduces the electricity imports cost which can be explained by reduction in the electricity imports (or net electricity demands) as demonstrated in Figure 43. In addition, comparing the scenarios with BST-conventional clarifier alternation demonstrates that implementing these power shifting options are less feasible during the peak of electricity grid (16:00 to 21:00) as they result in the highest electricity import costs for all the tariff structures.

Total operating costs of the scenarios discussed in this section are compared in Figure 59. The operating cost in this figure covers the entire study period (12 consecutive months) and are calculated for each of the 5 electricity tariffs presented in the Methods chapter. These cost values are normalized to each scenario's total QIR [47, 48] and are presented as dimensionless ratios, with the conventional clarifier scenario's in the denominator, to simplify the comparison of these scenarios.

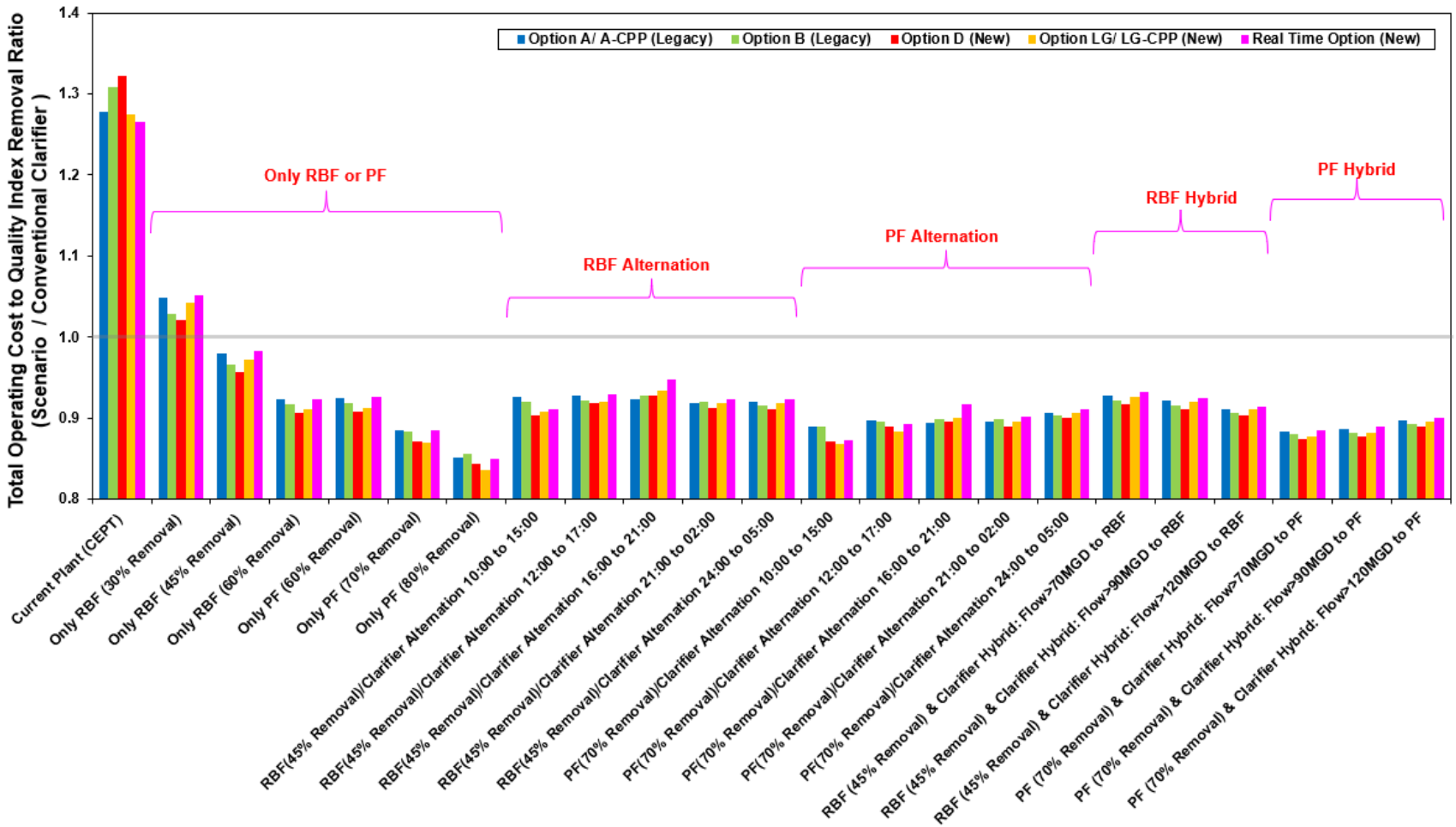

Figure 59. Sum of 12 consecutive months' plant operating cost by electricity tariff structures normalized to total quality index removal for all the scenarios with standalone advanced primary treatment technologies and their combinations with conventional clarifier (Scenarios 2 to 8). The results are presented as dimensionless ratios, with the conventional clarifier scenario in the denominator. The light gray horizontal line represents the conventional clarifier scenario's ratio of 1 for all the electricity tariffs.

Figure 59, surprisingly, portrays CEPT scenario as the least desirable scenario from the total operating cost standpoint. This scenario's high extent of the primary treatment removal without the need for additional electricity demand comparing to conventional clarifiers, in contrast with BST, leads to this scenario having the least net electricity demand and electricity import cost comparing to conventional clarifiers and other scenarios in this chapter. However, this scenario's cost of primary treatment enhancing chemical is so extensive that even with such an electricity cost-savings it still makes this scenario the most expensive option from total operating cost standpoint. More detailed comparison of chemicals cost as well as other operating cost categories such as natural gas and biosolid disposal is provided in the Figure 60. This observation significantly increases the value of the barrier separation technologies which can deliver higher extent of primary removal without the need for primary treatment expensive enhancing chemical agents.

As demonstrated in Figure 59, except CEPT and standalone RBF with 30% solid removal scenarios, all the BST and their combination with conventional clarifiers offer cost-savings over the conventional clarifier scenarios. This cost-saving seems to be maximized in scenarios where PF and its combination with conventional clarifier are utilized. According to Figure 59, the standalone PF scenario with 80% solid removal is the most cost-efficient option among these scenarios. Since this option also offers net electricity demand savings over conventional clarifier according to Figure 43, it is the best option for developing demand-side flexibility project at WARFs that utilize conventional clarifiers.

To better understand the more dominating role of other components of this facility's operating cost over electricity import cost, the contribution of these other components (i.e., natural gas imports, chemical additives and biosolid disposal) are compared in Figure 60. This figure covers the entire cost of each of these components during the study period (12 consecutive months). These cost values are normalized to each scenario's total QIR [47, 48] and are

presented as dimensionless ratios, with the conventional clarifier scenario's in the denominator, to simplify the comparison of these scenarios.

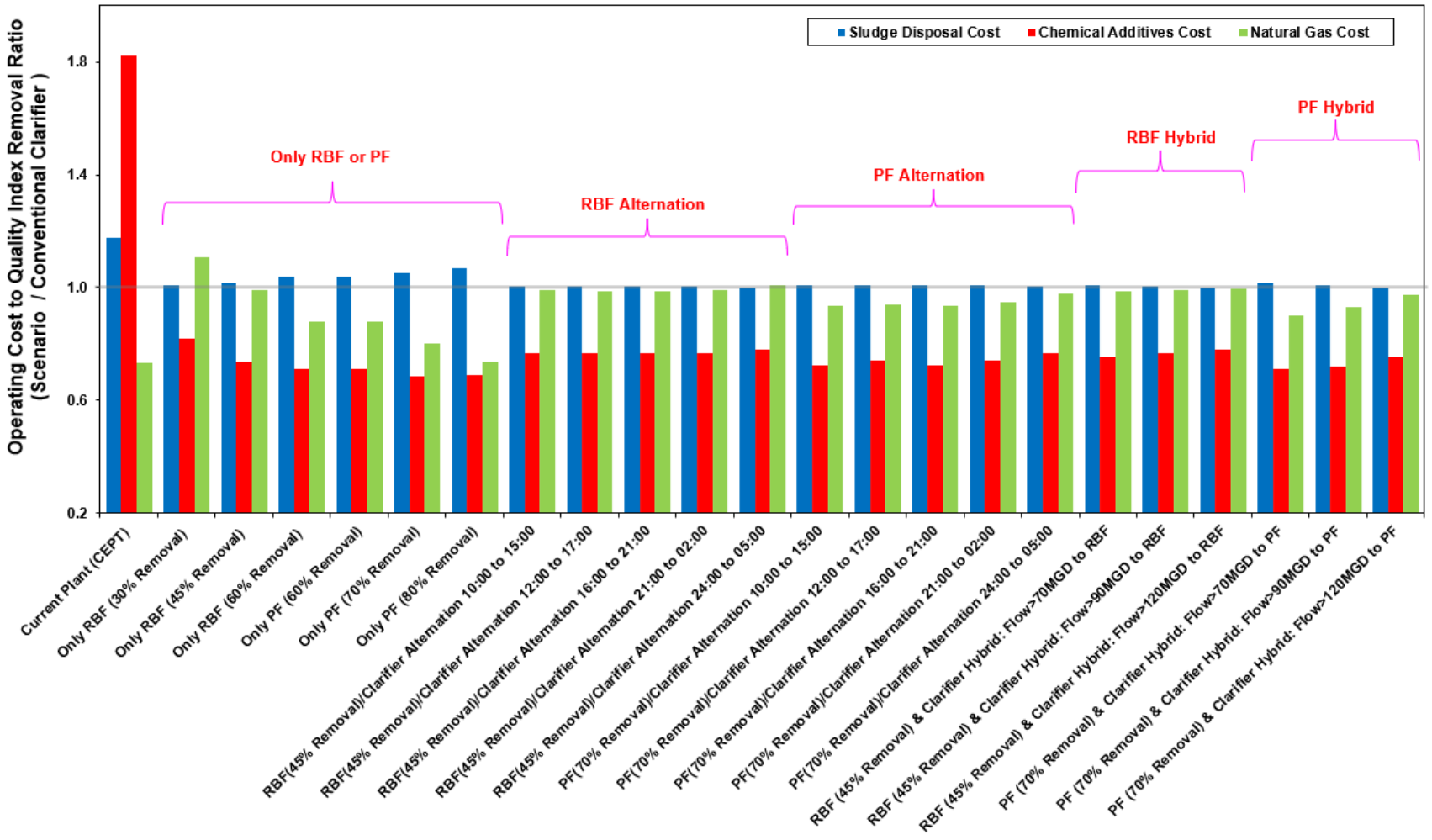

Figure 60. Sum of 12 consecutive months' plant operating cost by each non-electricity cost category normalized to total quality index removal for all the scenarios with standalone advanced primary treatment technologies and their combinations with conventional clarifier (Scenarios 2 to 8). The results are presented as dimensionless ratios, with the conventional clarifier scenario in the denominator. The light gray horizontal line represents the conventional clarifier scenario's ratio of 1 for all the operating costs categories.

Figure 60 demonstrates the significantly higher chemical additive cost of CEPT scenario comparing to the other scenarios which is due to addition of ferric chloride and anionic polymers to enhance the extent of primary treatment in this option. As indicated in the analysis provided for Figure 59, this significantly high cost explains the overall higher operating cost of this scenario comparing to all the other scenarios in this chapter. Figure 60 also demonstrates, an inverse correlation between the sludge thickening and dewater chemical additive usage and its cost and extent of primary treatment for BST scenarios here which translates into overall cost savings over conventional clarifier option for these scenarios. As explained before the extent of primary treatment is also inversely correlated to the natural gas usage and its cost as natural gas is substituted by the additional biogas production as result of increase in the extent of the primary treatment. Lastly, this figure demonstrates the direct correlation between the extent of primary removal and biosolid or sludge disposal cost which is more visible in the standalone scenarios.

Advanced Primary Treatment Cost-Effectiveness Dependency on External Factors

As explained in the operating cost analysis of this chapter, the cost of electricity import; natural gas; sludge thickening and dewatering chemical additives; CEPT chemical agents; and sludge disposal costs are assessed and combined to determine the overall cost-effectiveness of the scenarios discussed in this chapter. Each of these cost components relies on a fee rate and tariff structures that are developed outside of this WRRF's boundary by the utility providers, chemical vendors, or biosolid receiving or shipping company, which can dictate the faith and economic feasibility of the proposed scenarios inside this facility boundary. For example and as demonstrated in the previous section, the unit cost of the CEPT enhancing agent per plant influent volume (or flow) is the dominating factor that determines the overall operating cost ineffectiveness of CEPT scenario over conventional clarifier's despite its operating cost savings associated to less natural gas, sludge dewatering and thickening chemical and electricity usages.

In this section of this chapter, the effect of two of most contributing of these external factors to the overall operating cost of this WRRF is assessed. These are electricity tariffs and CEPT enhancing agent cost per facility's unit influent volume. For electricity tariffs this assessment is performed by defining and calculating a power price critical threshold ($*) below which each of the standalone BST scenarios (Scenarios 3 and 4) provide cost-savings over the conventional clarifier scenario (Scenario 1). This analysis and threshold will provide a blueprint for the electricity tariff domains that guarantee these scenarios' cost savings over conventional clarifier's. Equation 5 is used to determine this power price critical threshold ($*), electricity cost domain, or blueprint for which the decoupling of flow rate and load removal in primary treatment using standalone barrier separation (Scenarios 3 and 4) during the 24hr cycle is economically beneficial (i.e., the net cost or Cnet is positive).

$$\mathbf{C_{net}} = \int_{\mathbf{t=0}}^{\mathbf{t=24}} \mathbf{C_{PC}(t)} - \int_{\mathbf{t=0}}^{\mathbf{t=24}} \mathbf{C_{BS}(t)} > 0 \qquad \textbf{if} \qquad \mathbf{P} < \$^{*} \ \textbf{for a} \leq \mathbf{t} \leq \mathbf{b} \qquad \textbf{(Equation 5)}$$

Where: $\mathbf{C_{PC}}$ and $\mathbf{C_{BS}}$ are diurnal operating cost time function for the plant with standalone conventional clarifier and with standalone barrier separation respectively, **P** is cost of grid electricity in (USD kWh^{-1}), **$*** is a electricity price/tariff critical threshold at which the total operating cost of the WRRF with primary clarifier (baseline) is the same as barrier separations', and below which barrier separations' cost will be lower, **t** is time in (h) and **a** and **b** are hours of the day in ascending order ($0 \leq a < b < 24$).

This equation (inequality) has been further expanded and solved for **P** in Appendix D.

In case of CEPT scenario the effect of cost of primary treatment enhancing chemical additives per unit influent volume (or flow) needs to be also accounted for in the blueprint explained above. As such, the feasibility domain or blueprint defined for this scenario is for the critical ratio of these enhancing chemical additives cost rates per unit plant influent volume over electricity tariffs (Ω). Equation 6 is used to determine this critical ratio for which CEPT scenarios (Scenario 2) is cost-effective over conventional clarifiers (Scenario 1).

$$\mathbf{C_{net}} = \int_{\mathbf{t=0}}^{\mathbf{t=24}} \mathbf{C_{PC}(t)} - \int_{\mathbf{t=0}}^{\mathbf{t=24}} \mathbf{C_{CEPT}(t)} > \mathbf{0} \quad \mathbf{if} \quad \frac{\mathbf{Chem}}{\mathbf{P}} < \mathbf{\Omega} \quad \mathbf{for\ 0 \leq t \leq 24} \qquad (\mathbf{Equation\ 6})$$

Where: $\mathbf{C_{PC}}$ and $\mathbf{C_{CEPT}}$ are diurnal operating cost time function for the plant with standalone conventional clarifier and with standalone chemically enhanced primary treatment (CEPT) respectively; **P** is cost of electricity in (USD kWh^{-1}), **Chem** is cost of primary treatment enhancing chemical additives added to unit flow of the plant influent (USD $gallon^{-1}$), **Ω** is the critical ratio of unit price of chemical additives added to unit volume of primary treatment influent to enhance the treatment in (kWh $gallon^{-1}$) to electricity tariff at which the total operating cost of the WRRF with primary clarifier (baseline) is the same as CEPT, and below which CEPT's cost will be lower.

This equation (inequality) has been further expanded and rewritten to solve for **Ω** in Appendix D.

The cost-time equations introduced in the Equations 5 and 6 above account for the costs of electricity imports; CEPT chemical additives (only applicable to Scenario 2 and Ω); natural gas imports; additives used for sludge thickening and dewatering; and biosolids disposal which are calculated from the results of the simulations for each scenario for the entire study period and averaged for each hour of the day (averaged diurnal trends). As such, the instantaneous hourly and cumulative daily feasibility domains that are estimated here represent the entire study period although it only portrays one average diurnal hourly trend or cumulative daily range blueprint.

The average instantaneous or hourly electricity price critical thresholds ($*) in USD kWh^{-1} for each hour of the day below which each of the standalone barrier separation scenarios has cost savings over conventional clarifier's have been calculated using the result of their dynamic simulations and Equation 5 and illustrated in Figures 61 to 66. In these figures, the green range represents the electricity tariffs domains for which BST scenario has cost-savings over conventional clarifier scenario and red represents tariff domains that conventional clarifier option is more cost-effective. The boundary between these two color-zones represents $*. As indicated in the Methods chapter, electricity tariffs usually consist of other components such as metering and fixed and time-dependent demand charges in addition to energy charges. However, for this

analysis the electricity tariff assumed to be only consist of energy charges (delivery and generation) to make the assessment summarized in this section and in Figures 61 to 66 mathematically possible as only one variable could be calculated using Equation 5 (i.e., one equation and one variable).

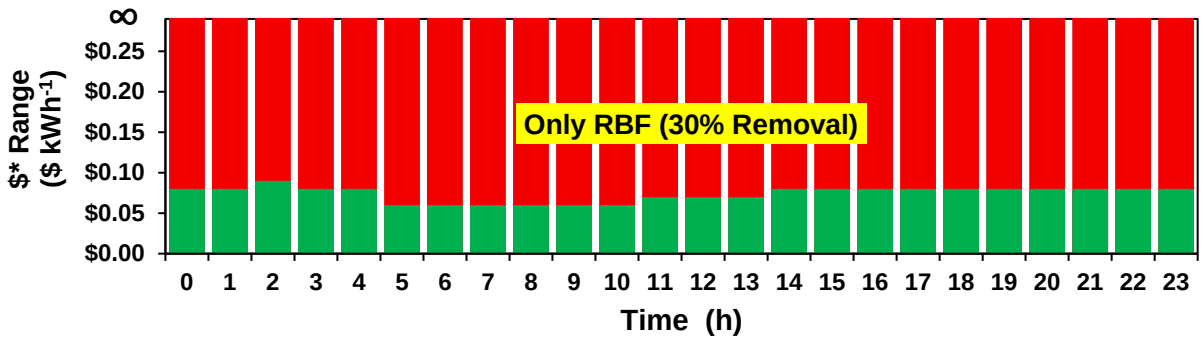

Figure 61. The instantaneous hourly electricity import cost domain for which standalone rotating-belt filtration (Only RBF) scenario with 30% TSS removal has operating cost savings over conventional clarifier's. Green range represents the electricity tariff domains for which this barrier separation technology scenario has cost-savings over the conventional clarifier's scenario and red represents tariff domains that conventional clarifier scenarios is more cost-efficient. The boundary between these two color-zones represents $*.

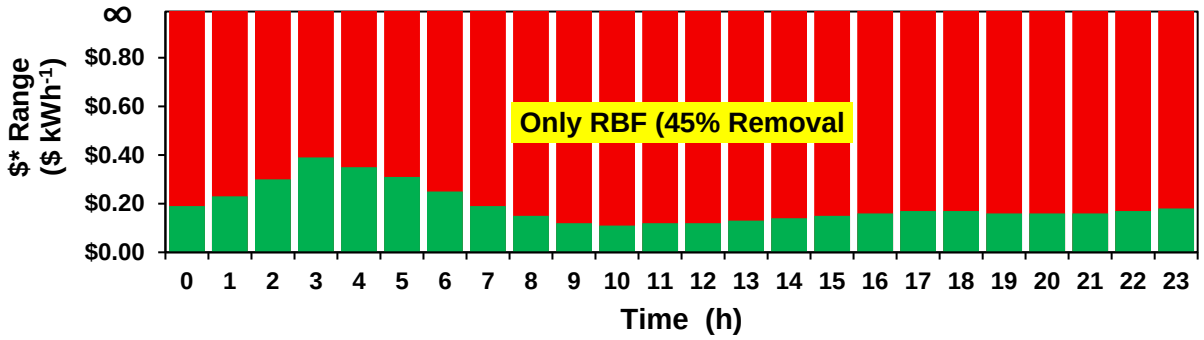

Figure 62. The instantaneous hourly electricity import cost domain for which standalone rotating-belt filtration (Only RBF) scenario with 45% TSS removal has operating cost savings over conventional clarifier's. Green range represents the electricity tariff domains for which this barrier separation technology scenario has cost-savings over the conventional clarifier's scenario and red represents tariff domains that conventional clarifier scenario is more cost-efficient. The boundary between these two color-zones represents $*.

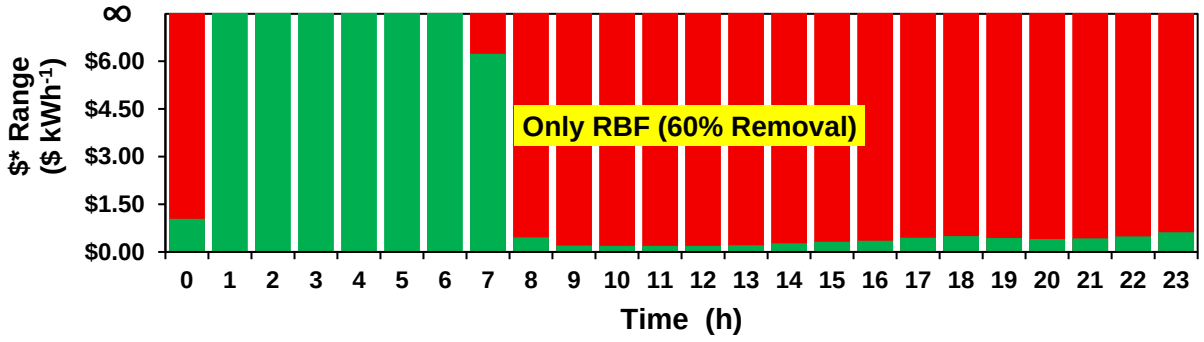

Figure 63. The instantaneous hourly electricity import cost domain for which standalone rotating-belt filtration (Only RBF) scenario with 60% TSS removal has operating cost savings over conventional clarifier's. Green range represents the electricity tariff domains for which this barrier separation technology scenario has cost-savings over the conventional clarifier's scenario and red represents tariff domains that conventional clarifier scenario is more cost-efficient. The boundary between these two color-zones represents $*.

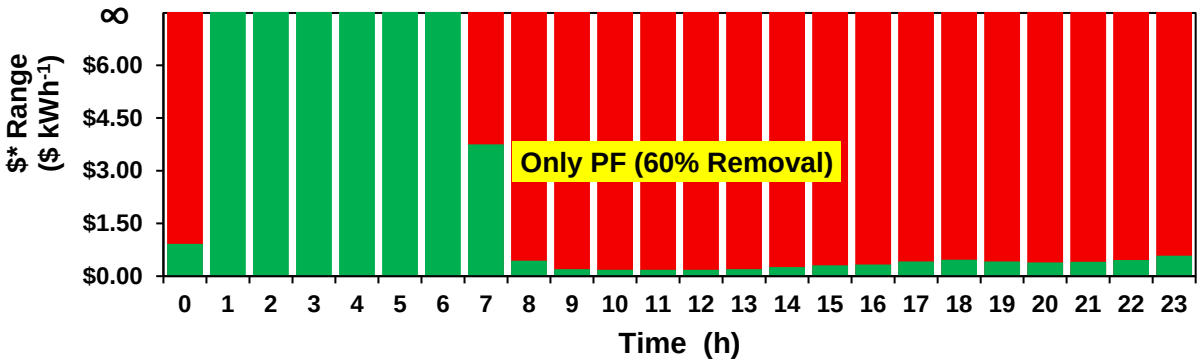

Figure 64. The instantaneous hourly electricity import cost domain for which standalone primary filtration (Only PF) scenario with 60% TSS removal has operating cost savings over conventional clarifier's. Green range represents the electricity tariff domains for which this barrier separation technology scenario has cost-savings over the conventional clarifier's scenario and red represents tariff domains that conventional clarifier scenario is more cost-efficient. The boundary between these two color-zones represents $*.

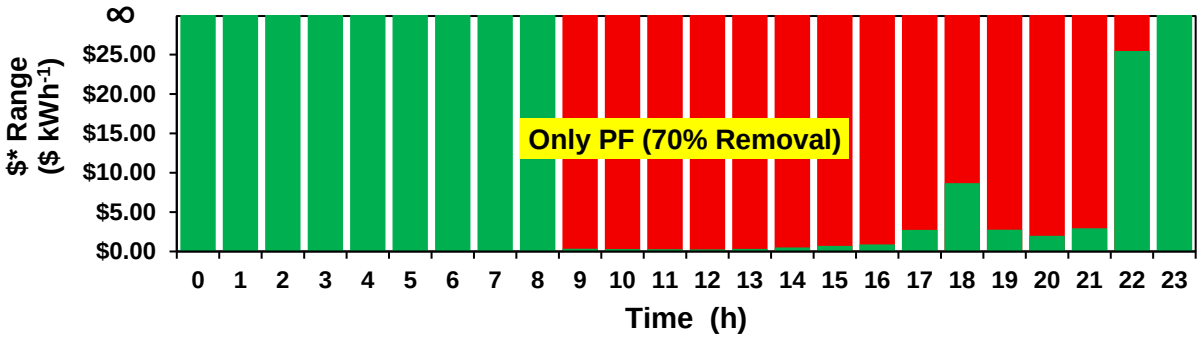

Figure 65. The instantaneous hourly electricity import cost domain for which standalone primary filtration (Only PF) scenario with 70% TSS removal has operating cost savings over conventional clarifier's. Green range represents the electricity tariff domains for which this barrier separation technology scenario has cost-savings over the conventional clarifier's scenario and red represents tariff domains that conventional clarifier scenario is more cost-efficient. The boundary between these two color-zones represents $*.

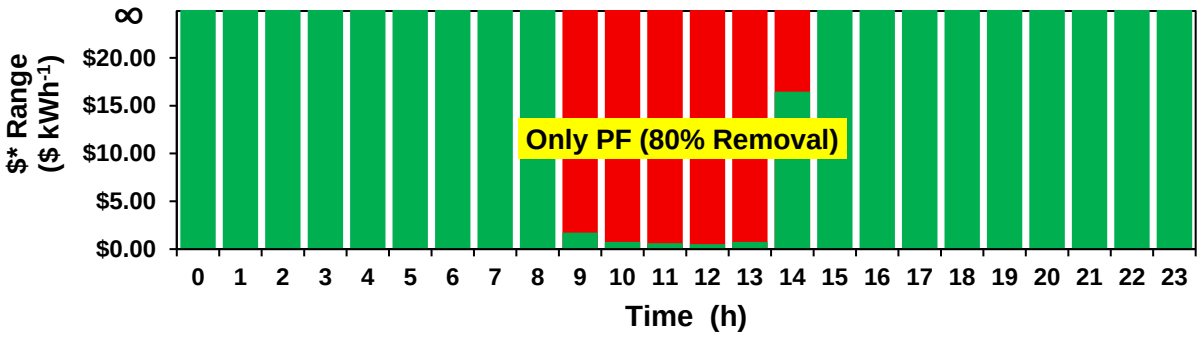

Figure 66. The instantaneous hourly electricity import cost domain for which standalone primary filtration (Only PF) scenario with 80% TSS removal has operating cost savings over conventional clarifier's. Green range represents the electricity tariff domains for which this barrier separation technology scenario has cost-savings over the conventional clarifier's scenario and red represents tariff domains that conventional clarifier scenario is more cost-efficient. The boundary between these two color-zones represents $*.

The Y-axis boundary in the bar charts presented in Figures 61 to 66 had to be selected independently for each of the scenarios in order to make all the green domains' boundaries visible for every hour of the day, as such, great care is needed when these bar charts are compared. In addition, the upper boundaries of these bar charts' Y-axis are set to be infinite (∞) to completely demonstrates the mathematical analysis performed using Equation 5 although electricity tariffs have finite ranges.

Figures 61 to 66 demonstrates that increase in the extent of a primary treatment (% solid removals) in these BST scenarios expands the domain of electricity costs for which barrier separation scenarios generate cost-savings over conventional clarifier's (i.e., larger $*). This expansion results in $* covering the entire mathematical price domain (0 to ∞ USD kWh^{-1}) for certain hours of the day for some of these BST scenarios; for example, 1:00 to 6:00 in standalone RBF scenario with 60% TSS removal. This can be interpreted as independency of this scenario operating cost-effectiveness over the conventional clarifier scenario from electricity tariffs for these hours. Further increase in the extent of a primary treatment in the standalone PF scenarios in Figures 64 to 66 demonstrates the expansion of these full price range domains (i.e., cost-effectiveness independency from the electricity tariff domains) to more hours of the day which reaches to 75% of the hours in a day in the standalone PF scenario with 80% TSS removal. This observation illustrates that the extent of the primary treatment in these BST scenarios is inversely correlated with the dominance of electricity tariffs as an external factor on determining the overall cost-savings of these scenarios over conventional clarifiers. In other words, the increase in the extent of the primary treatment diminishes the role of electricity tariffs in economic feasibility determination of these scenarios.

In order to simplify the comparison of these scenarios, the same analysis that was performed on hourly bases and presented in Figures 64 to 66 is also performed on average daily bases for the entire 12 months study period to come up with one as opposed to 24 electricity cost

domains for each scenario. The daily electricity tariff feasibility domain for the six BST scenarios discussed in this section are compared in Figure 67.

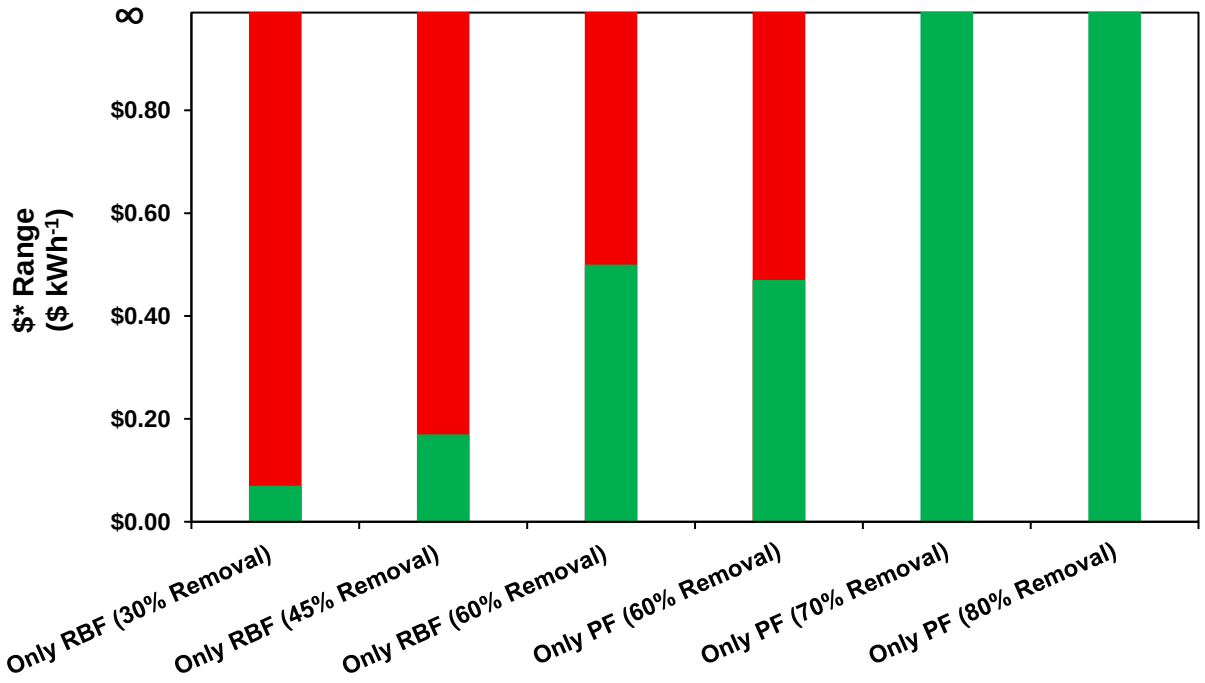

Figure 67. The cumulative daily electricity import cost domain for which each standalone barrier separation technology (primary filtration or PF and rotating-belt filtration or RBF) scenario has operating cost savings over conventional clarifier's. Green range represents the electricity tariff domains for this barrier separation technology scenario has cost-savings over the conventional clarifier's scenario and red represents tariff domains that conventional clarifier option is more cost efficient. The boundary between these two color-zones represents $*.

Similar to Figures 64 to 66, Figure 67 also demonstrates how upgrading to a BST with higher extent of removal expands the range of electricity tariffs that provides cost-savings over conventional clarifier scenario. It also demonstrates the PF scenarios with the % solid removal of the greater than or equal to 70% are the options that provide overall cost savings over conventional clarifiers independent from the electricity tariffs. This slightly changes the conclusion drawn from Figures 61 to 66 suggesting the role of electricity utility companies on dictating the feasibility of these BST through setting their tariff structures at least for some of the hours during the day. Figure 67 elucidates that although this conclusion may be applicable if we determine the feasibility on hourly bases, it may change when we assess the feasibility cumulatively over the

course of an average day for BST options that offer higher extent of removal (PF with solid removal ≥70%). This is due to the fact that the costs-saving of these scenarios over the conventional clarifier scenario for the hours that they are more cost-effective can be significant enough to compensate the hours that the facility losses money on electricity imports for by utilizing BSTs over conventional clarifiers. Therefore, the feasibility of some of these high performing BST become independent from electricity tariff structure. As explained before some key components of the grid electricity tariffs such as demand charges had to be excluded in this assessment. As such, further analysis using more advanced tariff calculating programs developed and used by electricity utility providers may need to be performed in the future studies to perform this assessment such that it will account for other component of the electricity tariffs.

In order to perform the similar assessment summarized in Figures 61 to 67 for CEPT scenario, the cost of primary treatment enhancing agents used for this scenario needs to be accounted for in addition to the electricity tariff as an outside controlling factor that has a role in dictating the cost-effectiveness of this scenario. As such for this scenario, a feasibility domain of ratio of cost of all enhancing chemical agents added per unit volume of the primary treatment influent to grid electricity cost (i.e., Ω in (USD m^{-3}) / (USD kWh^{-1}) or kWh m^{-3}) is determined using Equation 6 over which CEPT scenario is expected to provide overall operating cost-savings over conventional clarifiers. This domain has been illustrated in Figure 68 where green range represents the chemical additives to electricity costs ratios for which CEPT scenario has cost-savings over the conventional clarifier scenario and red represents ratios for which conventional clarifier option is more cost-efficient. The boundary between these two color-zones represents Ω. This figure provides the cost ratio domains in both SI and American units.

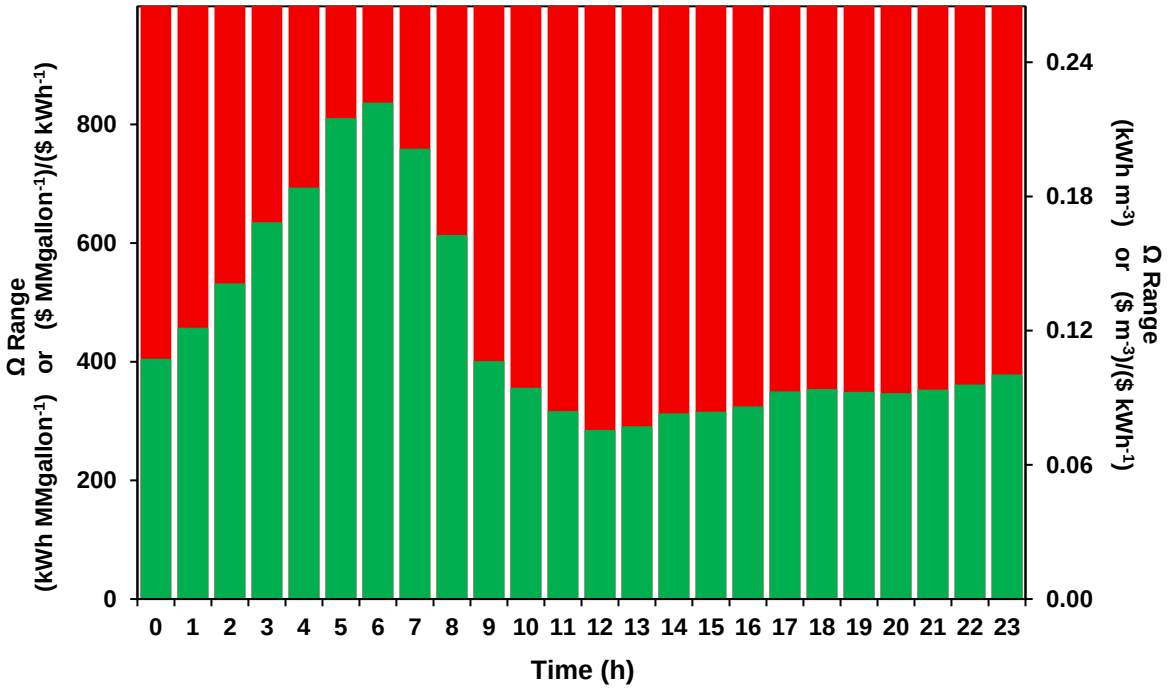

Figure 68. The instantaneous domain of primary treatment enhancing chemical additives to grid electricity costs ratio for which chemically enhanced primary treatment (CEPT) scenario has operating cost savings over conventional clarifier's. Green range represents the ratio domains for this CEPT scenario has cost-savings over the conventional clarifier's scenario and red represents the domains for which conventional clarifier option is more cost-efficient. The boundary between these two color-zones represents Ω.

Figure 68 illustrates the reverse dynamic pattern of the diurnal influent flow in Figure 6 for Ω. As demonstrated in Figure 59 in the operating cost comparison section of this chapter, the high cost of primary treatment enhancing chemical additive cost exceeds all the energy cost savings that this option provides accounting for any of the 5 electricity tariff structures used in this study. Therefore, these additives' cost seems to have more weight in determining the feasibility of this scenario over conventional clarifier comparing to grid electricity tariffs. Since the diurnal influent flow reaches its minimum at 6:00, less additive needs to be added to the influent at this time of the day which results in the expansion of the economic feasibility domain (Ω) in the Figure 68 or reduction of these additives' cost dominance in the cost-effectiveness of this scenario.

Similar to BST, the cumulative analysis is performed to determine the range of Ω on average daily basis for which CEPT scenario is more cost-effective than conventional clarifier

scenario. This cumulative feasibility range is concluded to be $0<\Omega<0.11$kWh m^{-3} ($0<\Omega<413.39$ kWh $MMgallon^{-1}$). The finite domines of Ω derived from the simultaneous hourly and cumulative daily analysis for CEPT scenario elucidates that the feasibility of a CEPT scenario is always dictated by the plant tariff structure and the cost of primary treatment enhancing chemical which is determined beyond the WRRF's boundary and by the electricity utility provider and chemical suppliers.

Summary

This chapter demonstrates that increasing the extent of the primary treatment by replacing or coupling the conventional primary clarifiers with the advanced primary treatment (APT) technologies focused on in this chapter, including chemically enhanced primary treatment (CEPT), primary filtration (PF), and rotating-belt filtration (RBF), results in net electricity demand savings at the WRRF studied here for only few of these scenarios (i.e., CEPT and PF-only with 80% TSS removal). This increase in the extent of removal also reduces the anthropogenic greenhouse gas emissions of this facility for the scenarios although it increases the facilities' overall carbon-footprint of all of them.

Comparing the scenarios analyzed in this study from the operating cost standpoint illustrates that electricity demand reduction and cost savings associated with increasing the extent of the primary treatment by these APTs does not necessarily result in overall cost savings. This is observed in the case of CEPT scenario, for instance, where the extensive cost of the primary treatment enhancing chemical agents exceed all the cost savings associated with this scenario's electricity demand and natural gas costs savings. This chapter also portrays that standalone PF scenarios or its combination with conventional clarifiers as the more economic feasible options form overall operating cost standpoint comparing to the other BST scenarios.

The dynamic analysis performed in this study also demonstrates that despite having higher net electricity demand than primary clarifier scenario, few of the PF-primary clarifier alternation scenarios result in electricity cost-savings for most of the tariff structures over the conventional clarifier scenario's. This observation elucidates the effect of timing of the electricity demand on its cost estimation and importance of dynamic assessment of electricity costs using dynamic tariff structures to prevent inaccurate cost estimation. Similar observation or determination has been reported in this chapter for the electricity imports' greenhouse gas emissions.

This chapter also demonstrates dependency of economic feasibility of APTs on external factors outside of the boundary of the WRRF. Two of the most contributing of these factors are electricity tariff structures and cost of the chemicals exclusively used for enhancing the primary treatment in CEPT scenarios. Detail analysis of the standalone BST technologies in this chapter, demonstrates that the cost-effectiveness of these technologies over conventional clarifiers' is independent from grid electricity tariff structures at least for a portion of the day for the scenarios with TSS removal of greater than 60%. This observation also highlights the effect of increase in the extent of primary treatment on reducing the dependency of these BST's economic feasibility on the grid's tariff structure. Similar assessment was performed for CEPT scenario by also accounting for the cost of this scenario's exclusive primary treatment enhancing chemical additives. This assessment concludes the dependency of this scenario's cost-effectiveness over conventional clarifiers on both electricity tariff structure and the cost of CEPT exclusive enhancing agents for every hour of the day.

CONCLUSION

This doctoral dissertation demonstrates the dynamic nature of water resource recovery facilities (WRRFs) and power grid through detail study of a large WRRF in the state of California. For this study a dynamic model of this WRRF was developed and calibrated and validated. This model then is used to study the effect of most recent three modifications at this the facility's activated sludge (AS) processes, including migration from carbon oxidizing to nitrogen oxidizing and removing configuration followed up with an expansion consisting of addition of a differently configured AS unit to the facility's existing one, on the facility's extent of removal, electricity demand, carbon-footprint, and operating cost. This comparison of different activated sludge configurations demonstrates the benefit of graduating from carbon oxidation to nitrogen oxidation and removal on the facility's effluent quality, power demand, operating cost and carbon-footprint. It also elucidates the current plant's additional room for energy efficiency improvement despite this configuration being the most cost-effective AS configuration among the three configurations analyzed here. Addressing this room for energy improvement using the few suggestions provided in this dissertation is also expected to reduce the environmental impact of this facility by improving the facility effluent quality and reducing its carbon-footprint in addition to some electricity demand cost-savings.

The assessment of all these activated sludge configurations unfirmly demonstrates the coincidence of this facility's peak of net electricity demand with the peak of electricity grid's diurnal tariff structures and carbon intensities. This coincidence demonstrates an amplifying effect on the electricity import's cost and greenhouse gas (GHG) emissions. This amplifying effect elucidates the importance of performing the operating cost and carbon-footprint assessment of this WRRF using a dynamic model results and dynamic gird electricity tariff and carbon intensity profiles which has been highlighted here as the main gap in many of the similar analysis at different WRRFs by other researchers.

The current plant configuration dynamic model is then utilized to study the effect of three different advanced primary treatment (APT) technologies on the facility's electricity demand, carbon-footprint, and operating cost. For this effort different scenarios using each of these three ATP technologies, including chemically enhanced primary treatment (CEPT), rotary belt filters (RBF) and primary filters (PF), have been developed and compared with standalone conventional primary clarifier scenario. Using the result of this comparison different hybrid and alternation scenarios have been also developed by combining conventional clarifiers with RBF or PF (i.e., barrier separations). This comparison demonstrates CEPT as the most power efficient with least anthropogenic greenhouse gas (GHG) emissions, yet the least cost-effective scenario due to the high cost of its exclusive primary treatment enhancing agents. Standalone PF scenarios with TSS removal equal to and greater 70% scenarios were demonstrated to be the most promising options of all due to their lower operating cost and anthropogenic GHG emissions comparing to standalone conventional clarifier scenario. This is despite the fact that not all the standalone PF scenarios, for example scenarios with TSS removal of equal to or less than 70% TSS removal, provide net electricity demand savings over conventional clarifier scenario.

The BST-conventional clarifier alternation scenarios also demonstrate the importance of dynamic assessment of the grid electricity import cost and GHG emissions using the results of this dynamic model and grid electricity tariffs and carbon intensity diurnal profiles. This is elucidated in scenarios that delivered electricity import cost and GHG emissions savings over conventional clarifiers despite their higher net electricity demand. These alternation scenarios also demonstrate the amplifying effect of the coincidence of this WRRF net electricity demand with the peak of power grid on its electricity import costs and GHG emissions and how breaking this coincidence, even for a small time period, can reduce these cost and emissions even when the total facility net electricity demand remain the same (e.g., PF-conventional clarifier alternation between 10:00 to 15:00 and 12:00 to 17:00). This observation also elucidates the cost

effectiveness of the load-shifting through the use of these BST-alternation at the facilities that are not willing to completely switch to the standalone BSTs studied in this dissertation from their existing standalone conventional clarifiers.

Lastly this study highlights the dependency of the cost-effectiveness of all these standalone APT scenarios over standalone conventional clarifier's on the factors beyond this WRRF's boundary such as electricity tariff structures and chemical additives cost. The dependency of the cost effectiveness of the standalone APT technologies here is further analyzed for electricity tariff structure and cost of CEPT's exclusive treatment enhancing agent. This analysis concludes that the increase in the extent of primary treatment in standalone BST scenarios reduces the dependency of their cost-effectiveness on gird tariff structure and demonstrates some of PF-only scenarios to be economically cost-effective over conventional clarifiers no matter what the cost of grid electricity is. Such a freedom from external factors could not be demonstrated for CEPT option, and this scenario cost-effectiveness is demonstrated to always depend on the cost of grid electricity and its exclusive treatment enhancing agents. It needs to be noted the only energy usage charge aspect of power grid tariffs could be used for this dependency analysis due to complexity of electricity demand cost calculations. As such, further analysis in collaboration with the facility's electricity utility provider needs to be performed as part of future studies.

In summary, by combining the most energy and cost effective primary and secondary treatment configurations analyzed in this research effort which deliver equal or less overall environmental impact than the current configuration, this WRRF can alleviate the adverse impacts of the Duck-Curve phenomenon such as recent increase in the power grid's electricity cost and carbon intensity during its new peak periods (i.e., demand-side flexibility project). Extending the results of this study to other WRRFs without considering these plants' characteristics, treatment goals, and distinct geometry differences as well as their site-specific dynamic grid electricity tariffs,

GHG intensities, and alpha factors, shall be prohibited. However, the methods developed, and recommendation summarized in this dissertation to develop a complete dynamic model can be applied to other WRRFs to achieve more accurate and representative results for these facilities. Such dynamic models then could be utilized to defined and study different demand-side flexibility project such as the ones introduced and studied here for these WRRFs.

RECOMMENDATIONS FOR FUTURE RESEARCH

Through different chapters of this dissertation miscellaneous recommendations have been made for future research and studies. This chapter summarizes these recommendations. As discussed in more details in the Methods chapter as well as Chapter 3, not all the data required to develop the dynamic model presented here was available. As such collecting the necessary field data at the sufficient frequency and accuracy prior to start of model development is the first recommendation for future modeling efforts to guarantee the most accurate results and to increase the efficiency of the modeling effort.

In addition to broad list of data collection challenges listed in Chapter 3 and as indicated in Methods section, no off-gas testing result and field alpha factor was available to model Activated Sludge 2 (AS2) in the current plant configuration. Therefore, conservative assumptions were made to come up with synthetic alpha factors required to model this section of the current plant's activated sludge unit that process 60% of the activated sludge influent at this facility. Due to activated sludge considerable contribution to the facility's overall electricity demand as demonstrated in Chapters 4 and 5 and AS2's larger share of treating the facility's overall activated sludge process influent, any error associated with the synthetic alpha factors used (in the absence of field data) to model this process unit will significantly impact the results of analysis performed in Chapters 4 and 6. As such, another recommendation for performing future dynamic modeling effort at this water resource recovery facility (WRRF) or any other facility is performing off-gas testing prior to the modeling effort and utilizing these field alpha factors as opposed to synthetic data.

Another recommendation for future research that has been discussed in this dissertation is to perform an energy efficiency assessment on AS2 at the current facility configuration as it does not meet the expectations of a Modified Ludzack-Ettinger (MLE) configuration in terms of energy efficiency and nitrification and denitrification. Thus, the next area that needs to be focused

on for future studies of this facility after performing off-gas testing at AS2 is to perform an energy efficiency study at this unit. One of the areas that this dissertation recommends to focus such an efficiency study on is the MLE recycle flow. Currently the facility is running this recycle stream at a flow equal to 200% of the influent flow to this activates sludge unit. As explained in more detail in Chapter 4, excess recycle stream deviates the functionality of this biological reactor from plug-flow to continuous stirred tank reactor (CSTR) configuration that will reduce its extent of the removal and performance.

Depending on the outcome of addressing the recommendations above, the assessments performed in Chapters 4 and 6 of this dissertation may need to be repeated to account for more accurate field data and optimized AS2 configuration. Since the cost of chemical additives used for sludge dewatering and thickening in this facility was shown to play a key role on determining the cost-effectiveness of the scenarios modeled in these two chapters, field cost ratings are recommended to be used instead of the simulation software's defaults if the assessment performed in these chapters are repeated in the future. In addition, the cost of these chemicals is also recommended to be accounted in the assessment performed in Chapter 6 to study the dependency of the barrier separation technologies (BST) and chemically enhanced primary treatment (CEPT) scenarios' cost-effectiveness on the external factor beyond this WRFF's boundary. As such, similar mathematical equation to Equation 6 will be used for both BST and CEPT scenarios. In addition, these dependency analyses are recommended to be performed in collaboration with electricity utility provider (Southern California Edison in case of this facility) in order to account for all the different components of the electricity tariff structures as opposed to only energy usage charges that was used for the analysis performed in Chapter 6 of this dissertation.

FUTURE OUTLOOK

In this dissertation work, some research gaps where identified that could be summarized as future research outlook here. As demonstrated in Chapter 6, primary filters (PF) scenarios with solid removal above certain thresholds demonstrate cost and energy savings over conventional clarifiers. As such, more PF scenarios with solid removal above these thresholds need to be reviewed to precisely determine the benefit of using this barrier separation technology over conventional clarifiers and to identify different configurations that can be used to develop demand-side flexibility project at the water resource recovery facilities (WRRFs) studied here.

The other research gap that should be mentioned here is the gap related to quantification of biogas fugitive emissions. As discussed in Chapters 3 and 4 of this dissertation, the margin of error in typical flow meters used in biogas service does not allow precise estimation of this fugitive emission through mass- or flow-balance calculations. As such, different methods need to be developed to quantify these emissions whose contribution to total facility carbon-footprint can be significant due to large global warming potential of methane (i.e., 25 [42]) as demonstrated in the sensitively analysis performed in Chapter 4 for the WRRF studied in this dissertation.

The other area that can be mentioned as a future outlook and a method to reduce electricity and operating costs of WRRFs is load leveling using electricity storage units or batteries. The result of such an analysis including its capital cost also need to be compared with cost savings and capital cost associated with implementation of PF scenarios that provide electricity and overall operating cost savings to determine the economic feasibility of costs-savings achieved by implementing this barrier separation technology over electricity storage.

The last area that could be mentioned under the future outlook section here based on the findings in this research effort is the need for studying the effect of the recent regulations that promote the diversion of food wastes to WRRFs as opposed to landfills for digestion and biogas

production. California Senate Bill 1383 (SB1383) is an example of such regulations [55, 56]. The effect of this change on the operation of the WRRFs subject to these regulations, especially on their extent of treatment, inhouse electricity generation, electricity demand, and operating cost, need to be assessed prior to complete implementation of them to educate these facilities about their operation needs to comply with such regulations.

REFERENCES

[1] H. O. R. Howlader, M. Furukakoi, H. Matayoshi and T. Senjyu, "Duck Curve Problem Solving Strategies with Thermal Unit Commitment by Introducing Pumped Storage Hydroelectricity & Renewable Energy," in 2017 IEEE 12th International Conference on Power Electronics and Drive Systems (PEDS), Honolulu, HI, 2017, pp., 2017.

[2] Howlader, H. O. R.; Sediqi, M. M.; Ibrahimi, A. M.; Senjyu, T., "Optimal Thermal Unit Commitment for Solving Duck Curve Problem by Introducing CSP, PSH and Demand Response," IEEE Access, vol. 6, pp. 4834-4844, 2018.

[3] J. Blondeau and J. Mertens, "Impact of intermittent renewable energy production on specific CO2 and NOx emissions from large scale gas-fired combined cycles," Journal of Cleaner Production, vol. 221, pp. 261-270, 2019.

[4] I. D'Adamo and P. Rosa, "Current state of renewable energies performances in the European Union: a new reference framework," Energy Conversion and Management, vol. 121, pp. 84-92, 2016.

[5] European Commission, "Second Report on the State of the Energy Union.," European Commission, 2017.

[6] M. A. Gonzalez-Salazar, L. Prchlik and T. Kirsten, "Review of the operational flexibility and emissions of gas- and coal-fired power plants in a future with growing renewables," Renewable & Sustainable Energy Reviews, vol. 82, pp. 1497-1513, 2018.

[7] B. Jones-Albertus, "Confronting the Duck Curve: How to Address Over-Generation of Solar Energy," 12 10 2017. [Online]. Available: https://www.energy.gov/eere/articles/confronting-duck-curve-how-address-over-generation-solar-energy.

[8] California Independent System Operator, "Today's Outlook," 22 05 2021. [Online]. Available: http://www.caiso.com/TodaysOutlook/Pages/index.html.

[9] M. C. Argyroua, P. Christodoulides and S. A. Kalogirou, "Energy storage for electricity generation and related processes: Technologies appraisal and grid scale applications," Renewable and Sustainable Energy Reviews, vol. 94, p. 804–821, 2018.

[10] H. Chen, T. Cong, W. Yang, C. Tan, Y. Li and Y. Ding, "Progress in electrical energy storage system: a critical review," Progress in Natural Science-Materials International, vol. 19, no. 3, pp. 291-312, 2009.

[11] A. Mayyas, D. Steward and M. Mann, "The case for recycling: Overview and challenges in the material supply chain for automotive li-ion batteries," Sustainable Materials and Technologies, vol. 19, pp. 2214-9937, 2019.

[12] A. S. Brouwer, M. Van Den Broek, W. Zappa, W. C. Turkenburg and A. Faaij, "Least-cost options for integrating intermittent renewables in low-carbon power systems," Applied Energy, vol. 161, p. 48–74, 2016.

[13] P. Denholm and T. Mai, "Timescales of energy storage needed for reducing renewable energy curtailment," Renewable Energy, vol. 130, p. 388–399, 2019.

[14] A. Zohrabian, S. Plata, D. Kim, A. E. Childress and K. T. Sanders, "Leveraging the water-energy nexus to derive benefits for the electric grid through demand-side management in the water supply and wastewater sectors," Wiley Interdisciplinary Reviews-Water, vol. 8, no. 3, pp. 1-23, May 2021.

[15] D. J. Reardon, "Turning down the power," Civil Engineering, vol. 65, no. 8, pp. 54-56, 1995.

[16] Metcalf and Eddy, Wastewater Engineering: Treatment and Resource Recovery, 5th ed., New York: McGraw-Hill Education, 2014.

[17] L. M. Jiang, M. Garrido-Baserba, D. Nolasco, A. Al-Omari, H. DeClippeleir, S. Murthy and D. Rosso, "Modelling oxygen transfer using dynamic alpha factors," Water Research, vol. 124, pp. 139-148, 2017.

[18] S. Y. Leu, D. Rosso, L. E. Larson and M. K. Stenstrom, "Real-Time Aeration Efficiency Monitoring in the Activated Sludge Process and Methods to Reduce Energy Consumption and Operating Costs," Water Environment Research, vol. 81, no. 12, pp. 2471-2481, 2009.

[19] WEF, Energy Conservation in Water and Wastewater Treatment Facilities,WEF Manual of Practice, New York, NY: McGraw-Hill, Inc., 2009.

[20] A. Botrous, O. Caliskaner, J. Hauser and M. W. Miller, "Primary Treatment," in Design of Water Resource Recovery Facilities, WEF_Ch10_p0595-0662, Water Environment Federation, 2017, pp. 595-662.

[21] R. Gori, L. Jiang, R. Sobhani and D. Rosso, "Effects of soluble and particulate substrate on the carbon and energy footprint of wastewater treatment processes," Water Research, no. 45, pp. 5858-5872, 2011.

[22] O. Caliskaner, G. Tchobanoglous, Z. Wu, R. Young, C. Paez, B. Davis, B. Mansell, P. Ackman, T. Reid and J. Dyson, "Performance of Full Scale and Demonstration-Scale Primary Filtration Projects," in Proceedings of the 2018 Water Environment Federation Technical Exhibition and Conference, New Orleans, Louisiana, 2018.

[23] O. Caliskaner, G. Tchobanoglous, T. Reid, R. Young, M. Downey and B. Kunzman, "Advanced Primary Treatment via Filtration to Increase Energy Savings and Plant Capacity," in Proceedings of the 89th Annual Water Environment Federation Technical Exposition and Conference, New Orleans, Louisiana, 2016.

[24] O. Caliskaner, G. Tchobanoglous, T. Reid, B. Davis, R. Young and M. Downey, "First Full-Scale Installation of Primary Filtration for Advanced Primary Treatment to Save Energy and Increased Capacity," in Proceedings of the 2017 Water Environment Federation Technical Exhibition and Conference, New Orleans, Louisiana, 2017.

[25] W. E. Steel, Water Supply and Sewerage, New York: McGraw-Hill, 1979.

[26] U.S. EPA, Design Manual for Phosphorus Removal (EPA-625/1-87-001), Cincinnati, Ohio: U.S. Environmental Protection Agency, 1987.

[27] H. Ødegaard, "Combining CEPT and Biofilm Systems.," in Proceedings of the International Water Agency Specialised Conference on BNR; Krakow, Poland., London, England, 2005.

[28] P. Sutton, B. Rusten, A. Ghanam, R. Dawson and H. Kelly, "Rotating Belt Screen: An Attractive alternative for Primary Treatment of Municipal Wastewater.," in Proceedings of the 81st Annual Water Environment Federation Technical Exposition and Conference, Chicago, Illinois, , 2008.

[29] F. Pasini, M. Garrido-Baserba, A. Ahmed, G. Nakhla, D. Santoro and D. Rosso, "Oxygen transfer and wide-plant energy assessment of primary screening in WRRFs," Water Environment Research, pp. 1-16, 2020.

[30] C. Degroot, E. Sheikholeslamzadeh, A. Soleymani, D. Santoro, D. Batstone and D. Rosso, "Modeling Rotating Belt Filter Performance and Nutrient Diversion Potential Using Computational Fluid Dynamics," in WA Specialist Conference on Nutrient Removal and Recovery. , Gdansk, Poland, 2015.

[31] C. Tien, Principles of filtration, Oxford, UK.: Elsevier, 2012.

[32] O. Caliskaner, G. Tchobanoglous, T. Reid, B. Kunzman, R. Young and N. Ramos, "Evaluation and Demonstration of Five Different Filteration Technologies as an Advanced Primary Treatment Method for Carbon Diversion," in Proceedings of the 88th Annual Water Environment Federation Technical Exposition and Conference, Alexandria, VA, 2015.

[33] R. Gori, F. Giaccherini, L. Jiang, R. Sobhani and D. Rosso, "Role of primary sedimentation on plant-wide energy recovery and carbon footprint," Water Science & Technology, vol. 68, no. 4, pp. 870-878, 2013.

[34] D. Rosso and M. Stenstrom, "Comparative economic analysis of the impacts of mean cell retention time and denitrification on aeration systems," Water Research, vol. 39, no. 16, pp. 3773-3780, 2005.

[35] D. Rosso and M. Stenstrom, "Energy-saving benefits of denitrification," Environmental Engineering, vol. 43, no. 3, pp. 29-38, 2007.

[36] L. Rieger, S. Gillot, G. Langergraber, T. Ohtsuki, A. Shaw, I. Takacs and S. Winkler, "Guidelines for Using Activated Sludge Models," IWA, London, 2013.

[37] EnviroSim, BioWin 6.1 Help Manual, Hamilton, Ontario: EnviroSim, 2020.

[38] Weather Underground, "John Wayne Airport Station," 22 05 2021. [Online]. Available: https://www.wunderground.com/history/monthly/us/ca/santa-ana/KSNA/date/2018-10.

[39] American Society of Civil Engineers, "ASCE Standard ASCE/EWRI 18-18," in Standard Guidelines for In-Process Oxygen Transfer Testing, Reston, VA: American Society of Civil Engineers, 2018.

[40] U.S. EPA, Design Manual Fine Pore Aeration Systems(EPA/625/1-89/023), Cincinnati, OH: U.S. Environmental Protection Agency, 1989.

[41] U.S. EPA, "Title 40 Part 98—Mandatory Greenhouse Gas Reporting-Subpart C—General Stationary Fuel Combustion Sources," 12 09 2016. [Online]. Available: https://www.ecfr.gov/cgi-bin/text-idx?SID=c928f22246db4fd098e7ed7cdf75a869&mc=true&node=pt40.23.98&rgn=div5#sp40.23.98.c.

[42] U.S. EPA, "Title 40 Part 98—Mandatory Greenhouse Gas Reporting-Subpart A—General Provision," 11 12 2014. [Online]. Available: https://www.ecfr.gov/cgi-bin/text-idx?SID=c928f22246db4fd098e7ed7cdf75a869&mc=true&node=pt40.23.98&rgn=div5#sp40.23.98.a.

[43] California Air Resource Board, "California Cap-and-Trade," 16 06 2019. [Online]. Available: https://www.arb.ca.gov/cc/capandtrade/guidance/cap_trade_overview.pdf.

[44] L. Tseng, A. K. Robinson, X. Zhang, X. Xu, J. Southon, A. J. Hamilton, R. Sobhani, M. K. Stenstrom and D. Rosso, "Identification of Preferential Paths of Fossil Carbon within Water Resource Recovery Facilities via Radiocarbon Analysis," Environmental Science & Technology, vol. 50, p. 12166−12178, 2016.

[45] R. Christian, "What California's 100% clean energy mandate means for the United States," PV magazine USA, 10 9 2018.

[46] Southern California Edison, "SCE - Document Library," 22 05 2021. [Online]. Available: https://library.sce.com/?10000_group.propertyvalues.property=jcr%3Acontent%2Fmetadata%2Fcq%3Atags&10000_group.propertyvalues.operation=equals&10000_group.propertyvalues.0_values=sce-document-library%3Aregulatory%2Fsce-tariff-books%2Felectric%2Fschedules%2.

[47] U. Jeppsson, M.-N. Pons, I. Nopens, J. Alex, J. Copp, K. Gernaey, C. Rosen, J.-P. Steyer and P. Vanrolleghem, "Benchmark simulation model no 2: general protocol and exploratory case studies," Water Science & Technology, vol. 56, no. 8, pp. 67-78, 2007.

[48] I. Nopens, L. Benedetti, U. Jeppsson, M.-N. Pons, J. Alex, J. B. Copp, K. V. Gernaey, C. Rosen, J.-P. Steyer and P. A. Vanrolleghem, "Benchmark Simulation Model No 2: finalisation of plant layout and default control strategy," Water Science & Technology, vol. 62, no. 9, pp. 1967-1974, 2010.

[49] A. A. Zorpas, C. Coumi, M. Drtil, I. Voukalli and P. Samaras, "Operation description and physicochemical characteristics of influent, effluent and the tertiary treatment from a sewage treatment plant of the Eastern Region of Cyprus under warm climates," Desalination and Water Treatment, vol. 22, no. 1-3, pp. 244-257, 2010.

[50] D. Rosso, L.-M. Jiang, R. Sobhani and B. Wett, "Energy Footprint Modelling: a tool for process optimisation in Large Wastewater Treatment Plants," Water Practice & Technology, vol. 7, no. 1, 2012.

[51] U.S. EPA Region 4 Laboratory Services and Applied Sciences Division, Wastewater Flow Measurement Operating Procedure, Athens, Georgia, 2020.

[52] J. Replogle, "Some observations on irrigation flow measurements at the end of the millennium," Applied Engineering in Agriculture, vol. 18, no. 1, pp. 47-55, 2002.

[53] J. Davis, "Understanding of Flowmeter Specification," Water and Waste Digest, 03 10 2005.

[54] P. Roeleveld and M. Van Loosdrecht, "Experience with guidelines for wastewater characterisation in The Netherlands," Water Science and Technology, vol. 45, no. 6, pp. 77-87, 2002.

[55] CalRecycle, 22 05 2021. [Online]. Available: https://www.aqmd.gov/docs/default-source/rule-book/Proposed-Rules/1118.1/calrecycle-prez-wgm2.pdf?sfvrsn=8.

[56] H. Jones, "SB 1383: A Revolution For Organic Waste," BioCycle, 17 3 2020.

[57] N. Emami, R. Sobhani and D. Rosso, "Diurnal variations of the energy intensity and associated greenhouse gas emissions for activated sludge processes," Water Science and Technology, vol. 77, no. 7, pp. 1838-1850, 2018.

[58] L. Chan, S.-Y. Leu, D. Rosso and M. Stenstrom, "The Relationship Between Mixed-Liquor Particle Size and Solids Retention Time in the Activated Sludge Process," Water Environment Research, vol. 83, no. 12, pp. 2178-2186, 2011.

[59] Z. Li and M. Stenstrom, "Impacts of SRT on Particle Size Distribution and Reactor Performance in Activated Sludge Processes," Water Environment Research, vol. 90, no. 1, pp. 48-56, 2018.

[60] MWH, Water Treatment: Principles and Design, 2nd ed., Hoboken, NJ: John Wiley & Sons, 2012.

[61] S.-Y. Leu, L. Chan and M. Stenstrom, "Toward Long SRT of Activated Sludge Processes: Benefits in Energy Saving, Effluent Quality, and Stability," Water Environment Research, vol. 8, pp. 7282-7295, 2010.

[62] J. L. Willis, Z. Yuan and S. Murthy, "Wastewater GHG Accounting Protocols as Compared to the State of GHG Science," Water Environment Research, vol. 88, no. 8, pp. 704-714, 2016.

[63] H. Monteith, H. Sahely, H. MacLean and D. Bagley, "A rational procedure for estimation of greenhouse-gas emissions from municipal wastewater treatment plants," Water Environment Research, vol. 77, no. 4, pp. 390-403, 2005.

[64] J. Foley and P. Lant, "Fugitive Greenhouse Gas Emissions from Wastewater Systems: WSAA Literature Review No.01.," Water Services Association of Australia, Melbourne, 2008.

[65] E. Musabandesu and F. Loge, "Load shifting at wastewater treatment plants: A case study for participating as an energy demand resource," Journal of Cleaner Prodcution, vol. 282, 2021.

[66] D. Rosso, R. Iranpour and M. Stenstrom, "Fifteen years of offgas transfer efficiency measurements on fine-pore aerators: key role of sludge age and normalized air flux," Water Environ. Res., vol. 77, pp. 266-273, 2005.

[67] S. Pabi, A. Amarnath, R. Goldstein and L. Reekie, "Electricity Use and Management in the Municipal Water Supply and Wastewater Industries," Electric Power Research Institute & Water Research Foundation, Palo Alto, California, 2013.

[68] R. Sobhani, L.-M. Jiang, A. M. Chau, J. Brown, E. Torres, Y. Shao and D. Rosso, "Energy Footprint Analysis of Orange County Sanitation District's Operations," in Water Environment Federation, Los Angeles, 2011.

APPENDICES

APPENDIX A: LIST OF ABBREVIATIONS

APT: Advanced Primary Treatment

AS: Activated Sludge

BOD: Biological Oxygen Demand

BST: Barrier Separation Technologies

CAISO: California Independent System Operator

CBOD: Carbonaceous Biological Oxygen Demand

CEPT: Chemically Enhanced Primary Treatment

COD: Chemical Oxygen Demand

CSTR: Continuous Stirred Tank Reactor

D-C: Duck-Curve

EQI: Effluent Quality Index

GHG: Greenhouse Gas

HRT: Hydraulic Retention Time

IQI: Influent Quality Index

L-E: Ludzack-Ettinger

Li-Ion: Lithium-Ion

MCRT: Mean Cell Residence Time

MLE: Modified Ludzack-Ettinger

MLSS: Mixed Liquor Suspended Solids

OTE: Oxygen Transfer Efficiency

PF: Primary Filtration (also Primary Filter)

PT: Primary Treatment

PV: Photovoltaic

QIR: Quality Index Removal

RBF: Rotating Belt Filtration or Micro-screening (also Rotating Belt Filter or Micro-screen)

sCOD: Soluble Chemical Oxygen Demand

SCE: Southern California Edison Company

TKN: Total Kjeldahl Nitrogen

TSS: Total Suspended Solids

WAS: Waste Activated Sludge (Stream)

WRRF: Water Resource Recovery Facility

APPENDIX B: PROCESS PARAMETERS USED FOR SIMULATIONS

Data collection was the most challenging phase of this research project and took more than two years. Key equipment size and configuration data were collected through a series of email data requests, site visits, and interviews with the plant engineers. In addition, literature data and Google map surveys were used where the data could not be provided by the plant. This collected process information has been summarized in this section for all the three facility configurations studied in this dissertation.

The tables below summarize the specifications and parameters used for simulation in addition to the simulation software's defaults:

Table B-1. Primary Treatment Specifications

Process Unit	Process Parameter	Current Plant	Step-Feed	Plug-Flow
Primary Clarifier	**Total Basins Count**	26	26	26
	Basins Count in Service	20	20	20
	Volume per Basin (1,000 m^3)	1.9	1.9	1.9
	Depth (m)	2.7	2.7	2.7
	Width (m)	12.0	12.0	12.0
	Length (m)	58.4	58.4	58.4
	Clarifier Model Parameters Used for CEPT:			
	BioWin CEPT Default Max Vesilind Settling Velocity (m/d)	150.0	150.0	150.0
	BioWin CEPT Default Vesilind Hindered Zone Settling Parameter (L/g)	0.40	0.40	0.40
	Calibrated Clarification Switching function (mg/L)	618.0	618.0	618.0
	BioWin CEPT Default Max Compactability Slope (mg/L)	50,000.0	50,000.0	50,000.0
	Clarifier Model Parameters Used for Conventional Clarifiers (non-CEPT)	BioWin's Default [37]	N/A	N/A

Table B-2a. Secondary Treatment Specifications – Activated Sludge 1

Process Unit	Process Parameter	Current Plant	Step-Feed	Plug-Flow
Activated Sludge 1	**Total Basins Count**	10	10	10
	Count of Basins in Service	6	10	10
	Volume per Basin (1,000 m^3)	5.3	5.3	5.3
	Zone Volume Breakdown (1,000 m^3):			
	Zone 1A	0.42	0.42	0.42
	Zone 1B	0.42	0.42	0.42
	Zone 2	0.82	0.82	0.82
	Zone 3	0.82	0.82	0.82
	Zone 4	0.92	0.92	0.92
	Zone 5	0.92	0.92	0.92
	Zone 6	0.92	0.92	0.92
	Depth (m)	4.57	4.57	4.57
	Width (m)	14	14	14
	Length (m)	83.8	83.8	83.8
	Fine Bubble Diffusers Diameter (m)	0.18	0.18	0.18
	Coarse Bubble Diffusers Diameter (m)	BioWin's Default [37]	BioWin's Default [37]	BioWin's Default [37]
	Diffuser Count per Zone per Basin:			
	Zone 1A	Anoxic w/ 6 Coarse Bubble Diffusers	Anoxic w/ 6 Coarse Bubble Diffusers	866
	Zone 1B	866	866	866
	Zone 2	1,732	1,732	1,732
	Zone 3	Anoxic	Anoxic	1,732
	Zone 4	1,732	1,732	1,732
	Zone 5	1,732	1,732	1,000
	Zone 6	1,626	1,626	1,000
Activated Sludge 1 Secondary Clarifier	**Total Basins Count**	26	26	26
	Count of Basins in Service	16	26	26
	Volume per Basin (1000 m^3)	2.95	2.95	2.95
	Depth (m)	4.88	4.88	4.88
	Width (m)	13.2	13.2	13.2
	Length (m)	45.9	45.9	45.9
	Clarifier Model Parameters Used for non-CEPT	BioWin's Default [37]	BioWin's Default [37]	BioWin's Default [37]

Table B-2b. Secondary Treatment Specifications – Activated Sludge 2

Process Unit	Process Parameter	Current Plant	Step-Feed	Plug-Flow
Activated Sludge 2	**Total Basins Count**	6	N/A	N/A
	Count of Basins in Service	6		
	Volume per Basin (1,000 m^3)	7.4		
	Zone Volume Breakdown (1,000 m^3):			
	Anoxic Zone	1.8		
	Aerobic Zone 1	2.8		
	Aerobic Zone 2	2.8		
	Depth (m)	7.92		
	Width (m)	13.7		
	Length (m)	69.19		
	Fine Bubble Diffusers Diameter (m)	0.23		
	Diffuser Count per Zone per Basin:			
	Anoxic Zone	Anoxic		
	Aerobic Zone 1	1,858		
	Aerobic Zone 2	1,721		
Activated Sludge 2 Secondary Clarifier	**Total Basins Count**	6	N/A	N/A
	Count of Basins in Service	6		
	Volume per Basin (1,000 m^3)	9.16		
	Depth (m)	4.88		
	Diameter (m)	48.9		
	Clarifier Model Parameters Used for Conventional Clarifiers (non-CEPT)	BioWin's Default [37]		

Table B-3. Digesters and Sludge Processing Specifications

Process Unit	Process Parameter	Current Plant	Step-Feed	Plug-Flow
Digesters:				
Small Digester	**Total Digester Count**	2	2	2
	Count of Digesters in Service	1	1	1
	Volume per Digester (1,000 m^3)	5.35	5.35	5.35
	Digester Head Space (% of Total Volume)	16%	16%	16%
	Height (m)	9.14	9.14	9.14
	Digester Wall Thickness (% of Diameter)	15.1%	15.1%	15.1%
	Diameter (m)	32.2	32.2	32.2
Large Digesters	**Total Digester Count**	8	8	8
	Count of Digesters in Service	8	8	8
	Volume per Digester (1,000 m^3)	7.28	7.28	7.28
	Digester Head Space (% of Total Volume)	16%	16%	16%
	Height (m)	9.14	9.14	9.14
	Digester Wall Thickness (% of Diameter)	15.1%	15.1%	15.1%
	Diameter (m)	37.5	37.5	37.5
Digested Sludge Dewatering	**% Removal**	Dynamic trend derived from field monthly data post calibration.	Dynamic trend derived from field monthly data post calibration.	Dynamic trend derived from field monthly data post calibration.
Digester Heat Loss per Year (C/day)	**October 2018 through April 2019 (post Calibration)**	0.145	0.145	0.145
	May 2018 through September 2019 accounting for additional natural gas import for electrcity peak shaving (post Calibration)	0.957	0.957	0.957
Sludge Thickeners	**Primary Sludge % Removal**	99.78%	99.78%	99.78%
	Secondary Sludge % Removal	99.78%	99.78%	99.78%

Table B-4. Energy Calculations Specifications

Process Unit	Process Parameter	Current Plant	Step-Feed	Plug-Flow
Blower	**Efficiency**	59.00%	59.00%	59.00%
Cogeneration	**%Fuel Energy Converted to Power**	35.00%	35.00%	35.00%
	Cogeneration Heat Recovery Steam Generator Heat Transfer Efficiency	55.0%	55.0%	55.0%
	%Fuel Energy Converted to Heat in Cogeneration (not accounting for heat exchanger efficiency)	18.18%	18.18%	18.18%
	Natural Gas Boiler Efficiency	60.0%	60.0%	60.0%
	Natural Gas LHV (kJ/kg)	51,810	51,810	51,810
	Pure Methane LHV (kJ/kg)	50,000	50,000	50,000
	Natural Gas HHV/LHV Ratio	1.11	1.1100	1.11

Table B-5. Power demand intensities (power demand per unit flow of wastewater treated) for each process unit replaced the default values in the simulation software.

Process Unit	Power Intensity (Wh/m^3)	Source of Factor
Primary Clarifier	2.09E+01	Derived from Plant Data
Influent Lift Pumps	7.84E+01	Derived from Plant Data
Other Power Consumption (ex, pumping, odor control, control system, etc.)	5.27E+01	Derived from Plant Data
Secondary Clarifier	1.60E+01	[67]
Trickling Filters	1.47E+02	[68]
Digester (Mixing and Biogas Compression)	6.30E+02	Derived from Plant Data
Thickening (Centrifuge)	6.19E+02	[67]
Digested Sludge Dewatering (Centrifuge)	4.15E+03	[67]
Rotating Belt Filter Driver Train and Pumping	8.60E+01	[67]
Primary Filter Driver Train and Pumping	8.78E+01	[67]

To perform the modelling, plant influent data has been collected for October 2018 through September 2019 using the plant's current data collection system and interviews with plant engineers. This period was selected to have the most updated data series available before the start of the COVID 19 pandemic. The start of the stay-at-home order in the state of California in February 2020 in response to this pandemic was expected (and later was confirmed by the plant engineers) to temporarily change the influent trends and dynamics of the plant until the end of the pandemic. Therefore, the plant data collected during this pandemic was not used for this modelling exercise. In addition, large data gaps associated with the transition to centrifuge sludge dewatering technology at the plant resulted in not selecting October 2019 through January 2020.

APPENDIX C: ELECTRICITY CUSTOMER AND DEMAND CHARGES

Table C-1. Average of 2-50 kV & >50 kV voltage categories' customer and demand charges for each power tariff option.

Cost Category			Option A/ A-CPP	Option B	Option LG/ LG-CPP	Option D	Real Time Option
Customer Charge ($/Meter/Month)			$914.32	$914.32	$914.32	$914.32	$914.32
Facilities Related Demand	**Charge [Excess of CRC] ($/kW)**		$8.10	$12.45	$6.37	$8.58	$8.58
	Standby [CRC] ($/kW)		$4.70	$4.70	$3.85	$3.85	$3.85
Time Related Demand Charge ($/kW)	**Backup Demand**	**Summer Season - On-Peak**	$11.47	$11.47	$14.55	$14.55	$3.13
		Winter Season - Weekdays (4-9 pm) for Option D and LGs OR Mid-Peak for Option As and B	$0.00	$0.00	$2.77	$3.56	$0.83
	Supplemental Demand	**Summer Season - On-Peak**	$0.00	$16.67	$0.00	$28.88	$6.41
		Winter Season - Weekdays (4-9 pm) for Option D and LGs OR Mid-Peak for Option As and B	$0.00	$5.29	$0.00	$6.83	$1.67

Table C-2. Time-of-Use periods applicable to time related demand charges for each power tariff option.

Time of Use Subject to Demand Charges		Option A/ A-CPP	Option B	Option LG/ LG-CPP	Option D	Real Time Option
Weekdays Summer Season - On-Peak for All Options	**Start Time**	12	12	16	16	16
	End Time	18	18	21	21	21
Weekdays Winter Season - Weekdays (4-9 pm) for Option D and LG	**Start Time**	N/A	N/A	16	16	16
	End Time	N/A	N/A	21	21	21
Weekdays Summer Mid-Peak for Option As and B#1	**Start Time**	8	8	N/A	N/A	N/A
	End Time	12	12	N/A	N/A	N/A
Weekdays Summer Mid-Peak for Option As and B#2	**Start Time**	18	18	N/A	N/A	N/A
	End Time	23	23	N/A	N/A	N/A
Weekdays Winter Mid-Peak for Option As and B	**Start Time**	8	8	N/A	N/A	N/A
	End Time	21	21	N/A	N/A	N/A

* N/A: Not Applicable

APPENDIX D: ADVANCED PRIMARY TREATMENT TECHNOLOGIES' COST-EFFECTIVENESS DEPENDENCY ANALYSIS METHOD

Barrier Separations: **(Equation D-1)**

$$\int C_{BS} - \int C_{PC} < 0$$

$$\int [C_{BS-NG} + C_{BS-SLDG} + C_{BS-ELECT} + C_{BS-CHEM}] - \int [C_{PC-NG} + C_{PC-SLDG} + C_{PC-ELECT} + C_{PC-CHEM}] < 0$$

$$\int [(C_{BS-NG} - C_{PC-NG}) + (C_{BS-SLDG} - C_{PC-SLDG}) + (C_{BS-CHEM} - C_{PC-CHEM})] + \int [C_{BS-ELECT} - C_{PC-ELECT}] < 0$$

$$Assume: \Psi = \int [(C_{BS-NG} - C_{PC-NG}) + (C_{BS-SLDG} - C_{PC-SLDG}) + (C_{BS-CHEM} - C_{PC-CHEM})]$$

$$\Psi < \int -[C_{BS-ELECT} - C_{PC-ELECT}]$$

$$\Psi < \int -\$^{*} \times [E_{BS-NET} - E_{PC-NET}]$$

$$\Psi < \$^{*} \times \int -[E_{BS-NET} - E_{PC-NET}]$$

$$if \int -[E_{BS-NET} - E_{PC-NET}] < 0 \rightarrow \frac{\Psi}{\int -[E_{BS-NET} - E_{PC-NET}]} > \$^{*}$$

$$if \int -[E_{BS-NET} - E_{PC-NET}] > 0 \rightarrow \frac{\Psi}{\int -[E_{BS-NET} - E_{PC-NET}]} < \$^{*}$$

Where:

C_{BS}: Total operating cost of barrier separation (RBF or PF) scenarios
C_{PC}: Total operating cost of Baseline or Primary Clarifiers scenario
C_{BS-NG}: Natural gas cost of barrier separation scenarios
$C_{BS-SLDG}$: Sludge disposal cost of barrier separation scenarios
$C_{BS-ELECT}$: Net electricity demand (grid electricity demand) cost of barrier separation scenarios
$C_{BS-CHEM}$: Chemical additive cost of barrier separation scenarios
C_{PC-NG}: Natural gas cost of Baseline scenario
$C_{PC-SLDG}$: Sludge disposal cost of Baseline scenario
$C_{PC-ELECT}$: Net electricity demand (grid electricity demand) cost of Baseline scenario
$C_{PC-CHEM}$: Chemical additive cost of Baseline scenario
$\$^{*}$: a power price critical threshold when $\int C_{PC}(t) = \int C_{BS}(t)$ and below or above which $\int C_{PC}(t) > \int C_{BS}(t)$
E_{BS-NET}: Net electricity demand (grid electricity demand) of barrier separation scenarios
E_{PC-NET}: Net electricity demand (grid electricity demand) of Baseline scenario

Chemically Enhanced Primary Treatment: (Equation D-2)

$$\int C_{CEPT} - \int C_{PC} < 0$$

$$\int [C_{CEPT-NG} + C_{CEPT-SLDG} + C_{CEPT-ELECT} + C_{CEPT-TotCHEM}] - \int [C_{PC-NG} + C_{PC-SLDG} + C_{PC-ELECT} + C_{PC-TotCHEM}] < 0$$

$$\int [(C_{CEPT-NG} - C_{PC-NG}) + (C_{CEPT-SLDG} - C_{PC-SLDG}) + (C_{CEPT-CHEM} - C_{PC-CHEM})|_{NoneCEPT-CHEM} + C_{FeCl_3+Polymer}] +$$

$$\int [C_{CEPT-ELECT} - C_{PC-ELECT}] < 0$$

$$\int [(C_{CEPT-NG} - C_{PC-NG}) + (C_{CEPT-SLDG} - C_{PC-SLDG}) + \int [C_{CEPT-CHEM} - C_{PC-CHEM}]|_{NoneCEPT-CHEM} + \int [(\alpha + \beta) \times F] +$$

$$\int [C_{CEPT-ELECT} - C_{PC-ELECT}] < 0$$

$$Assume: \Psi = \int [(C_{BS-NG} - C_{PC-NG}) + (C_{BS-SLDG} - C_{PC-SLDG})] + \int [C_{CEPT-CHEM} - C_{PC-CHEM})|_{NoneCEPT}]$$

$$\Psi + \int [(\alpha + \beta) \times F] + \int [C_{CEPT-ELECT} - C_{PC-ELECT}] < 0$$

$$Assume: C = \$ * E$$

$$\Psi + \int [(\alpha + \beta) \times F] + \int \$^* \times [E_{BS-NET} - E_{PC-NET}] < 0$$

$$\Psi + (\alpha + \beta) \times \int [F] + \$^* \times \int [E_{BS-NET} - E_{PC-NET}] < 0$$

$$Assume: \frac{\$^*}{(\alpha + \beta)} = \frac{1}{\Omega}$$

$$Assume: (\alpha + \beta) > 0 \,\&\, \$^* > 0 \Rightarrow \Omega > 0 \,\&\, 1/\Omega > 0$$

$$\frac{\Psi + (\alpha + \beta) \int [F] + \$^* \int [E_{CEPT-NET} - E_{PC-NET}]}{(\alpha + \beta)} < 0$$

$$\frac{\Psi}{(\alpha + \beta)} + \int [F] + \frac{\$^*}{(\alpha + \beta)} \int [E_{CEPT-NET} - E_{PC-NET}] < 0$$

$$if \int -[E_{CEPT-NET} - E_{PC-NET}] > 0 \rightarrow \frac{\frac{\Psi}{(\alpha + \beta)} + \int [F]}{\int -[E_{CEPT-NET} - E_{PC-NET}]} < \frac{1}{\Omega}$$

$$if \int -[E_{CEPT-NET} - E_{PC-NET}] < 0 \rightarrow \frac{\frac{\Psi}{(\alpha + \beta)} + \int [F]}{\int -[E_{CEPT-NET} - E_{PC-NET}]} > \frac{1}{\Omega}$$

Where:

C_{CEPT}: Total operating cost of Chemically Enhanced Primary Treatment (CEPT) scenarios
C_{PC}: Total operating cost of Baseline or Primary Clarifiers scenario
$C_{CEPT-NG}$: Natural gas cost of CEPT scenarios

$C_{CEPT-SLDG}$: Sludge disposal cost of CEPT scenarios
$C_{CEPT-ELECT}$: Net electricity demand (grid electricity demand) cost of CEPT scenarios
$C_{CEPT-TotCHEM}$: Chemical additive cost of CEPT scenarios including FeCl3 and Anionic Polymer added to chemically enhance the primary treatment
$*: Cost of power purchased from the grid
C_{PC-NG}: Natural gas cost of Baseline scenario
$C_{PC-SLDG}$: Sludge disposal cost of Baseline scenario
$C_{PC-ELECT}$: Net electricity demand (grid electricity demand) cost of Baseline scenario
$C_{PC-TotCHEM}$: Chemical additive cost of Baseline scenario
$[C_{CEPT-CHEM} - C_{PC-CHEM}]|_{NoneCEPT-CHEM}$: Difference between cost of chemical usage in PC and CEPT scenarios not accounting for the cost of FeCl3 and Anionic Polymer added to enhance the primary treatment in CEPT
α: Cost of $FeCl_3$ per unit of primary treatment influent added only in CEPT scenarios and assumed not to vary during the day
β: Cost of Anionic Polymer per unit of primary treatment influent added only in CEPT scenarios and assumed not to vary during the day
F: Hourly flow of primary treatment influent
$E_{CEPT-NET}$: Net electricity demand (grid electricity demand) of CEPT scenarios
E_{PC-NET}: Net electricity demand (grid electricity demand) of Baseline scenario

APPENDIX E: ADDITIONAL RESULTS

I. Total Electricity Demand and Generation Comparison for Primary Treatment Scenarios

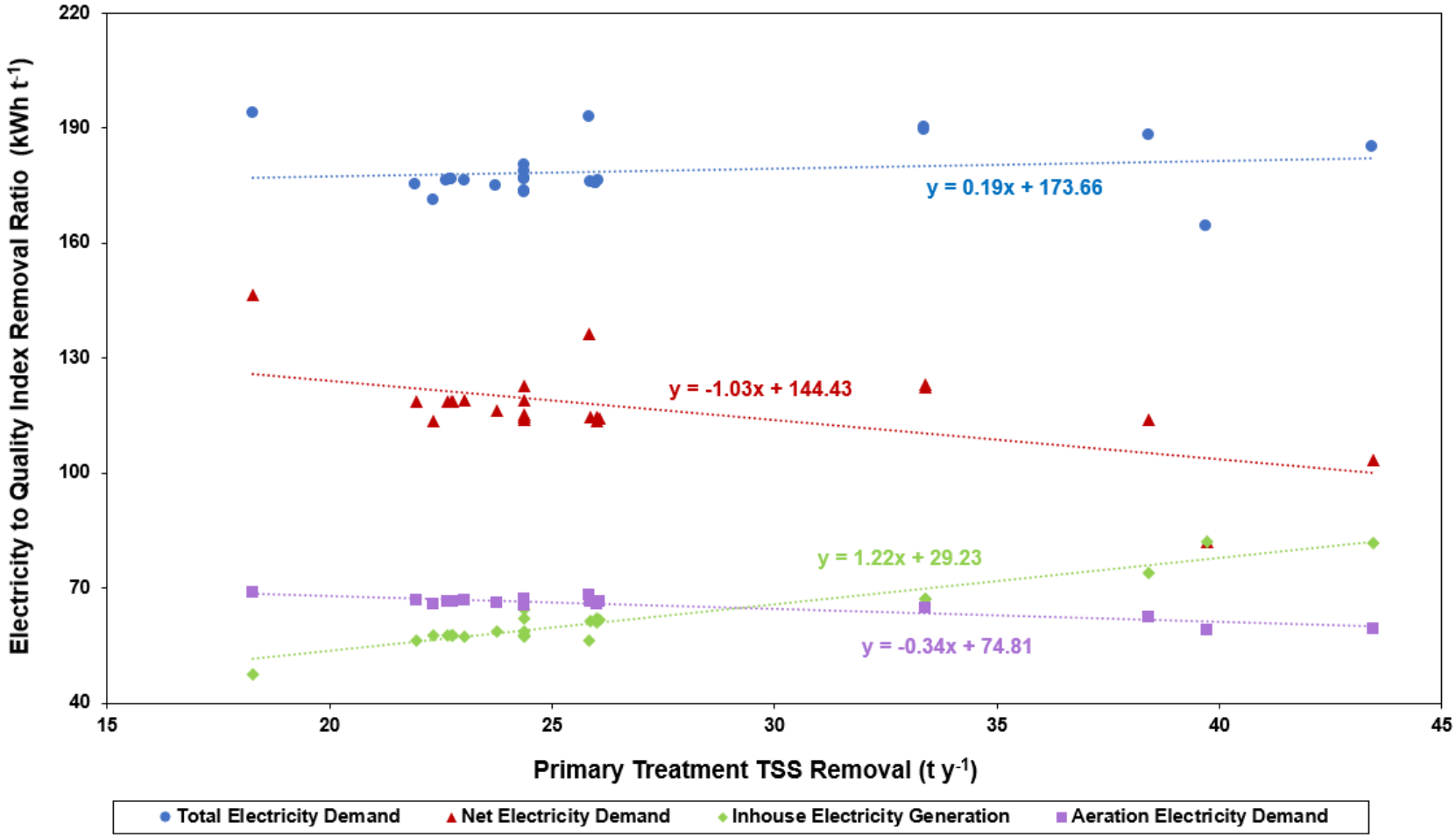

Figure E-1. Sum of 12 consecutive months' electricity generations and demands comparison normalized to total quality index removal for all the advanced primary treatment scenarios. The dotted trendline and their matching color equations demonstrate the ascending and descending trend of each electricity data category.

II. Total Greenhouse Gas Emissions Comparison for Primary Treatment Scenarios

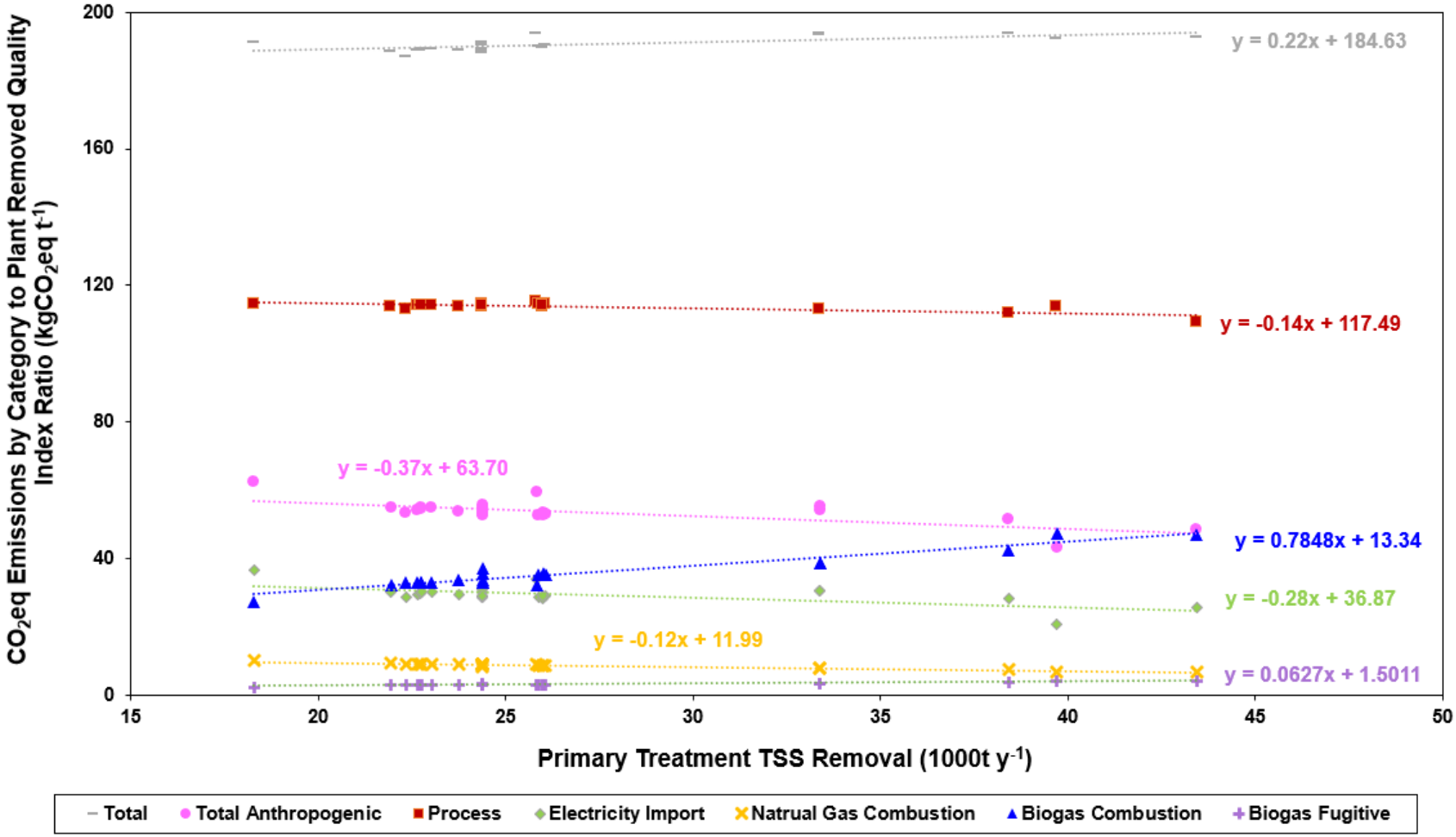

Figure E-2. Comparison of sum of 12 consecutive months' greenhouse gas (GHG) emissions normalized to total quality index removal by emission source type for all the advanced primary treatment scenarios. The dotted trendline and their matching color equations demonstrate the ascending and descending trend of each GHG emission data category. Anthropogenic total GHG emission is defined as total GHG excluding about 87.18% of activated sludge process emissions [44]**, CO_2 emissions produced in digesters, and CO_2 portion of biogas combustion.**

III. Average Diurnal Total Anthropogenic Greenhouse Gas Emissions Comparison for Primary Treatment Scenarios

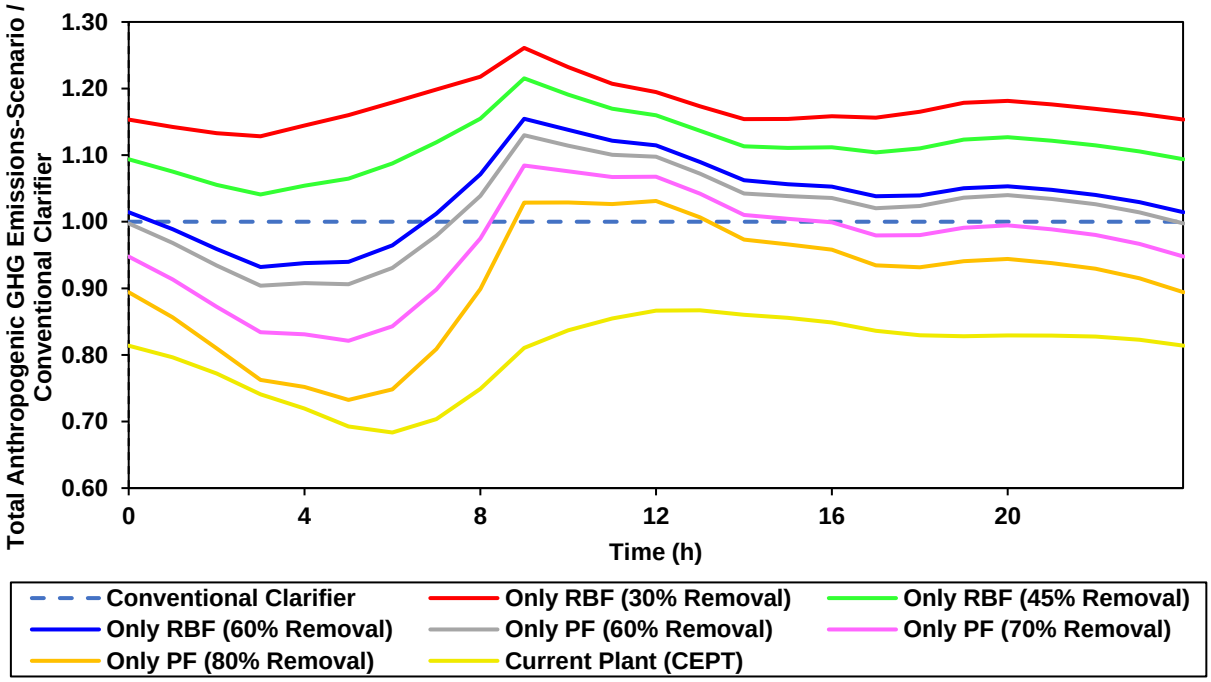

Figure E-3. Comparison of standalone primary treatment technologies' average total anthropogenic greenhouse gas emissions diurnal trends normalized to quality index removal presented as dimensionless ratios, with the conventional clarifier scenario's in the denominator.

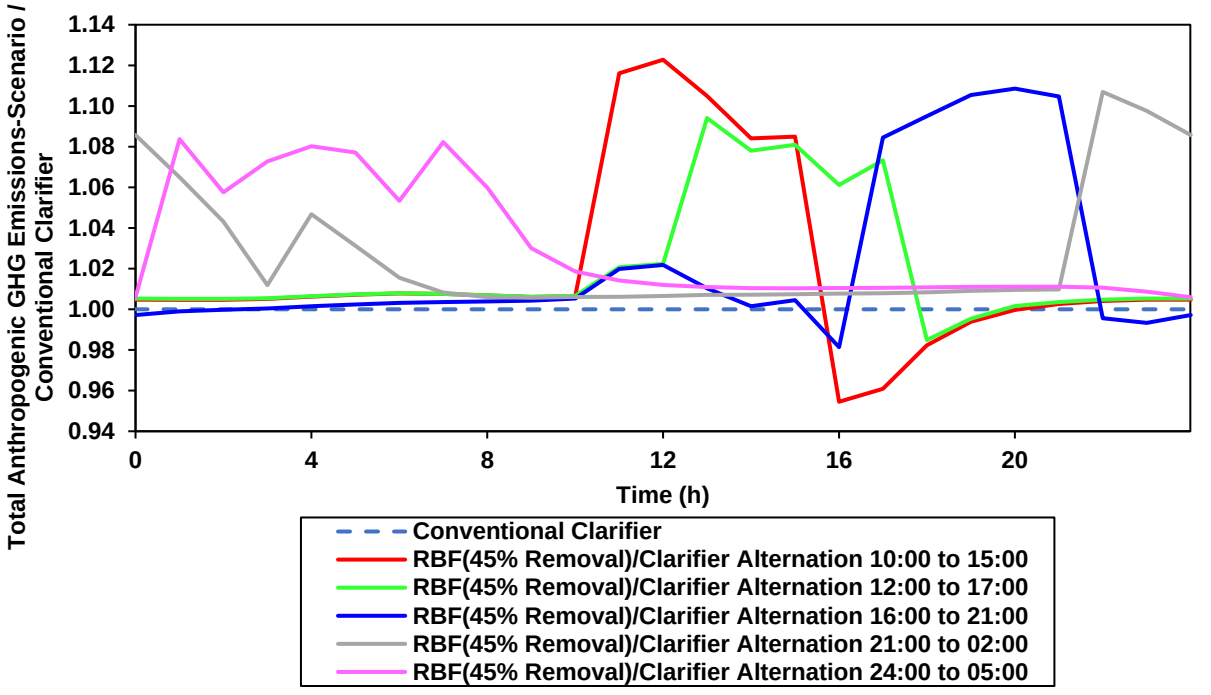

Figure E-4. Comparison of rotating-belt filtration and conventional clarifier alternation scenarios' average total anthropogenic greenhouse gas emissions diurnal trends normalized to quality index removal presented as dimensionless ratios, with the conventional clarifier scenario's in the denominator.

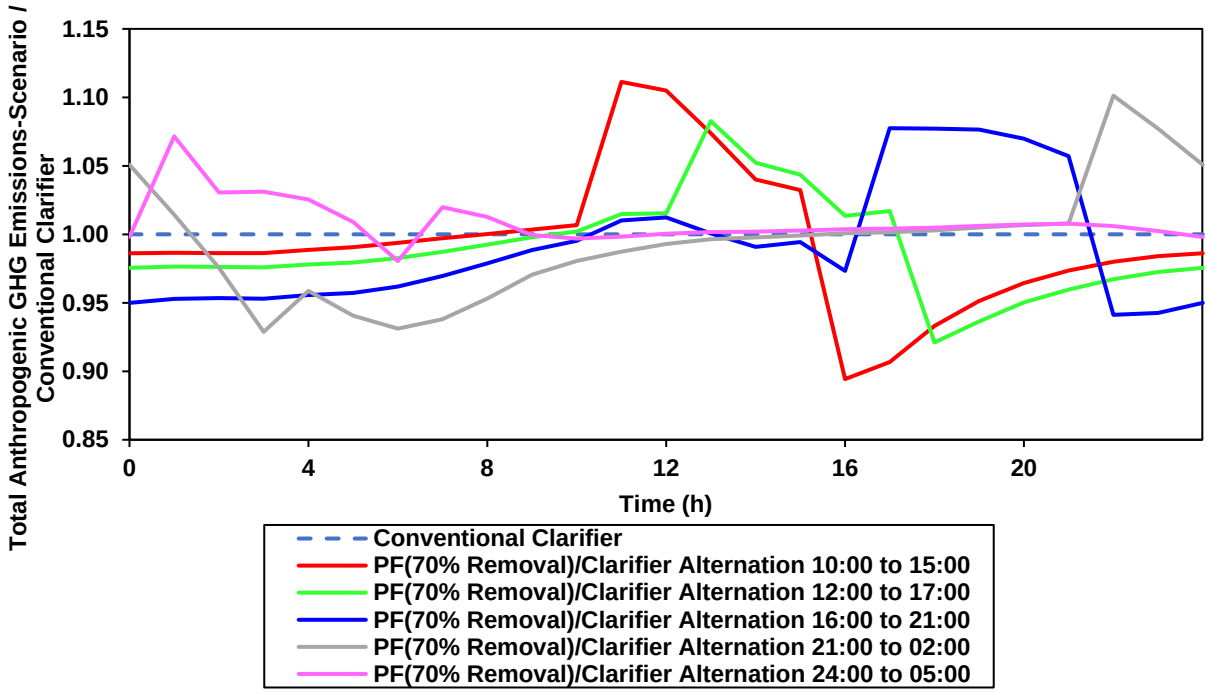

Figure E-5. Comparison of primary filtration and conventional clarifier alternation scenarios' average total anthropogenic greenhouse gas emissions diurnal trends normalized to quality index removal presented as dimensionless ratios, with the conventional clarifier scenario's in the denominator.

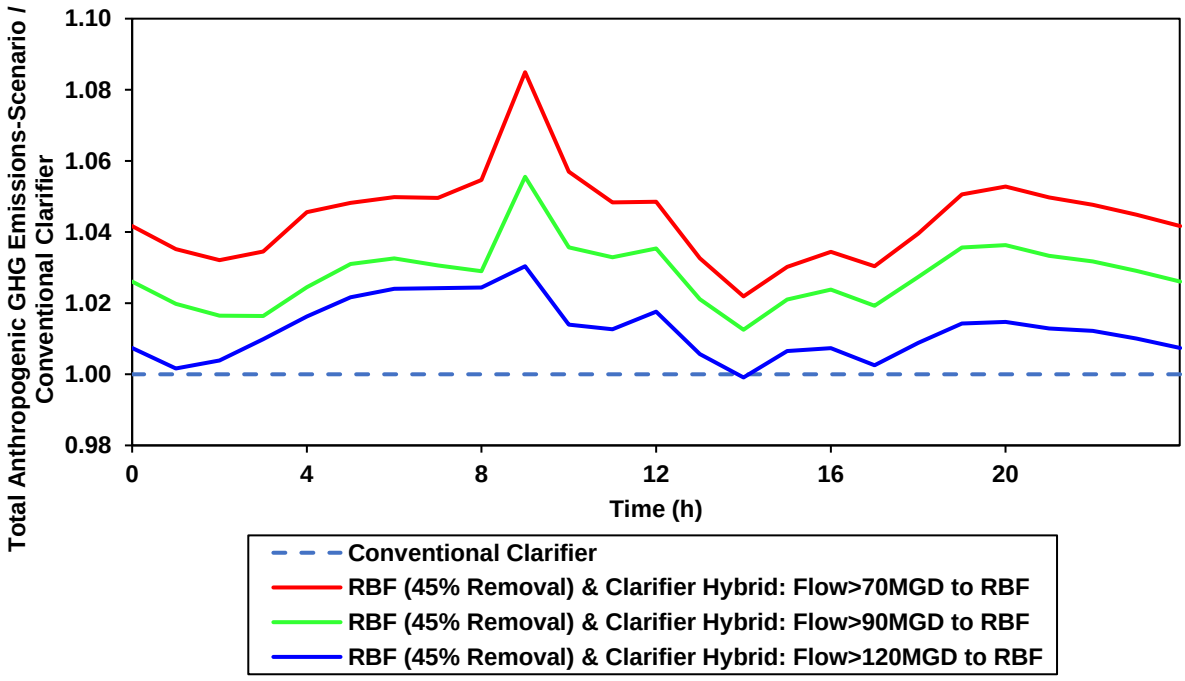

Figure E-6. Comparison of rotating-belt filtration and conventional clarifier hybrid scenarios' average total anthropogenic greenhouse gas emissions diurnal trends normalized to quality index removal presented as dimensionless ratios, with the conventional clarifier scenario's in the denominator.

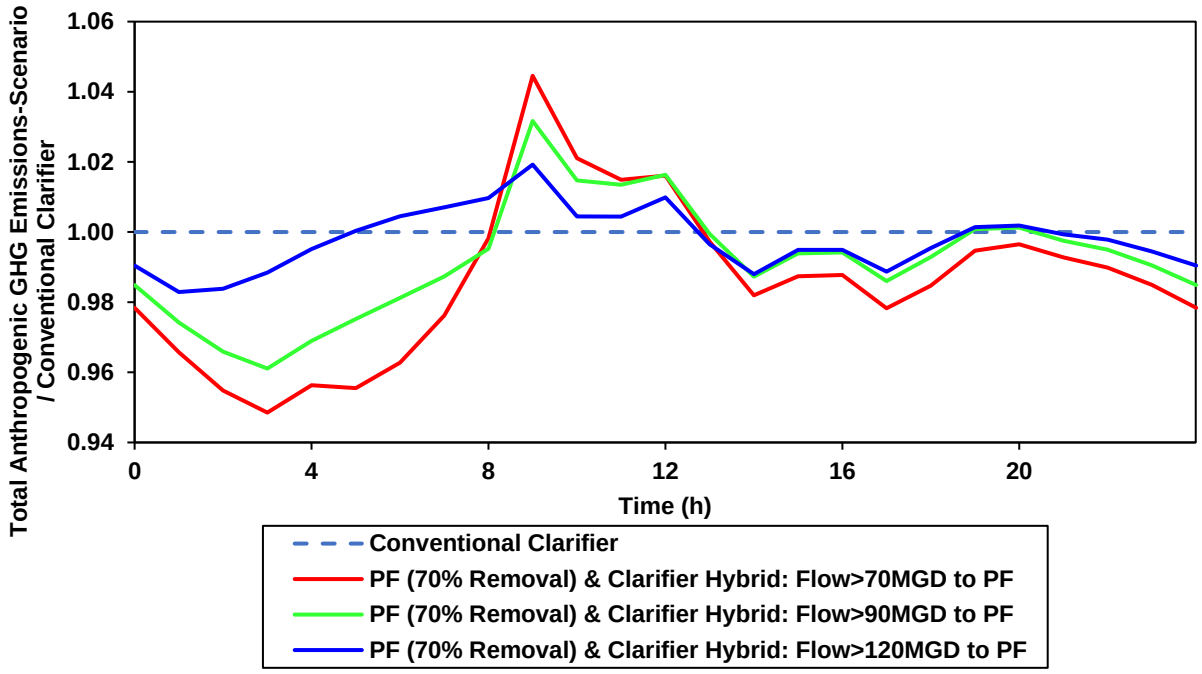

Figure E-7. Comparison of primary filtration and conventional clarifier hybrid scenarios' average total anthropogenic greenhouse gas emissions diurnal trends normalized to quality index removal presented as dimensionless ratios, with the conventional clarifier scenario's in the denominator.

IV. Average Diurnal Total Greenhouse Gas Emissions Comparison for Primary Treatment Scenarios

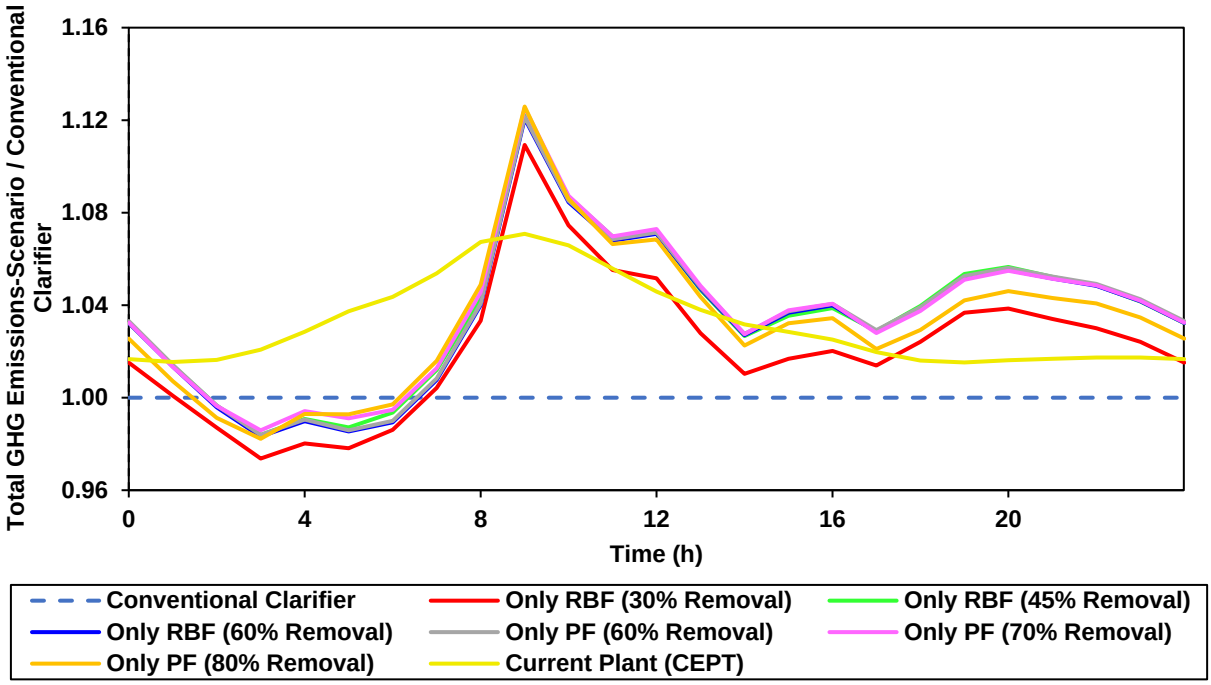

Figure E-8. Comparison of standalone primary treatment technologies' average total greenhouse gas emissions diurnal trends normalized to quality index removal presented as dimensionless ratios, with the conventional clarifier scenario's in the denominator.

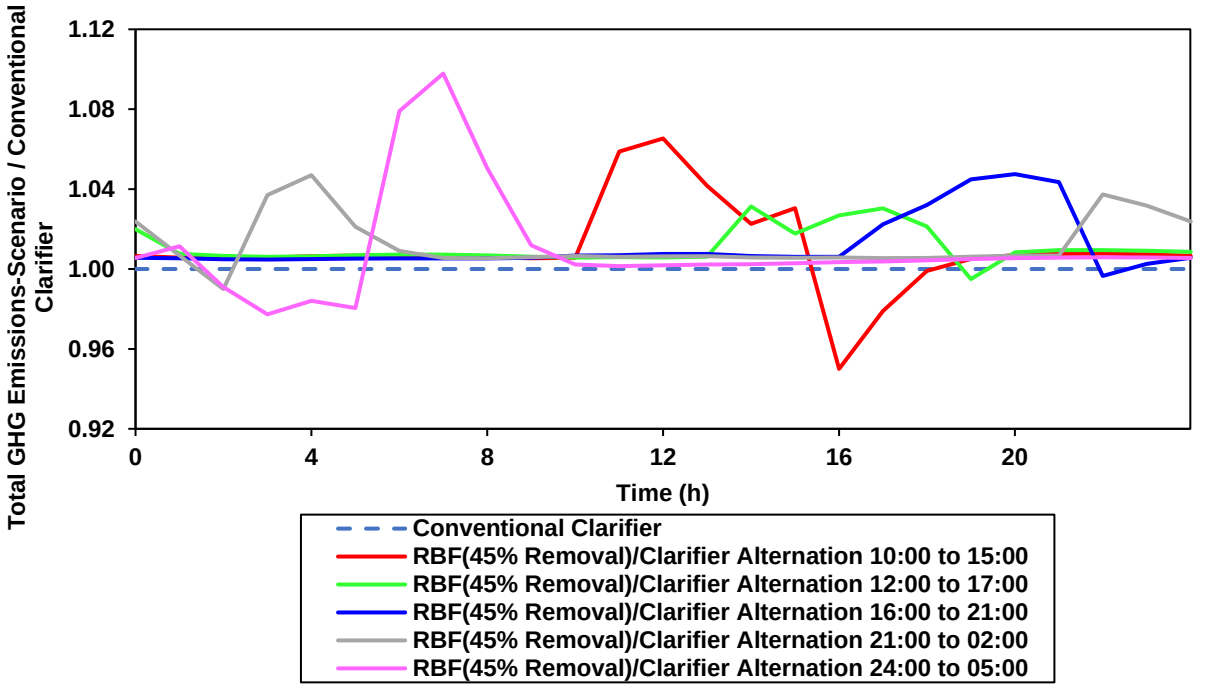

Figure E-9. Comparison of rotating-belt filtration and conventional clarifier alternation scenarios' average total greenhouse gas emissions diurnal trends normalized to quality index removal presented as dimensionless ratios, with the conventional clarifier scenario's in the denominator.

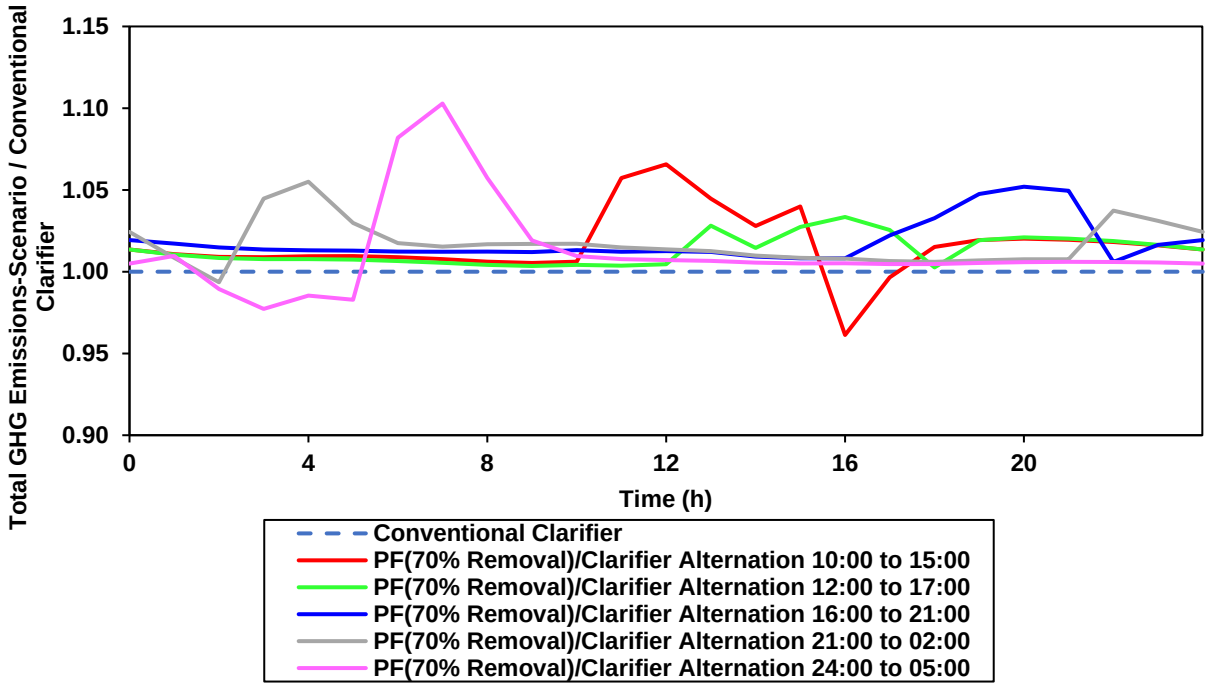

Figure E-10. Comparison of primary filtration and conventional clarifier alternation scenarios' average total greenhouse gas emissions diurnal trends normalized to quality index removal presented as dimensionless ratios, with the conventional clarifier scenario's in the denominator.

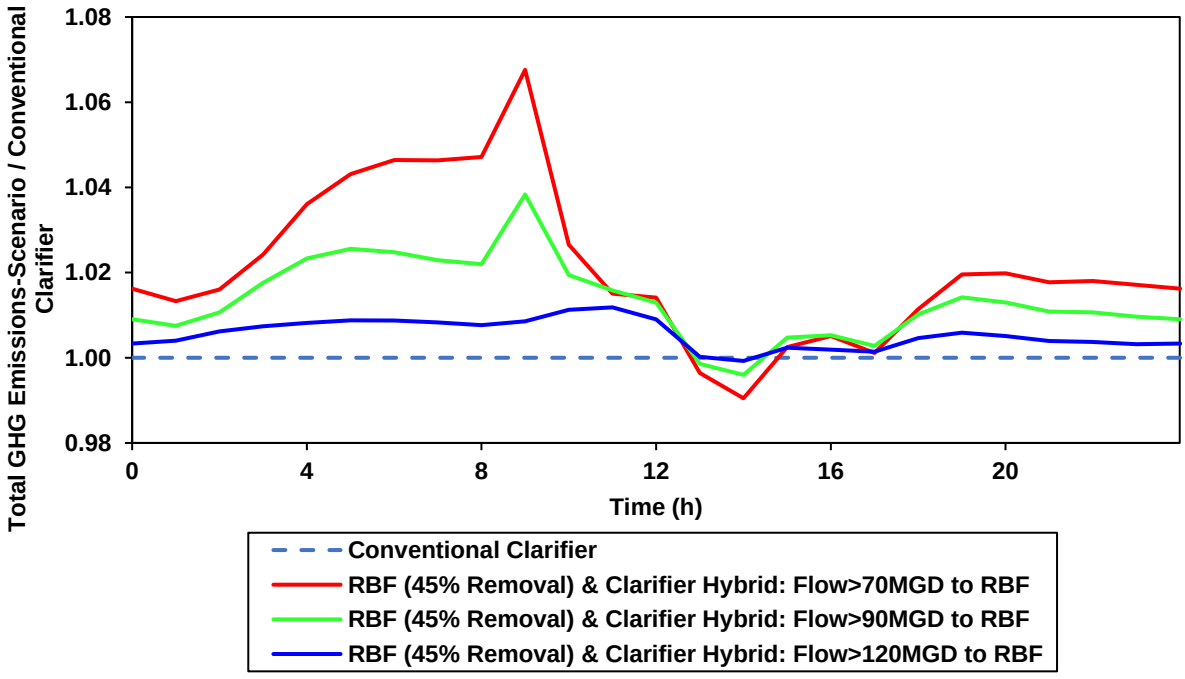

Figure E-11. Comparison of rotating-belt filtration and conventional clarifier hybrid scenarios' average total greenhouse gas emissions diurnal trends normalized to quality index removal presented as dimensionless ratios, with the conventional clarifier scenario's in the denominator.

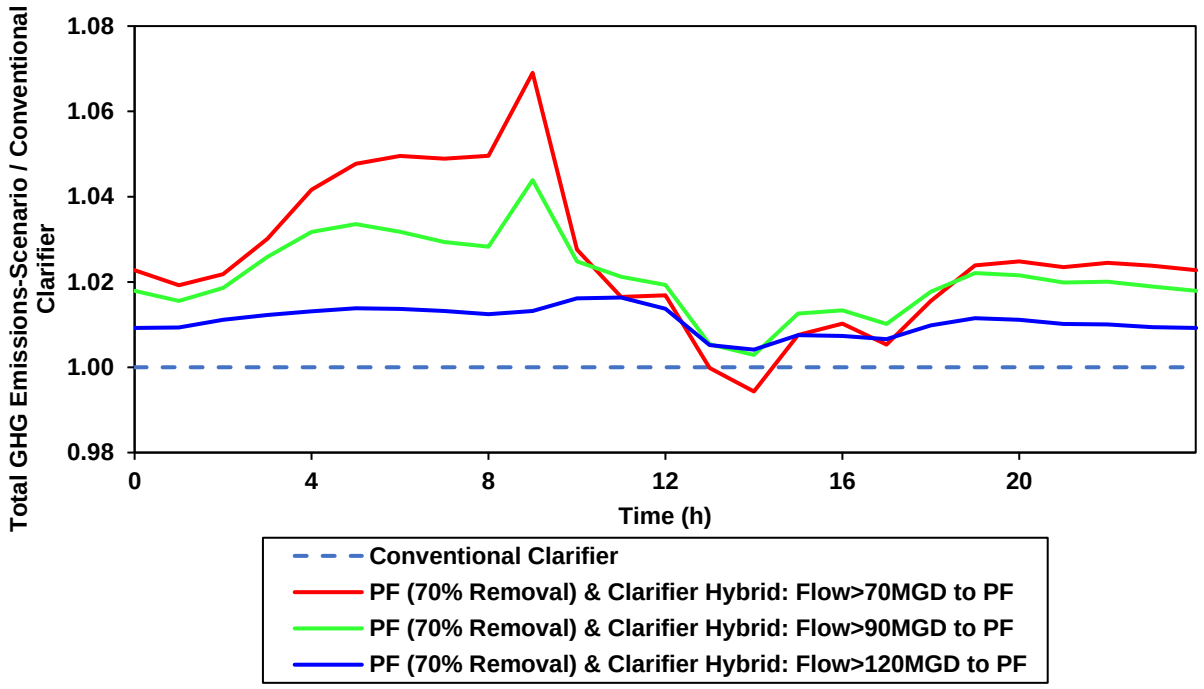

Figure E-12. Comparison of primary filtration and conventional clarifier hybrid scenarios' average total greenhouse gas emissions diurnal trends normalized to quality index removal presented as dimensionless ratios, with the conventional clarifier scenario's in the denominator.

V. Average Diurnal Electricity Import Cost Comparison for Primary Treatment Scenarios

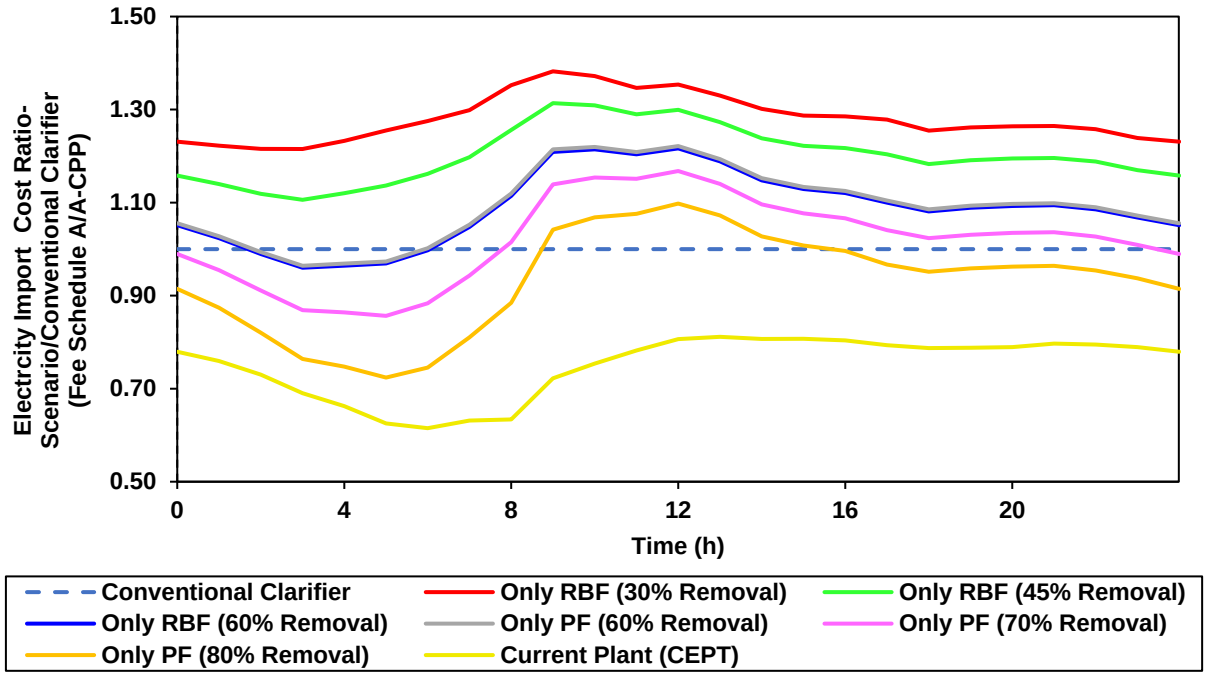

Figure E-13. Comparison of standalone primary treatment technologies' average electricity import cost (per Fee Schedule A/A-CPP) diurnal trends normalized to quality index removal presented as dimensionless ratios, with the conventional clarifier scenario's in the denominator.

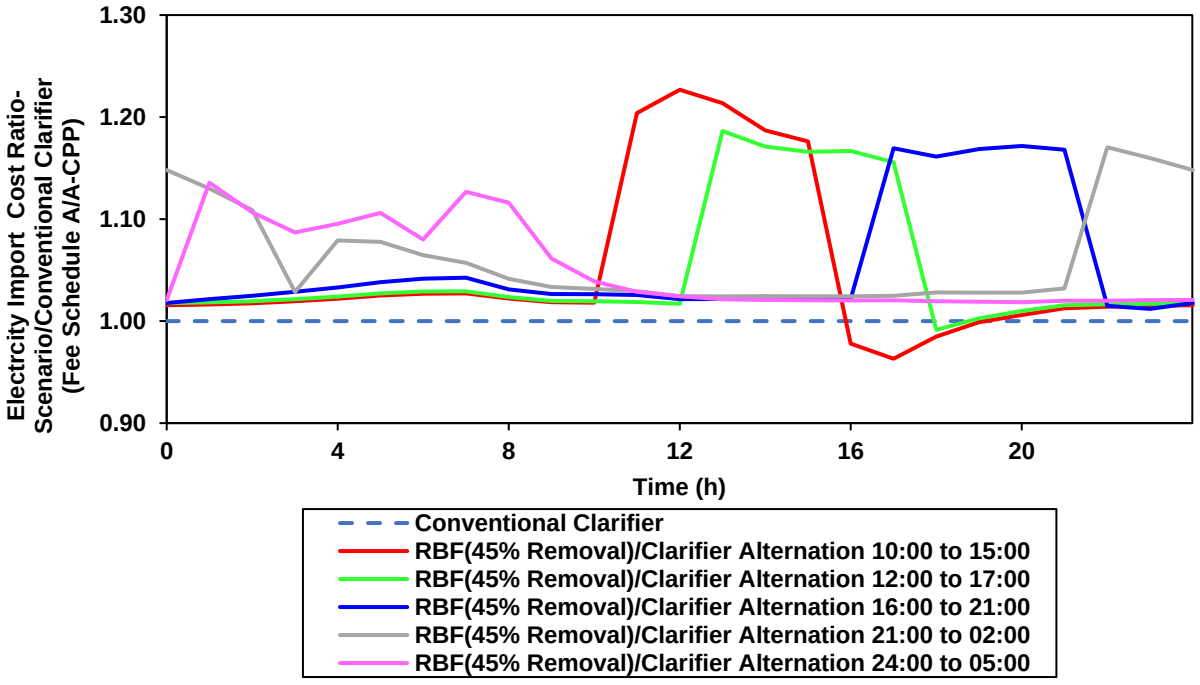

Figure E-14. Comparison of rotating-belt filtration and conventional clarifier alternation scenarios' average electricity import cost (per Fee Schedule A/A-CPP) diurnal trends normalized to quality index removal presented as dimensionless ratios, with the conventional clarifier scenario's in the denominator.

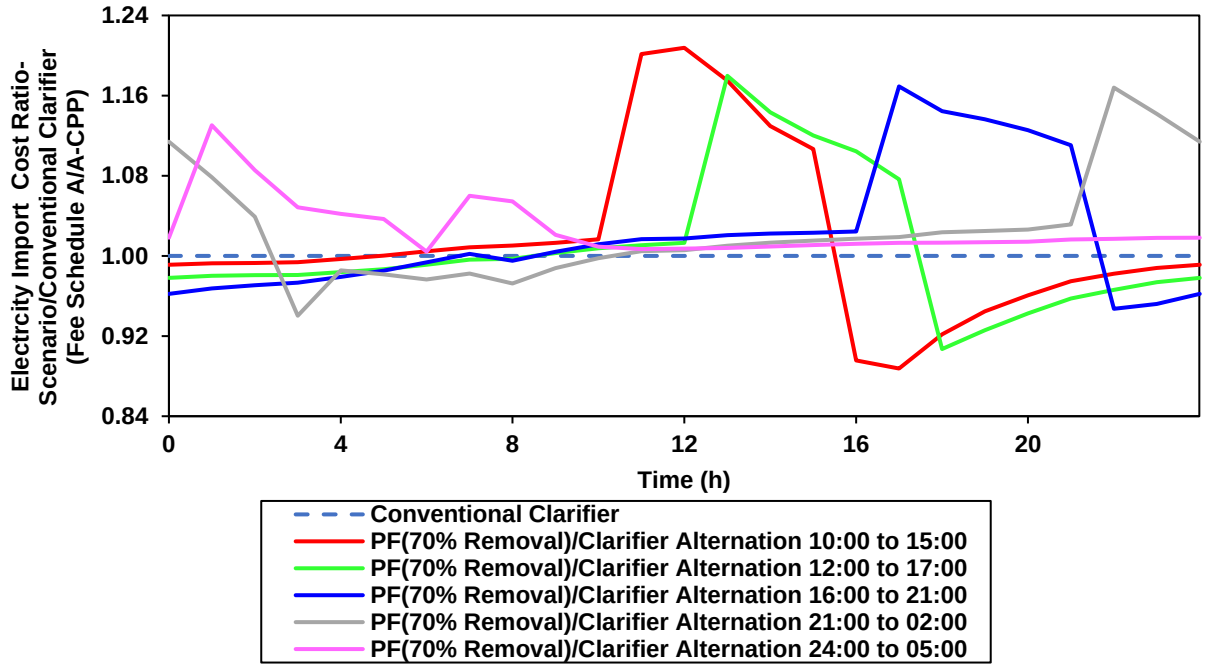

Figure E-15. Comparison of primary filtration and conventional clarifier alternation scenarios' average electricity import cost (per Fee Schedule A/A-CPP) diurnal trends normalized to quality index removal presented as dimensionless ratios, with the conventional clarifier scenario's in the denominator.

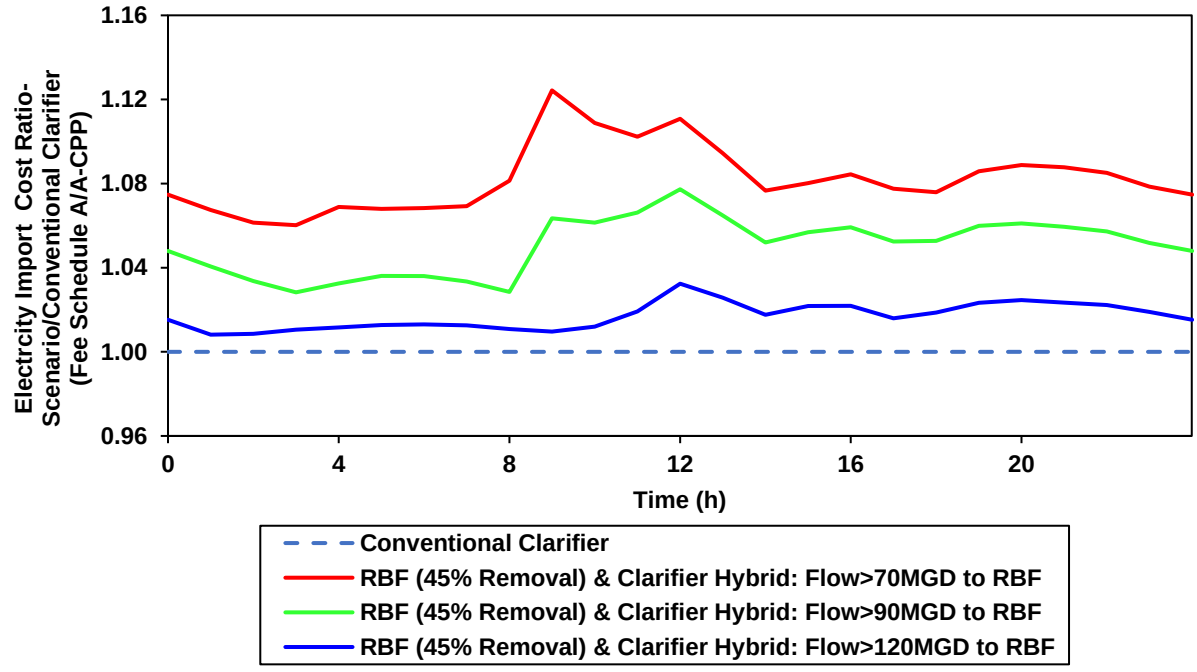

Figure E-16. Comparison of rotating-belt filtration and conventional clarifier hybrid scenarios' average electricity import cost (per Fee Schedule A/A-CPP) diurnal trends normalized to quality index removal presented as dimensionless ratios, with the conventional clarifier scenario's in the denominator.

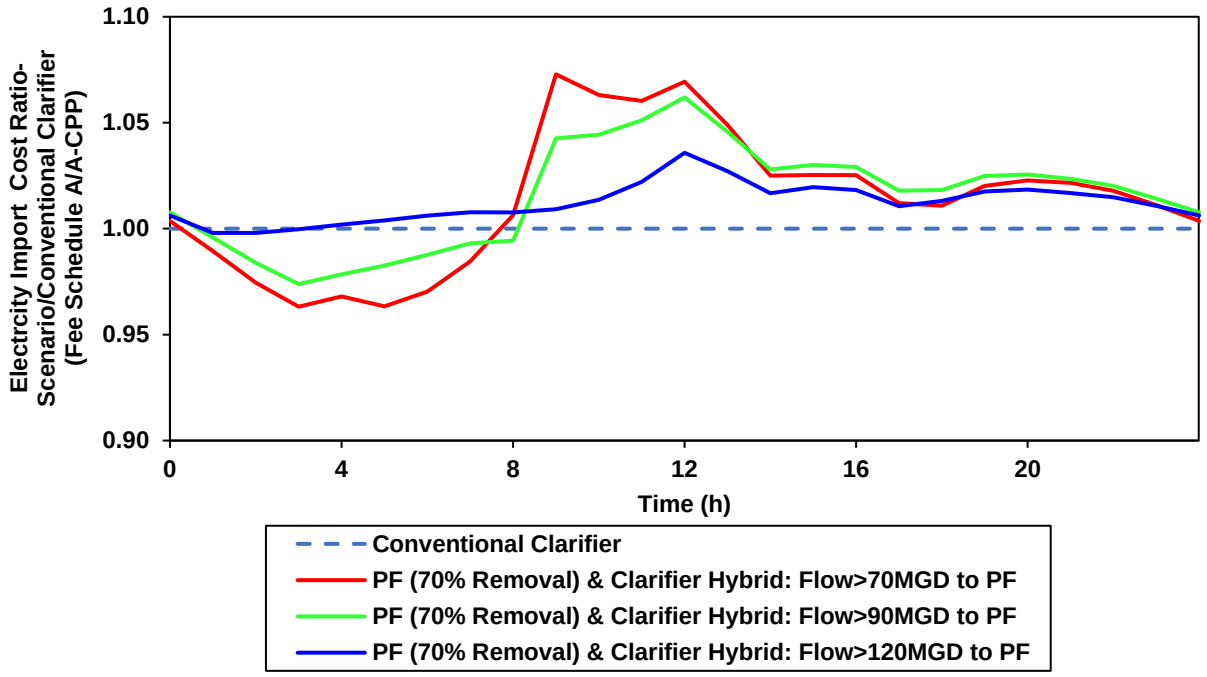

Figure E-17. Comparison of primary filtration and conventional clarifier hybrid scenarios' average electricity import cost (per Fee Schedule A/A-CPP) diurnal trends normalized to quality index removal presented as dimensionless ratios, with the conventional clarifier scenario's in the denominator.

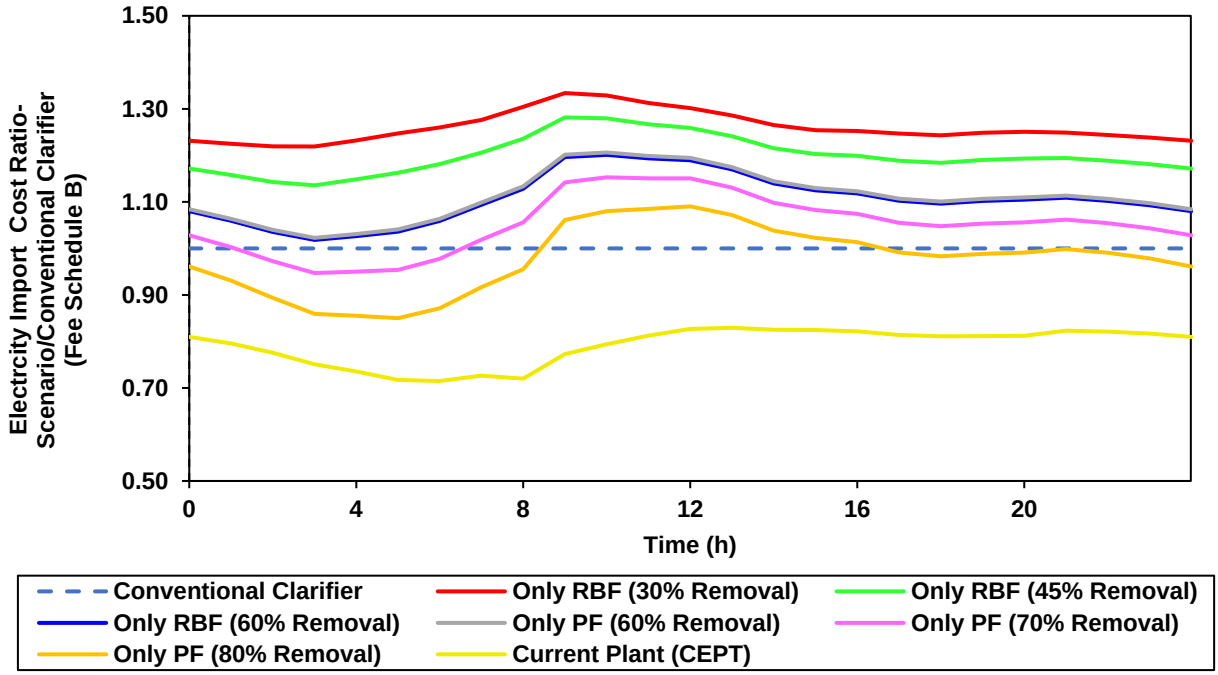

Figure E-18. Comparison of standalone primary treatment technologies' average electricity import cost (per Fee Schedule B) diurnal trends normalized to quality index removal presented as dimensionless ratios, with the conventional clarifier scenario's in the denominator.

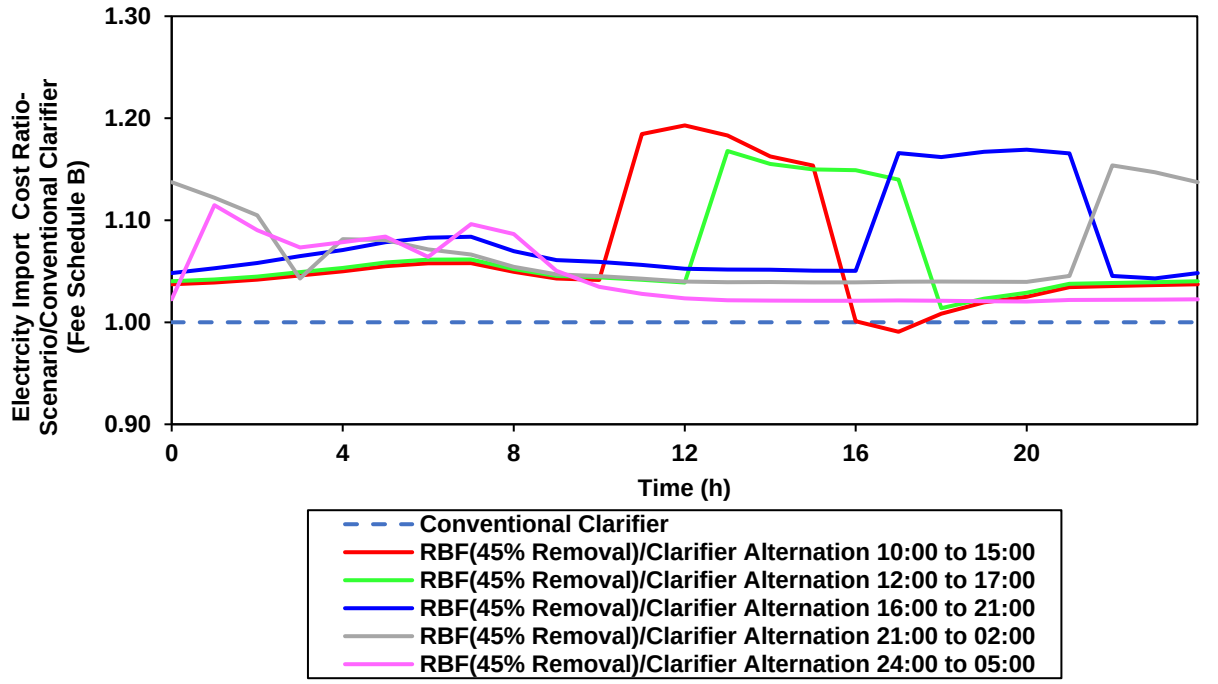

Figure E-19. Comparison of rotating-belt filtration and conventional clarifier alternation scenarios' average electricity import cost (per Fee Schedule B) diurnal trends normalized to quality index removal presented as dimensionless ratios, with the conventional clarifier scenario's in the denominator.

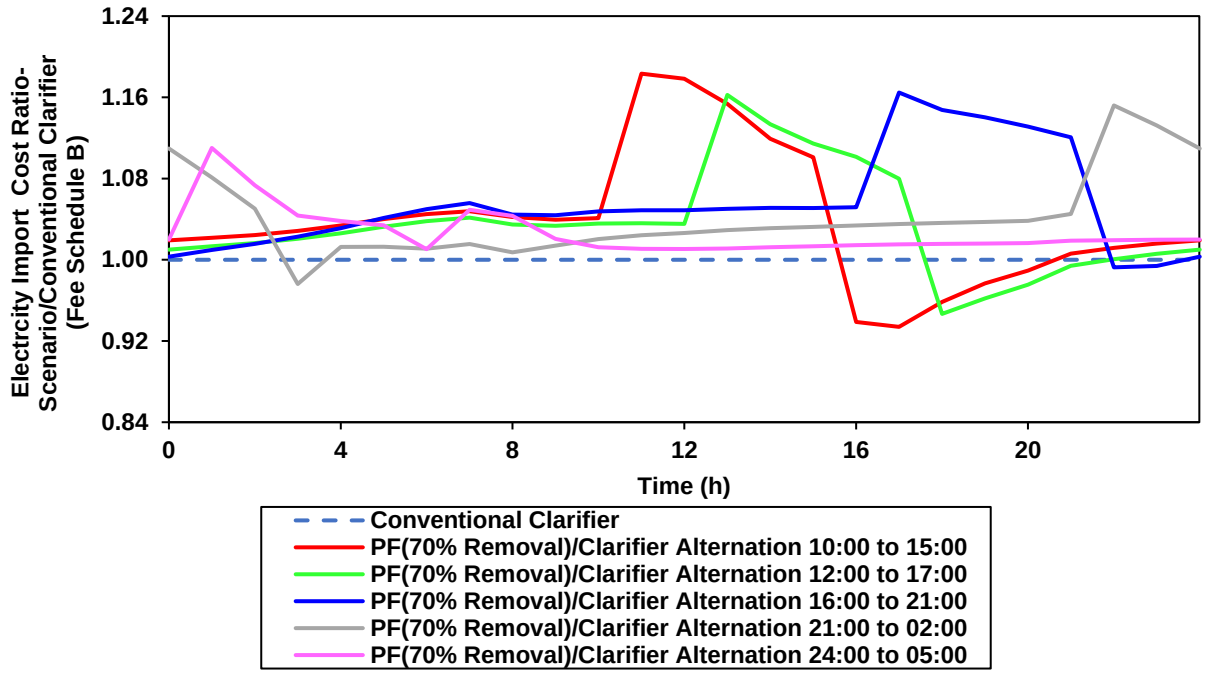

Figure E-20. Comparison of primary filtration and conventional clarifier alternation scenarios' average electricity import cost (per Fee Schedule B) diurnal trends normalized to quality index removal presented as dimensionless ratios, with the conventional clarifier scenario's in the denominator.

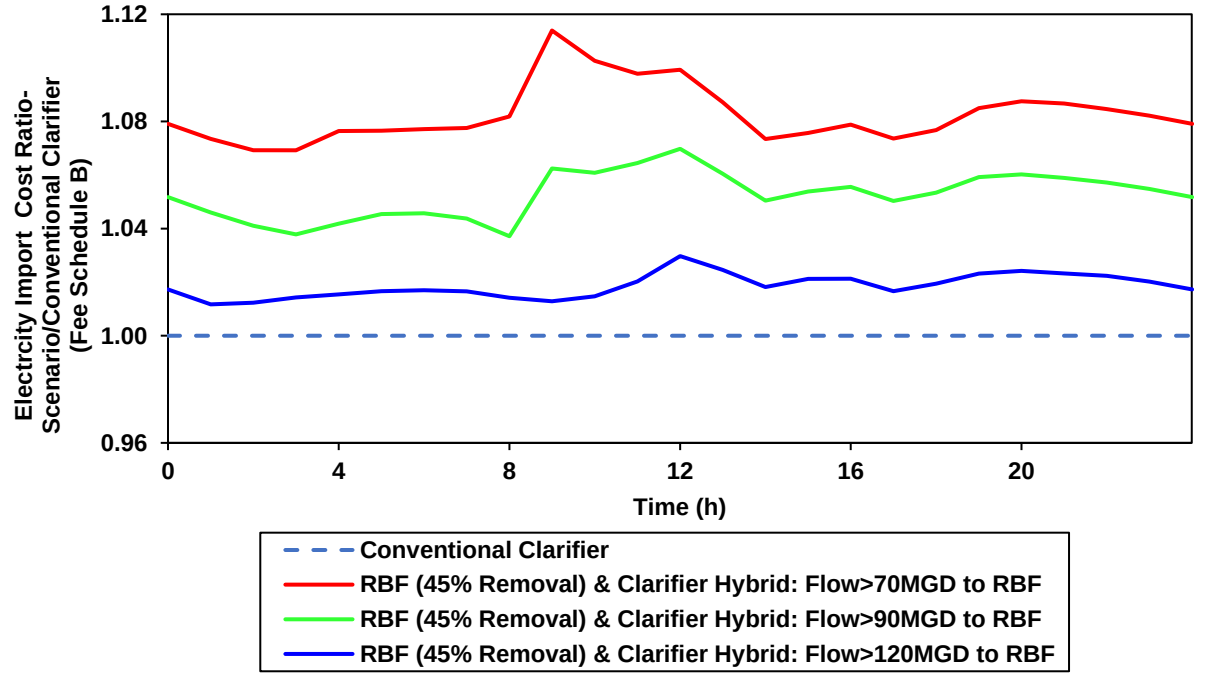

Figure E-21. Comparison of rotating-belt filtration and conventional clarifier hybrid scenarios' average electricity import cost (per Fee Schedule B) diurnal trends normalized to quality index removal presented as dimensionless ratios, with the conventional clarifier scenario's in the denominator.

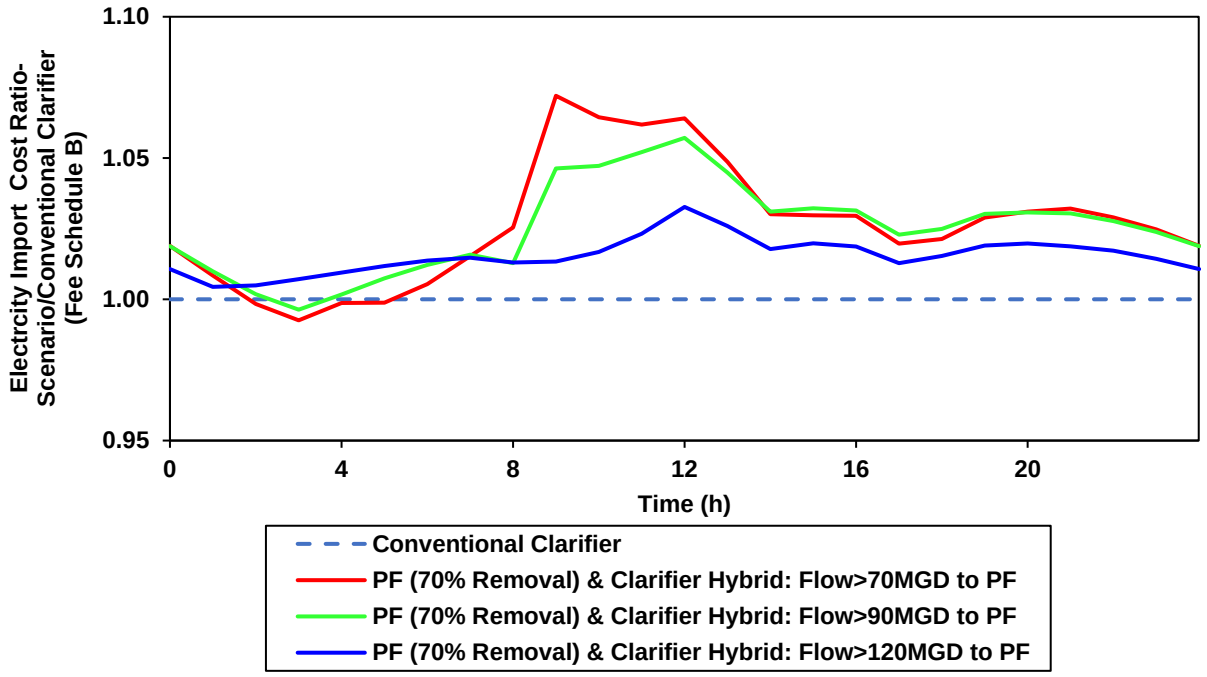

Figure E-22. Comparison of primary filtration and conventional clarifier hybrid scenarios' average electricity import cost (per Fee Schedule B) diurnal trends normalized to quality index removal presented as dimensionless ratios, with the conventional clarifier scenario's in the denominator.

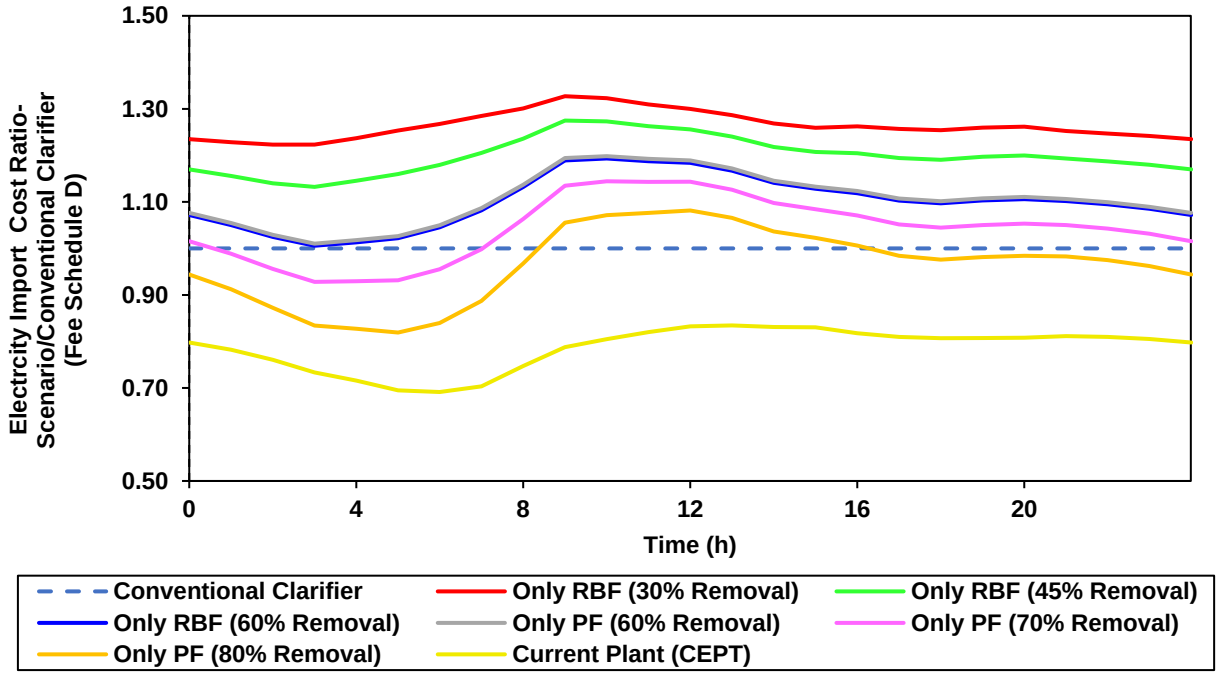

Figure E-23. Comparison of standalone primary treatment technologies' average electricity import cost (per Fee Schedule D) diurnal trends normalized to quality index removal presented as dimensionless ratios, with the conventional clarifier scenario's in the denominator.

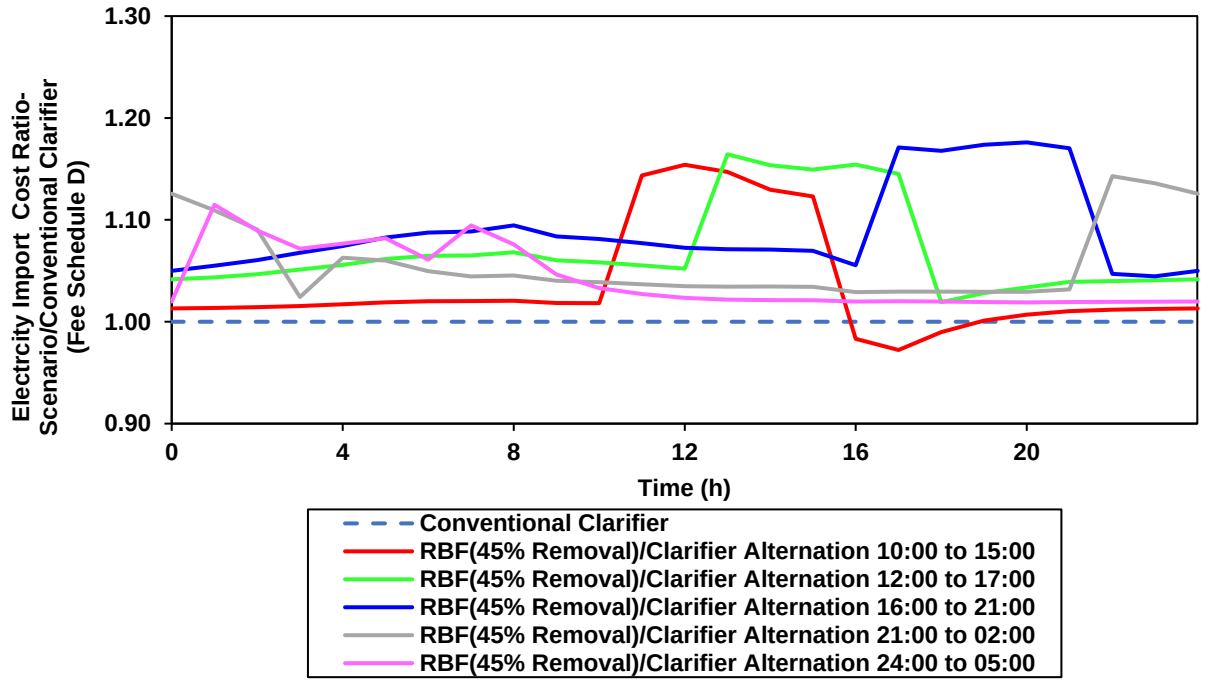

Figure E-24. Comparison of rotating-belt filtration and conventional clarifier alternation scenarios' average electricity import cost (per Fee Schedule D) diurnal trends normalized to quality index removal presented as dimensionless ratios, with the conventional clarifier scenario's in the denominator.

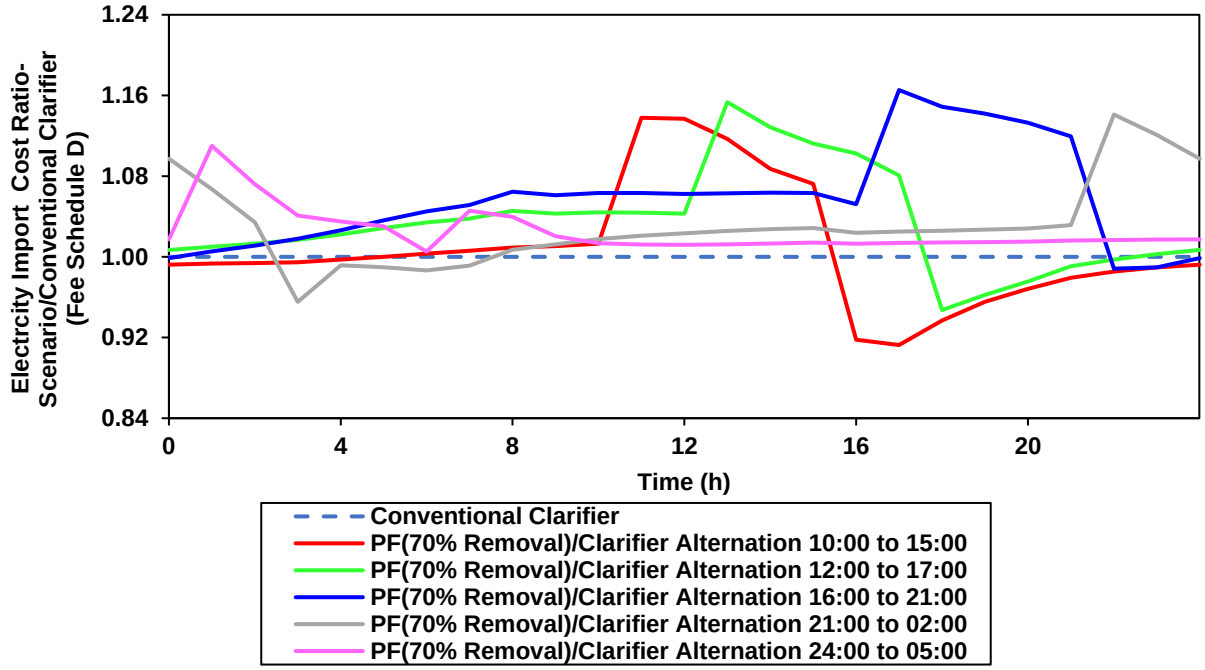

Figure E-25. Comparison of primary filtration and conventional clarifier alternation scenarios' average electricity import cost (per Fee Schedule D) diurnal trends normalized to quality index removal presented as dimensionless ratios, with the conventional clarifier scenario's in the denominator.

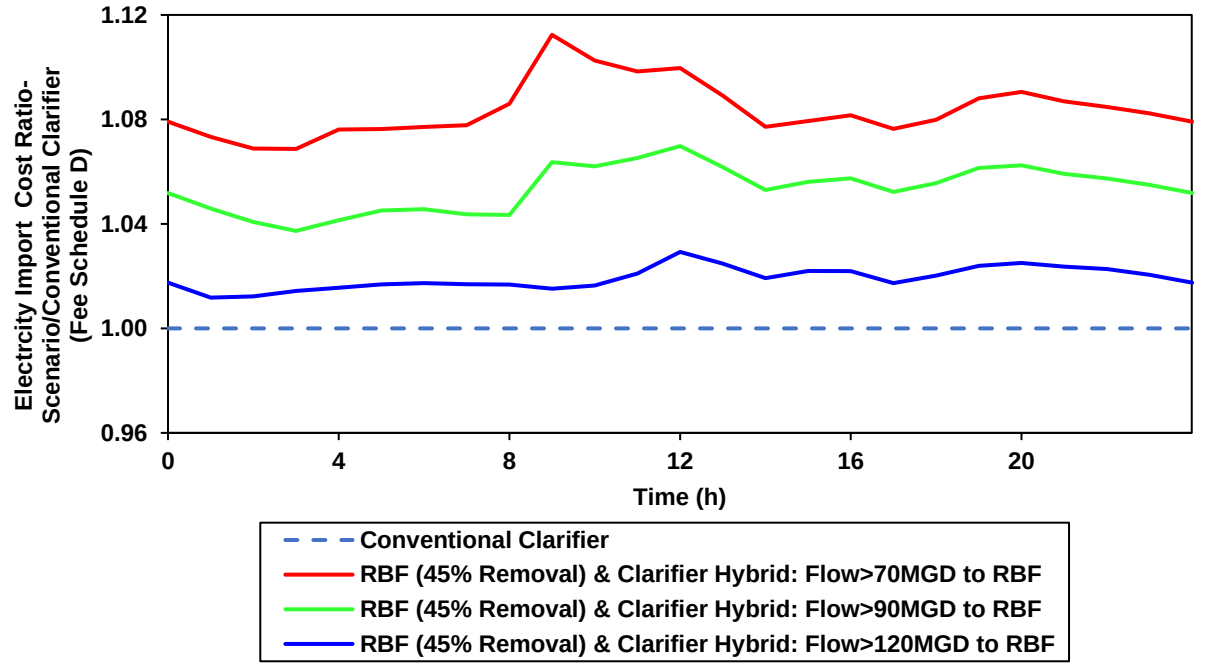

Figure E-26. Comparison of rotating-belt filtration and conventional clarifier hybrid scenarios' average electricity import cost (per Fee Schedule D) diurnal trends normalized to quality index removal presented as dimensionless ratios, with the conventional clarifier scenario's in the denominator.

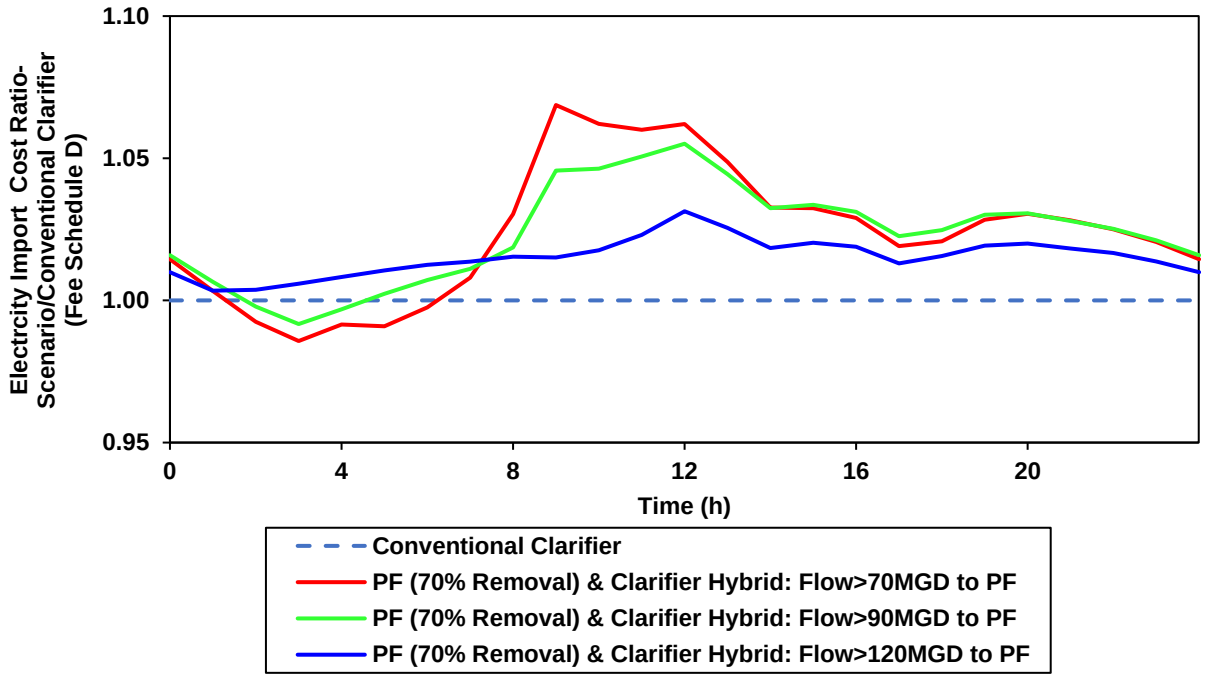

Figure E-27. Comparison of primary filtration and conventional clarifier hybrid scenarios' average electricity import cost (per Fee Schedule D) diurnal trends normalized to quality index removal presented as dimensionless ratios, with the conventional clarifier scenario's in the denominator.

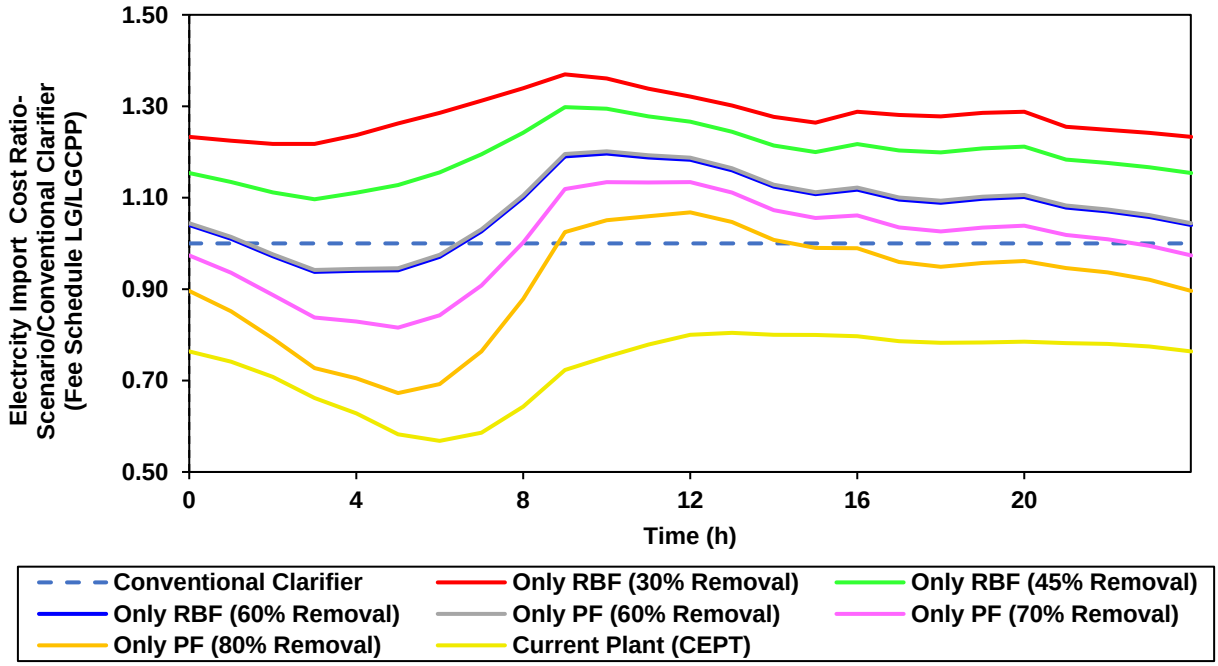

Figure E-28. Comparison of standalone primary treatment technologies' average electricity import cost (per Fee Schedule LG/LG-CPP) diurnal trends normalized to quality index removal presented as dimensionless ratios, with the conventional clarifier scenario's in the denominator.

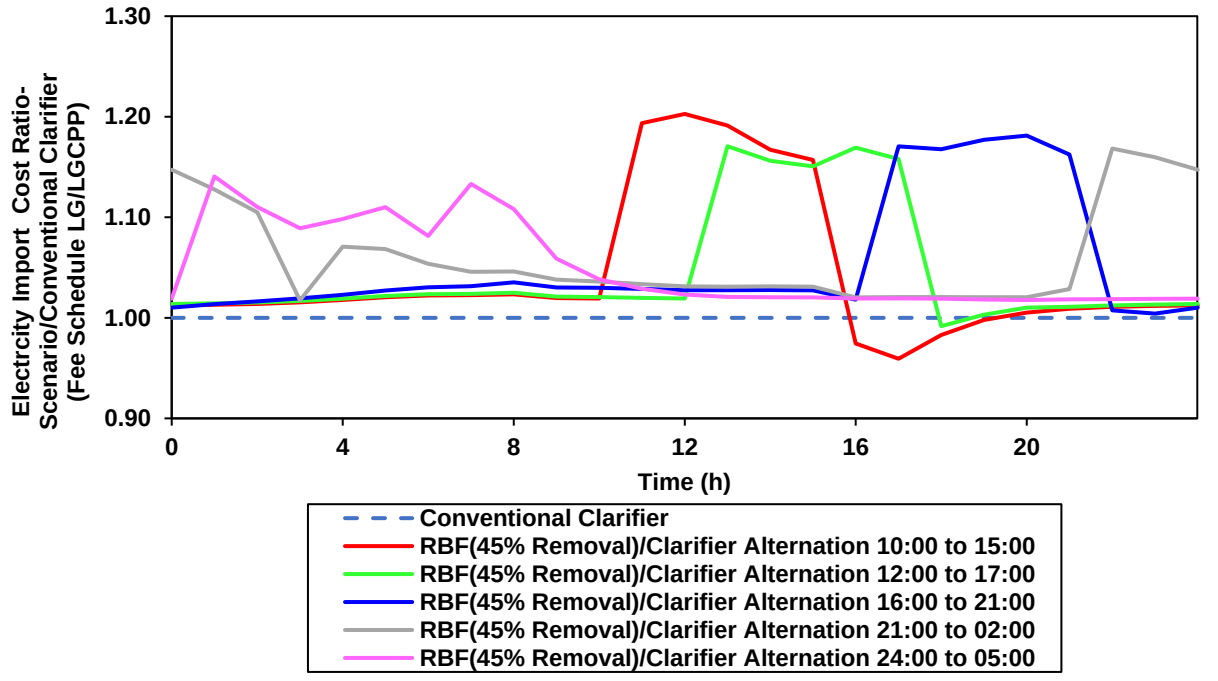

Figure E-29. Comparison of rotating-belt filtration and conventional clarifier alternation scenarios' average electricity import cost (per Fee Schedule LG/LG-CPP) diurnal trends normalized to quality index removal presented as dimensionless ratios, with the conventional clarifier scenario's in the denominator.

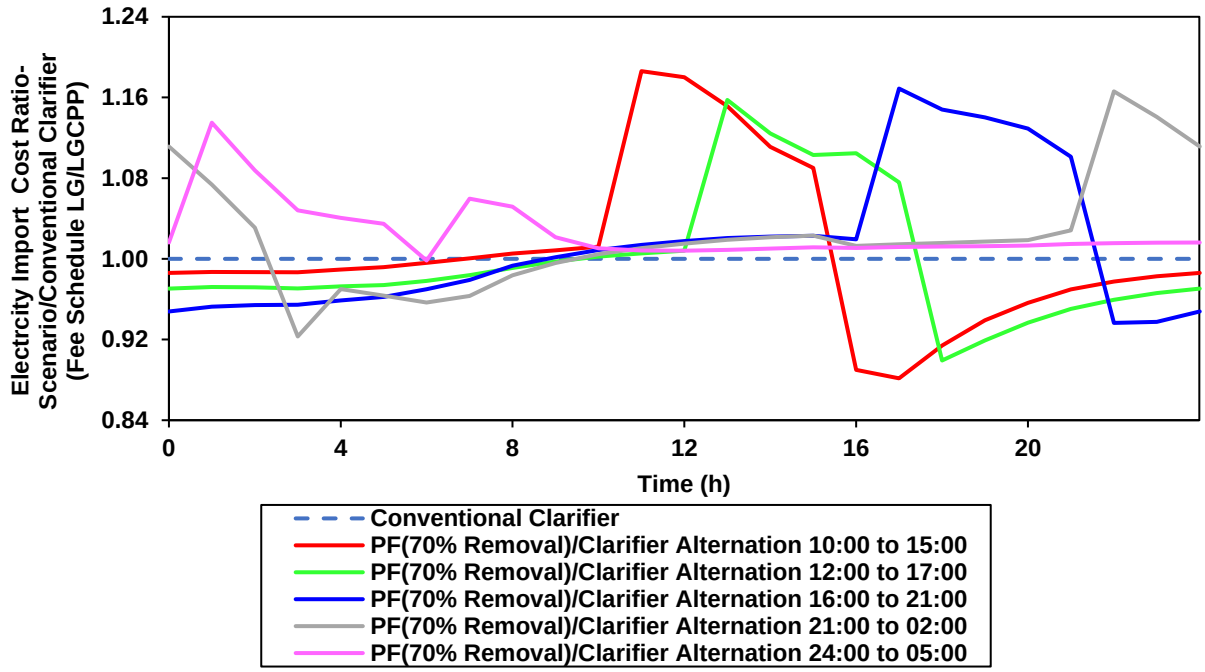

Figure E-30. Comparison of primary filtration and conventional clarifier alternation scenarios' average electricity import cost (per Fee Schedule LG/LG-CPP) diurnal trends normalized to quality index removal presented as dimensionless ratios, with the conventional clarifier scenario's in the denominator.

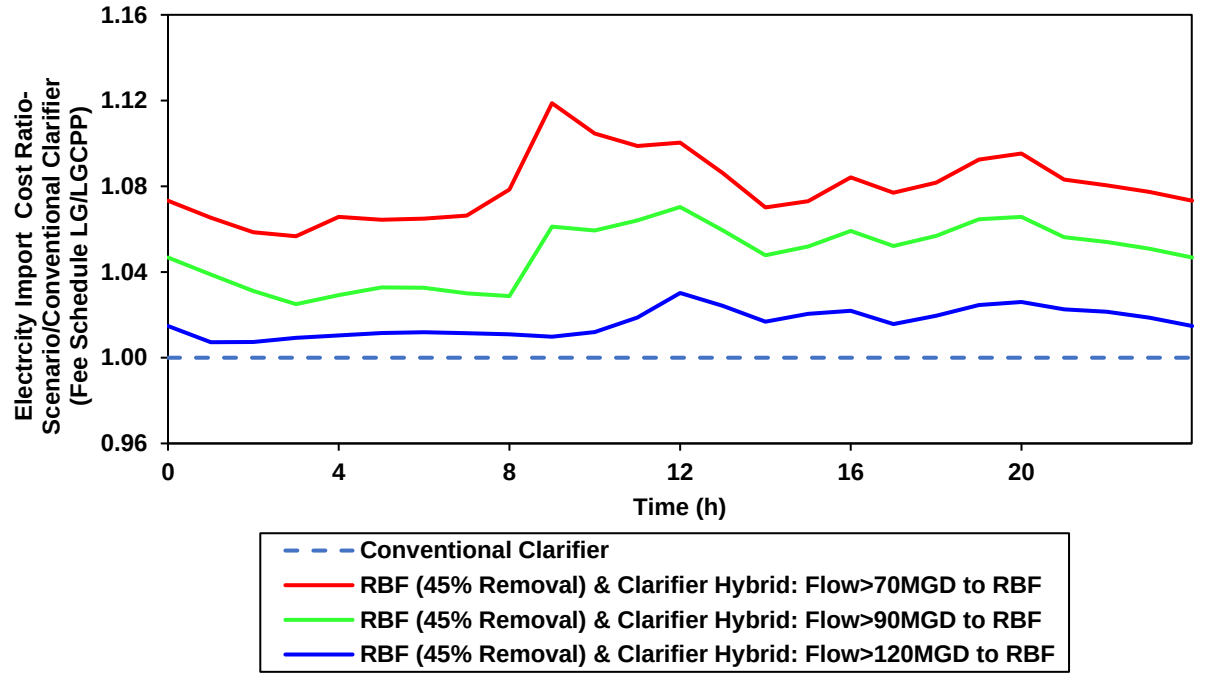

Figure E-31. Comparison of rotating-belt filtration and conventional clarifier hybrid scenarios' average electricity import cost (per Fee Schedule LG/LG-CPP) diurnal trends normalized to quality index removal presented as dimensionless ratios, with the conventional clarifier scenario's in the denominator.

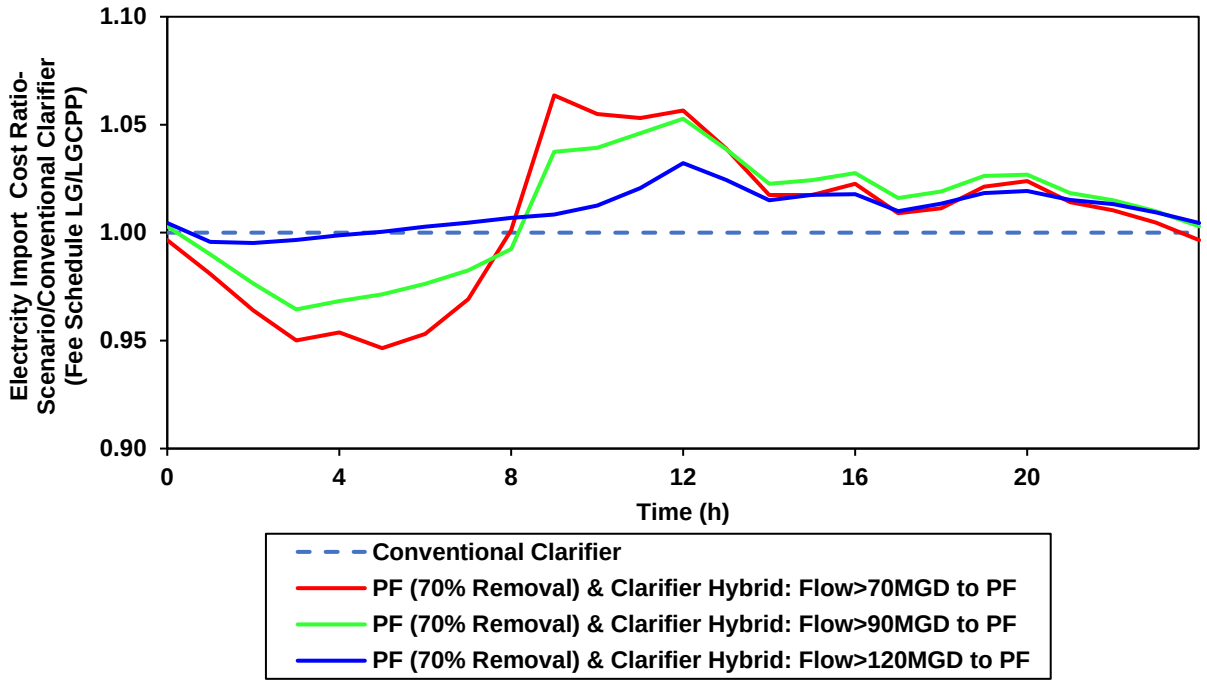

Figure E-32. Comparison of primary filtration and conventional clarifier hybrid scenarios' average electricity import cost (per Fee Schedule LG/LG-CPP) diurnal trends normalized to quality index removal presented as dimensionless ratios, with the conventional clarifier scenario's in the denominator.

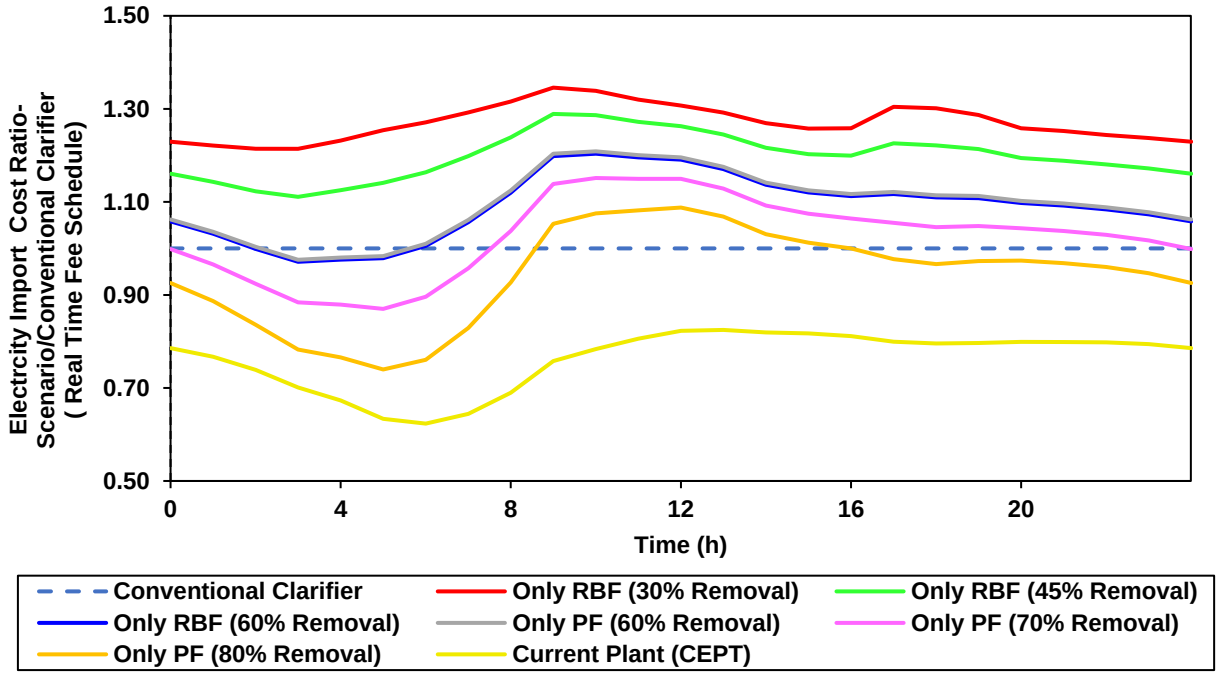

Figure E-33. Comparison of standalone primary treatment technologies' average electricity import cost (per Real Time Fee Schedule) diurnal trends normalized to quality index removal presented as dimensionless ratios, with the conventional clarifier scenario's in the denominator.

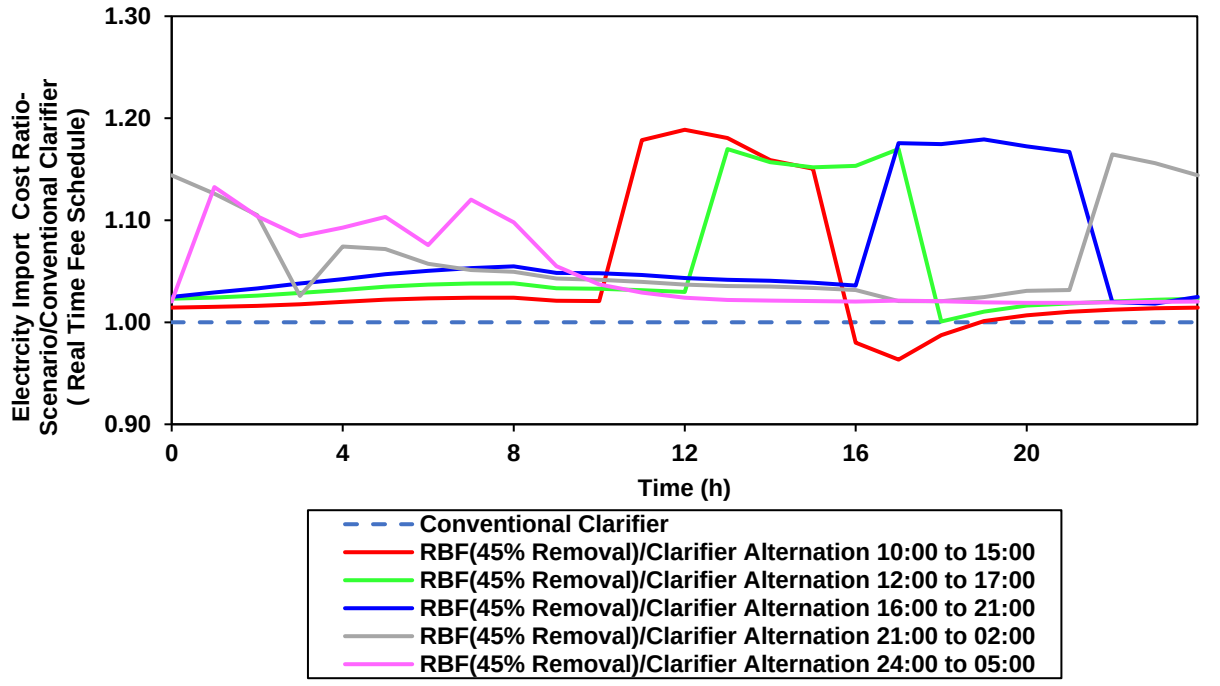

Figure E-34. Comparison of rotating-belt filtration and conventional clarifier alternation scenarios' average electricity import cost (per Real Time Fee Schedule) diurnal trends normalized to quality index removal presented as dimensionless ratios, with the conventional clarifier scenario's in the denominator.

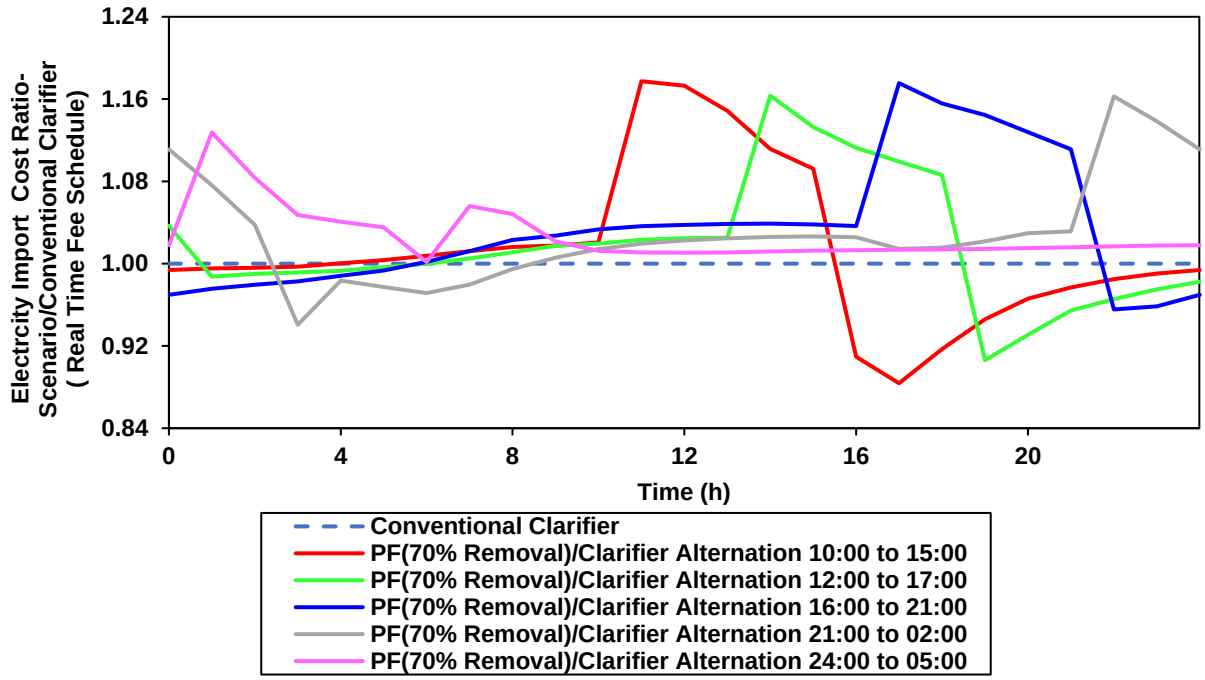

Figure E-35. Comparison of primary filtration and conventional clarifier alternation scenarios' average electricity import cost (per Real Time Fee Schedule) diurnal trends normalized to quality index removal presented as dimensionless ratios, with the conventional clarifier scenario's in the denominator.

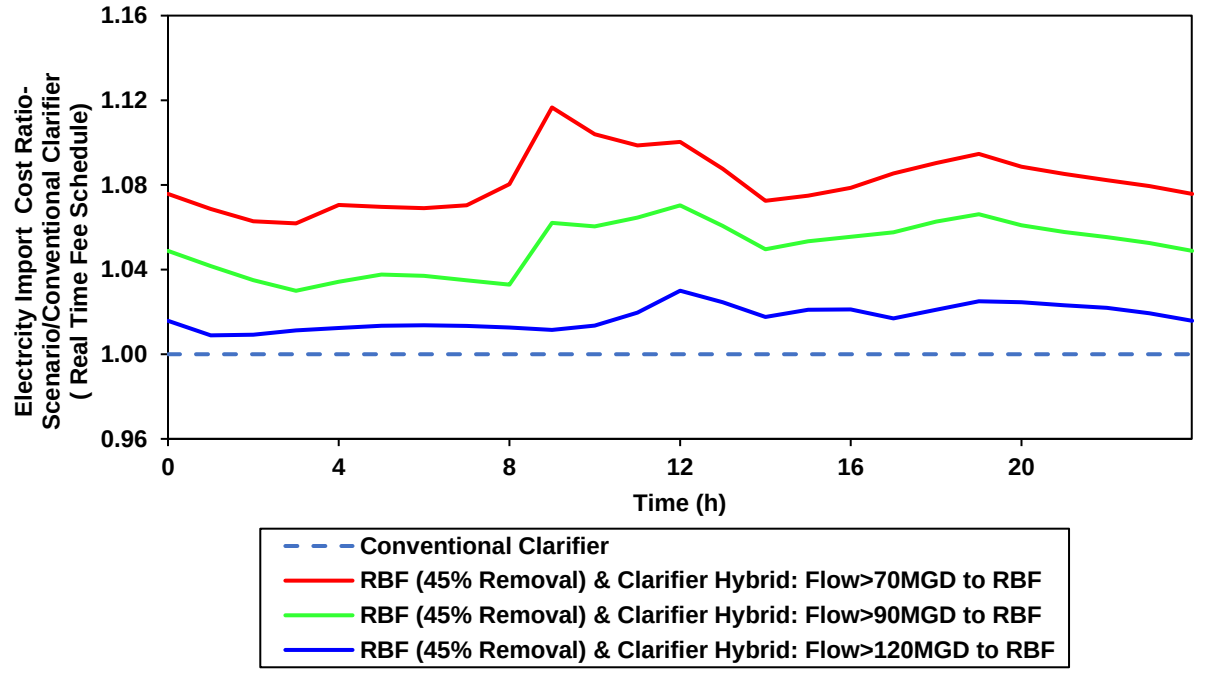

Figure E-36. Comparison of rotating-belt filtration and conventional clarifier hybrid scenarios' average electricity import cost (per Real Time Fee Schedule) diurnal trends normalized to quality index removal presented as dimensionless ratios, with the conventional clarifier scenario's in the denominator.

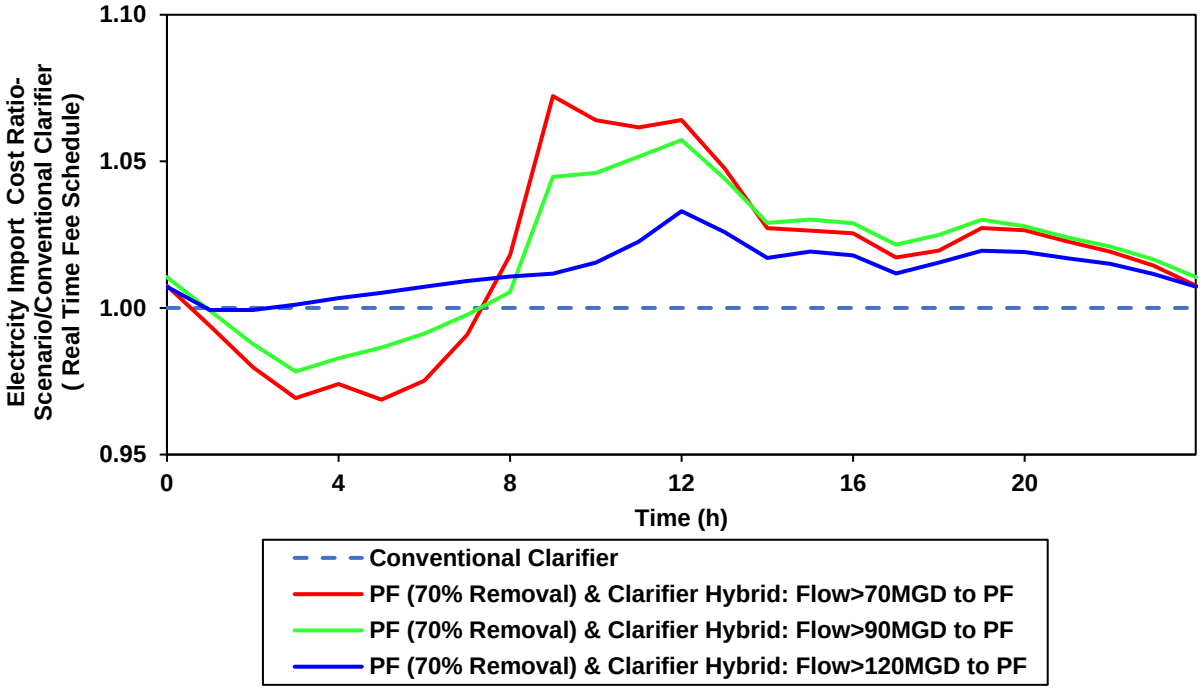

Figure E-37. Comparison of primary filtration and conventional clarifier hybrid scenarios' average electricity import cost (per Real Time Fee Schedule) diurnal trends normalized to quality index removal presented as dimensionless ratios, with the conventional clarifier scenario's in the denominator.

VI. Average Diurnal Operating Cost Comparison for Primary Treatment Scenarios

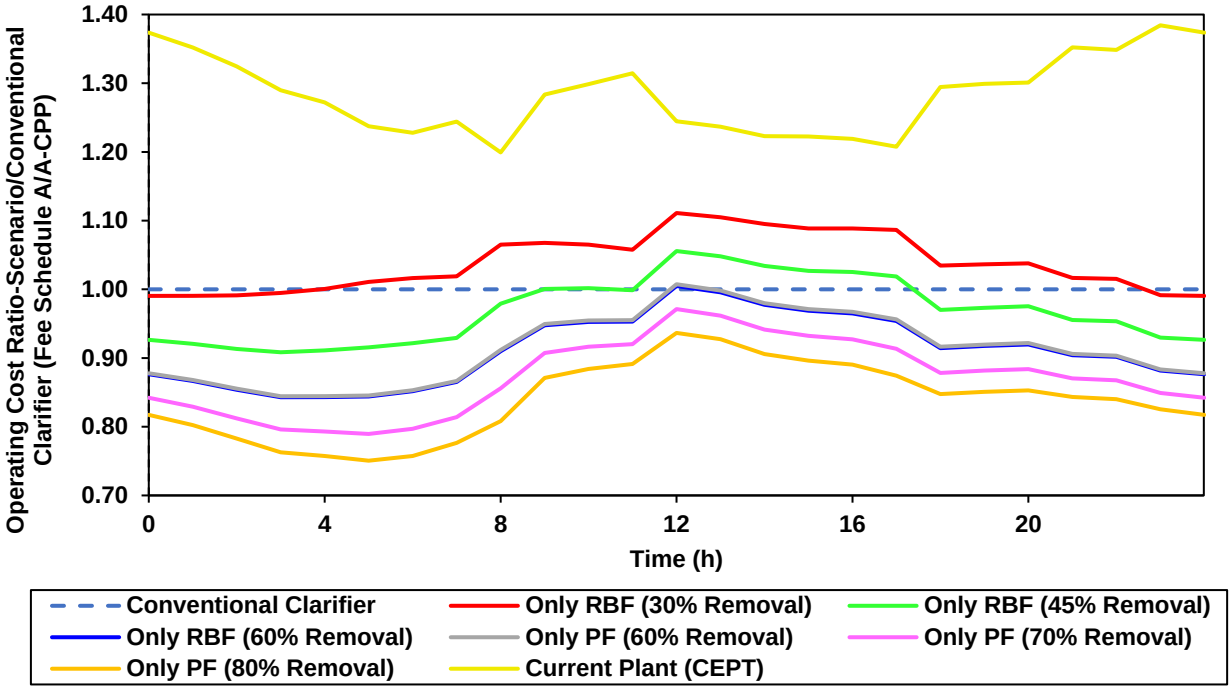

Figure E-38. Comparison of standalone primary treatment technologies' average operating cost (per electricity Fee Schedule A/A-CPP) diurnal trends normalized to quality index removal presented as dimensionless ratios, with the conventional clarifier scenario's in the denominator.

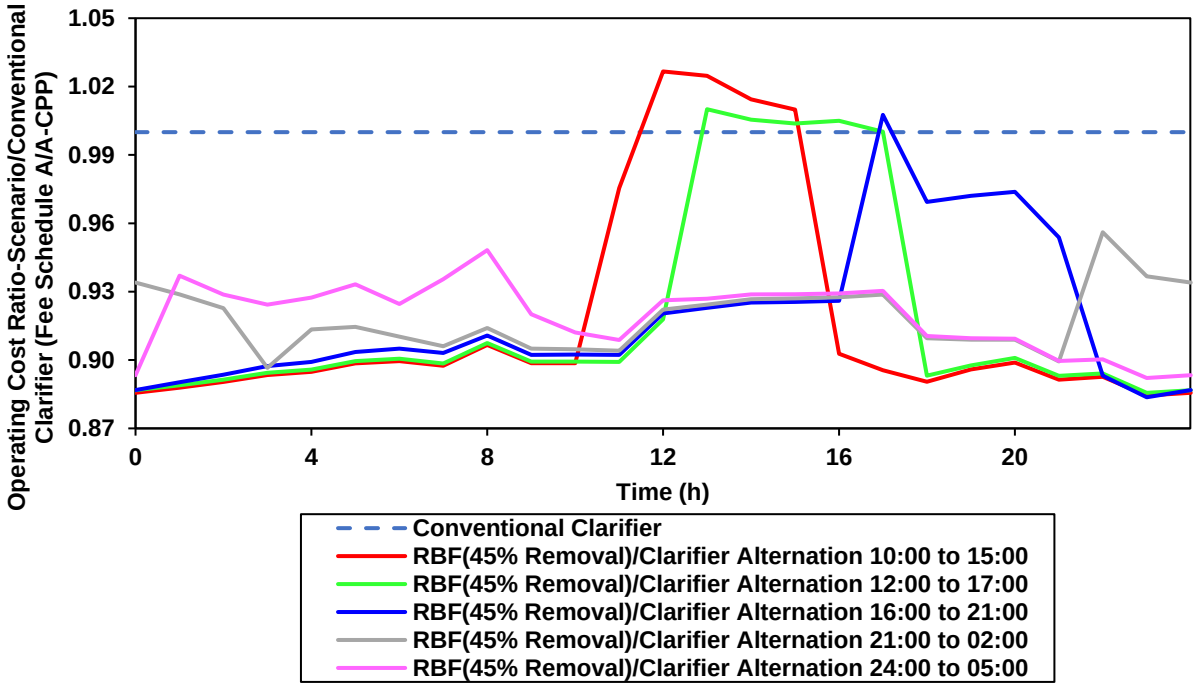

Figure E-39. Comparison of rotating-belt filtration and conventional clarifier alternation scenarios' average operating cost (per electricity Fee Schedule A/A-CPP) diurnal trends normalized to quality index removal presented as dimensionless ratios, with the conventional clarifier scenario's in the denominator.

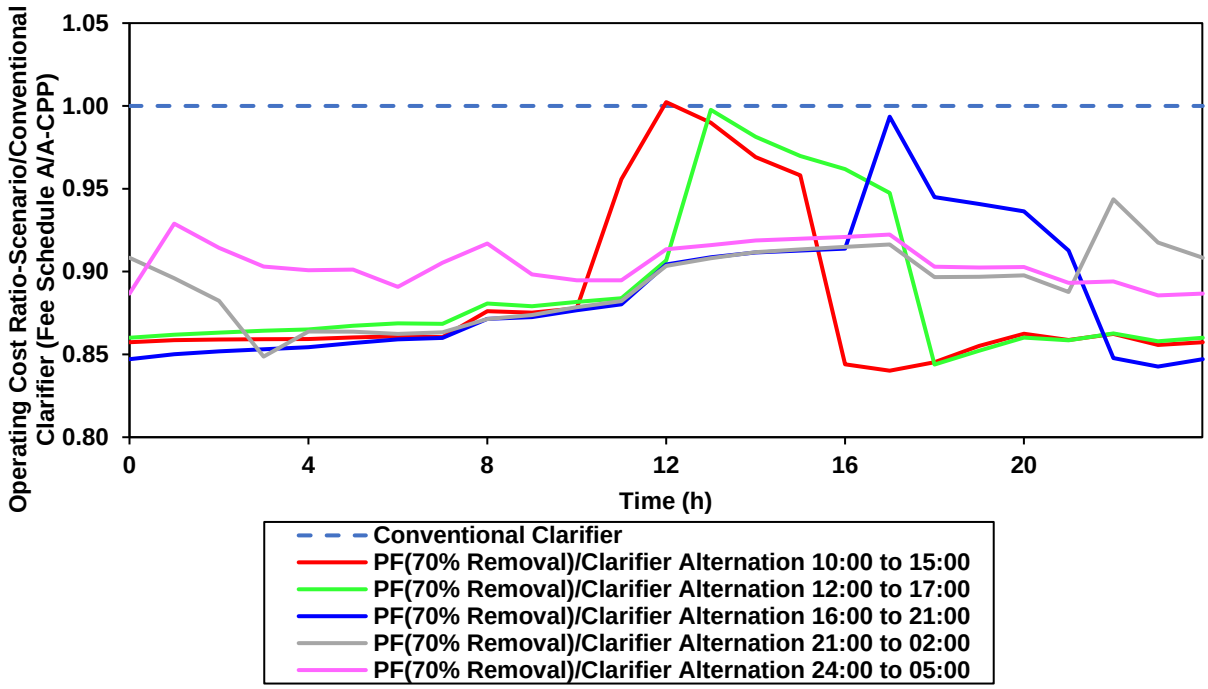

Figure E-40. Comparison of primary filtration and conventional clarifier alternation scenarios' average operating cost (per electricity Fee Schedule A/A-CPP) diurnal trends normalized to quality index removal presented as dimensionless ratios, with the conventional clarifier scenario's in the denominator.

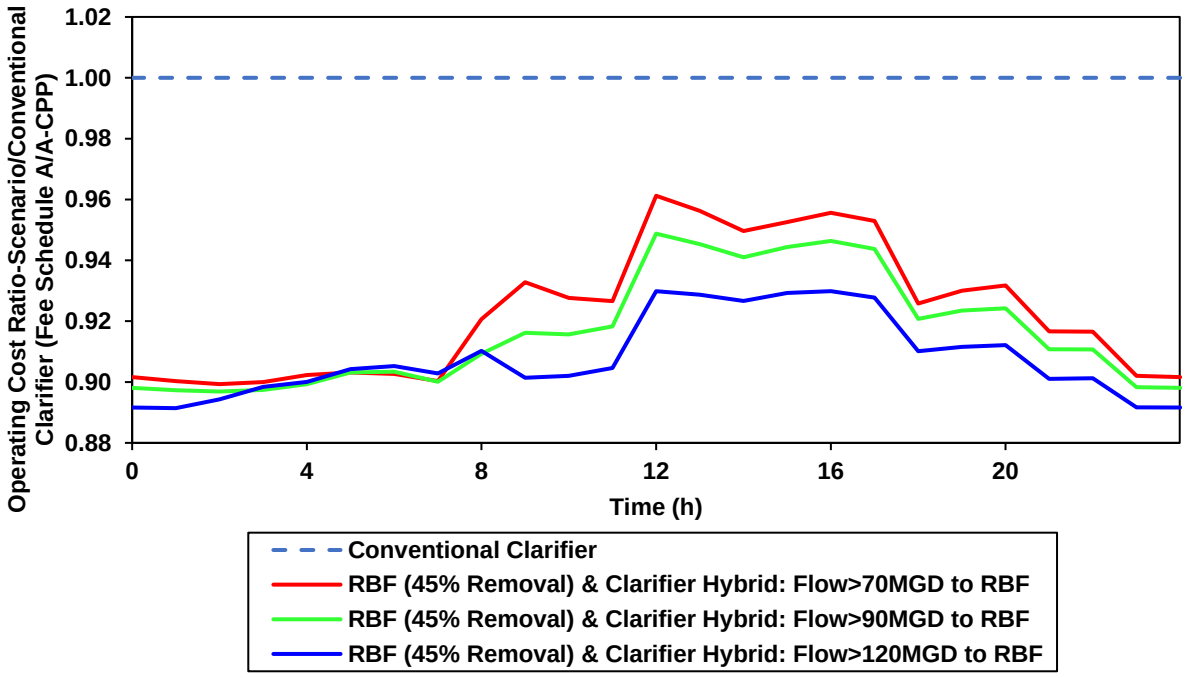

Figure E-41. Comparison of rotating-belt filtration and conventional clarifier hybrid scenarios' average operating cost (per electricity Fee Schedule A/A-CPP) diurnal trends normalized to quality index removal presented as dimensionless ratios, with the conventional clarifier scenario's in the denominator.

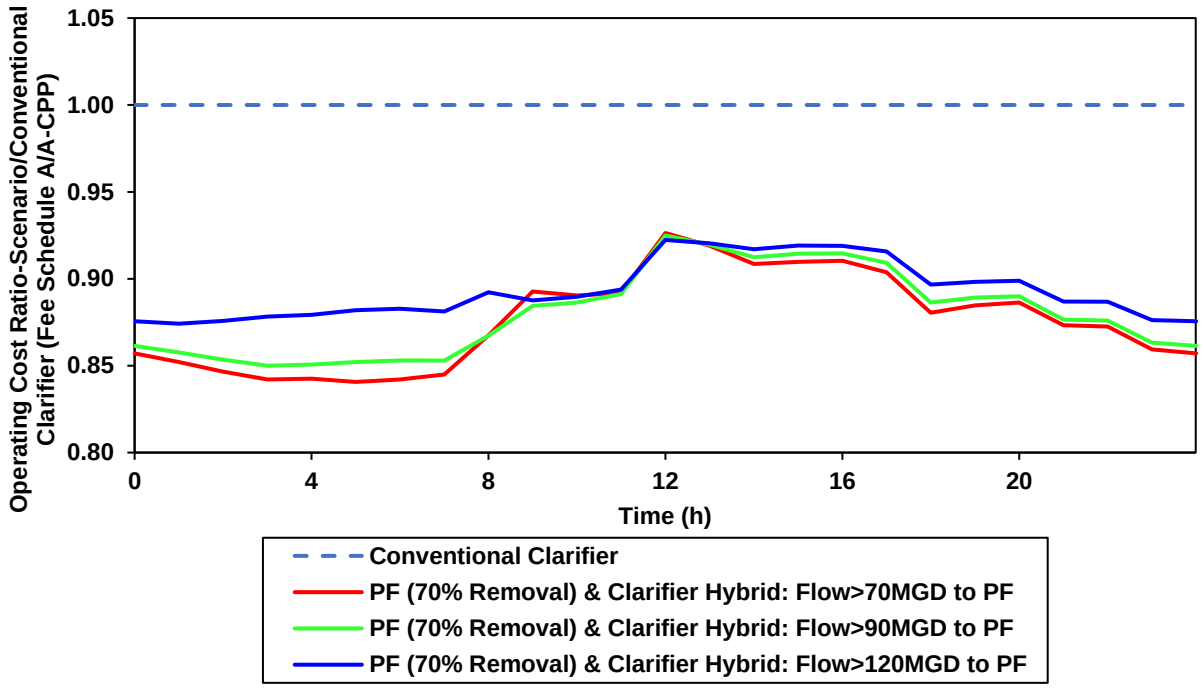

Figure E-42. Comparison of primary filtration and conventional clarifier hybrid scenarios' average operating cost (per electricity Fee Schedule A/A-CPP) diurnal trends normalized to quality index removal presented as dimensionless ratios, with the conventional clarifier scenario's in the denominator.

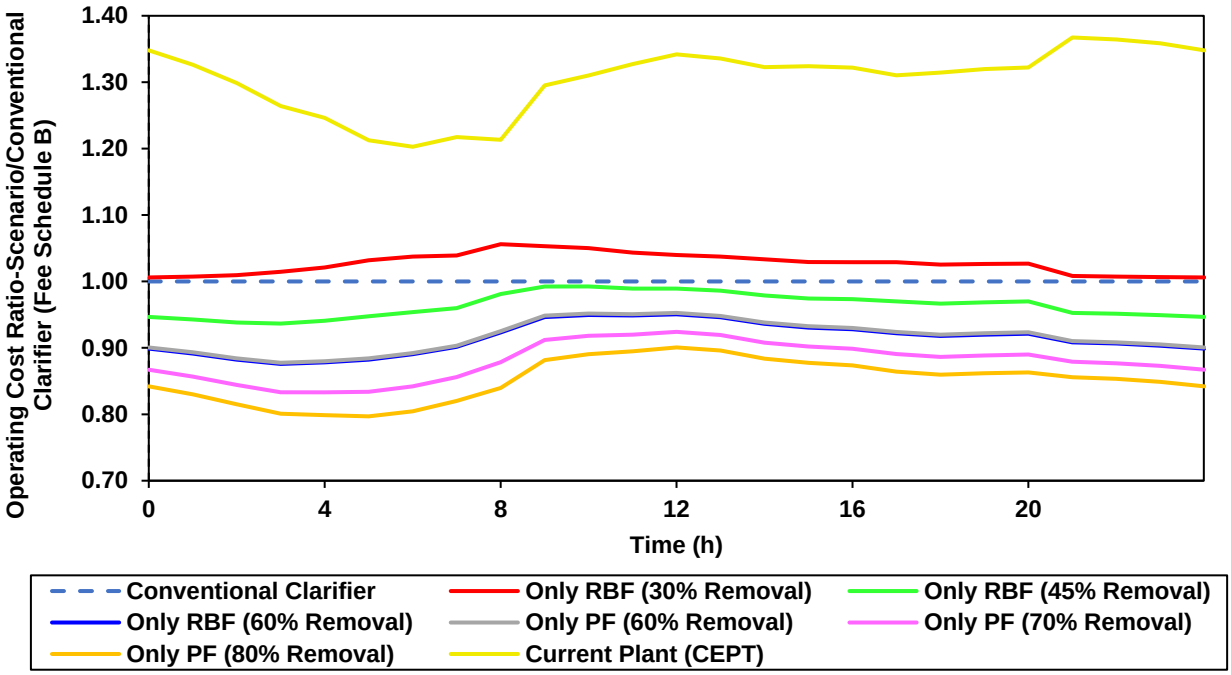

Figure E-43. Comparison of standalone primary treatment technologies' average operating cost (per electricity Fee Schedule B) diurnal trends normalized to quality index removal presented as dimensionless ratios, with the conventional clarifier scenario's in the denominator.

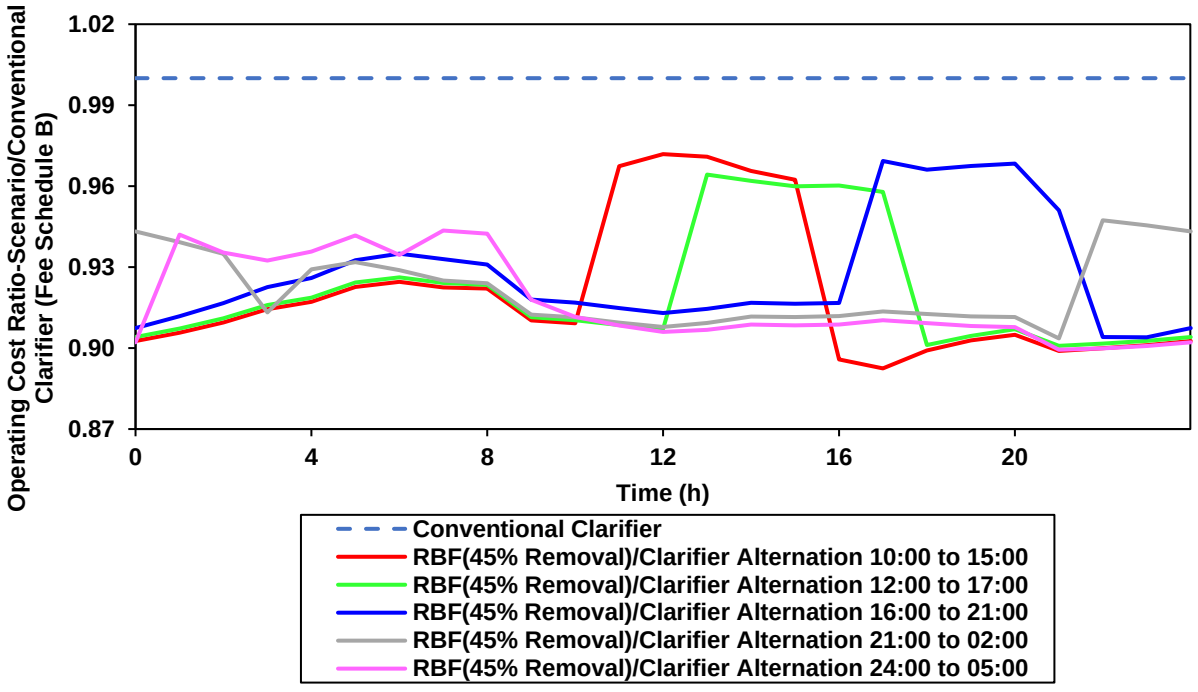

Figure E-44. Comparison of rotating-belt filtration and conventional clarifier alternation scenarios' average operating cost (per electricity Fee Schedule B) diurnal trends normalized to quality index removal presented as dimensionless ratios, with the conventional clarifier scenario's in the denominator.

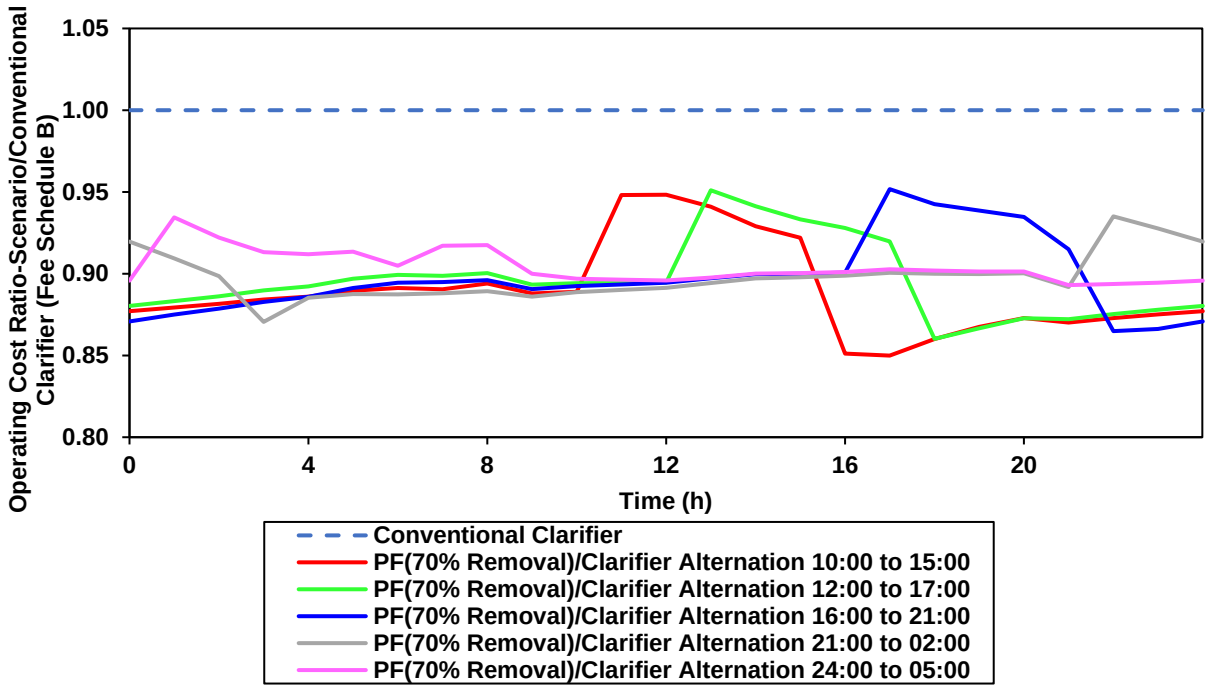

Figure E-45. Comparison of primary filtration and conventional clarifier alternation scenarios' average operating cost (per electricity Fee Schedule B) diurnal trends normalized to quality index removal presented as dimensionless ratios, with the conventional clarifier scenario's in the denominator.

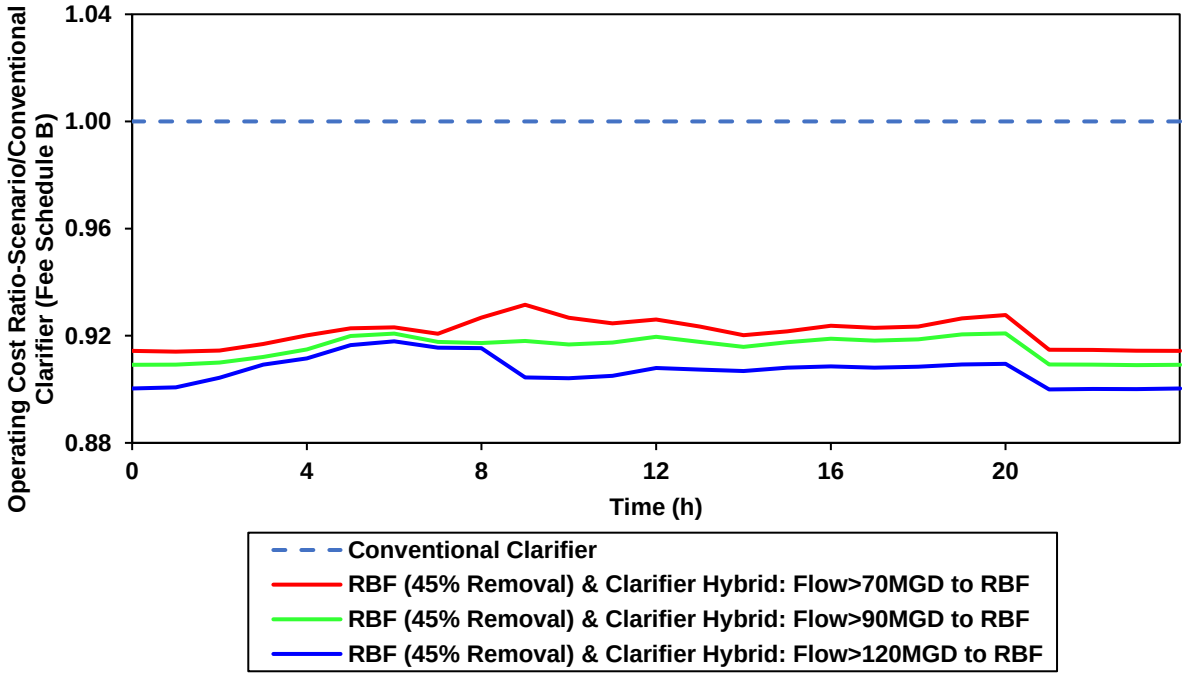

Figure E-46. Comparison of rotating-belt filtration and conventional clarifier hybrid scenarios' average operating cost (per electricity Fee Schedule B) diurnal trends normalized to quality index removal presented as dimensionless ratios, with the conventional clarifier scenario's in the denominator.

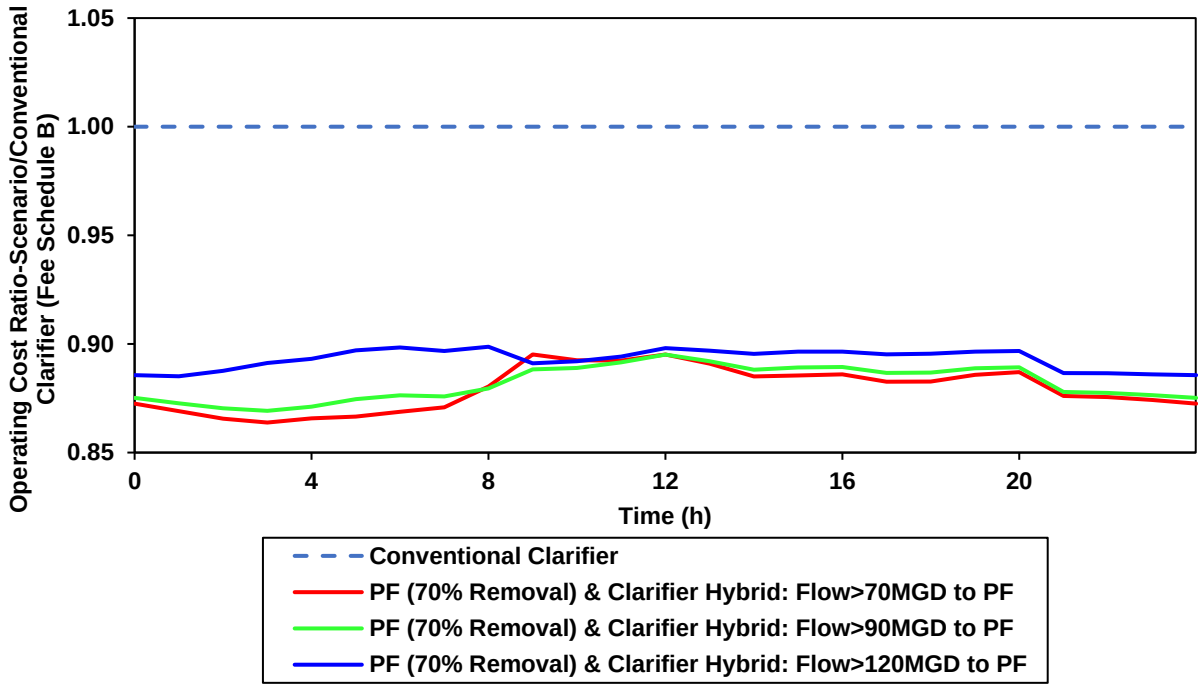

Figure E-47. Comparison of primary filtration and conventional clarifier hybrid scenarios' average operating cost (per electricity Fee Schedule B) diurnal trends normalized to quality index removal presented as dimensionless ratios, with the conventional clarifier scenario's in the denominator.

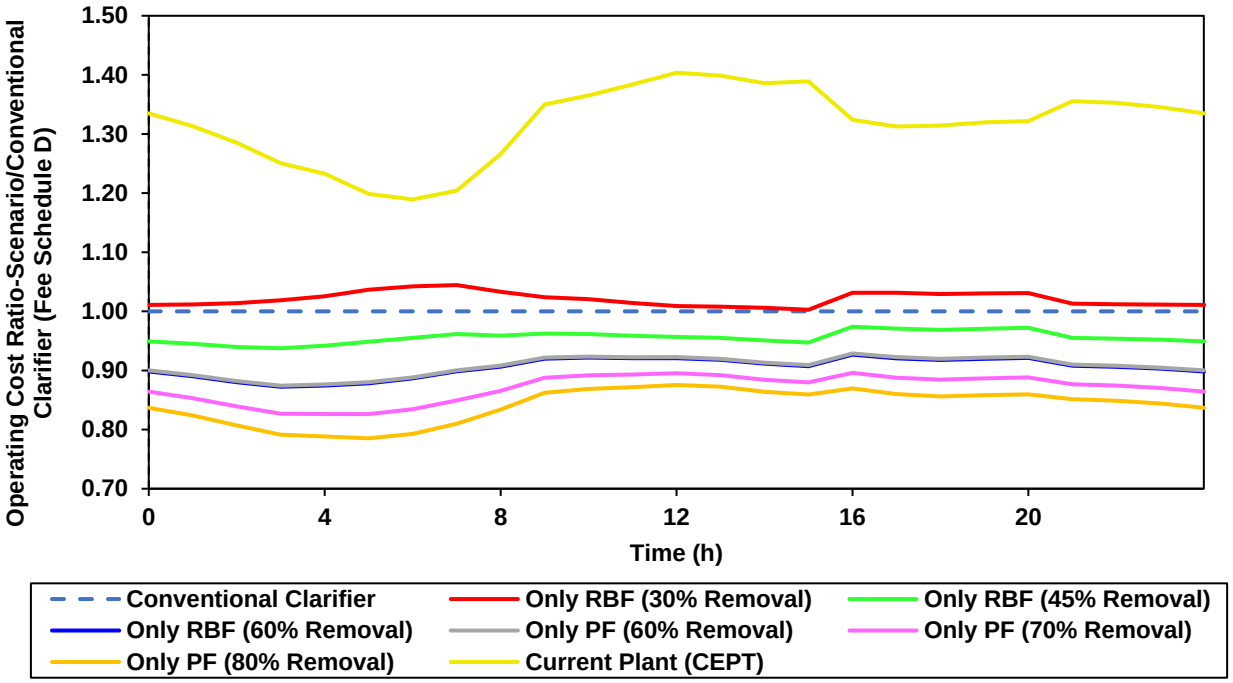

Figure E-48. Comparison of standalone primary treatment technologies' average operating cost (per electricity Fee Schedule D) diurnal trends normalized to quality index removal presented as dimensionless ratios, with the conventional clarifier scenario's in the denominator.

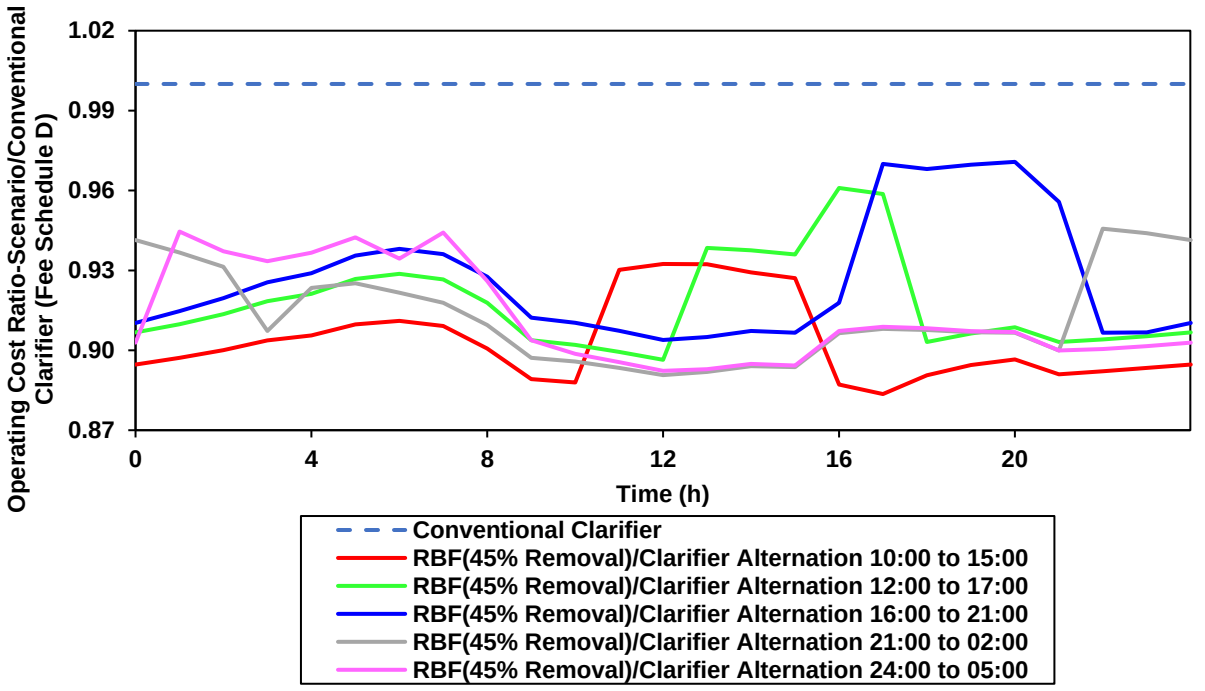

Figure E-49. Comparison of rotating-belt filtration and conventional clarifier alternation scenarios' average operating cost (per electricity Fee Schedule D) diurnal trends normalized to quality index removal presented as dimensionless ratios, with the conventional clarifier scenario's in the denominator.

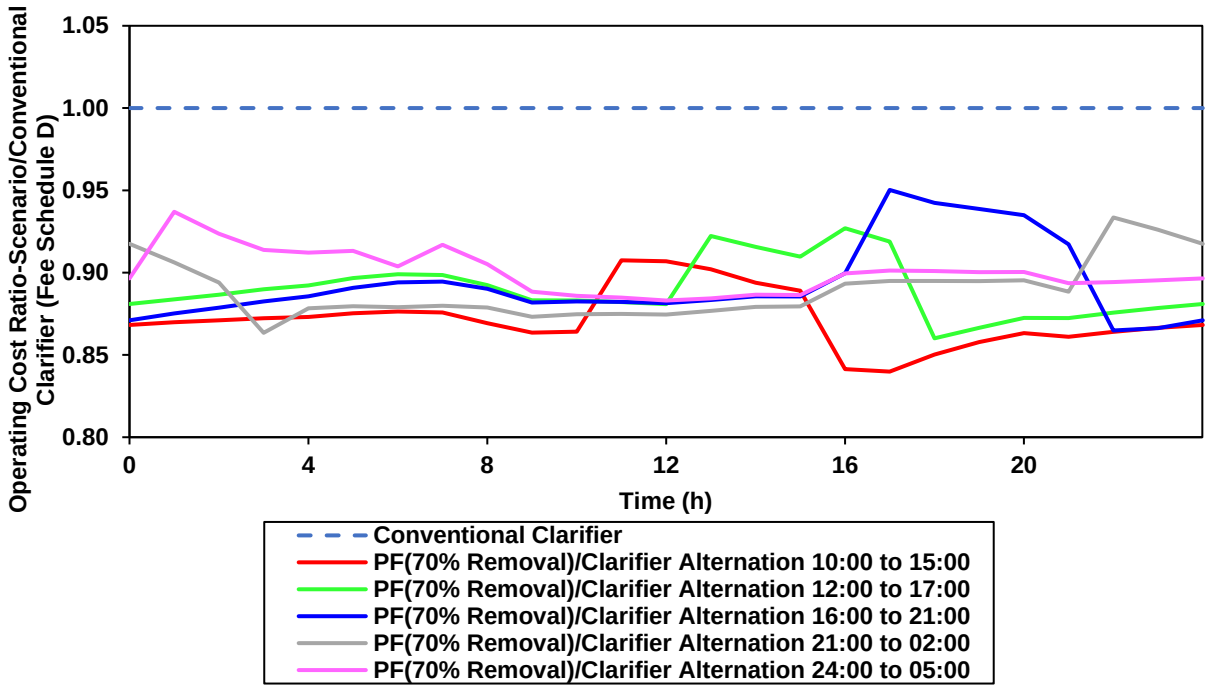

Figure E-50. Comparison of primary filtration and conventional clarifier alternation scenarios' average operating cost (per electricity Fee Schedule D) diurnal trends normalized to quality index removal presented as dimensionless ratios, with the conventional clarifier scenario's in the denominator.

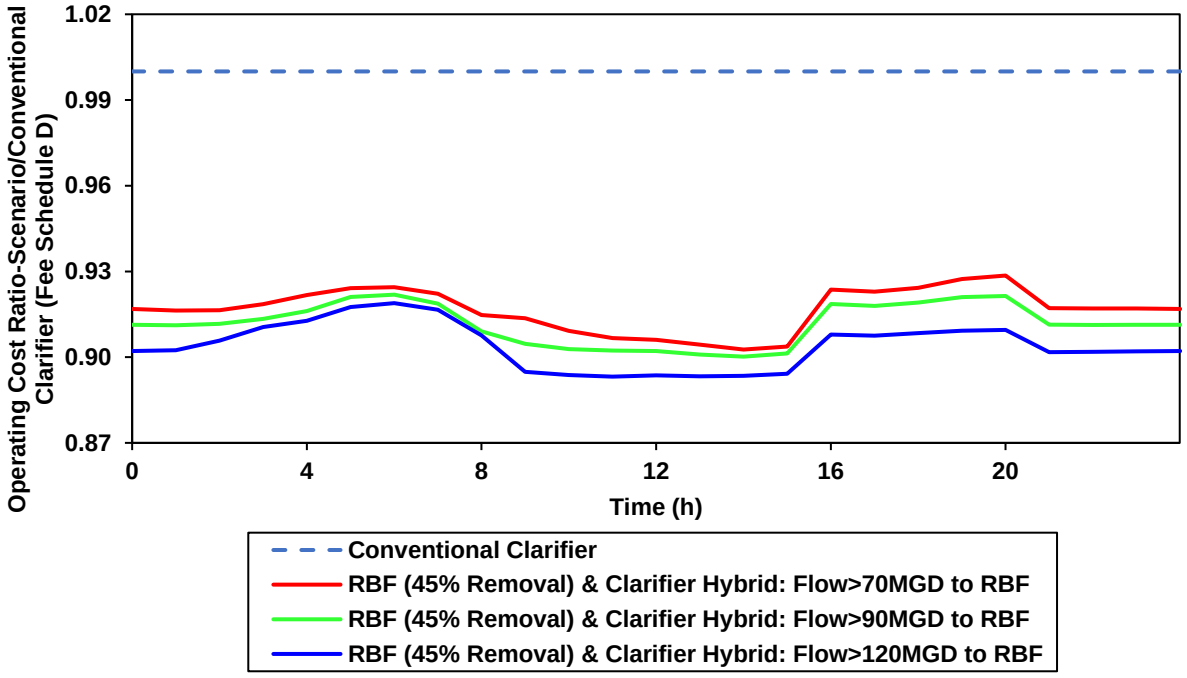

Figure E-51. Comparison of rotating-belt filtration and conventional clarifier hybrid scenarios' average operating cost (per electricity Fee Schedule D) diurnal trends normalized to quality index removal presented as dimensionless ratios, with the conventional clarifier scenario's in the denominator.

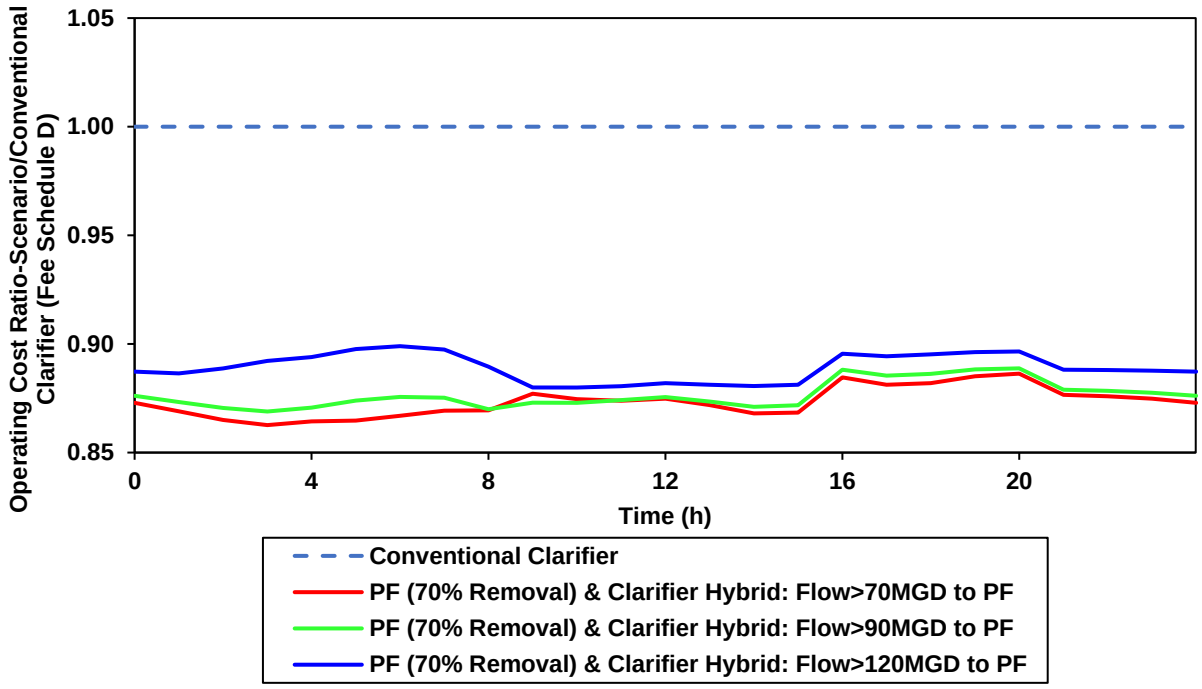

Figure E-52. Comparison of primary filtration and conventional clarifier hybrid scenarios' average operating cost (per electricity Fee Schedule D) diurnal trends normalized to quality index removal presented as dimensionless ratios, with the conventional clarifier scenario's in the denominator.

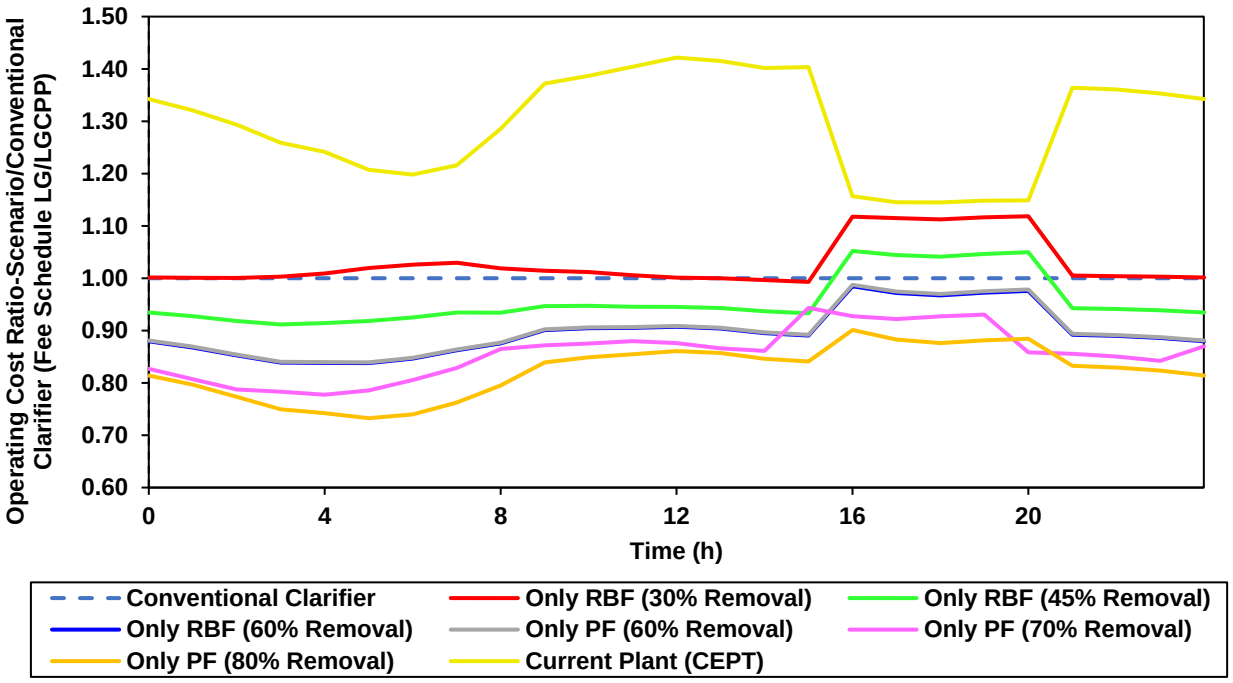

Figure E-53. Comparison of standalone primary treatment technologies' average operating cost (per electricity Fee Schedule LG/LG-CPP) diurnal trends normalized to quality index removal presented as dimensionless ratios, with the conventional clarifier scenario's in the denominator.

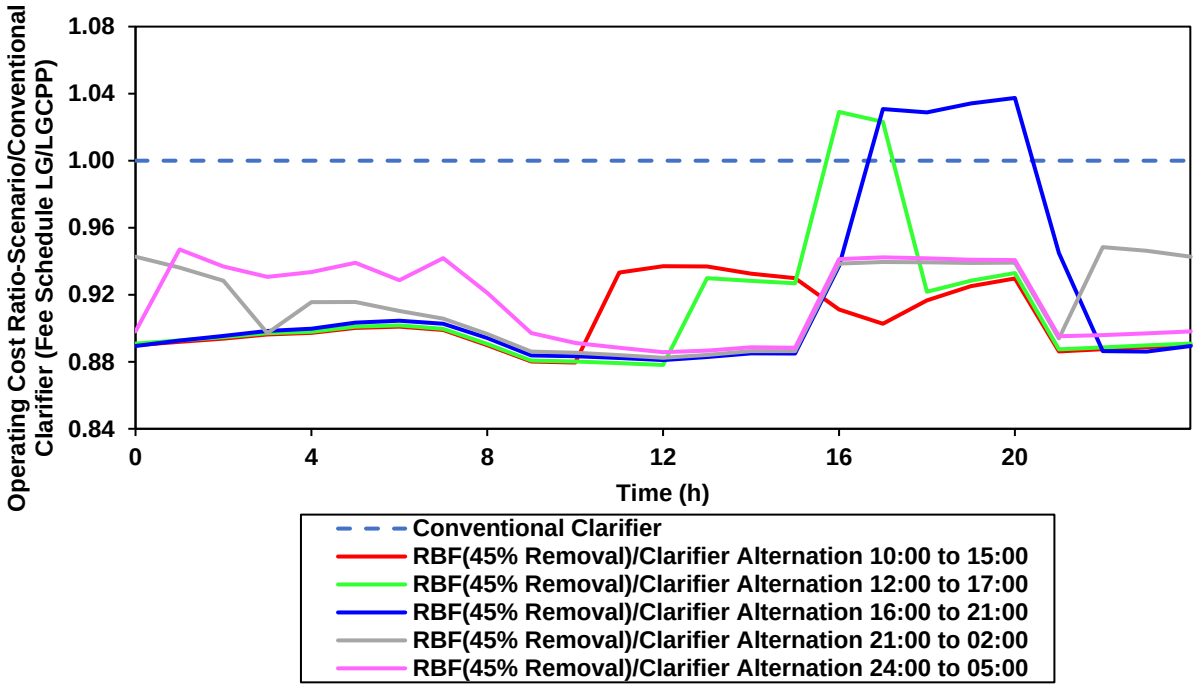

Figure E-54. Comparison of rotating-belt filtration and conventional clarifier alternation scenarios' average operating cost (per electricity Fee Schedule LG/LG-CPP) diurnal trends normalized to quality index removal presented as dimensionless ratios, with the conventional clarifier scenario's in the denominator.

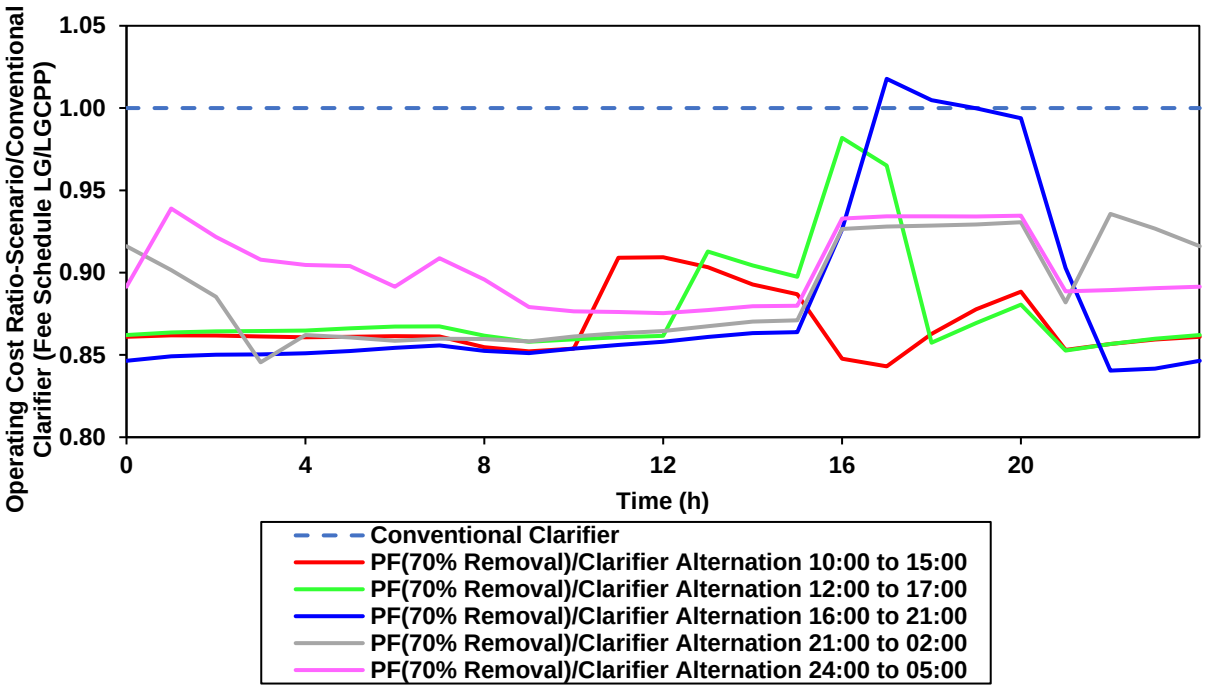

Figure E-55. Comparison of primary filtration and conventional clarifier alternation scenarios' average operating cost (per electricity Fee Schedule LG/LG-CPP) diurnal trends normalized to quality index removal presented as dimensionless ratios, with the conventional clarifier scenario's in the denominator.

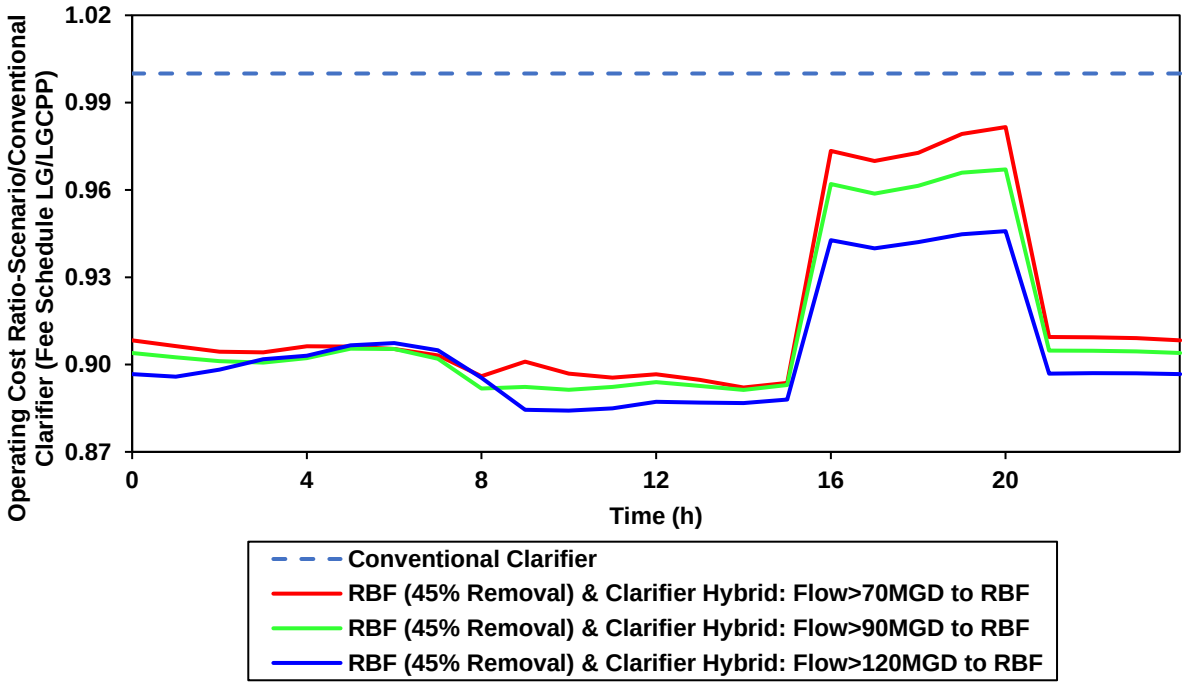

Figure E-56. Comparison of rotating-belt filtration and conventional clarifier hybrid scenarios' average operating cost (per electricity Fee Schedule LG/LG-CPP) diurnal trends normalized to quality index removal presented as dimensionless ratios, with the conventional clarifier scenario's in the denominator.

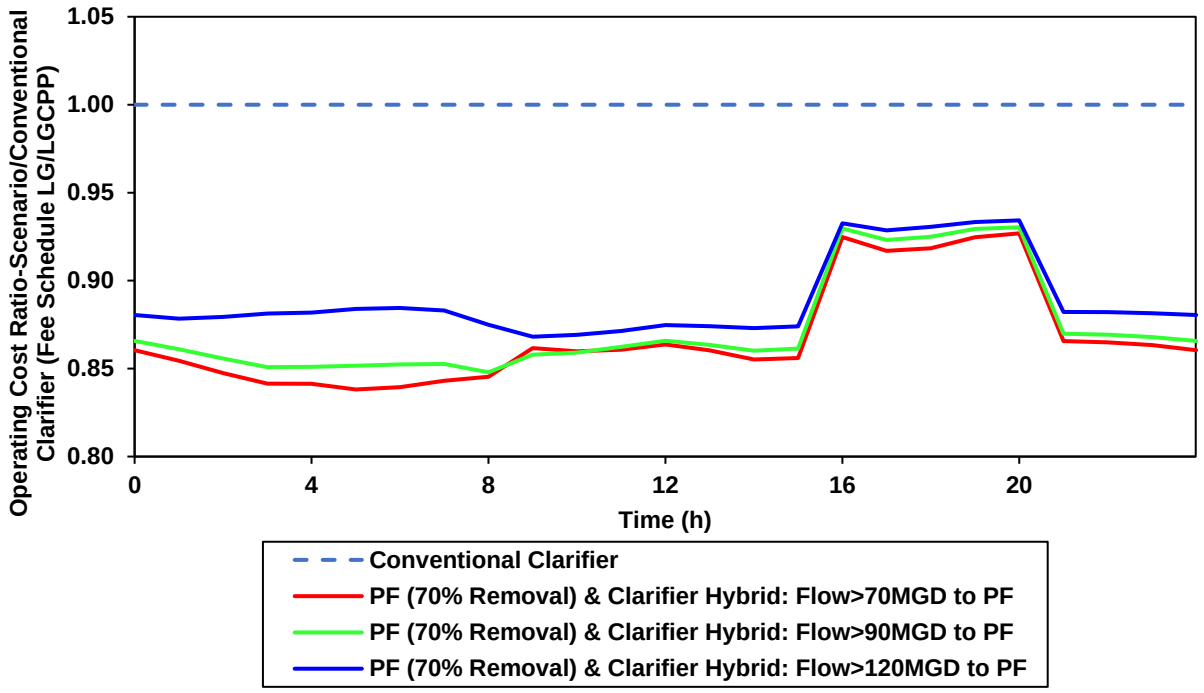

Figure E-57. Comparison of primary filtration and conventional clarifier hybrid scenarios' average operating cost (per electricity Fee Schedule LG/LG-CPP) diurnal trends normalized to quality index removal presented as dimensionless ratios, with the conventional clarifier scenario's in the denominator.

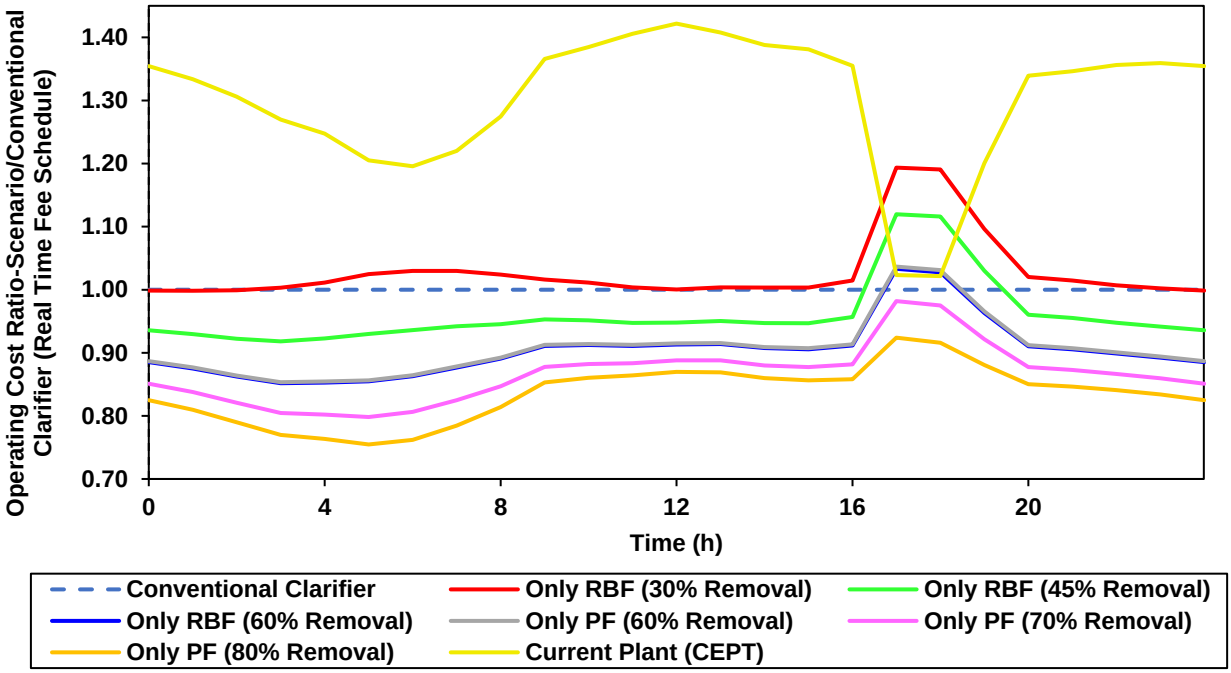

Figure E-58. Comparison of standalone primary treatment technologies' average operating cost (per electricity Real Time Fee Schedule) diurnal trends normalized to quality index removal presented as dimensionless ratios, with the conventional clarifier scenario's in the denominator.

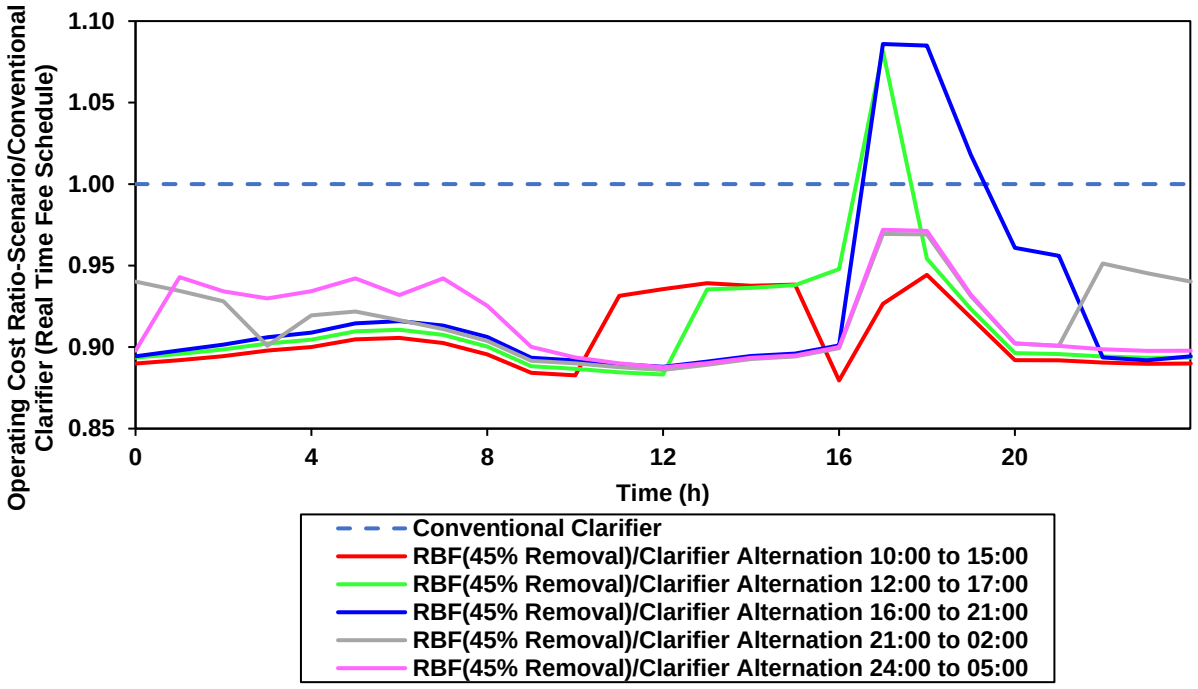

Figure E-59. Comparison of rotating-belt filtration and conventional clarifier alternation scenarios' average operating cost (per electricity Real Time Fee Schedule) diurnal trends normalized to quality index removal presented as dimensionless ratios, with the conventional clarifier scenario's in the denominator.

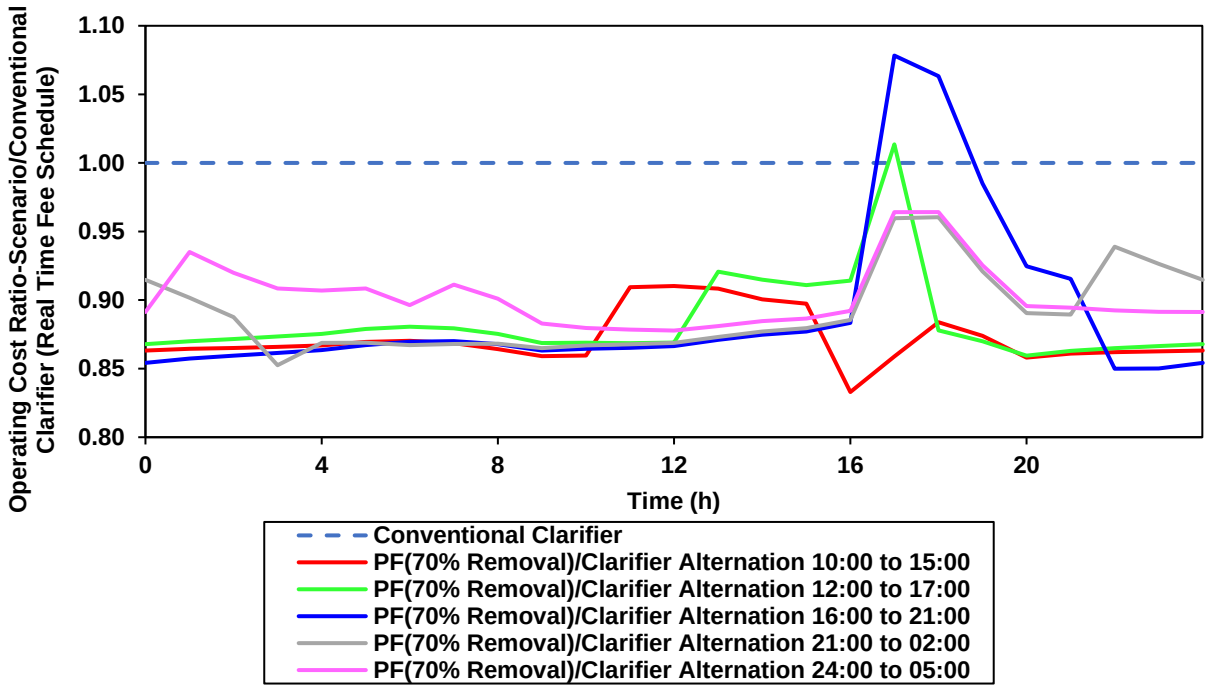

Figure E-60. Comparison of primary filtration and conventional clarifier alternation scenarios' average operating cost (per electricity Real Time Fee Schedule) diurnal trends normalized to quality index removal presented as dimensionless ratios, with the conventional clarifier scenario's in the denominator.

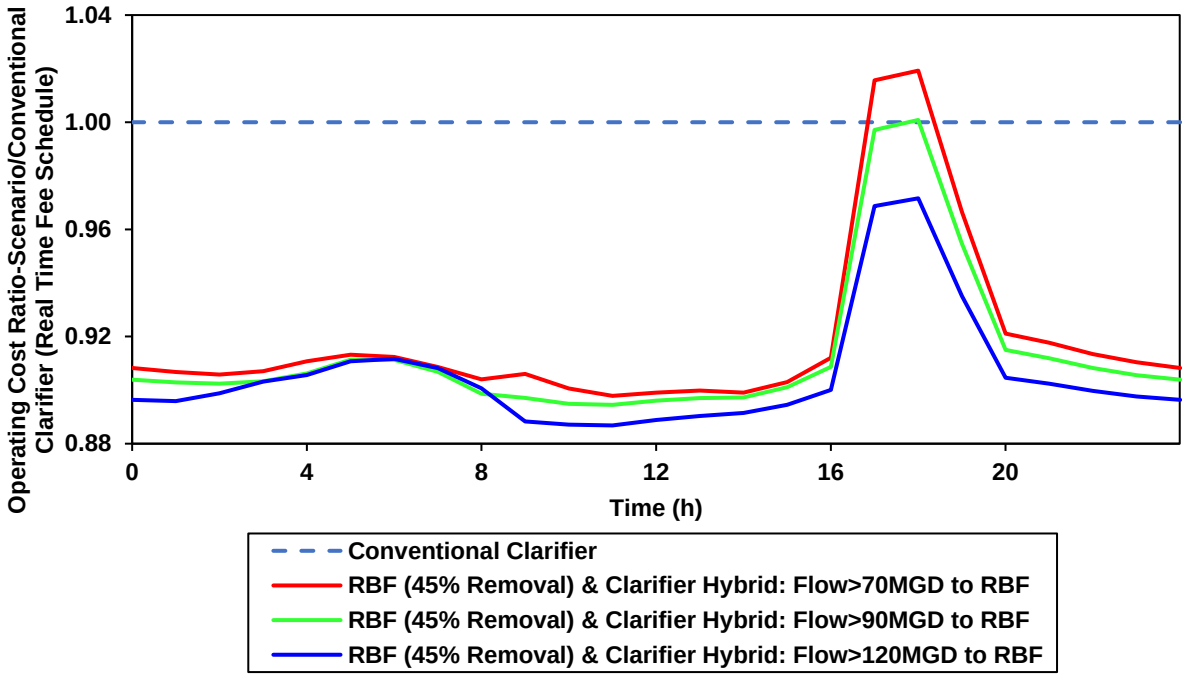

Figure E-61. Comparison of rotating-belt filtration and conventional clarifier hybrid scenarios' average operating cost (per electricity Real Time Fee Schedule) diurnal trends normalized to quality index removal presented as dimensionless ratios, with the conventional clarifier scenario's in the denominator.

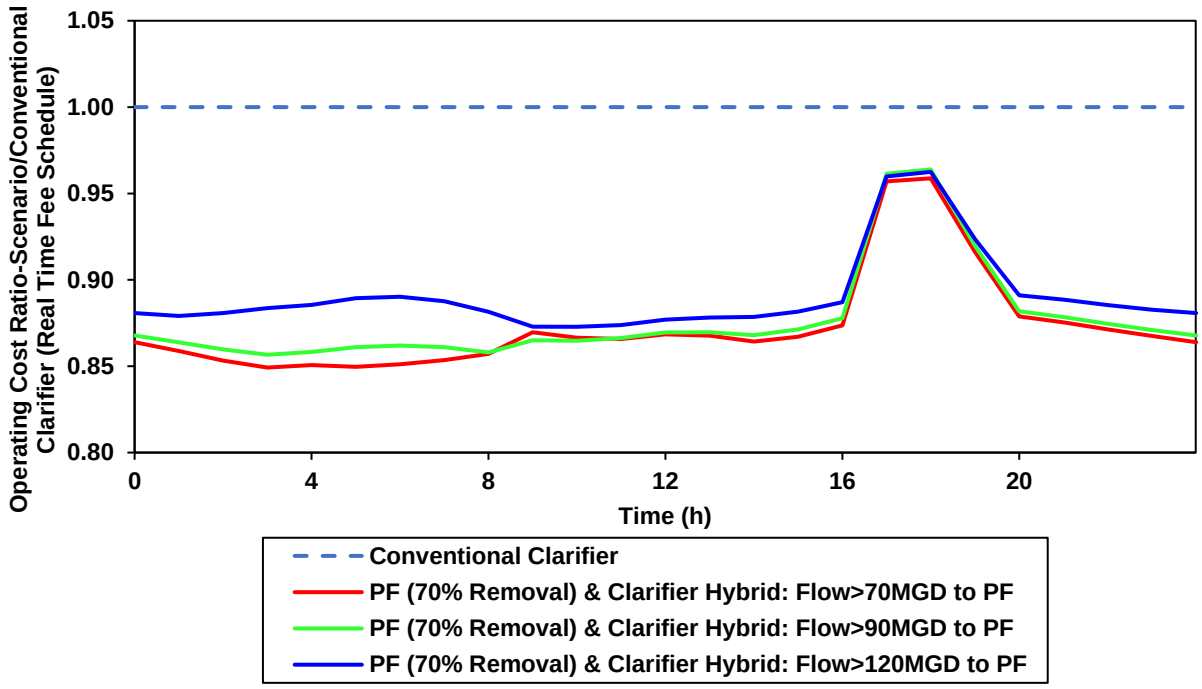

Figure E-62. Comparison of primary filtration and conventional clarifier hybrid scenarios' average operating cost (per electricity Real Time Fee Schedule) diurnal trends normalized to quality index removal presented as dimensionless ratios, with the conventional clarifier scenario's in the denominator.

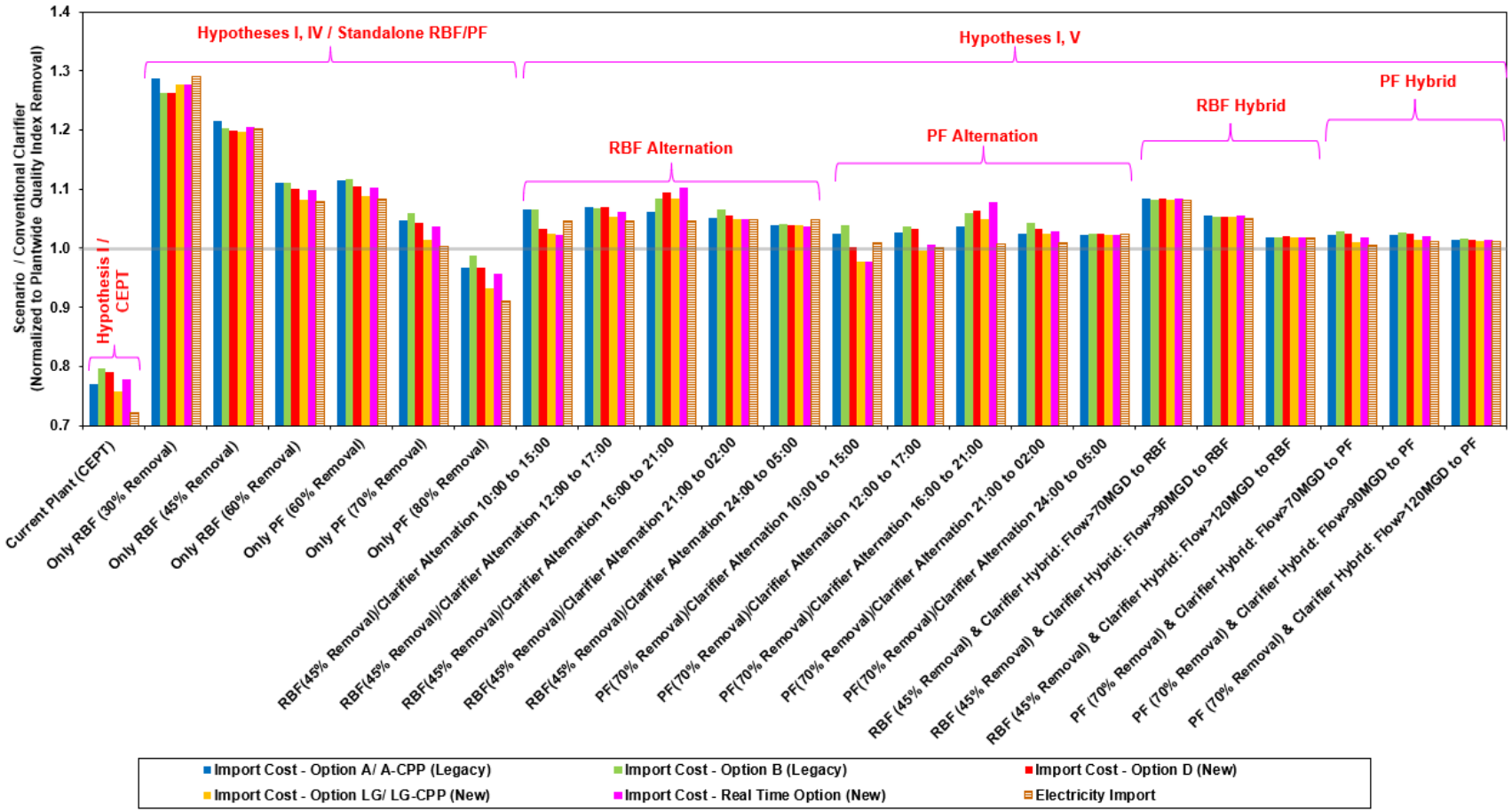

Figure E-63. Sum of 12 consecutive months' electricity import and its cost for each tariff structure normalized to total quality index removal for all the scenarios with standalone advanced primary treatment technologies and their combinations with conventional clarifier (Scenarios 2 to 8). The results are presented as dimensionless ratios, with the conventional clarifier scenario in the denominator. The light gray horizontal line represents the conventional clarifier scenario's ratio of 1 for all the electricity import and cost categories presented here.